



# Lawrence Berkeley Laboratory

UNIVERSITY OF CALIFORNIA

## Materials & Molecular Research Division

BROADBAND EXCITATION IN NUCLEAR MAGNETIC RESONANCE

R. Tycko  
(Ph.D. Thesis)

October 1984



#### LEGAL NOTICE

This book was prepared as an account of work sponsored by an agency of the United States Government. Neither the United States Government nor any agency thereof, nor any of their employees, makes any warranty, express or implied, or assumes any legal liability or responsibility for the accuracy, completeness, or usefulness of any information, apparatus, product, or process disclosed, or represents that its use would not infringe privately owned rights. Reference herein to any specific commercial product, process, or service by trade name, trademark, manufacturer, or otherwise, does not necessarily constitute or imply its endorsement, recommendation, or favoring by the United States Government or any agency thereof. The views and opinions of authors expressed herein do not necessarily state or reflect those of the United States Government or any agency thereof.

BROADBAND EXCITATION IN NUCLEAR MAGNETIC RESONANCE

Robert Tycko

This work was supported by the Director, Office of Energy Research,  
Office of Basic Energy Sciences, Materials Sciences Division of the  
U. S. Department of Energy under Contract Number DE-AC03-76SF00098.





## BROADBAND EXCITATION IN NUCLEAR MAGNETIC RESONANCE

Robert Tycko

## ABSTRACT

Theoretical methods for designing sequences of radio frequency (rf) radiation pulses for broadband excitation of spin systems in nuclear magnetic resonance (NMR) are described. The sequences excite spins uniformly over large ranges of resonant frequencies arising from static magnetic field inhomogeneity, chemical shift differences, or spin couplings, or over large ranges of rf field amplitudes. Specific sequences for creating a population inversion or transverse magnetization are derived and demonstrated experimentally in liquid and solid state NMR.

One approach to broadband excitation is based on principles of coherent averaging theory. A general formalism for deriving pulse sequences is given, along with computational methods for specific cases. This approach leads to sequences that produce strictly constant transformations of a spin system. The importance of this feature in NMR applications is discussed.

A second approach to broadband excitation makes use of iterative schemes, i.e. sets of operations that are applied repetitively to a given initial pulse sequences, generating a series of increasingly complex sequences with increasingly desirable properties. A general mathematical framework for analyzing iterative schemes is developed. An

iterative scheme is treated as a function that acts on a space of operators corresponding to the transformations produced by all possible pulse sequences. The fixed points of the function and the stability of the fixed points are shown to determine the essential behavior of the scheme. Iterative schemes for broadband population inversion are treated in detail. Algebraic and numerical methods for performing the mathematical analysis are presented.

Two additional topics are treated. The first is the construction of sequences for uniform excitation of double-quantum coherence and for uniform polarization transfer over a range of spin couplings. Double-quantum excitation sequences are demonstrated in a liquid crystal system. The second additional topic is the construction of iterative schemes for narrowband population inversion. The use of sequences that invert spin populations only over a narrow range of rf field amplitudes to spatially localize NMR signals in an rf field gradient is discussed.

## Acknowledgements

The work described here would not have come about if Professor Alexander Pines had not posed problems, provided ideas, and made constructive criticism. In particular, I thank Professor Pines for setting high standards as to what constitutes interesting research.

John Guckenheimer's willingness to share his expertise in mathematical dynamics has been a significant factor in the development of the methods described in Chapters VII, VIII, and IX. I have learned a great deal from Dan Weitekamp, who has also contributed directly to the work described in Chapter VI. Herman Cho and Erika Schneider have worked on the computations and experiments described in Chapters IV and V.

Lastly, my interest in the problems that are focus of this dissertation began in a collaboration with Jean Baum. For that, as well as for her friendship, I thank her.

## TABLE OF CONTENTS

---

Chapter I:	Introduction.....	1
Chapter II:	Quantum Mechanical Background.....	8
A.	The rotating frame.....	8
1.	Laboratory frame Hamiltonian.....	8
2.	Rotating frame transformation.....	9
3.	Observations in the rotating frame.....	12
B.	Nuclear spin interactions.....	15
1.	Zeeman interaction.....	15
2.	Rf interaction.....	15
3.	Chemical shifts.....	17
4.	Dipole couplings.....	18
5.	Quadrupole couplings.....	18
6.	Scalar couplings.....	20
C.	Pulse sequence propagators.....	21
1.	General remarks.....	21
2.	Isolated spins and two-level systems.....	22
3.	Coupled spins.....	25
D.	Broadband excitation problems.....	27
1.	Population inversion.....	27
2.	Creation of transverse magnetization.....	33
Chapter III:	Previous Work in Broadband Excitation.....	38



A. Adiabatic inversion .....	38
B. Composite pulses .....	40
C. Broadband population inversion by phase-modulated pulses .....	48

#### Chapter IV: Coherent Averaging Approach to Broadband Excitation:

Formalism and Computational Methods .....	53
A. Motivation .....	53
B. The Magnus expansion .....	58
1. Derivations .....	58
2. A parameter differentiation theorem .....	60
C. Application to the construction of composite pulses .....	63
1. Formal approach .....	63
2. A simple example .....	66
3. Numerical methods: resonance offsets and rf inhomogeneity .....	68
4. Numerical methods: dipole and quadrupole couplings .....	73
5. Limitations of the methods .....	78

#### Chapter V: Coherent Averaging Approach to Broadband Excitation:

Results .....	80
A. Motivation .....	80
B. Rf inhomogeneity .....	81
1. Composite $\pi$ pulses .....	81
2. Composite $\pi/2$ pulses .....	87
C. Resonance offsets .....	91

1. Composite $\pi$ pulses.....	91
2. Composite $\pi/2$ pulses.....	91
D. The importance of constant net rotations.....	97
E. Dipole and quadrupole couplings.....	100
1. Composite $\pi$ pulses.....	100
2. Composite $\pi/2$ pulses.....	112
 Chapter VI:     Broadband Excitation in Other NMR Techniques.....	123
A. Motivation.....	123
B. Theory of broadband double-quantum excitation.....	126
1. Fictitious two-level systems.....	126
2. Composite double-quantum excitation sequences.....	130
3. Reduced composite sequences.....	131
4. The double-quantum experiment.....	133
C. Broadband double-quantum excitation results.....	138
1. Experiments and spectra.....	138
2. Effects of pulse imperfections.....	139
D. Extensions and applications.....	142
1. Liquid state NMR.....	142
2. $^{13}\text{C}$ spectroscopy in solids.....	143
3. Quadrupolar spin-1 nuclei.....	144
E. Broadband polarization transfer.....	145
1. Background.....	145
2. Polarization transfer in an I-S spin system.....	147
3. Polarization transfer in an $I_n$ -S spin system.....	153

Chapter VII:     Iterative Schemes: Fixed Point Theory and Application	
--	--

to Broadband Population Inversion.....	155
A. Background.....	155
1. Definition of iterative schemes.....	155
2. Iterative schemes as functions on the propagator space.....	156
3. An example of a function.....	158
a. Iterates, fixed points, and attractors.....	158
b. Basins of attractors.....	161
4. Remarks.....	162
B. Iterative schemes for broadband population inversion....	163
1. Propagator space for an isolated spin or two-level system.....	163
2. An iterative scheme and the corresponding function..	164
3. Stability of the fixed points.....	167
a. The origin.....	167
b. The equator.....	169
4. Schemes for which the equator of $SO(3)$ is superstable.....	173
C. Numerical analysis of iterative schemes in $SO(3)$ .....	180
1. Motivation.....	180
2. Maps of basins.....	183
3. Maps of fixed points and the flow of iterates.....	187
D. Generation of pulse sequences for broadband population inversion.....	193
E. Summary of principles of the fixed point theory.....	199

Inversion.....	202
A. Motivation.....	202
B. Generation of pulse sequences.....	203
C. Application to the spatial localization of NMR signals...	207
D. Resonance offset behavior.....	214
 Chapter IX: Fixed Point Theory Analyses of Other Iterative	
Schemes.....	219
A. Motivation.....	219
B. Heteronuclear decoupling in liquids.....	219
1. Waugh's theory of decoupling.....	219
2. MLEV decoupling sequences.....	222
3. Remarks.....	224
C. Composite pulses.....	227
1. Recursive expansion procedure.....	227
2. Composite $\pi$ pulses.....	229
3. Remarks.....	232
D. Selective excitation of multiple quantum coherence.....	233
 Chapter X: Conclusion.....	237
 Appendix A: Experimental Methods.....	239
1. Spectrometers.....	239
2. NMR probes.....	241
3. Samples.....	244
4. Additional remarks on techniques.....	245



Appendix B: Computer Programs.....	247
1. Simulations.....	247
2. Derivation of pulse sequences in the coherent averaging theory approach.....	247
3. Generation of maps for iterative schemes.....	257
References.....	273



## Chapter I: Introduction

This dissertation describes theoretical approaches to the problem of broadband excitation in nuclear magnetic resonance (NMR), and gives experimental results that verify the theoretical work.

In most pulsed NMR experiments, a sequence of radio frequency (rf) radiation pulses is applied to a sample containing magnetic nuclei initially at equilibrium in a large, static magnetic field. The typical experimental arrangement is shown in Figure I.1. The rf pulses excite the nuclei to a non-equilibrium spin state, from which much weaker rf signals are emitted and recorded. That state may be specified in detail by a density operator. However, there is often one property of the spin state that is of particular interest. That property may then be considered to be the response of the spin system to the applied rf pulses. Figure I.2 gives a schematic representation of the excitation process.

The response is determined not only by the specific sequence of rf pulses, i.e. the individual pulse lengths and rf phases, but also by a set of experimental parameters. Thus, for a given pulse sequence, the response of the spin system can be plotted as a function of one of the experimental parameters, with the other parameters fixed at some nominal values. An example of the form of such a plot is given in Figure I.3. When the parameter  $\lambda$  takes on its nominal value  $\lambda_0$ , the response  $R(\lambda)$  has the desired value  $R_0$ . In some small range of values of  $\lambda$  around  $\lambda_0$ ,  $R(\lambda)$  is approximately  $R_0$ . The range of  $\lambda$  for which  $R(\lambda) \approx R_0$  defines the bandwidth of excitation with respect to  $\lambda$ .

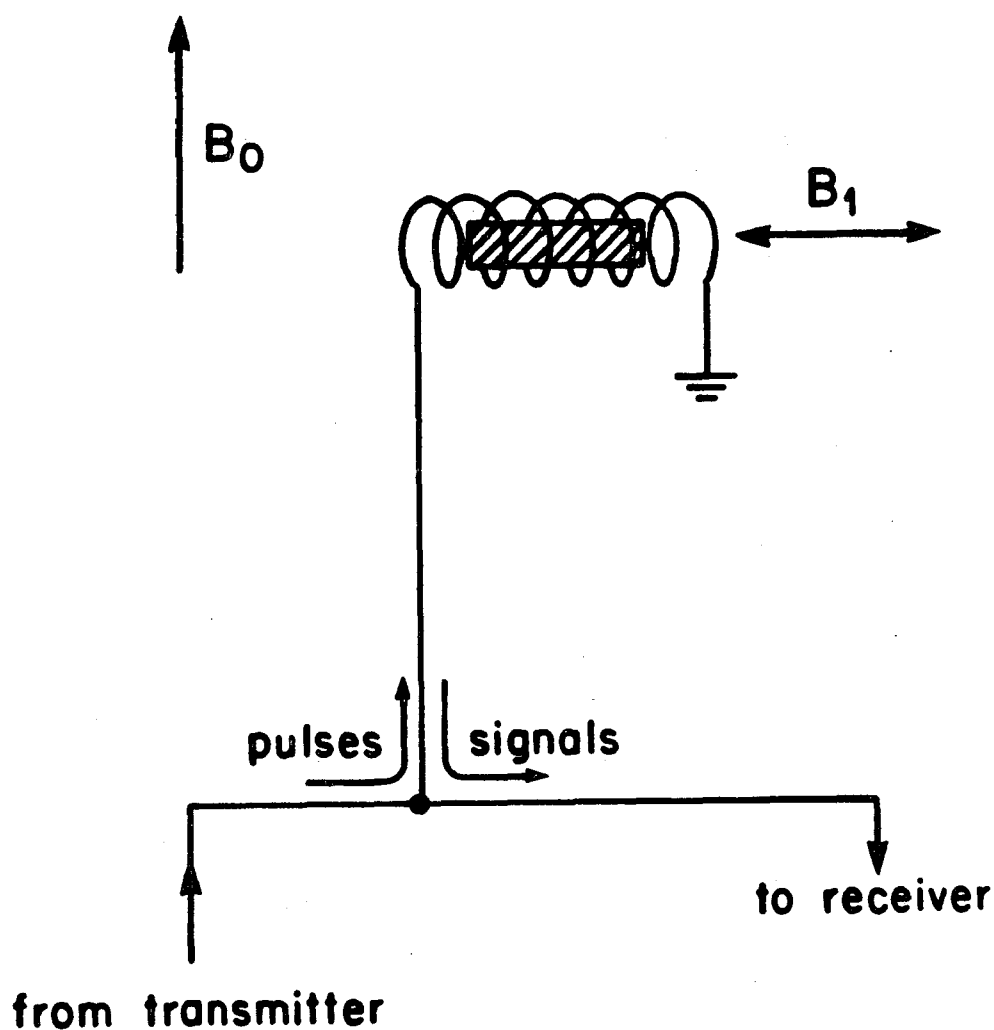


Figure I.1: Experimental set up for pulsed NMR. A sample is placed in the coil of a tuned circuit in a large static magnetic field  $B_0$ . Rf pulses create an oscillating field  $B_1$  perpendicular to the static field. Oscillating rf signals emitted by the sample are detected.



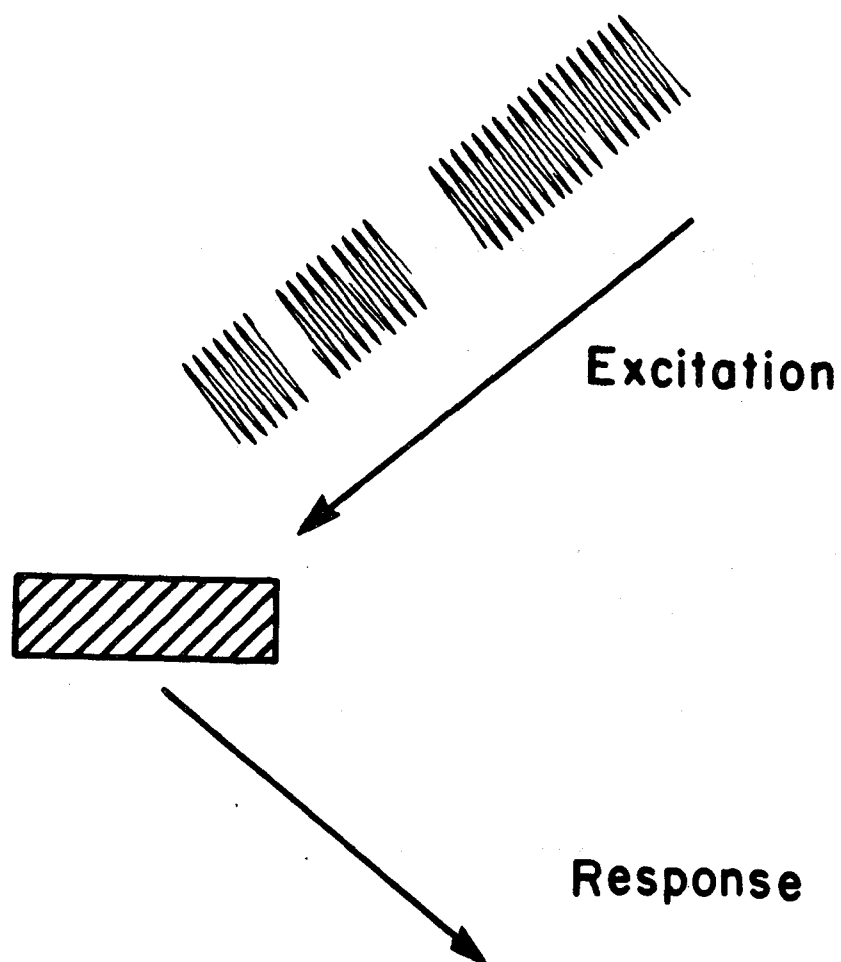


Figure 1.2: An NMR experiment can be viewed as a measurement of the response of a sample to a given excitation. The excitation is typically a sequence of rf pulses with well defined lengths and phases, possibly separated by delays.

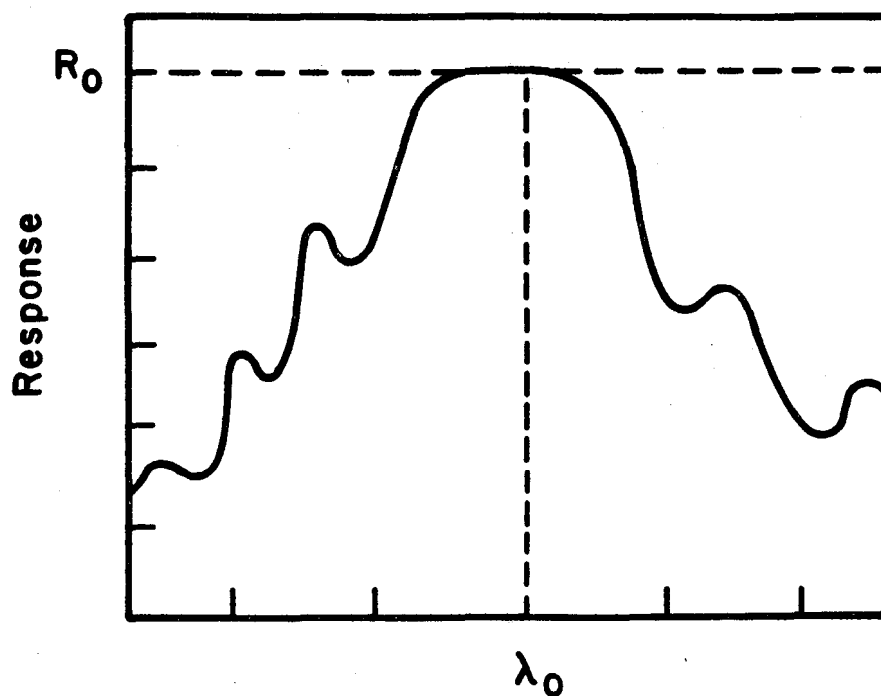


Figure I.3: The measured response is a function of experimental parameters that are properties of the sample or imperfections in the excitation sequence. Sequences are designed so that the desired response  $R_0$  is obtained when the parameter  $\lambda$  has its nominal value  $\lambda_0$ . A broadband excitation sequence produces the response  $R_0$  over a large range of  $\lambda$  around  $\lambda_0$ .

Specifically, there are two responses that are the focus of much of this dissertation. The first is the inversion of spin populations, which corresponds to rotating nuclear magnetization from its equilibrium direction parallel to the static field to the direction antiparallel to the field. The second is the creation of a coherence between spin states that corresponds to rotating the magnetization so that it lies in a plane transverse to the static field. The experimental parameters considered are the difference between the rf frequency and the spins' resonant frequency, called the resonance offset, the rf amplitude, and the strengths of spin couplings.

Certain standard excitation sequences for which  $R(\lambda_0) = R_0$  are used in NMR experiments. These are usually the simplest possible sequences, consisting of a single pulse or a small number of pulses. There are many applications in which the bandwidths of the standard excitation sequences are inadequate, however. Thus, there is a need for pulse sequences that produce the desired response over larger ranges of the experimental parameters. The derivation of such sequences is the problem of broadband excitation in NMR.

The work described in this dissertation was motivated mainly by the intrinsic interest of the problem. The emphasis has been on the development and demonstration of general theoretical methods, rather than on the specific pulse sequences. No particular chemical or physical system has been investigated in detail. However, many uses for broadband excitation exist. These typically take the form of improvements on existing NMR techniques or extensions of the range of applications of those techniques. For example, broadband excitation makes relaxation studies possible in strongly coupled spin systems such

as occur in solids. Various applications for broadband excitation are discussed at the appropriate points in the text.

In addition to the NMR applications, many of the results are directly transferrable to other forms of coherent spectroscopy, i.e. spectroscopy that employs pulses of radiation with a well-defined phase, including pulsed electron spin resonance and coherent optics.

The chapters that follow are intended to be written at a level that is comprehensible to anyone with experience in quantum mechanics. An effort has been made to avoid unnecessary NMR jargon and to provide at least a brief explanation of the jargon when it is necessary. This is meant to be in keeping with the overall presentation of broadband excitation as a problem with intrinsic interest. However, there are sections in which lapses into jargon are unavoidable, particularly in discussions of applications. On the other hand, certain elementary facts may seem to be treated in excessive detail. This has been done where it is felt that a detailed treatment is lacking in textbooks and other dissertations.

The chapters fall into three groups. Chapters II and III are introductory. Chapter II gives the necessary quantum mechanical formalism, including the requisite, but brief list of Hamiltonian terms. The specific broadband excitation problems that are treated in detail are defined, along with the experimental parameters that are considered. Chapter III reviews earlier work in the area of broadband excitation, emphasizing the theoretical approaches used and the need for new approaches.

Chapters IV and V present one approach to broadband excitation, based on a formalism that is widely used in coherent averaging theory in



NMR. The application of the formalism to broadband excitation, including computational methods, is described in Chapter IV; the results, including experimental verifications, are described in Chapter V. Chapter VI shows how certain results from Chapter V can be extended to apparently unrelated broadband excitation problems by means of a formal analogy. The examples of broadband excitation of double-quantum coherence and broadband polarization transfer are treated in detail. Experimental results for broadband double-quantum excitation are given.

The third group of chapters describes a different approach to generating pulse sequences, namely the use of iterative schemes. In Chapter VII, iterative schemes for broadband population inversion are developed and demonstrated. They serve as an example that illustrates a theoretical framework for analyzing iterative schemes in general. That framework depends on treating an iterative scheme as a function on a space of operators. The performance of an iterative scheme is shown to be dictated largely by fixed points of the function. Algebraic and numerical methods for carrying out the fixed point analysis are described. Chapter VIII extends the iterative schemes to the construction of pulse sequences for narrowband population inversion. Finally, Chapter IX contains fixed point analyses of iterative schemes derived by other authors.

Much of the work presented in this dissertation has been published elsewhere, although sometimes in less detail. The publications are listed as references 1 through 9.

## CHAPTER II: Quantum Mechanical Background

### A. The rotating frame

#### 1. Laboratory frame Hamiltonian

The interactions of nuclear spin systems that occur in many NMR experiments can be described by a laboratory frame Hamiltonian of the following general form [10,11]:

$$\mathcal{H}_L = -\omega_0 I_z + 2\omega_1(t) I_x \cos(\omega t + \phi) + \mathcal{H}_{int} \quad (II.1)$$

$\mathcal{H}_L$  has the units of radians per second, or energy divided by  $\hbar$ .

$-\omega_0 I_z$  is the Zeeman interaction of a spin system, with total spin angular momentum vector operator  $\underline{I}$ , with a static magnetic field along z.  $\omega_0$ , the Larmor frequency, is equal to  $\gamma B_0$ , where  $B_0$  is the magnitude of the static field and  $\gamma$  is the gyromagnetic ratio.  $\gamma$  is a characteristic property of each nuclear isotope. Eq. (II.1) assumes that all nuclei are the same isotopes, for example all  $^1\text{H}$  nuclei, so that they share a common  $\gamma$ . In common NMR language,  $\mathcal{H}_L$  is said to be the Hamiltonian for a homonuclear system.

$2\omega_1(t) I_x \cos(\omega t + \phi)$  is the term that describes the interaction with a linearly oscillating rf field perpendicular to the static field.

$\omega_1(t)$  equals  $-\gamma B_1(t)/2$ , where  $B_1(t)$  is the rf magnetic field amplitude.  $\omega$  and  $\phi$  are the frequency and phase of the rf. Typically, the rf field is applied in pulses that are ideally square, so that  $\omega_1(t)$  is

piecewise-constant, taking on the values 0 and  $\omega_1^0$  only.  $\omega_1^0$  will be referred to as the nominal rf amplitude. Also typically,  $\omega$  is constant and  $\phi$  is piecewise-constant.

$\mathcal{H}_{\text{int}}$  stands for all other interactions. These include internal couplings between pairs of spins and between spins and internal fields.

The dominant term in Eq.(II.1) is the interaction with the static field.  $\omega_0/2\pi$  generally ranges from about 10 MHz to about 500 MHz, depending on the isotope and the static field strength.  $\omega_1^0/2\pi$  and all the contributions to  $\mathcal{H}_{\text{int}}$  are usually at least 100 times smaller. Thus, to a good approximation the eigenstates of  $\mathcal{H}_L$  when the rf is turned off are eigenstates of  $I_z$ . They occur in Zeeman manifolds characterized by the eigenvalue  $m$  of  $I_z$  and separated in energy by increments of roughly  $\omega_0$ . When the rf is turned on, it induces a coherent mixing of the eigenstates if  $\omega$  is about equal to  $\omega_0$ .

## 2. Rotating frame transformation

The well-characterized, and therefore uninformative, interaction with the static field can be largely removed, the oscillatory time dependence of the rf can be made to vanish, and the important parts of  $\mathcal{H}_{\text{int}}$  can be made apparent by a transformation to a new frame of reference called the rotating frame [10-12]. Rather than dealing with the rotating frame transformation specifically, it is useful for the development in later chapters to describe the general quantum mechanical procedure for a change of reference frames [13].

A change of reference frames is defined by a unitary transformation  $A(t)$ , which may be time-dependent. If  $|\psi(t)\rangle$  is the state of a system

at time  $t$  in the original frame, the state at time  $t$  in the new frame is  $|\phi(t)\rangle$ :

$$|\phi(t)\rangle = A(t) |\psi(t)\rangle \quad (\text{II.2})$$

Given that  $\mathcal{H}$  is the Hamiltonian in the original frame, the Hamiltonian  $\mathcal{H}'$  in the new frame may be found by the following argument. In their respective frames,  $|\psi(t)\rangle$  and  $|\phi(t)\rangle$  evolve according to the Schrodinger equation:

$$i\frac{d}{dt}|\psi(t)\rangle = \mathcal{H}|\psi(t)\rangle \quad (\text{II.3})$$

$$i\frac{d}{dt}|\phi(t)\rangle = \mathcal{H}'|\phi(t)\rangle \quad (\text{II.4})$$

Substituting Eq.(II.2) into Eq.(II.4):

$$i\left(\frac{dA}{dt}\right)|\psi\rangle + iA\frac{d}{dt}|\psi\rangle = \mathcal{H}'|\phi\rangle \quad (\text{II.5})$$

Using Eq.(II.3):

$$\left[i\left(\frac{dA}{dt}\right) + A\right]|\psi\rangle = \mathcal{H}'|\phi\rangle \quad (\text{II.6})$$

Eq.(II.6) implies that:

$$\mathcal{H}' = i\left(\frac{dA}{dt}\right)A^{-1} + A\mathcal{H}A^{-1} \quad (\text{II.7})$$

This expression for  $\mathcal{H}'$  holds even if  $\mathcal{H}$  is time-dependent.

The specific example of the rotating frame transformation employs

a unitary transformation given by:

$$A(t) = \exp(-i\omega I_z t) \quad (II.8)$$

Applying Eq.(II.7) to Eq.(II.1):

$$\begin{aligned} \mathcal{H}'_L = & \Delta\omega I_z + 2\omega_1(t)(I_x \cos\omega t + I_y \sin\omega t)\cos(\omega t + \phi) \\ & + A\mathcal{H}_{int}A^{-1} \end{aligned} \quad (II.9)$$

where  $\Delta\omega = \omega - \omega_0$  is the resonance offset. The rf interaction in  $\mathcal{H}'_L$  contains terms that oscillate at  $2\omega$  and terms that do not oscillate. Similarly,  $A\mathcal{H}_{int}A^{-1}$  is generally a sum of constant terms and terms that oscillate at multiples of  $\omega$ . Since  $\omega \approx \omega_0$ , and  $\omega_0$  is much larger than  $\omega_1^0$  and much larger than the magnitude of  $\mathcal{H}_{int}$ , it is a good approximation to retain only the non-oscillatory terms in  $\mathcal{H}'_L$ .  $\mathcal{H}'_L$  then becomes  $\mathcal{H}$ , given by:

$$\mathcal{H} = \Delta\omega I_z + \omega_1(t)(I_x \cos\phi + I_y \sin\phi) + \mathcal{H}_{int}^{(0)} \quad (II.10)$$

where  $\mathcal{H}_{int}^{(0)}$  is the constant part of  $A\mathcal{H}_{int}A^{-1}$ . Specifically,  $\mathcal{H}_{int}^{(0)}$  is the part of  $\mathcal{H}_{int}$  that commutes with  $I_z$ .  $\mathcal{H}$  in Eq.(II.10) is usually taken to be the Hamiltonian in the rotating frame.

The step from  $\mathcal{H}'_L$  to  $\mathcal{H}$  can also be accomplished by averaging in time over a single period  $\tau = 2\pi/\omega$ . At multiples of  $\tau$ , the laboratory frame and the rotating frame coincide, since  $A(n\tau) = 1$ . This derivation of an approximate effective Hamiltonian by averaging a time-dependent one is an example of a procedure that will be employed

extensively in Chapters IV and V.

Finally, the replacement of  $\mathcal{H}_{\text{int}}$  by  $\mathcal{H}_{\text{int}}^{(0)}$  may also be justified by perturbation theory, which states that the lowest order effect of the perturbation  $\mathcal{H}_{\text{int}}$  on the unperturbed energies established by  $-\omega_0 I_z$  comes from the part of  $\mathcal{H}_{\text{int}}$  that commutes with  $-\omega_0 I_z$ .

### 3. Observations in the rotating frame

The rotating frame is more than a mathematical trick. Due to the usual design of an NMR spectrometer, experimental observations are actually made in the rotating frame. To show this, it is first necessary to present the quantum statistical mechanical description of spin systems and observables.

A spin system is described by a density operator,  $\rho(t)$ . If the system is in a pure state  $|\psi(t)\rangle$ , the corresponding density operator is:

$$\rho(t) = |\psi(t)\rangle\langle\psi(t)| \quad (\text{II.11})$$

The system may also be, and generally is, in a mixed state, or an incoherent superposition of states. In that case, it can not be described by a single ket, but can be described by the density operator:

$$\rho(t) = \sum_{nm} c_{nm}(t) |n\rangle\langle m| \quad (\text{II.12})$$

where  $\{|n\rangle\}$  is a complete basis of orthonormal states, possibly eigenstates of the Hamiltonian.  $\rho(t)$  is hermitian, so that  $c_{nm} = c_{mn}^*$ .

Any other complete set of operators can be used in place of  $\{|n\rangle\langle m|\}$  as a basis in which to express the density operator.

The evolution of  $\rho(t)$  is governed by the Liouville equation:

$$\frac{d\rho(t)}{dt} = i[\rho(t), \mathcal{H}] \quad (\text{II.13})$$

The formal solution to Eq.(II.13) is:

$$\rho(t) = U(t)\rho(0)U(t)^{-1} \quad (\text{II.14})$$

where the time evolution operator  $U(t)$  may generally be written:

$$U(t) = T \exp(-i \int_0^t \mathcal{H}(t') dt') \quad (\text{II.15})$$

using the Dyson time-ordering operator  $T$ .  $U(t)$  is commonly called the propagator in the NMR literature. The same propagator governs the evolution of pure states:

$$|\psi(t)\rangle = U(t) |\psi(0)\rangle \quad (\text{II.16})$$

Given the density operator, the expectation value  $b$  of an observable, hermitian operator  $B$  can be expressed as a trace:

$$b = \text{Tr}(B\rho) \quad (\text{II.17})$$

The laboratory frame observable in an NMR experiment is typically the  $x$  component of the bulk nuclear magnetization. The corresponding observable operator is proportional to  $I_x$ . Thus, the observed signal

$S(t)$  is:

$$S(t) = \text{Tr}[I_x U_L(t) \rho(0) U_L(t)^{-1}] \quad (\text{II.18})$$

Here  $U_L(t)$  is the propagator in the laboratory frame. Eqs.(II.2) and (II.8) imply that the propagator  $U(t)$  in the rotating frame is related to that in the laboratory frame by:

$$U_L(t) = \exp(i\omega I_z t) U(t) \quad (\text{II.19})$$

Substituting Eq.(II.19) into Eq.(II.18), it can be shown that:

$$\begin{aligned} S(t) = & \text{Tr}[I_x U(t) \rho(0) U(t)^{-1}] \cos \omega t \\ & + \text{Tr}[I_y U(t) \rho(0) U(t)^{-1}] \sin \omega t \end{aligned} \quad (\text{II.20})$$

The coefficient of  $\cos \omega t$  in  $S(t)$  is the expectation value of the x component of spin angular momentum in the rotating frame; the coefficient of  $\sin \omega t$  is the expectation value of the y component.

Experimentally, the signal  $S(t)$  is divided in two and mixed separately with two rf reference signals, one proportional to  $\cos \omega t$  and the other proportional to  $\sin \omega t$ . The two results after mixing are then passed through separate, low-pass audio filters. This process of mixing and filtering has the effect of extracting signals that are proportional to the coefficients of  $\cos \omega t$  and  $\sin \omega t$ . The two extracted signals are stored as the real and imaginary parts of a complex signal  $S_+(t)$ :

$$S_+(t) = \text{Tr}[I_+ U(t) \rho(0) U(t)^{-1}] \quad (\text{II.21})$$



with  $I_{\pm} = I_x \pm iI_y$ . The experimental arrangement is illustrated in Figure II.1.

Thus, experiments are actually performed in the rotating frame, with the two measured signal channels corresponding to the rotating frame x and y components of spin angular momentum. In subsequent discussions, the rotating frame will be assumed unless otherwise stated.

## B. Nuclear spin interactions

### 1. Zeeman interaction

The Zeeman interaction with the static field has already been introduced and has been shown to give rise to the  $\Delta\omega I_z$  term in Eq.(II.10). The offset  $\Delta\omega$  can be the result of a missetting of the rf frequency, or it can be the result of spatial inhomogeneity of the static field. In the latter case,  $\Delta\omega$  is a function of spatial position.

### 2. Rf interaction

The interaction with rf fields has been shown to give rise to the  $\omega_1(t)(I_x \cos\phi + I_y \sin\phi)$  term in Eq.(II.10). As mentioned earlier,  $\omega_1(t)$  has the nominal value  $\omega_1^0$  during a pulse. However,  $\omega_1(t)$  is always inhomogeneous in space, so that the rf interaction can be written:

$$\begin{aligned} \mathcal{H}_{rf} = & \omega_1^0(I_x \cos\phi + I_y \sin\phi) \\ & + \delta\omega_1(I_x \cos\phi + I_y \sin\phi) \end{aligned} \quad (II.22)$$

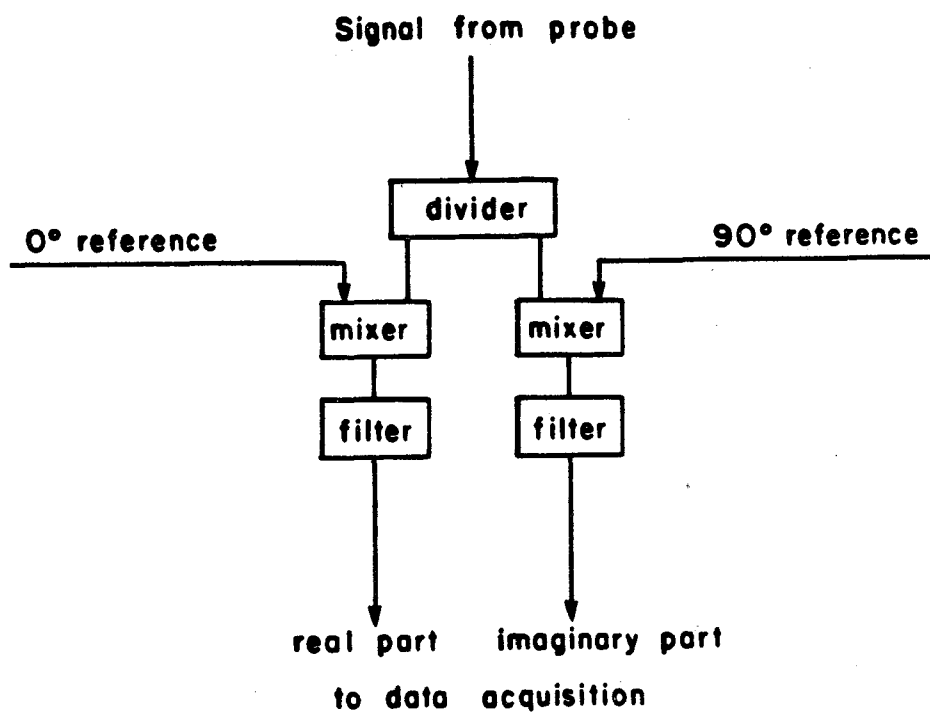


Figure II.1: Typical design of an NMR receiver that allows observations to be made in the rotating frame. Signals near the rf carrier frequency are mixed independently with rf references with a  $90^\circ$  phase difference. The complex audio signal after filtering corresponds to the the x and y magnetization components in the rotating frame.

where  $\delta\omega_1$  is a function of position. The significance of rf inhomogeneity depends on the design of the coil that produces the rf fields and on the relative sizes of the coil and the sample.

### 3. Chemical shifts

The chemical shifts are one contribution to  $\mathcal{H}_{\text{int}}$ , with the form:

$$\mathcal{H}_{\text{CS}} = -\sum_i \delta_i I_{zi} \quad (\text{II.23})$$

The sum in Eq.(II.21) is over individual nuclei. The chemical shift is a shift in the apparent Larmor frequency of a nucleus due to its chemical environment, specifically due to local fields set up by electron currents. The shift is proportional to the static field, so that chemical shifts are measured as fractions of the Larmor frequency, in parts per million (ppm). For hydrogen nuclei (protons) in organic liquids, the chemical shift range is about 10 ppm; for  $^{13}\text{C}$  nuclei, it is about 200 ppm.

The resonance offset term and the chemical shift terms are clearly similar in form. In subsequent discussions, particularly in problems involving isolated spins or systems of spins with identical chemical shifts, the offset and chemical shift terms are combined and referred to collectively as the resonance offset.

#### 4. Dipole couplings

Another contribution to  $\mathcal{H}_{\text{int}}$  is the dipole coupling:

$$\mathcal{H}_d = \sum_{i>j} d_{ij} [I_{zi} I_{zj} - (1/3) I_i \cdot I_j] \quad (\text{II.24})$$

$\mathcal{H}_d$  is the interaction of the magnetic moment of one nucleus with the magnetic field created by the dipole moment of another nucleus. The sum in Eq.(II.24) is over all pairs of nuclei. The coupling constants  $d_{ij}$  are given by:

$$d_{ij} = 3\gamma^2 \frac{(1 - 3\cos^2 \theta_{ij})}{2r_{ij}^3} \quad (\text{II.25})$$

$r_{ij}$  is the distance between nuclei  $i$  and  $j$ ;  $\theta_{ij}$  is the angle between the internuclear vector and the static field direction, i.e. the  $z$  axis. Dipole couplings on the order of 50 kHz are common in proton NMR of organic solids. If there are rapid molecular motions, the right-hand side of Eq.(II.25) is replaced by its time average. "Rapid" means that the motions occur on a time scale that is small compared to  $1/d_{ij}$ . Such motions reduce the effective coupling constants if the motions are anisotropic, as in the rotation of methyl groups in organic solids or the restricted movements of liquid crystals. If the motion is isotropic, as in the tumbling of small molecules in liquids, the coupling constants average to zero.

#### 5. Quadrupole couplings

Quadrupole couplings also contribute to  $\mathcal{H}_{\text{int}}$ . The quadrupole

coupling is an interaction between the quadrupole moment of the nuclear charge distribution and electric field gradients at the nucleus, set up by the electronic charge distribution. It can be put in the form of a nuclear spin interaction through the Wigner-Eckart theorem [10,11,14]. If the field gradients have axial symmetry, the result is:

$$\mathcal{H}_Q = \sum_i \omega_{Qi} [I_{zi}^2 - (1/3)I_i^2] \quad (\text{II.26})$$

$$\omega_{Qi} = \frac{3eQ_i V_{zzi}}{8I(2I-1)} (3\cos^2\theta_i - 1) \quad (\text{II.27})$$

where  $eQ_i$  and  $V_{zzi}$  are respectively the quadrupole moment and the electric field gradient along the unique direction for the  $i^{\text{th}}$  spin.  $\theta_i$  is the angle between the static field direction and the unique field gradient direction. Quadrupole couplings of several hundred kilohertz are common in solid state deuterium NMR.

For a nucleus to have a quadrupole coupling, it must have a total spin quantum number greater than 1/2. For spin-1/2 nuclei,  $[I_{zi}^2 - (1/3)I_i^2]$  is zero. Eq.(II.26) also applies to non-axially symmetric field gradients, but the orientational dependence of  $\omega_{Qi}$  is more complicated.

The remarks about the averaging of the dipole coupling constants by molecular motions apply identically to  $\omega_{Qi}$ . In particular, quadrupole couplings are averaged away in liquids.

$\mathcal{H}_Q$  and  $\mathcal{H}_d$  have an obvious similarity of form. As discussed later, they are both irreducible tensor operators of the type  $T_{20}$ .

## 6. Scalar couplings

The final contribution to  $\mathcal{H}_{\text{int}}$  that plays a role in subsequent discussions is the isotropic J coupling, or scalar coupling:

$$\mathcal{H}_J = \sum_{i>j} J_{ij} \mathbf{I}_i \cdot \mathbf{I}_j \quad (\text{II.28})$$

The scalar coupling is an indirect coupling between two nuclear spins, mediated by electron orbitals that cover both nuclei. The  $J_{ij}$  are generally much smaller than the  $d_{ij}$ , the  $\omega_{Qi}$ , and  $\omega_1^0$ . Scalar couplings between protons in liquid state NMR are usually less than 15 Hz. Couplings between protons and  $^{13}\text{C}$  nuclei are less than 200 Hz. The scalar coupling is thus negligible except over rather long time periods. It has important effects only where mentioned explicitly.

The form in Eq.(II.28) applies when the chemical shift differences of coupled nuclei are smaller than or comparable to  $J_{ij}$ . When  $|\delta_i - \delta_j| \gg |J_{ij}|$ , the following form may be used:

$$\mathcal{H}_J = \sum_{i>j} J_{ij} I_{zi} I_{zj} \quad (\text{II.29})$$

Eq.(II.29) retains only the part of  $\mathcal{H}_J$  that commutes with  $\mathcal{H}_{\text{CS}}$ . The elimination of non-commuting parts can be justified by perturbation theory, or by an averaging argument such as the one that led to the replacement of  $\mathcal{H}_{\text{int}}$  by  $\mathcal{H}_{\text{int}}^{(0)}$  in Eq.(II.10). Systems in which Eq.(II.29) applies are often called "first-order" or "weakly coupled" systems.

## C. Pulse sequence propagators

### 1. General remarks

The effect of an rf pulse sequence on a spin system is given by the propagator, defined most generally in Eq.(II.13). Eq.(II.13) can be viewed in several ways. The exponential operator can be expanded in a series:

$$U(t) = T[1 - i \int_0^t \mathcal{H}(t') dt' - (1/2) (\int_0^t \mathcal{H}(t') dt')^2 + \dots] \quad (\text{II.30})$$

The time-ordering operator performs the following function:

$$T\mathcal{H}(t_1)\mathcal{H}(t_2) = \begin{cases} \mathcal{H}(t_1)\mathcal{H}(t_2), & t_1 > t_2 \\ \mathcal{H}(t_2)\mathcal{H}(t_1), & t_1 < t_2 \end{cases} \quad (\text{II.31})$$

which converts Eq.(II.30) to:

$$U(t) = 1 - i \int_0^t dt_1 \mathcal{H}(t_1) - \int_0^t dt_1 \int_0^{t_1} dt_2 \mathcal{H}(t_1)\mathcal{H}(t_2) + \dots \quad (\text{II.32})$$

Eq.(II.32) is the Dyson series expression for a propagator [15].

If the Hamiltonian is piecewise-constant, equal to  $\mathcal{H}_1, \mathcal{H}_2, \mathcal{H}_3$ , etc. during successive intervals of length  $t_1, t_2, t_3$ , etc., the propagator can be written:

$$U(t) = \exp(-i\mathcal{H}_n t_n) \dots \exp(-i\mathcal{H}_2 t_2) \exp(-i\mathcal{H}_1 t_1) \quad (\text{II.33})$$

$$t = \sum_i t_i \quad (\text{II.34})$$

If the Hamiltonian varies continuously in time, imagine dividing the total time interval  $t$  into many small subintervals during which the Hamiltonian is essentially constant. Then an expression like Eq.(II.33) holds to an increasingly good approximation as the number of subintervals increases. Thus, for a general time-dependent Hamiltonian:

$$U(t) = \lim_{N \rightarrow \infty} \exp[-i\mathcal{H}(t)t/N] \dots \exp[-i\mathcal{H}(2t/N)t/N] \exp[-i\mathcal{H}(t/N)t/N] \quad (\text{II.35})$$

The expression in Eq.(II.15) can be thought of as shorthand for Eq.(II.35).

The rotating frame Hamiltonian during an ideal pulse sequence is piecewise-constant. A pulse sequence composed of  $n$  contiguous pulses may be represented by the notation  $(\theta_1)_{\phi_1} (\theta_2)_{\phi_2} \dots (\theta_n)_{\phi_n}$ , where  $\theta_i = \omega_1^0 \tau_i$ , with  $\tau_i$  and  $\phi_i$  being the length and phase of the  $i^{\text{th}}$  pulse.  $\theta_i$  is frequently called the flip angle of the pulse.

Propagators for Hamiltonians that are not piecewise-constant are considered in detail in Chapter IV.

## 2. Isolated spins and two-level systems

In liquid state NMR, it is generally a good approximation to consider the individual nuclei to be isolated spins during a pulse, since the scalar couplings are very small compared to typical values of  $\omega_1^0$ . In treating the effect of a pulse sequence on a system of uncoupled, isolated spins, it is sufficient to consider



a single spin, with angular momentum operator  $\underline{I}$ . The Hamiltonian during a pulse of length  $\tau$  is:

$$\mathcal{H} = \Delta\omega I_z + \omega_1 I_\phi \quad (11.36)$$

$$I_\phi = I_x \cos\phi + I_y \sin\phi \quad (11.37)$$

The propagator is:

$$U(\tau) = \exp[-i(\Delta\omega/\omega_1^0 I_z + \omega_1/\omega_1^0 I_\phi)\omega_1^0 \tau] \quad (11.38)$$

The propagator is therefore specified by four quantities: a phase  $\phi$ , a flip angle  $\omega_1^0 \tau$ , a relative offset  $\Delta\omega/\omega_1^0$ , and a relative rf amplitude  $\omega_1/\omega_1^0$ .

Any unitary operator of the form:

$$R = \exp(-i\alpha \cdot \underline{I}) \quad (11.39)$$

is a rotation operator in the operator space spanned by  $\{I_x, I_y, I_z\}$ . The length of  $\alpha$  is the net rotation angle and the direction of  $\alpha$  is the rotation axis. The sense of the rotation is established by the relation:

$$\exp(-iI_x\theta)I_y\exp(iI_x\theta) = I_y\cos\theta + I_z\sin\theta \quad (11.40)$$

Eq.(11.40) holds if  $\{x,y,z\}$  is cyclically permuted, as well.

$U(\tau)$  clearly has the form of a rotation operator. The overall propagator for a sequence of contiguous pulses is the product of the propagators for the individual pulses. Since any product of rotations

is equivalent to some single net rotation, the propagator for any pulse sequence is a rotation operator.

The pulse sequence propagator acts on the initial density operator, transforming it to a final density operator. If the initial density operator describes a spin system at equilibrium, it is given by:

$$\rho(0) = \exp(-\mathcal{H}_L/kT)/\text{Tr}[\exp(-\mathcal{H}_L/kT)] \quad (\text{II.41})$$

where  $\mathcal{H}_L$  is the laboratory frame Hamiltonian with no rf fields present. Since the dominant term in  $\mathcal{H}_L$  is the Zeeman term, and since  $\omega_0 \ll kT$  at temperatures above a few degrees K even for proton NMR in the highest fields currently available, it is a good approximation to write:

$$\rho(0) = [1 + \omega_0 I_z/kT]/N \quad (\text{II.42})$$

Here  $N$  is the total number of spin states, or the dimension of the system. This is the high temperature approximation [10,11,16]. The unit operator part of  $\rho(0)$  commutes with all propagators and does not contribute to observed signals. Therefore, it is usually dropped along with the constant of proportionality multiplying  $I_z$ , which only determines the absolute signal amplitude, leaving an initial density operator of  $I_z$ . Rf pulses then rotate the density operator to some linear combination of  $I_x$ ,  $I_y$ , and  $I_z$ . The density operator is therefore always in the form:

$$\rho(t) = \underline{M}(t) \cdot \underline{I} \quad (\text{II.43})$$

where  $\underline{M}$  is a unit magnetization vector, or Bloch vector [17]. It is sometimes useful to picture the effect of a pulse sequence on an isolated spin as the trajectory of  $\underline{M}(t)$  on a unit sphere, as will be seen in Chapter III.

That a pulse sequence propagator is a rotation and that the state of the spin system may be described by a Bloch vector are both consequences of the linear form of the Hamiltonian and of the commutation rules for angular momentum operators. The above discussion therefore applies to isolated spins with any total spin quantum number, not just to spin-1/2 nuclei. However, the state of any quantum mechanical two-level system, of which a spin-1/2 nucleus is an example, can be described by a Bloch vector [18]. Its time development can be described as a series of rotations. This is because the 2X2 matrices corresponding to  $\{1, I_x, I_y, I_z\}$  form a complete basis for all 2X2 matrices. Both the Hamiltonian and the density operator may always be written as linear combinations of  $I_x, I_y$ , and  $I_z$  plus constants, regardless of the physical origin of the system and the Hamiltonian.

### 3. Coupled spins

If dipole or quadrupole couplings exist, the Hamiltonian has terms that are bilinear in the angular momentum operators. The pulse sequence propagator is no longer a rotation, but is a more general unitary

transformation. For a pulse of length  $\tau$ , the propagator is:

$$\begin{aligned}
 U(\tau) = \exp\{ & -i[(\Delta\omega/\omega_1^0)I_z - \sum(\delta_i/\omega_1^0)I_z \\
 & + \sum(\omega_{Qi}/\omega_1^0)(I_z^2 - (1/3)I_i^2) \\
 & + \sum(d_{ij}/\omega_1^0)(I_{zi}I_{zj} - (1/3)I_i \cdot I_j) \\
 & + (\omega_1/\omega_1^0)I_\phi] \omega_1^0 \tau \} \quad (II.44)
 \end{aligned}$$

The propagator is therefore specified by a phase, a flip angle, a relative offset, a relative rf amplitude, and sets of relative chemical shifts, relative quadrupole couplings, and relative dipole couplings.

The initial density operator is still  $I_z$ . There are certain important cases in which the evolution of the density operator can be calculated analytically after reasonable simplifying assumptions. There are other cases in which symmetry in the pulse sequence places restrictions on the evolution. These will be encountered later. In general, however, the evolution can only be calculated numerically. The results depend on the specific network of couplings.

If the density operator is expressed according to Eq.(II.12), with  $\{|n\rangle\}$  being eigenstates of  $I_z$  and of the Hamiltonian, certain names can be assigned to the coefficients  $c_{nm}$  that make up the density matrix. The diagonal element  $c_{nn}$  is the population of the state  $|n\rangle$ . An off-diagonal element  $c_{nn'}$  is a coherence between states  $|n\rangle$  and  $|n'\rangle$ . If:

$$I_z |n\rangle = m_n |n\rangle \quad (II.45)$$

$$I_z |n'\rangle = m_{n'} |n'\rangle \quad (II.46)$$

the coherence is called an  $(m_n - m_{n'})$ -quantum coherence, e.g. a

zero-quantum, single-quantum, double-quantum, or in general a multiple-quantum coherence.

Only single-quantum coherence contributes to observable signal, in particular only single-quantum coherence  $c_{nn}$ , that satisfies:

$$\text{Tr}(I_+ |n\rangle\langle n'|) = 0 \quad (\text{II.47})$$

or:

$$\langle n'| I_+ |n\rangle = 0 \quad (\text{II.48})$$

#### D. Broadband excitation problems

##### 1. Population inversion

The pulse sequence propagator in general depends on dimensionless experimental parameters such as the relative offset, the relative rf amplitude, and the relative couplings. The object of broadband excitation is the development of pulse sequences whose propagators are nearly independent of one or several of those parameters over some large range of values. Two specific types of pulse sequences are of particular interest because of their many applications in NMR. The first is a sequence that inverts spin populations. Spin population inversion is defined by the following property:

$$U(\tau) I_z U(\tau)^{-1} = -I_z \quad (\text{II.49})$$

or:

$$\{U(\tau), I_z\} = 0 \quad (\text{II.50})$$

where the curly brackets indicate an anticommutator. A pulse sequence that inverts populations takes an initial density operator of  $I_z$  to a final density operator of  $-I_z$ . For a more general initial condition, population inversion corresponds to an exchange of the total populations of the  $m^{\text{th}}$  and  $(-m)^{\text{th}}$  Zeeman manifolds, for all  $m$ . To see this, write the initial density operator as:

$$\rho(0) = \sum_m \sum_{m'} \sum_s \sum_{s'} c_{mm's's'}(0) |m,s\rangle \langle m',s'| \quad (\text{II.51})$$

The states  $|m,s\rangle$  are eigenstates of  $I_z$ , with eigenvalue  $m$ , and of  $\mathcal{H}$  without the rf interaction, with eigenvalue  $\omega_s$ . The total population  $p_m(t)$  of the  $m^{\text{th}}$  Zeeman manifold is defined by:

$$p_m(t) = \sum_s c_{mmss}(t) \quad (\text{II.52})$$

Using the fact that:

$$c_{mmss}(\tau) = \text{Tr}[|m,s\rangle \langle m,s| \rho(\tau)] \quad (\text{II.53})$$

the total population of the  $(-m)^{\text{th}}$  Zeeman manifold at the end of the inverting sequence may be written:

$$p_{-m}(\tau) = \sum_{m'} \sum_{m''} \sum_{s'} \sum_{s''} \sum_m c_{m'm''s's''}(0) \text{Tr}[|-m,s\rangle \langle -m,s| U(\tau) |m',s'\rangle \langle m'',s''| U(\tau)^{-1}] \quad (\text{II.54})$$

Because of Eq.(II.50):

$$U(\tau)|ms\rangle = \sum_t a_{mst}|-m,t\rangle \quad (II.55)$$

Then Eq.(II.54) becomes:

$$p_{-m}(\tau) = \sum_{m'} \sum_{m''} \sum_s \sum_{s'} \sum_t \sum_{t'} c_{m'm''s's'}(0) a_{m's't} a_{m''s't'}^* \times \text{Tr}(|-m,s\rangle\langle -m,s| -m',t\rangle\langle -m'',t'|) \quad (II.56)$$

Using the unitarity of  $U(\tau)$  and the fact that:

$$\text{Tr}(|-m,s\rangle\langle -m,s| -m',t\rangle\langle -m'',t'|) = \delta_{m,m'} \delta_{m,m''} \delta_{s,t} \delta_{s,t'} \quad (II.57)$$

$p_{-m}(\tau)$  reduces to:

$$p_{-m}(\tau) = \sum_{s'} c_{mm's's'}(0) \quad (II.58)$$

which is  $p_m(0)$ .

Any  $U(\tau)$  that satisfies Eq.(II.49) can be rewritten as:

$$U(\tau) = \exp(-iI_x \pi) A \quad (II.59)$$

where  $A$  is a unitary operator that commutes with  $I_z$ . This is so because:

$$A = \exp(iI_x \pi) U(\tau) \quad (II.60)$$

and:

$$\exp(iI_x\pi)U(\tau)I_z = \exp(iI_x\pi)U(\tau)I_zU(\tau)^{-1}\exp(-iI_x\pi) \quad (II.61)$$

$$= I_z\exp(iI_x\pi)U(\tau) \quad (II.62)$$

For an isolated spin, the only possibility for the form of a propagator that inverts populations is:

$$U(\tau) = \exp(-iI_x\pi)\exp(2iI_z\phi) \quad (II.63)$$

or equivalently:

$$U(\tau) = \exp(-iI_\phi\pi) \quad (II.64)$$

It is sometimes useful to picture the inversion of an isolated spin as a Bloch vector trajectory from +z to -z on a unit sphere.

The extent of inversion is measured by the quantity W, defined by:

$$W = -\text{Tr}[I_zU(\tau)I_zU(\tau)^{-1}]/\text{Tr}(I_z^2) \quad (II.65)$$

Thus, W is the negative of the expectation value of the final z component of spin angular momentum, normalized to a maximum value of 1. W = 1 corresponds to complete population inversion, while W = -1 corresponds to equilibrium populations. For an isolated spin, -W is the final z component of the Bloch vector.

The standard method for inverting populations in pulsed NMR experiments is to use a single  $\pi$  pulse, i.e. a pulse with a flip angle of  $\pi$ . To illustrate the need for broadband inversion sequences, and to



give a benchmark against which the later sequences can be compared, Figure II.2 shows theoretical plots and experimental data for the extent of inversion by a single pulse as a function of the relative offset and the relative rf amplitude. These results apply to a system of isolated spins. It is clear that the inversion bandwidth is quite limited with respect to both the offset and the rf amplitude. The exact expression for the inversion in this case is:

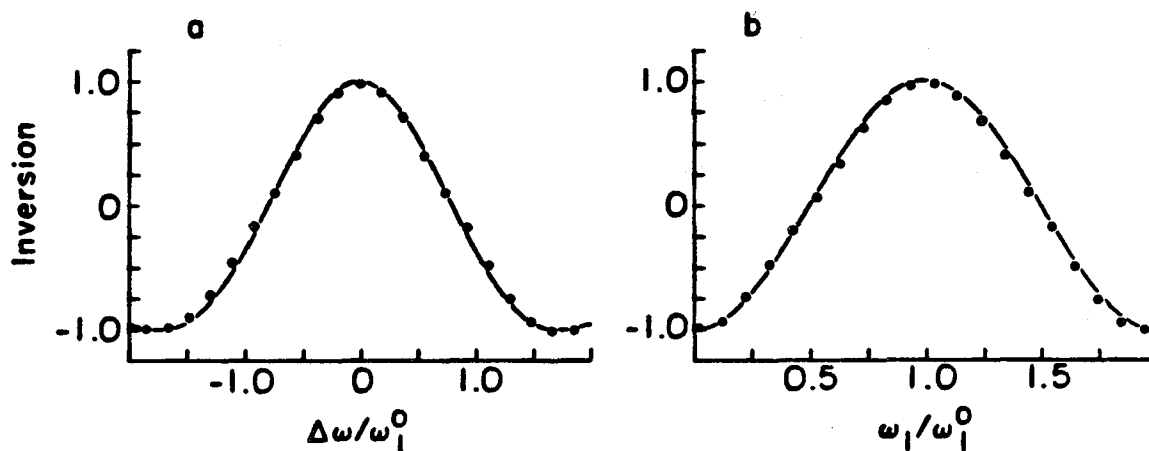
$$W = -(\cos^2 \chi \cos \zeta + \sin^2 \chi) \quad (\text{II.66})$$

$$\chi = \tan^{-1}(\Delta\omega/\omega_1) \quad (\text{II.67})$$

$$\zeta = \pi(\omega_1^2 + \Delta\omega^2)^{1/2}/\omega_1^0 \quad (\text{II.68})$$

Two criteria for defining a broadband inversion sequence may be used. The more liberal one is that the pulse sequence propagator be in the form of Eq.(II.59) over a large range of some experimental parameter, such as the relative offset or rf amplitude, but with  $A$  allowed to be a function of that parameter. For such a pulse sequence, populations will be inverted over a large range of the parameter. An initial density operator of  $I_z$  will be transformed to  $-I_z$ . However, other initial density operators will in general be transformed to a final form that is still a function of the parameter.

A more stringent requirement is that the propagator be strictly constant over a range of the parameter. Then an arbitrary initial condition will be transformed in a constant way. There are certain important applications of broadband inversion sequences in which the more stringent requirement is necessary. These are discussed in Chapter V. It is particularly useful to generate a pulse sequence with a



XBL 846-2382

Figure II.2: The extent of population inversion produced by a single  $\pi$  pulse as a function of the resonance offset  $\Delta\omega$ (a) and the true rf amplitude  $\omega_1$  (b). Simulations (solid lines) and experimental proton NMR measurements (dots) are shown. The experimental measurements were performed on  $\text{H}_2\text{O}_{(l)}$  with a nominal rf amplitude  $\omega_1^0/2\pi = 21.6$  kHz. Broadband inversion sequences (composite  $\pi$  pulses) are designed to have larger inversion bandwidths than those shown here.

constant propagator of the form of Eq.(II.64), even in a coupled spin system.

## 2. Creation of transverse magnetization

The second type of pulse sequence that is of special importance is one that takes  $I_z$  to a linear combination of  $I_x$  and  $I_y$ , i.e.:

$$U(\tau)I_zU(\tau)^{-1} = I_x\sin\phi - I_y\cos\phi \quad (\text{II.69})$$

This corresponds to the creation of transverse magnetization from longitudinal magnetization. For an isolated spin, the sequence yields a Bloch vector trajectory from +z to a point on the equator of a unit sphere. In a coupled spin system, the density operator may evolve into a general linear combination of operators at intermediate times between 0 and  $\tau$ .

A general form for  $U(\tau)$  satisfying Eq.(II.69) is:

$$U(\tau) = \exp(-iI_z\phi)\exp(-iI_x\pi/2)B \quad (\text{II.70})$$

where  $B$  is a unitary operator that commutes with  $I_z$ . That  $B$  commutes with  $I_z$  if  $U(\tau)$  satisfies Eq.(II.69) may be shown as follows:

$$B = \exp(iI_x\pi/2)\exp(iI_z\phi)U(\tau) \quad (\text{II.71})$$

$$BI_z = [\exp(iI_x\pi/2)\exp(iI_z\phi)U(\tau)I_zU(\tau)^{-1}\exp(-iI_z\phi) \\ \times \exp(-iI_x\pi/2)]\exp(iI_x\pi/2)\exp(iI_z\phi)U(\tau) \quad (\text{II.72})$$

$$= I_zB \quad (\text{II.73})$$

For an isolated spin, the only possible form for  $U(\tau)$  is:

$$U(\tau) = \exp(-iI_z\phi_1)\exp(-iI_x\pi/2)\exp(-iI_z\phi_2) \quad (II.74)$$

The extent of the creation of transverse magnetization can be measured by the quantity  $M_{xy}$ , defined by:

$$M_{xy} = (M_x^2 + M_y^2)^{1/2} \quad (II.75)$$

$$M_\alpha = \text{Tr}[I_\alpha U(\tau) I_z U(\tau)^\dagger] / \text{Tr}(I_\alpha^2) \quad (II.76)$$

$M_{xy}$  is proportional to the signal amplitude observed immediately following the pulse sequence. The signal phase  $\phi$  is defined by:

$$\tan\phi = M_y/M_x \quad (II.77)$$

If the pulse sequence propagator is in the form of Eq.(II.70) over a large range of some experimental parameter,  $M_{xy}$  will be constant and equal to 1.  $\phi$  may still vary, reflecting variations in  $\phi$  in Eq.(II.70).

The standard way to create transverse magnetization in NMR is with a single  $\pi/2$  pulse, i.e. a pulse with a flip angle of  $\pi/2$ . Figure II.3 shows plots of the signal amplitude and phase following a  $\pi/2$  pulse, with an rf phase of zero, as a function of the relative offset. Figure II.4 shows the signal amplitude as a function of the relative rf amplitude; the phase is constant. Again, these results apply to isolated spins. The exact expressions are:

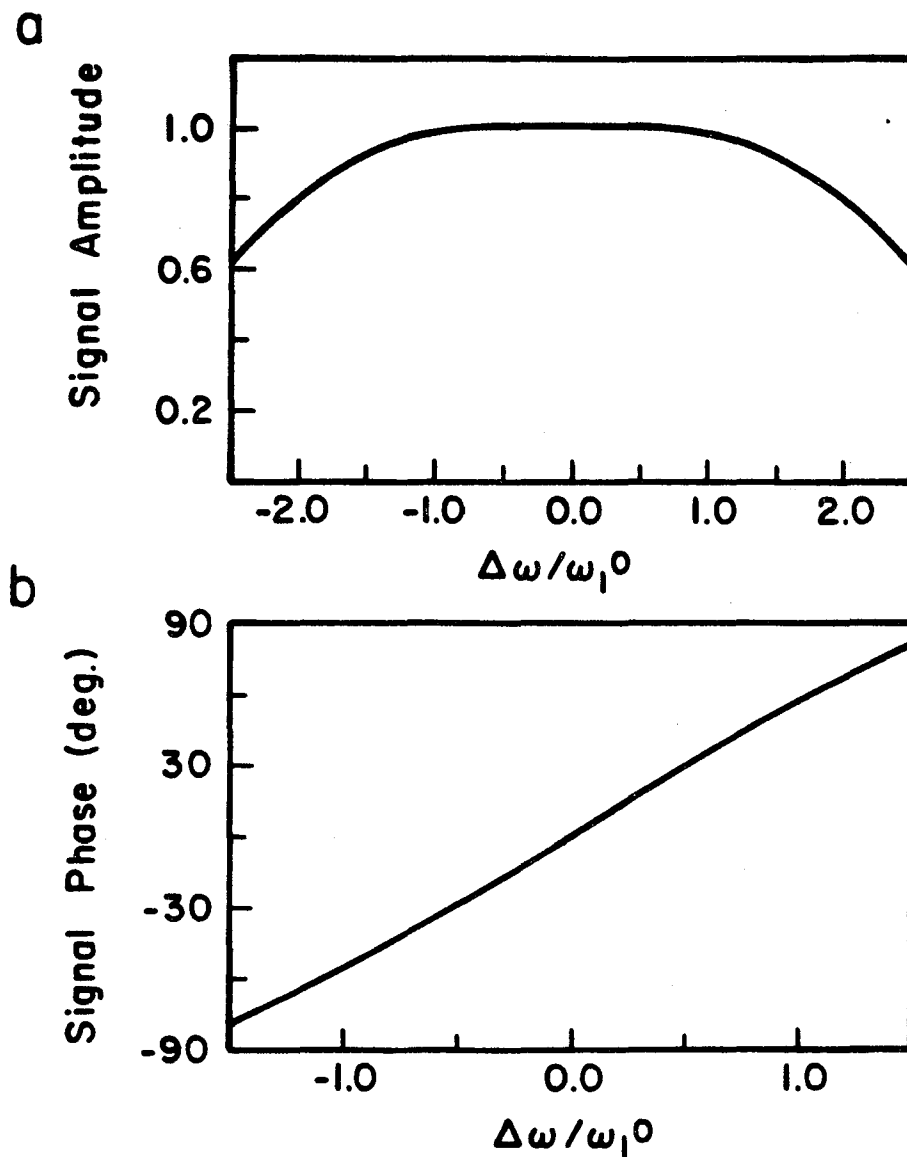


Figure II.3: Simulations of the NMR signal amplitude and phase following excitation by a single  $\pi/2$  pulse as a function of the relative resonance offset. The signal amplitude bandwidth is large, but the signal phase is a strong, approximately linear, function of the offset. Composite  $\pi/2$  pulses may be designed to give a constant signal phase over a larger bandwidth.

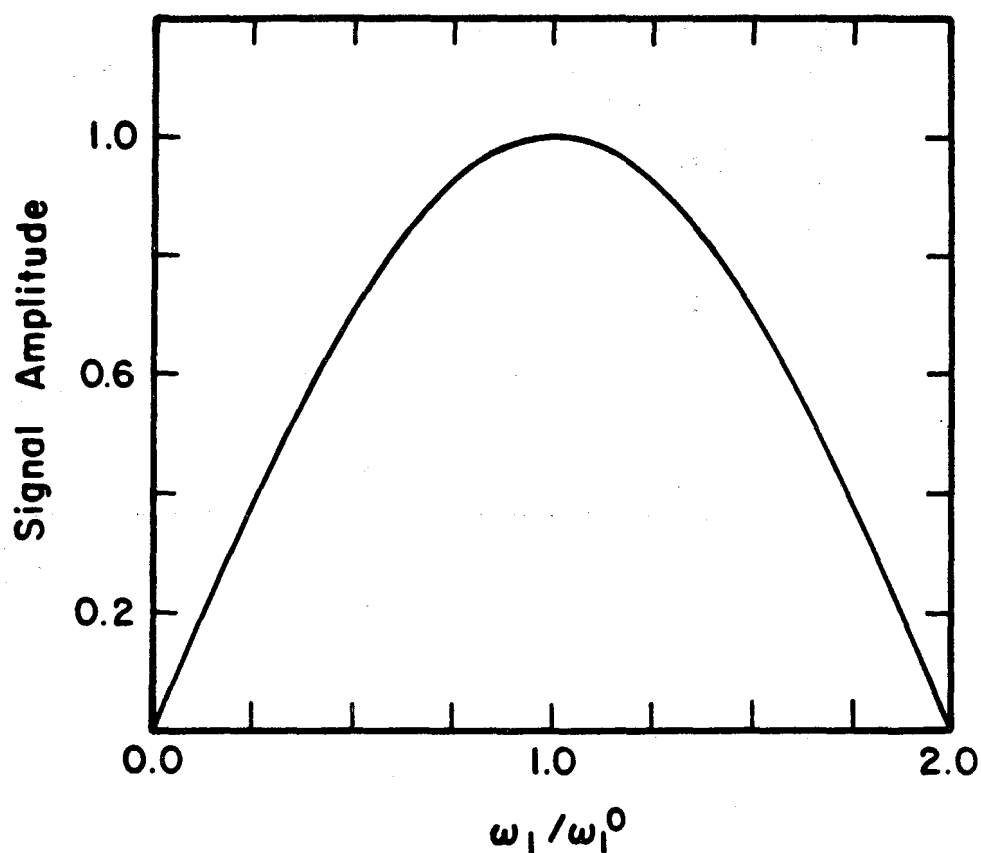


Figure II.4: Simulation of the NMR signal amplitude following excitation by a single  $\pi/2$  pulse as a function of the relative rf amplitude. Composite  $\pi/2$  pulses may be designed to produce uniform excitation over a larger range of rf amplitudes.

$$M_{xy} = \cos\chi[\sin^2\chi(1-\cos\zeta)^2 + \sin^2\zeta]^{1/2} \quad (II.78)$$

$$\tan\phi = \sin\zeta/[\sin\chi(\cos\zeta - 1)] \quad (II.79)$$

where  $\chi$  and  $\zeta$  are defined in Eqs.(II.67) and (II.68). Figure II.3 indicates that  $M_{xy}$  is fairly constant over a large range of offsets, but  $\phi$  varies approximately linearly with offset. Figure II.4 indicates that  $M_{xy}$  is not constant as a function of the rf amplitude.

Again, two criteria may be used to define broadband creation of transverse magnetization. If the propagator is only required to be in the form of Eq.(II.70),  $M_{xy}$  will be constant but  $\phi$  may vary. A general initial density operator will not be transformed in a constant way. In certain applications, it is important that  $U(\tau)$  be strictly constant. In particular, it is useful for  $U(\tau)$  to be a constant rotation, in the form of Eq.(II.74).

Finally, rotations of the form of Eq.(II.74) perform many other functions in addition to the creation of transverse magnetization. Some of these are discussed in later chapters.

## Chapter III: Previous Work in Broadband Excitation

### A. Adiabatic inversion

An early method for broadband population inversion is the adiabatic rapid passage [10,17]. In this technique, a long, continuous rf pulse is given and either the rf frequency or the static field strength is swept so that the resonance offset goes from a large positive value to a large negative value, or vice versa, for all spins. If the sweep is accomplished in a time that is short compared to spin relaxation times, and long compared to  $1/\omega_1^0$ , then populations are inverted to a high degree of accuracy in isolated spin systems.

The performance of an adiabatic sweep can be explained generally in terms of the Adiabatic Theorem of quantum mechanics [13]. In this specific case, however, a simple argument leads to a more detailed understanding. Consider the rotating frame Hamiltonian during a linear field sweep:

$$\mathcal{H} = \Delta\omega(t)I_z + \omega_1 I_x \quad (\text{III.1})$$

$$\Delta\omega(t) = -kt, \quad -t_0 \leq t \leq t_0 \quad (\text{III.2})$$

$\Delta\omega(t)$  and  $\omega_1$  are the z and x components of an effective field  $\omega_{\text{eff}}$ , with a time-dependent magnitude and direction.  $k$  is the sweep rate. In a new reference frame related to the rotating frame by the transformation  $T(t)$ :



$$T(t) = \exp[iI_y\theta(t)] \quad (\text{III.3})$$

$$\theta(t) = \pi/2 - \tan^{-1}[\Delta\omega(t)/\omega_1] \quad (\text{III.4})$$

the Hamiltonian is:

$$\mathcal{H}_T = \omega_{\text{eff}} I_z - \left(\frac{d\theta}{dt}\right) I_y \quad (\text{III.5})$$

If  $\omega_{\text{eff}} \gg \frac{d\theta}{dt}$  at all times during the sweep, in the new frame it appears as if the field is always nearly aligned with the z axis. This is the condition that the sweep be slow, placing an upper limit on k. If  $\theta(-t_0) \approx 0$ , the initial density operator in the new frame is approximately  $I_z$ . This is the condition that the sweep start far above resonance. If  $\mathcal{H}_T$  is always nearly proportional to  $I_z$ , the density matrix remains approximately equal to  $I_z$  in the new frame throughout the sweep. At the end of the sweep, the rotating frame is related to the new frame by  $T(t_0)^{-1}$ . If  $\theta(t_0) \approx \pi$ , then the final density operator in the rotating frame is approximately  $-I_z$ . This is the condition that the sweep end far below resonance. The degree of accuracy of the inversion is determined by the extent to which the various conditions are satisfied. It is generally sufficient to have  $\omega_{\text{eff}} > 5\left(\frac{d\theta}{dt}\right)$ ,  $\theta(-t_0) < 0.1$ , and  $\theta(t_0) > \pi - 0.1$ . Such a sweep requires a total time  $2t_0 > 2\pi \times 100/\omega_1$ .

Broadband inversion with respect to the resonant frequency is possible since, for a linear sweep, the condition  $\omega_{\text{eff}} \gg \frac{d\theta}{dt}$  is satisfied for all resonant frequencies once it is satisfied for any particular frequency. To invert spins over a large range of resonant frequencies, it is only necessary to begin the sweep far above the

highest resonant frequency and end it far below the lowest resonant frequency. Calculated plots of inversion as a function of the resonance "offset", i.e. the displacement from the central frequency of the sweep, are shown in Figure III.1 for sweeps of various lengths.

Broadband inversion with respect to the rf amplitude is possible since the condition  $\omega_{\text{eff}} \gg \frac{d\theta}{dt}$  is satisfied for all values of  $\omega_1$  greater than  $\omega_1^0$  once it is satisfied for  $\omega_1^0$ . Eventually,  $\omega_1$  may become so large that  $\theta$  is no longer nearly 0 and  $\pi$  at  $-t_0$  and  $t_0$ , respectively. This places the upper limit on the inversion bandwidth in  $\omega_1$ , but that upper limit can be made as large as desired by using a large  $t_0$ . Simulations of inversion as a function of the rf amplitude for sweeps of various lengths are shown in Figure III.2.

Thus, the inversion bandwidths with respect to the resonant frequency and the rf amplitude are ultimately limited only by the total time allowed for the sweep. The time is in turn limited by spin relaxation and by spin couplings, in other words by the time scale on which it is a good approximation to consider spins as being isolated.

## B. Composite pulses

The use of a sequence of single-frequency, phase-shifted pulses to perform the functions of a single  $\pi$  or  $\pi/2$  pulse, but over a larger bandwidth, was first suggested and demonstrated by Levitt and Freeman [19-28]. Those authors introduced the name "composite pulse" to describe such a sequence. A composite pulse offers several advantages over an adiabatic sweep. First, an adiabatic sweep does not apply to the creation of transverse magnetization over a range of resonant

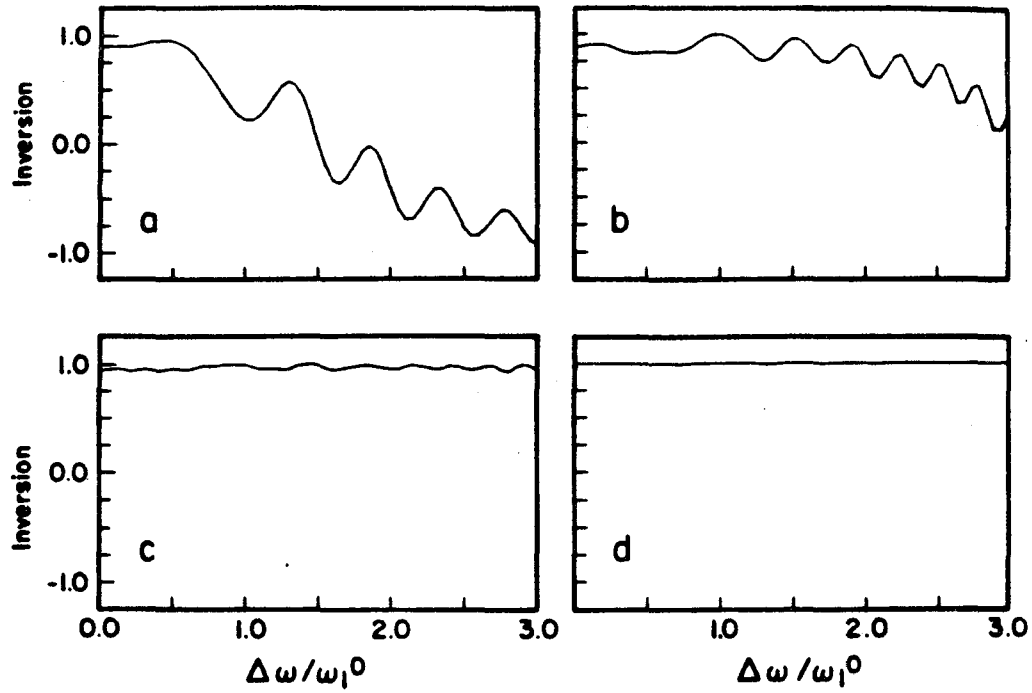


Figure III.1: Simulations of inversion as a function of the relative offset for linear frequency sweeps with a sweep rate  $k/(\omega_1^0)^2 = 0.2$ . The overall lengths of the sweeps are  $2\omega_1^0 t_0 = 15.82$  (a), 31.46 (b), 62.86 (c), 200.0 (d). The offset is the difference between the resonant frequency and the central frequency of the sweep.

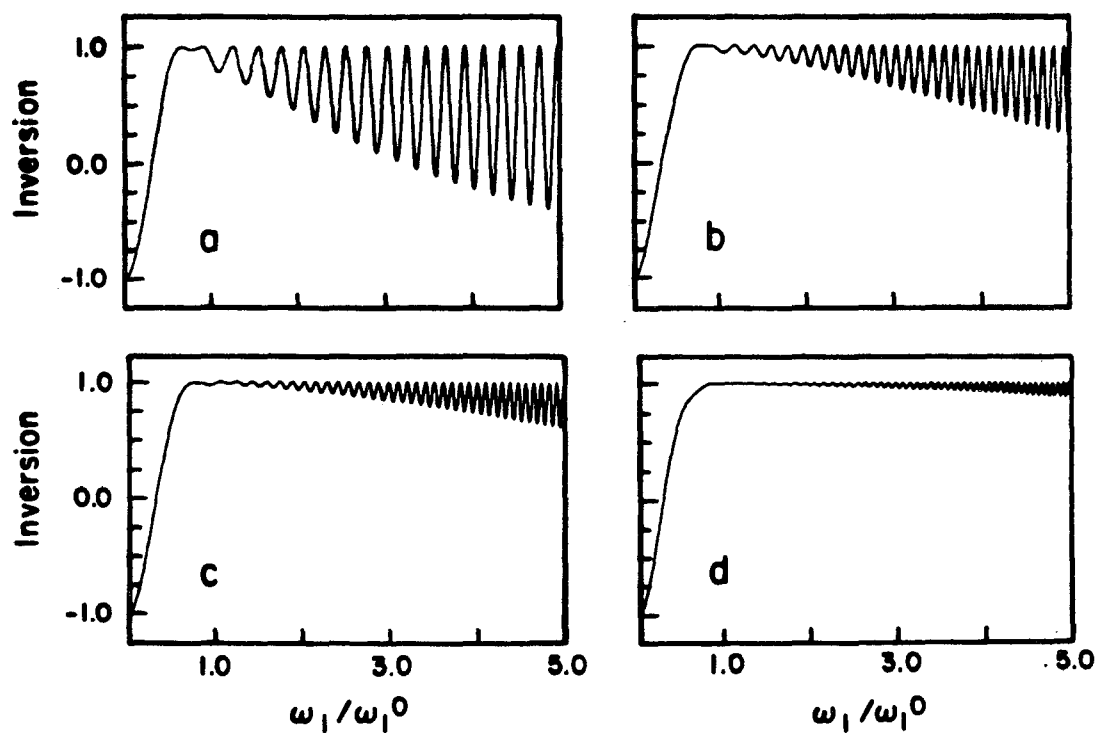


Figure III.2: Simulations of inversion as a function of the relative rf amplitude for linear frequency sweeps with a sweep rate  $k/(\omega_1^0)^2 = 0.2$ . The overall lengths of the sweeps are  $2\omega_1^0 t_0 = 31.46$  (a), 62.86 (b), 100.0 (c), 200.0 (d).

frequencies, while composite pulses that invert populations and that create transverse magnetization may be derived. Second, fairly large bandwidths are accessible with composite pulses that are more than ten times shorter in time than an adiabatic sweep. Third, composite pulses that have large bandwidths with respect to spin couplings may be derived, while an adiabatic sweep is generally not effective in a coupled spin system. Fourth, composite pulses that have constant net propagators may be derived, with important consequences that will be discussed later. Finally, composite pulses are easily given experimentally on modern pulsed NMR spectrometers, while the capability to perform field or frequency sweeps usually does not exist.

The original derivation of composite pulses by Levitt and Freeman [19] and by Freeman, Kemsell, and Levitt [20] relied on Bloch vector pictures and computer simulations. Bloch vector trajectories were examined as a function of  $\Delta\omega/\omega_1^0$  or  $\omega_1/\omega_1^0$ . The phases and flip angles of pulses were chosen so that the deviation from the ideal trajectory, i.e. the trajectory with  $\Delta\omega = 0$  and  $\omega_1 = \omega_1^0$ , in one pulse was compensated by the deviations in other pulses. Important examples are the composite  $\pi$  pulses of the form  $90_0^\theta 90_0$ . Regardless of  $\theta$ , a  $90_0^\theta 90_0$  sequence inverts spins when  $\Delta\omega = 0$  and  $\omega_1 = \omega_1^0$ . When  $\theta = 0$ , the sequence reduces to a single  $\pi$  pulse. By choosing  $\theta \neq 0$ , it is possible to extend the inversion bandwidths in  $\omega_1$  and  $\Delta\omega$ . Intuitively, this can be understood by an argument based on a Bloch vector. Consider the case where  $\omega_1 < \omega_1^0$ . The first  $90_0$  pulse takes the Bloch vector from  $+z$  to a point in the  $yz$  plane short of the  $y$  axis. If a perfect  $180^\circ$  rotation could be given about the  $y$  axis, the Bloch vector would move to a point in the  $yz$  plane related to the previous point by a reflection in the  $xy$  plane.

Then the final  $90_0$  pulse would take the Bloch vector to  $-z$ , completing the inversion. Of course, if a range of  $\omega_1$  values is present, it is impossible to give a perfect  $180^\circ$  rotation for the entire sample. However, it is at least conceivable that  $90_0 180_{90} 90_0$  may have a larger bandwidth than  $180_0$ . For variations in  $\Delta\omega$ , the argument is not as simple, since variations in  $\Delta\omega$  affect the direction of the rotation axis for a pulse as well as the rotation angle. However, simulations of the trajectories and of the resulting inversion as a function of  $\Delta\omega$  show that  $90_0 240_{90} 90_0$  has a large inversion bandwidth, covering offsets of  $\Delta\omega < 0.5\omega_1^0$ . Simulations of the inversion as a function of  $\Delta\omega$  and  $\omega_1$  for various  $90_0 \theta_{90} 90_0$  sequences are shown in Figure III.3.

Later derivations of composite pulses by Levitt and Freeman [21] employed a more mathematical analysis, treating pulse sequences as products of rotation operators. The propagator  $U$  for  $90_0 180_{90} 90_0$  as a function of the rf amplitude is as follows:

$$U = \exp[-iI_x(\pi/2 + \epsilon)] \exp[-iI_y(\pi + 2\epsilon)] \exp[-iI_x(\pi/2 + \epsilon)] \quad (\text{III.6})$$

$$\epsilon = \pi(\omega_1 - \omega_1^0)/2\omega_1^0 \quad (\text{III.7})$$

To first order in  $\epsilon$ :

$$U = \exp(-iI_x\pi/2) \exp(-iI_y\pi) \exp(-iI_x\pi/2) \exp(2iI_z\epsilon) \quad (\text{III.8})$$

$$= \exp(-iI_x\pi) \exp[iI_z(\pi + 2\epsilon)] \quad (\text{III.9})$$

Eq.(III.9) has the form of Eq.(II.63)

Similarly, the propagator for  $90_0 270_{90} 90_0$  as a function of  $\Delta\omega$

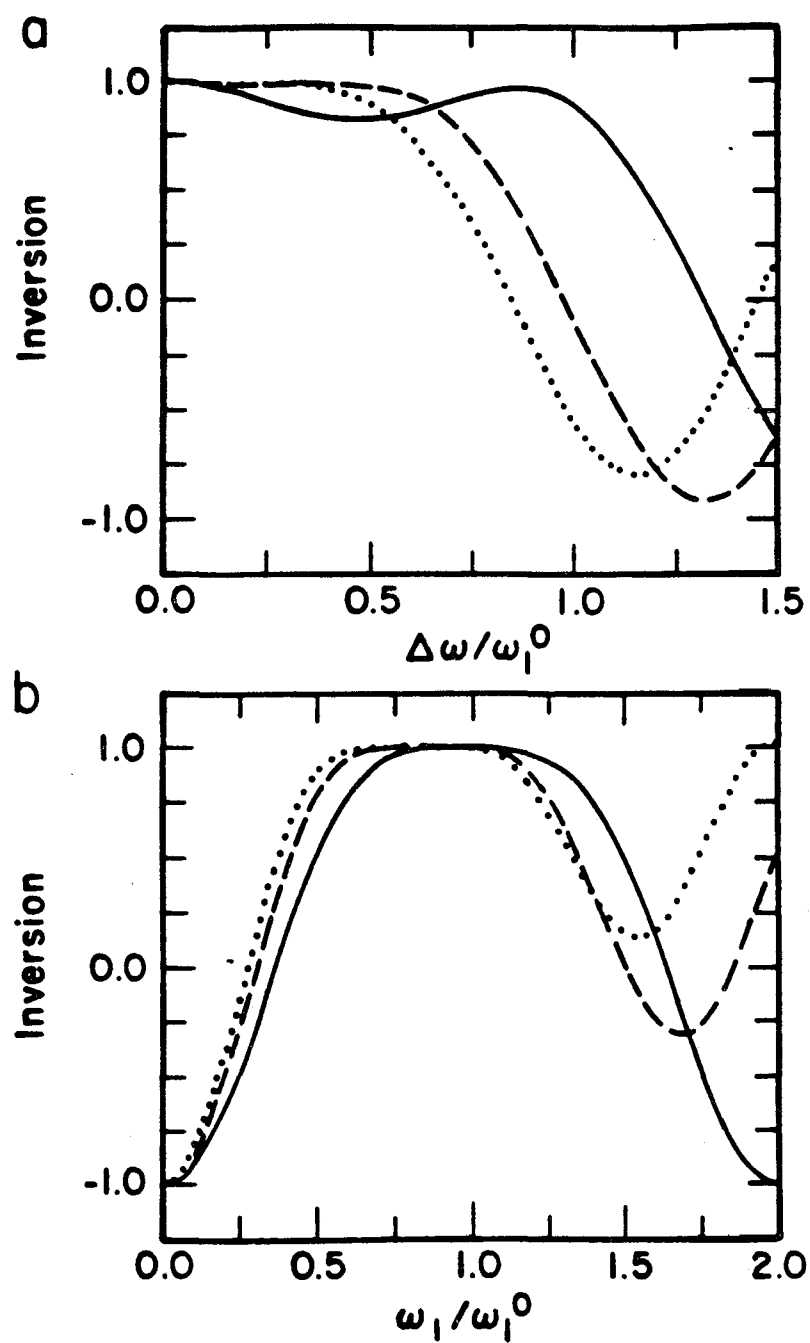


Figure III.3: Simulations of the extent of population inversion as a function of resonance offset (a) and rf amplitude (b) for the composite  $\pi$  pulses  $90_0 180_{90} 90_0$  (solid lines),  $90_0 240_{90} 90_0$  (dashed lines), and  $90_0 270_{90} 90_0$  (dotted lines).

can be written:

$$U = \exp(iI_y\chi)\exp(-iI_x\zeta/2)\exp(-iI_y\chi)\exp(-iI_x\chi) \\ \times \exp(-3iI_y\zeta/2)\exp(iI_x\chi)\exp(iI_y\chi)\exp(-iI_x\zeta/2)\exp(-iI_y\chi) \quad (\text{III.10})$$

with  $\chi$  and  $\zeta$  defined in Eqs.(II.67) and (II.68), with  $\omega_1 = \omega_1^0$ .

To first order in  $\Delta\omega/\omega_1^0$ :

$$U = \exp(-iI_x\pi/2)\exp(-3iI_y\pi/2)\exp(-iI_x\pi/2) \quad (\text{III.11})$$

$$= \exp(-iI_x\pi)\exp(3iI_z\pi/2) \quad (\text{III.12})$$

Eq.(III.12) has the form of Eq.(II.63). In addition, the propagator for  $90_0 270_{90} 90_0$  is independent of  $\Delta\omega$  to first order in  $\Delta\omega/\omega_1^0$ , i.e. it is a constant net rotation.

Further work by Levitt [22,23] involved evaluating the final density matrix as a function of  $\omega_1$  or  $\Delta\omega$  in a Taylor series expansion about the value at  $\omega_1 = \omega_1^0$  and  $\Delta\omega = 0$ . Simple geometric conditions were derived under which the first-order correction term in the expansion could be made to vanish. For example, for the case of variations in  $\omega_1$ , it can be shown that the first-order term vanishes for a two-pulse sequence if the ideal Bloch vector trajectories during the two pulses have the same arc length and are antitangential. One sequence that satisfies those conditions is  $90_0 180_{120}$ , assuming an initial Bloch vector aligned with the z axis.  $90_0 180_{120}$  takes Bloch vectors from +z to points in the xy plane to a good approximation over the range  $0.8\omega_1^0 < \omega_1 < 1.2\omega_1^0$ . From there, the sequence  $180_{120} 90_0$  takes the vectors from



the xy plane to -z, along trajectories that are approximately related to the trajectories during  $90_0 180_{120}$  by reflection in the xy plane. For  $\omega_1 = \omega_1^0$ , the reflection symmetry is exact. Thus,  $90_0 360_{120} 90_0$  is suggested as a composite  $\pi$  pulse that covers a range of rf amplitudes.

On the whole, the composite pulse work of Levitt, Freeman, et al. is of great practical importance. They have suggested simple sequences that significantly improve upon the bandwidths of single pulses. Additionally, they have demonstrated the usefulness of composite pulses in spin-lattice relaxation time measurements [19,20], Carr-Purcell multiple spin echo experiments [21], two-dimensional NMR experiments [28], and heteronuclear decoupling experiments [24,25,29-32].

Certain limitations of the theoretical approaches described above provided the motivation for developing new approaches to the derivation of composite pulses, as described in this dissertation. First, the reliance on Bloch vector pictures and computer simulations and the treatment of pulse sequence propagators as products of rotations limits the development of composite pulses to isolated spin problems. In coupled spin systems, the vector pictures do not apply. It is not possible to perform definitive computer simulations that apply to all coupled systems. The pulse sequence propagators are more complicated, without corresponding simple geometric pictures. Second, while it appears reasonable to expect that the bandwidths of composite pulses may improve as the number of individual pulses increases, the original methods of Levitt and Freeman do not provide a systematic method for deriving successively longer sequences with increasing bandwidths. An attempt to go beyond first-order arguments is cumbersome and not particularly successful [23], leading ultimately to a reliance on

computer simulations and optimizations. Third, composite pulses are derived from the standpoint of a particular initial spin density operator, namely  $I_z$ . The result is pulse sequences that are not strictly constant over any bandwidth, except in the fortuitous example of the  $90_0 270_{90} 90_0$  sequence. Finally, no methods are proposed for generating sequences for broadband excitation with respect to more than one experimental parameter at a time.

In the following chapters, theoretical methods for deriving composite pulses that overcome the above limitations are presented. In addition, further developments by other authors that have been made concurrently with the work described in the following chapters are discussed where appropriate.

### C. Broadband population inversion by phase-modulated pulses

Before moving on to the main body of the dissertation, an approach to broadband population inversion in systems of isolated spins that bridges between composite pulses and adiabatic inversion will be discussed briefly. The central idea is that, as the number of phase-shifted pulses in a composite pulse increases, the composite pulse may begin to resemble a single rf pulse with a continuously modulated phase. Conversely, if a continuously modulated pulse with broadband inversion properties is known, it may be possible to generate composite pulses by approximating the continuously varying phase function by a piecewise-constant function.

Pines has suggested using a particular pulse first proposed by Allen and Eberly [33], which can be written in the form:

$$\omega_1(t) = (\omega_1^0/\sin\gamma)\text{sech}(\omega_1^0 t) \quad (\text{III.13})$$

$$\dot{\phi}(t) = -\omega_1^0 \cot\gamma \tanh(\omega_1^0 t) \quad (\text{III.14})$$

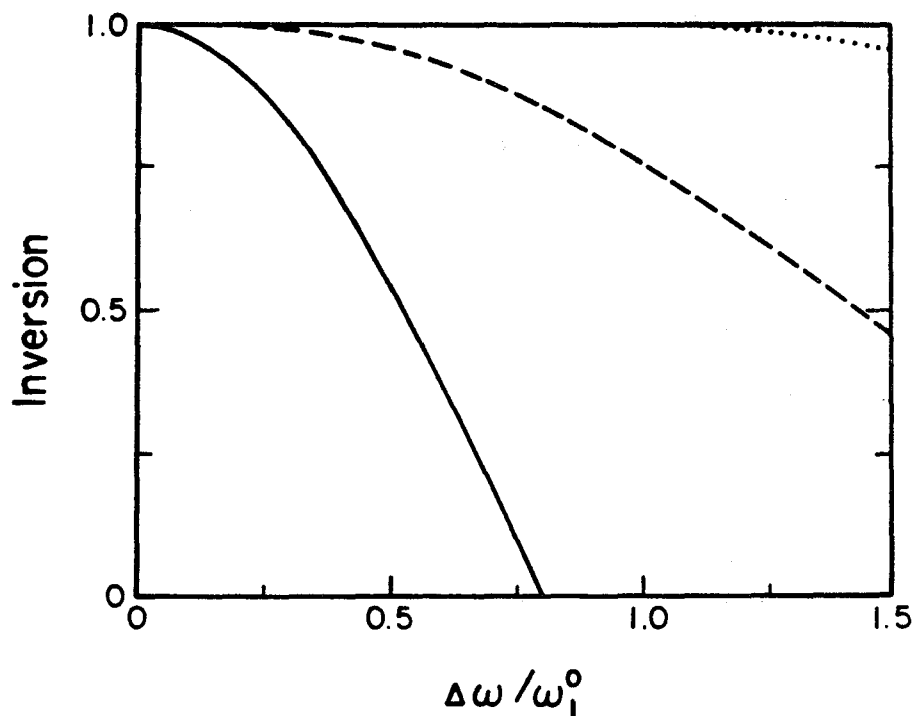
where  $\dot{\phi}(t)$  is the time derivative of the rf phase. Work by Baum, Tycko, and Pines [7,8] shows that this pulse inverts spins on resonance for any value of  $\gamma$ , and that the inversion bandwidths in both  $\omega_1$  and  $\Delta\omega$  become as large as desired as  $\gamma$  approaches 0. The same behavior holds for an equivalent pulse with a constant amplitude, defined by:

$$\omega_1(t) = \omega_1^0, \quad -\pi/(2\omega_1^0 \sin\gamma) < t < \pi/(2\omega_1^0 \sin\gamma) \quad (\text{III.15})$$

$$\dot{\phi}(t) = -\omega_1^0 \cos\gamma \tan(\omega_1^0 \sin\gamma) t \quad (\text{III.16})$$

The pulse of Eqs.(III.15) and (III.16) is equivalent to that of Eqs.(III.13) and (III.14) in the sense that the inverting trajectory for a Bloch vector with  $\Delta\omega = 0$  is the same for the two pulses. Inversion plots as a function of the resonance offset for pulses of the form of Eqs.(III.15) and (III.16) are shown in Figure III.4.

Composite pulses may be derived from the continuously modulated pulse by considering the on-resonance inverting trajectory. If  $N$  points are chosen along the trajectory, with the first point at  $+z$  and the last point at  $-z$ , a sequence of  $N-1$  pulses can be found such that it causes an on-resonance Bloch vector to move between successive points. As  $N$  becomes larger, the pulse sequence derived by this "connect the dots" method approximates the continuously modulated pulse. This approach to generating composite pulses is particularly well suited for generating long sequences with very large bandwidths, although short sequences

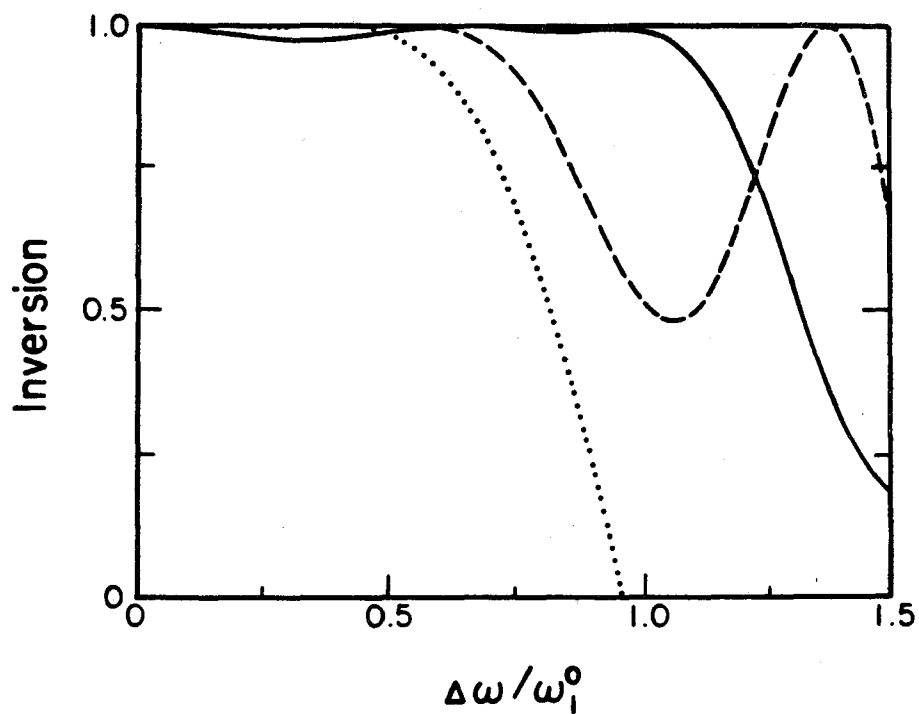


XB. 835-956+

Figure III.4: Simulations of population inversion as a function of offset for phase modulated pulses of the form in Eqs.(III.15) and (III.16), with  $\gamma = \pi/2$  (solid line), 0.245 (dashed line), and 0.111 (dotted line).  $\gamma = \pi/2$  corresponds to a single  $\pi$  pulse.

resembling those of Figure III.2 can also be derived. Inversion results for some derived composite pulse sequences are shown in Figure III.5.

A continuously modulated pulse such as that of Eqs.(III.15) and (III.16) becomes an adiabatic frequency sweep for small  $\gamma$ . This is because phase modulation and frequency modulation are equivalent: the time derivative of the phase is indistinguishable from a frequency shift. Eq.(III.16) may therefore be interpreted as a frequency sweep from far above resonance to far below resonance. As  $\gamma$  becomes smaller, the maximum sweep rate becomes smaller and the sweep becomes adiabatic. Note, however, that the sweep is not linear, i.e. the sweep rate is not constant. Far from resonance, the sweep is very rapid. This is permitted as long as the condition  $\omega_{\text{eff}} \gg \frac{d\theta}{dt}$  is satisfied, as discussed in section A. In fact, the varying sweep rate allows the adiabatic inversion to be accomplished in less time than the standard, linear sweep. Thus, the phase-modulated pulse considered here is an example of an efficient adiabatic sweep when  $\gamma$  is small, and inverts spins on resonance regardless of  $\gamma$ . Further details of this work are given in references 7 and 8.



XBL 835-9570

Figure III.5: Simulations of population inversion as a function of offset for composite  $\pi$  pulses derived from continuously phase modulated pulses. Shown are  $84_{94}^{251}0_{94}$  (dotted line),  $64_{322}^{122}96_{310}^{122}96_{64}^{322}$  (dashed line), and  $39_{419}^{54}209_{66}^{139}84_{70}^{267}0_{84}^{70}66_{139}^{54}209_{39}^{419}$  (solid line).

## Chapter IV: Coherent Averaging Approach to Broadband Excitation: Formalism and Computational Methods

### A. Motivation

As explained in Chapter II, the problem of broadband excitation in NMR is the problem of finding a pulse sequence for which the net propagator has a desired form, independent of the relative strength of a particular term in the Hamiltonian. Similar problems occur in other areas of NMR, although for different reasons. An important example is the area of high resolution NMR in solids [34,35]. The spectra of abundant nuclei in solids, for example protons ( $^1\text{H}$ ) in crystalline organic compounds, are typically broad and largely structureless. They are dominated by homonuclear dipole couplings, with values ranging from 0 to about 50 kHz. The large number of non-degenerate transitions between the coupled spin states makes it impossible to resolve individual transitions. However, if a pulse sequence for which the net propagator is independent of the couplings is given repetitively while the NMR signals are observed, a spectrum can be obtained which corresponds to an effective Hamiltonian in which there are no couplings. That spectrum has resolved lines whose positions are determined by chemical shifts. Pulse sequences of this sort are called line-narrowing sequences [34-44].

Other examples that may be related to the broadband excitation problem include experiments where the desired propagator is not necessarily independent of the values of coupling constants, but has

particular symmetry properties regardless of the specific couplings. Time-reversal experiments are one such example [45-47]. Pulse sequences may be constructed such that an overall rf phase shift of  $\pi/2$  converts the propagator to its inverse. The inverse propagator reverses the net evolution in time brought about by the original propagator.

The formalism for describing line-narrowing, time-reversal, and other such experiments in which a pulse sequence is designed to produce a propagator of some desired form is provided by coherent averaging theory, originally formulated by Haeberlen and Waugh [37]. The essential idea of coherent averaging theory is that a pulse sequence acts on the spin Hamiltonian, rather than on the spin state, averaging it in such a way that it may be replaced by some other effective Hamiltonian. If the pulse sequence has a total length  $\tau$ , the propagator for the true, time-dependent Hamiltonian is the same as the propagator for the constant, effective Hamiltonian acting for a time  $\tau$ .

A coherent averaging theory analysis of a proposed pulse sequence begins with the separation of the Hamiltonian into two parts:

$$\mathcal{H} = \mathcal{H}_{\text{rf}}(t) + V \quad (\text{IV.1})$$

where  $\mathcal{H}_{\text{rf}}(t)$  is the piecewise-constant interaction with ideal rf fields and  $V$  contains all other interactions, possibly including terms that represent imperfections in the rf pulses. The propagator for  $\mathcal{H}_{\text{rf}}(t)$  alone, a product of rotation operators, is  $U_{\text{rf}}(t)$ , with  $U_{\text{rf}}(0) = 1$ . In a frame of reference related to the rotating frame by the transformation  $U_{\text{rf}}(t)^{-1}$ , the Hamiltonian is  $\mathcal{V}(t)$ , defined by:



$$\tilde{V}(t) = U_{rf}(t)^{-1} V U_{rf}(t) \quad (IV.2)$$

The new frame of reference is an interaction representation in the terminology of time-dependent perturbation theory. Most applications of coherent averaging theory are to pulse sequences consisting of a train of pulses separated by delays in which the rf is switched off. It is often assumed, at least as a first approximation, that the pulses are of very large amplitude and are very short compared to the total length of the sequence. Then the rotations induced by the pulses can be considered to be instantaneous; this is the "delta function" pulse limit. In that limit  $\tilde{V}(t)$  is piecewise-constant if  $V$  is constant. The interaction representation is called the "toggling frame" in the delta function pulse limit.

Frequently, it is more realistic to take the finite pulse lengths and amplitudes into account. Line-narrowing sequences designed explicitly for finite pulse lengths have been demonstrated by Burum, Linder, and Ernst [44]. During a pulse,  $\tilde{V}(t)$  varies continuously in time. This is necessarily the situation in broadband excitation problems, in which parameters such as  $\Delta\omega/\omega_1^0$  and  $d_{ij}/\omega_1^0$  are deliberately not negligible.

The propagator for  $\tilde{V}(t)$  is  $U_V(t)$ . The overall propagator for the pulse sequence,  $U(\tau)$ , is then:

$$U(\tau) = U_{rf}(\tau) U_V(\tau) \quad (IV.3)$$

Eq.(IV.3) can be interpreted to mean that the overall evolution in the rotating frame can be calculated by first transforming to the

interaction representation at  $t = 0$ , calculating the evolution in the interaction representation up to  $t = \tau$ , and finally transforming back to the rotating frame at  $t = \tau$ . Note that the rotating frame and the interaction representation coincide at  $t = 0$ , since  $U_{rf}(0)^{-1} = 1$ .

Eq.(IV.3) is reminiscent of the forms for desired propagators introduced in Eqs.(II.57) and (II.68). Those forms involve the product of a pure rotation operator and another unitary operator of a more general type, just as in Eq.(IV.3). The resemblance suggests that a coherent averaging theory approach may be appropriate in broadband excitation problems.

It is necessary to evaluate  $U_V(\tau)$ , the propagator for a time-dependent Hamiltonian. Coherent averaging theory uses the Magnus expansion [48-51] to express  $U_V(\tau)$  as the exponential of an effective Hamiltonian:

$$U_V(\tau) = \exp(-iV_{\text{eff}}\tau) \quad (\text{IV.4})$$

$$V_{\text{eff}} = V^{(0)} + V^{(1)} + V^{(2)} + \dots \quad (\text{IV.5})$$

The Magnus expansion is a power series expansion in  $|V|\tau$ . The derivation of the Magnus expansion, the form of the terms  $V^{(i)}$ , and other properties are discussed in the next section. In most applications of coherent averaging theory, a pulse sequence is found for which  $V^{(0)}$  has the desired form and  $V^{(1)}$  vanishes. Provided that  $|V|\tau$  is small, higher terms are considered negligible. Then  $V_{\text{eff}} \approx V^{(0)}$ . In line-narrowing applications, sequences for which  $V^{(0)}$  has only terms that are linear in the angular momentum operators are used. In time-reversal applications, sequences for which  $V^{(0)}$  becomes  $-V^{(0)}$  under

an overall rf phase shift of  $\pi/2$  are used.

The two major requirements for the applicability of coherent averaging theory are that  $U_{\text{rf}}(\tau) = 1$  and that the state of the spin system only be observed at times that are multiples of  $\tau$ . A pulse sequence for which  $U_{\text{rf}}(\tau) = 1$  is commonly called a cycle. The requirement that the pulse sequence be cyclic makes  $U(\tau)$  equal to  $U_V(\tau)$ , as follows from Eq.(IV.3). If the pulse cycle is repeated, and if signals are only observed at multiples of  $\tau$ , the spin system appears to be evolving under the Hamiltonian  $V_{\text{eff}} = V^{(0)}$ . The pulse sequence does not affect the evolution explicitly, i.e. two different pulse sequences with the same  $V_{\text{eff}}$  give the same evolution. It is in this way that the pulse sequence acts on the Hamiltonian to create a new, effective Hamiltonian.

Only certain parts of coherent averaging theory are applicable to broadband excitation problems. These are the separations of the Hamiltonian and the propagator according to Eqs.(IV.1) and (IV.3) and the use of the Magnus expansion to evaluate  $U_V(\tau)$ . The requirement that  $U_{\text{rf}}(\tau) = 1$  certainly does not apply.  $U_{\text{rf}}$  is instead required to be a rotation that inverts spin populations or creates transverse magnetization. Another difference is that broadband excitation sequences are typically given as individual units. They are not meant to be applied repetitively and contiguously, as line-narrowing and time-reversal sequences are. Therefore, the idea of observing signals stroboscopically at multiples of  $\tau$  plays no role. The related idea of evolution under a constant effective Hamiltonian is only of importance insofar as the Magnus expansion is used to evaluate  $U_V(\tau)$ . Because the broadband excitation work only uses the Magnus expansion and the

interaction representation, which is standard in time-dependent perturbation theory, and does not use the additional ideas of coherent averaging theory, the phrase "coherent averaging theory" has not been used to describe that work in publications. It should be appreciated, however, that the prevalence of coherent averaging theory in NMR provides the background and inspiration for the approach to broadband excitation described below.

## B. The Magnus expansion

### 1. Derivations

As originally formulated by Magnus [48], the Magnus expansion is the solution to the problem of finding a linear operator  $\Omega(t)$  such that:

$$U(t) = \exp[\Omega(t)] \quad (\text{IV.6})$$

if  $U(t)$  satisfies:

$$\frac{dU(t)}{dt} = A(t)U(t) \quad (\text{IV.7})$$

$$U(0) = 1 \quad (\text{IV.8})$$

where  $A(t)$  is another linear operator. The Schrodinger equation for the propagator is a special case of Eqs.(IV.7) and (IV.8) in which  $iA(t)$  is hermitian and  $U(t)$  is unitary.

Magnus showed that  $\Omega(t)$  satisfies:

$$\frac{d\Omega}{dt} = \sum_{n=0} \beta_n [\dots [[A, \Omega], \Omega], \Omega] \dots] \quad (IV.9)$$

where the  $\beta_n$  are related to Bernoulli numbers.  $\beta_n$  is the coefficient of an  $n$ -fold commutator. Eq.(IV.9) can be solved for  $\Omega(t)$  by iterative integration.

Other derivations of the Magnus expansion that lead to a solution for  $\Omega(t)$  by iterative integration have been given by Pechukas and Light [49] and by Wilcox [50]. For the case where  $A(t) = -i\tilde{V}(t)$  and  $\Omega(\tau) = -iV_{\text{eff}}\tau$ , as in Eq.(IV.4), the result is an expansion of  $V_{\text{eff}}$  as in Eq.(IV.5), with:

$$V^{(0)} = \frac{1}{\tau} \int_0^\tau dt \tilde{V}(t) \quad (IV.10)$$

$$V^{(1)} = \frac{-i}{2\tau} \int_0^\tau dt \int_0^{t_1} dt_2 [\tilde{V}(t_1), \tilde{V}(t_2)] \quad (IV.11)$$

$$V^{(2)} = \frac{-1}{6\tau} \int_0^\tau dt_1 \int_0^{t_1} dt_2 \int_0^{t_2} dt_3 \{ [\tilde{V}(t_1), [\tilde{V}(t_2), \tilde{V}(t_3)]] \\ + [\tilde{V}(t_3), [\tilde{V}(t_2), \tilde{V}(t_1)]] \} \quad (IV.12)$$

$V^{(n)}$  is always a sum of terms that involve  $(n+1)$ -fold integrals of  $n$ -fold commutators of  $\tilde{V}(t)$  with itself at different times.  $V^{(n)}$  is hermitian for all  $n$ , so that the approximation to  $U_V(\tau)$  arrived at by truncating the expansion for  $V_{\text{eff}}$  at any point is always unitary. An explicit, non-recursive formula for  $V^{(n)}$  has been derived by Bialynicki-Birula et al. [51]. If  $\tilde{V}(t)$  commutes with itself at all times, the only non-zero term is  $V^{(0)}$ , which is simply the average of  $\tilde{V}(t)$ . Even if  $\tilde{V}(t)$  does not commute with itself at all times,  $V^{(n)}$  vanishes for all odd  $n$  if  $\tilde{V}(t) = \tilde{V}(\tau - t)$  [52]. A pulse sequence for

which  $\tilde{V}(t) = \tilde{V}(\tau - t)$  is said to be symmetrized.

A particularly simple derivation of the Magnus expansion goes as follows. Assume that the Hamiltonian is  $\lambda\tilde{V}(t)$ . Eq.(II.30) then implies:

$$U_V(\tau) = 1 - i\lambda \int_0^\tau dt_1 V(t_1) - \lambda^2 \int_0^\tau dt_1 \int_0^{t_1} dt_2 V(t_1)V(t_2) + \dots \quad (\text{IV.13})$$

Further assume that:

$$U_V(\tau) = \exp[-i(\lambda V^{(0)} + \lambda^2 V^{(1)} + \lambda^3 V^{(2)} + \dots)\tau] \quad (\text{IV.14})$$

$$\begin{aligned} &= 1 - i(\lambda V^{(0)} + \lambda^2 V^{(1)} + \dots)\tau \\ &\quad - (\lambda V^{(0)} + \lambda^2 V^{(1)} + \dots)^2 \tau^2 / 2 + \dots \end{aligned} \quad (\text{IV.15})$$

Equating the operator coefficients of  $\lambda^n$  in the expressions for  $U_V(\tau)$  in Eqs.(IV.13) and (IV.15) gives Eqs.(IV.10) through (IV.12). While this derivation allows the Magnus expansion terms to be calculated, it does not demonstrate a priori the commutator structure of those terms.

## 2. A parameter differentiation theorem

Suppose that the Hamiltonian for some system is proportional to a parameter  $\lambda$ :

$$H(t) = \lambda V(t) \quad (\text{IV.16})$$

In the previous section, such a form was used to derive the Magnus expansion, with powers of  $\lambda$  serving merely as labels for various orders.

Here,  $\lambda$  is intended to have physical significance, for example as a parameter that determines the overall size of coupling constants in an interaction representation. The propagator for a time  $\tau$  is a function of  $\lambda$ ,  $U_V(\tau, \lambda)$ , with derivatives  $U_V^{(n)}$  at  $\lambda = 0$  defined by:

$$U_V^{(n)} = \left. \frac{d^n}{d\lambda^n} U_V(\tau, \lambda) \right|_{\lambda=0} \quad (\text{IV.17})$$

A theorem that relates the derivatives of the propagator to the Magnus expansion can be stated as follows:  $U_V^{(n)}$  vanishes for  $1 < n < N$  if and only if  $V^{(m)}$  vanishes for  $0 < m < N-1$ .

The theorem follows most directly by using Eq.(IV.15), which implies:

$$U_V^{(n)} = \left. \frac{d^n}{d\lambda^n} \left[ 1 - i(\lambda V^{(0)} + \lambda^2 V^{(1)} + \dots)\tau + \dots + \frac{\tau^k}{k} (-i)^k (\lambda V^{(0)} + \lambda^2 V^{(1)} + \dots)^k + \dots \right] \right|_{\lambda=0} \quad (\text{IV.18})$$

The only terms inside the square brackets that contribute to  $U_V^{(n)}$  are those that are proportional to  $\lambda^n$ . The highest-order Magnus expansion term that contributes is therefore  $V^{(n-1)}$ , so  $U_V^{(n)}$  vanishes for  $1 < n < N$  if  $V^{(m)}$  vanishes for  $0 < m < N-1$ .

The converse may be proved inductively:

$$U_V^{(1)} = -iV^{(0)}\tau \quad (\text{IV.19})$$

so that  $V^{(0)}$  vanishes if  $U_V^{(1)}$  vanishes. If it is assumed that  $U_V^{(n)}$  vanishes for  $1 < n < N$  and that  $V^{(m)}$  vanishes for  $0 < m < N-2$ , Eq.(IV.18) yields:

$$U_V^{(N)} = -in V^{(N-1)}_\tau \quad (IV.20)$$

Therefore,  $V^{(N-1)}$  vanishes as well, so  $V^{(m)}$  vanishes for  $0 < m < N-1$  if  $U_V^{(n)}$  vanishes for  $1 < n < N$ .

If the overall propagator is given by Eq.(IV.3), the derivatives of the overall propagator are:

$$\left. \frac{d^n U(\tau; \lambda)}{d\lambda^n} \right|_{\lambda=0} = U_{rf}(\tau) U_V^{(n)} \quad (IV.21)$$

The theorem is then a mathematical statement of the idea that the propagator for a pulse sequence for which  $V^{(n)}$  vanishes up to some order  $N$  should be independent of the values of the parameters in  $V(t)$  over some range of values. That range of values should increase as  $N$  increases. This is the essential idea of the coherent averaging approach to broadband excitation. Conversely, if it is known that the overall propagator is independent of some parameter, then it must be that  $V^{(n)}$  vanishes up to some order. This fact is of importance in theories of heteronuclear decoupling, particularly in liquid state NMR [32,53,54].

Finally, the theorem suggests that the Magnus expansion terms can be calculated by numerically evaluating the derivatives of a pulse sequence propagator. The practicality and utility of such a calculation have not yet been demonstrated, but it may be useful as a means for verifying more direct calculations or as a replacement for direct calculations when they are excessively complicated.



## C. Application to the construction of composite pulses

### 1. Formal approach

The coherent averaging approach to constructing composite pulses employs the strategy summarized by Eqs.(IV.1) through (IV.5) and (IV.10) through (IV.12). Two types of composite pulses are considered, composite  $\pi$  pulses and composite  $\pi/2$  pulses, although other types may be constructed similarly. A composite  $\pi$  pulse is defined by the condition:

$$\text{Tr}[I_z U_{\text{rf}}(\tau) I_z U_{\text{rf}}(\tau)^{-1}] = -\text{Tr}(I_z^2) \quad (\text{IV.21})$$

A composite  $\pi/2$  pulse is defined by the condition:

$$\text{Tr}[I_z U_{\text{rf}}(\tau) I_z U_{\text{rf}}(\tau)] = 0 \quad (\text{IV.22})$$

Broadband excitation with respect to four interactions is considered. For resonance offsets or chemical shifts,  $V$  is taken to be:

$$V = \Delta\omega I_z \quad (\text{IV.23})$$

For rf amplitude inhomogeneity:

$$V = \delta\omega_1 [I_x \cos\phi(t) + I_y \sin\phi(t)] \quad (\text{IV.24})$$

For dipole couplings:

$$V = \sum_{i>j} d_{ij} [I_{zi} I_{zj} - (1/3) \underline{I}_i \cdot \underline{I}_j] \quad (\text{IV.25})$$

For quadrupole couplings:

$$V = \omega_Q [I_z^2 - (1/3) I^2] \quad (\text{IV.26})$$

Simultaneous broadband excitation with respect to several interactions can be treated by taking  $V$  to be the sum of the interactions. The order of a composite pulse is defined by the number of Magnus expansion terms that vanish. An  $M^{\text{th}}$  order composite pulse has:

$$V^{(j)} = 0, \quad 0 < j < M \quad (\text{IV.27})$$

Eq.(IV.27) ensures that  $U_V(\tau) \approx 1$  for some range of  $\Delta\omega$ ,  $\delta\omega_1$ ,  $d_{ij}$ , or  $\omega_Q$  around zero. Then the overall propagator is  $U(\tau) \approx U_{\text{rf}}(\tau)$ , i.e. a constant pure rotation. This is a unique and important feature of composite pulses derived with a coherent averaging approach. Zeroth order and first order composite pulses are demonstrated in Chapter V, with an emphasis on features that result from the constancy of  $U(\tau)$ .

The problem now is to find a pulse sequence that satisfies Eqs.(IV.21) or (IV.22) and (IV.27). In other applications of coherent averaging theory, specific pulse cycles are found by some combination of experience, intuition, inspection, and inspiration. Typically, a cycle is chosen to have the desired  $V^{(0)}$  in the delta function pulse limit. Higher-order terms and effects of finite pulse lengths and pulse

imperfections are made to vanish by symmetrization and by combining variants of the basic cycle to form longer supercycles [41,46], or by readjusting the lengths of delays and the flip angles of pulses [42,43]. Theorems that indicate when variants of a cycle can be combined to form a superior supercycle have been developed [41,46].

The approach to finding composite pulses is conceptually different. It is essentially a "brute force" technique. Consider a general  $N$ -pulse sequence. With the phase of the first pulse arbitrarily set to zero, the sequence has  $2N-1$  variable parameters, namely  $N$  flip angles and  $N-1$  phases. Eqs.(IV.21) or (IV.22) and (IV.27) are a set of simultaneous equations in those variables. If  $N$  is chosen to be large enough, it may be expected that there is a solution to that set of equations. Such a solution is the desired composite pulse. The procedure therefore consists of constructing expressions for the appropriate equations in terms of the flip angles and phases and then finding the simultaneous solution.

The choice of  $N$  is not obvious. Each of the equations is an operator equation, and is therefore composed of several component equations. The equations are non-linear. Still, experience shows that solutions can usually be found when the number of variables approximately equals the number of equations, although this is not guaranteed.

In simple cases, of which an example is given below, the equations can be written out by hand and solved analytically. In most cases, this is tedious and essentially impossible. Therefore, computer programs are usually used, as described later.

## 2. A simple example

In this section, zeroth order composite  $\pi$  pulses for broadband excitation with respect to resonance offsets are derived, with the general form  $\alpha_0\beta_0\alpha_0$ . There are clearly three variables, the two flip angles  $\alpha$  and  $\beta$  and the phase  $\phi$ . The pure rf propagator for such a sequence is:

$$U_{rf}(t) = \begin{cases} \exp(-iI_x\omega_1^0 t), & 0 \leq t \leq \alpha/\omega_1^0 \\ \exp(-iI_z\phi)\exp(-iI_x\omega_1^0 t')\exp(iI_z\phi)\exp(-iI_x\alpha), & 0 \leq t' \leq \beta/\omega_1^0 \\ \exp(-iI_x\omega_1^0 t'')\exp(-iI_z\phi)\exp(-iI_x\beta)\exp(iI_z\phi)\exp(-iI_x\alpha), & 0 \leq t'' \leq \alpha/\omega_1^0 \end{cases} \quad (IV.28)$$

with:

$$t' = t - \alpha/\omega_1^0 \quad (IV.29)$$

$$t'' = t - (\alpha + \beta)/\omega_1^0 \quad (IV.30)$$

Using Eq.(IV.28), and with  $\tau = (2\alpha + \beta)/\omega_1^0$ :

$$U_{rf}(\tau)I_zU_{rf}(t)^{-1} = aI_x + bI_y + cI_z \quad (IV.31)$$

$$c = -\sin^2\alpha\sin^2\phi - \sin^2\alpha\cos\beta\cos^2\phi - 2\sin\alpha\cos\alpha\sin\beta\cos\phi + \cos^2\alpha\cos\beta \quad (IV.32)$$

The condition that the pulse sequence be a composite  $\pi$  pulse is

Eq.(IV.21), which becomes  $c = -1$ . This condition is satisfied when:

$$\cos\phi = \frac{\cos\alpha\sin\beta}{\sin\alpha(1 - \cos\beta)} \quad (IV.33)$$

Any  $\alpha_0 \beta_0 \alpha_0$  sequence for which Eq.(IV.33) holds inverts populations when  $\Delta\omega = 0$ . The next step is to evaluate  $\tilde{V}(t)$ . Using Eq.(IV.28) and the definition of  $\tilde{V}(t)$  in Eq.(IV.2):

$$\tilde{V}(t) = \Delta\omega[a(t)I_x + b(t)I_y + c(t)I_z] \quad (IV.34)$$

with:

$$a(t) = \begin{cases} 0, & 0 < t < \alpha/\omega_1^0 \\ -\sin\phi\sin\omega_1^0 t', & 0 < t' < \beta/\omega_1^0 \\ \sin\phi\cos\phi(1 - \cos\beta)\sin\omega_1^0 t'' - \sin\phi\sin\beta\cos\omega_1^0 t'', & 0 < t'' < \alpha/\omega_1^0 \end{cases} \quad (IV.35)$$

$$b(t) = \begin{cases} \sin\omega_1^0 t, & 0 < t < \alpha/\omega_1^0 \\ \cos\phi\cos\alpha\sin\omega_1^0 t' + \sin\alpha\cos\omega_1^0 t', & 0 < t' < \beta/\omega_1^0 \\ (\cos^2\phi\cos\beta\cos\alpha + \sin^2\phi\cos\alpha - \cos\phi\sin\beta\sin\alpha)\sin\omega_1^0 t'' \\ + (\cos\phi\sin\beta\cos\alpha + \cos\beta\sin\alpha)\cos\omega_1^0 t'', & 0 < t'' < \alpha/\omega_1^0 \end{cases} \quad (IV.36)$$

$$c(t) = \begin{cases} \cos\omega_1^0 t, & 0 < t < \alpha/\omega_1^0 \\ \cos\alpha\cos\omega_1^0 t' - \cos\phi\sin\alpha\sin\omega_1^0 t', & 0 < t' < \beta/\omega_1^0 \\ -(\cos\phi\sin\beta\cos\alpha + \cos^2\phi\cos\beta\sin\alpha + \sin^2\phi\sin\alpha)\sin\omega_1^0 t'' \\ + (\cos\beta\cos\alpha - \cos\phi\sin\beta\sin\alpha)\cos\omega_1^0 t'', & 0 < t'' < \alpha/\omega_1^0 \end{cases} \quad (IV.37)$$

$V^{(0)}$  can now be calculated by integrating Eqs.(IV.35),(IV.36), and (IV.37). For the special case  $\phi = \pi/2$ , the result is:

$$V^{(0)} = \Delta\omega[(\cos\beta - 1 - \sin\alpha\sin\beta)I_x + (1 + \sin\beta\sin\alpha - \cos^2\alpha + \cos\beta\sin^2\alpha)I_y$$

$$+ (\sin\beta\cos\alpha + \cos\beta\sin\alpha\cos\alpha + \sin\alpha\cos\alpha)I_z]/(2\alpha + \beta) \quad (\text{IV.38})$$

The requirement  $V^{(0)} = 0$  is satisfied, along with Eq.(IV.33), whenever  $\alpha$  is an odd multiple of  $\pi/2$  and  $\beta = 2n\pi - \alpha$  for an integer  $n$ . Thus, the sequence  $90_0 270_{90} 90_0$  derived with other methods by Levitt and Freeman [21] and by Levitt [23] belongs to a class of zeroth order composite  $\pi$  pulses in the coherent averaging approach.

For an arbitrary  $\phi$ , the expression for  $V^{(0)}$  is considerably longer. However, it can be shown that  $V^{(0)} = 0$  whenever Eq.(IV.33) and the equation  $\beta = 2n\pi - \alpha$  are satisfied.

### 3. Numerical methods: resonance offsets and rf inhomogeneity

The example in the previous section illustrates the complexity of the equations that must be solved to derive composite pulses. Even for a sequence with only three variables,  $\tilde{V}(t)$  does not have a simple form. If longer sequences are used in an effort to find higher-order composite pulses, the expression for  $\tilde{V}(t)$  soon becomes unwieldy. The same holds for the expression for  $U_{rf}(\tau)I_zU_{rf}(\tau)^{-1}$ . The number of terms in  $V^{(1)}$  is roughly the square of the number of terms in  $V^{(0)}$ , and each term involves roughly twice as many trigonometric functions of the flip angles and phases. Additionally, while in the resonance offset and rf inhomogeneity cases the only operators that appear in  $\tilde{V}(t)$  and  $V^{(n)}$  are  $I_x$ ,  $I_y$ , and  $I_z$ , due to the closed commutation relations of the angular momentum operators, in the dipole and quadrupole coupling cases there are more operator components to each equation. For all of these

reasons, it is generally not feasible to generate the equations explicitly by hand and solve them analytically. Instead, computer programs that evaluate the required expressions and search for solutions to the equations are written.

As an example of the way such a program works, consider the construction of a first order composite  $\pi$  pulse with compensation for resonance offsets of the form  $(\theta_1)_0(\theta_2)_{\phi_2}(\theta_3)_{\phi_3}\dots(\theta_N)_{\phi_N}$ . For a given choice of the  $N$  variable flip angles and  $N-1$  variable phases, the program first checks to see if the sequence inverts populations when  $\Delta\omega = 0$ . If  $N$  is small, a general expression for the coefficient of  $I_z$  in  $U_{rf}(\theta_i, \phi_i) I_z U_{rf}(\theta_i, \phi_i)^{-1}$  can be derived by hand. The program evaluates that expression for the specific choice of flip angles and phases. Otherwise, the coefficient of  $I_z$  can be extracted after applying the  $N$  rotations that make up  $U_{rf}$  to an initial operator  $I_z$  in a loop in the program. If the result differs from  $-1$  by more than a specified tolerance, that choice of flip angles and phases is discarded and a new choice is made. If the result equals  $-1$  to within the specified tolerance, the equation  $V^{(0)} = 0$  is tested.

For the resonance offset case:

$$\tilde{V}(t) = \Delta\omega \tilde{Y}_z(t) \quad (\text{IV.39})$$

with:

$$\tilde{Y}_z(t) = U_{rf}(t)^{-1} I_z U_{rf}(t) \quad (\text{IV.40})$$

During the  $n^{\text{th}}$  pulse,  $\tilde{Y}_z(t)$  has the form:

$$\tilde{Y}_z^n(t_n) = I_z(c_{1n}\sin\omega_1^0 t_n + c_{2n}\cos\omega_1^0 t_n) + I_y(c_{3n}\sin\omega_1^0 t_n + c_{4n}\cos\omega_1^0 t_n)$$

$$+ I_x(c_{5n}\sin\omega_1^0 t_n + c_{6n}\cos\omega_1^0 t_n), \quad 0 < t_n < \theta_n/\omega_1^0 \quad (\text{IV.41})$$

where:

$$t_n = t - (\theta_1 + \theta_2 + \dots + \theta_{n-1})/\omega_1^0 \quad (\text{IV.42})$$

The coefficients  $c_{in}$  are calculated according to the expression:

$$\begin{aligned} \gamma_z^n(t_n) = & \exp(iI_x\theta_1)\exp(-iI_z\phi_2)\dots\exp(iI_x\theta_{n-1})\exp[-iI_z(\phi_n - \phi_{n-1})] \\ & \times (I_z\cos\omega_1^0 t_n + I_y\sin\omega_1^0 t_n)\exp[iI_z(\phi_n - \phi_{n-1})]\exp(-iI_x\theta_{n-1})\dots \\ & \times \exp(iI_z\phi_2)\exp(-iI_x\theta_1) \end{aligned} \quad (\text{IV.43})$$

by applying the indicated rotations about z and x in a loop in the program.

$V^{(0)}$  is then proportional to:

$$\begin{aligned} \sum_n \omega_1^0 \int_0^{\theta_n/\omega_1^0} dt I_z^n(t) = & \sum_n I_z[c_{1n}(1 - \cos\theta_n) + c_{2n}\sin\theta_n] + I_y[c_{3n}(1 - \cos\theta_n) \\ & + c_{4n}\sin\theta_n] + I_x[c_{5n}(1 - \cos\theta_n) + c_{6n}\sin\theta_n] \end{aligned} \quad (\text{IV.44})$$

The total coefficients of  $I_x$ ,  $I_y$ , and  $I_z$  in Eq.(IV.44) are calculated individually and checked to see if they are within a specified tolerance of zero. If not, a new choice of flip angles and phases is made and the program begins again. If so, the equation  $V^{(1)} = 0$  is checked.

There are two contributions to  $V^{(1)}$ . The first is from commutators of  $\tilde{I}_z(t)$  during one pulse with  $\tilde{I}_z(t)$  during another pulse. These are proportional to:

$$\begin{aligned} \sum_{m>n} (\omega_1^0)^2 \left[ \int_0^{\theta_m/\omega_1^0} dt \tilde{I}_z^m(t), \int_0^{\theta_n/\omega_1^0} dt \tilde{I}_z^n(t) \right] = & \sum_{m>n} [iI_x g(m,n,3,4,1,2) \\ & + iI_y g(m,n,1,2,5,6) + iI_z g(m,n,5,6,3,4)] \end{aligned} \quad (\text{IV.45a})$$



$$\begin{aligned}
g(m,n,i,j,k,l) = & [c_{im}(1 - \cos\theta_m) + c_{jm}\sin\theta_m][c_{kn}(1 - \cos\theta_n) + c_{ln}\sin\theta_n] \\
& - [c_{km}(1 - \cos\theta_m) + c_{lm}\sin\theta_m][c_{in}(1 - \cos\theta_n) + c_{jn}\sin\theta_n]
\end{aligned}
\tag{IV.45b}$$

The contribution from commutators of  $\tilde{I}_z(t)$  at one time during a pulse with  $\tilde{I}_z(t)$  at a different time during the same pulse is proportional to:

$$\begin{aligned}
\sum_n (\omega_1^0)^2 \int_0^{\theta_n/\omega_1^0} dt \int_0^t dt' [\tilde{I}_z^n(t), \tilde{I}_z^n(t')] = & i \sum_n (\sin\theta_n - \theta_n) [I_x(c_{1n}c_{4n} - c_{3n}c_{2n}) \\
& + I_y(c_{2n}c_{5n} - c_{1n}c_{6n}) + I_z(c_{3n}c_{6n} - c_{4n}c_{5n})]
\end{aligned}
\tag{IV.46}$$

The sums of the coefficients of  $I_x$ ,  $I_y$ , and  $I_z$  in Eqs.(IV.45) and (IV.46) are calculated and checked to see if they are within a specified tolerance of zero. If so, the values of the flip angles and phases are saved.

All possible combinations of flip angles and phases within specified ranges and in specified increments are tested. The tolerances within which Eqs.(IV.21) or (IV.22) and (IV.27) must be satisfied are made sufficiently small that only a small number of flip angle and phase combinations are saved. Simulations of the performance of the composite pulses are used to select the best composite pulse from those that satisfy the required equations within the specified tolerances. Differences in the performance of various composite pulses may be attributed to differences in the higher-order Magnus expansion terms that are not calculated. The flip angles and phases may be further refined, when the required equations have not been solved exactly, by reducing the tolerances and searching through flip angles and phases in smaller increments in the neighborhood of the flip angles and phases

that have previously been saved.

A similar procedure is used to derive composite pulses that are broadband with respect to the rf amplitude. In that case, Eq.(IV.39) is replaced by:

$$\tilde{V}(t) = \delta\omega_1 \tilde{I}_\phi(t) \quad (\text{IV.47})$$

with:

$$\tilde{I}_\phi(t) = U_{\text{rf}}(t)^{-1} (I_x \cos\phi + I_y \sin\phi) U_{\text{rf}}(t) \quad (\text{IV.48})$$

During the  $n^{\text{th}}$  pulse,  $\tilde{I}_\phi(t)$  is the constant operator  $\tilde{I}_{\phi_n}$ :

$$\begin{aligned} \tilde{I}_{\phi_n} = & \exp(iI_{x1}\theta_1) \exp(-iI_{z2}\phi_2) \dots \exp(iI_{xn}\theta_{n-1}) \exp(iI_{zn}\phi_{n-1}) (I_x \cos\phi_n + I_y \sin\phi_n) \\ & \times \exp(-iI_{zn}\phi_{n-1}) \exp(-iI_{xn}\theta_{n-1}) \dots \exp(iI_{z2}\phi_2) \exp(-iI_{x1}\theta_1) \quad (\text{IV.49}) \end{aligned}$$

The fact that  $\tilde{I}_\phi(t)$  is piecewise-constant simplifies the expressions for  $V^{(0)}$  and  $V^{(1)}$ :

$$V^{(0)} \propto \sum_n \theta_n I_{\phi_n} \quad (\text{IV.50})$$

$$V^{(1)} \propto \sum_{m>n} \theta_m \theta_n [I_{\phi_m}, I_{\phi_n}] \quad (\text{IV.51})$$

Computer programs, written in FORTRAN, that are used to find first order composite  $\pi$  pulses are given in Appendix B. The programs follow the procedure described above.

#### 4. Numerical methods: dipole and quadrupole couplings

As pointed out in Chapter II.B, the dipole and quadrupole interactions have similar forms. This is made particularly clear by rewriting Eq.(IV.25) as:

$$V = \sum_{i>j} \frac{d_{ij}}{2} [(I_{zij}^2 - \frac{1}{3}I_{ij}^2) - (I_{zi}^2 - \frac{1}{3}I_i^2) - (I_{zj}^2 - \frac{1}{3}I_j^2)] \quad (IV.52)$$

with:

$$\tilde{I}_{ij} = \tilde{I}_i + \tilde{I}_j \quad (IV.53)$$

The right-hand sides of both Eq.(IV.52) and Eq.(IV.26) consist of terms of the form:

$$T_{20} = \frac{1}{6}(3I_z^2 - I^2) \quad (IV.54)$$

The notation  $T_{20}$  indicates that this is the  $m = 0$  component of a second rank irreducible tensor operator  $\{T_{2m}\}$ . An irreducible tensor operator with respect to rotations of the form  $\exp(-i\alpha \cdot \tilde{I})$  is defined by the relations [14,55]:

$$[I_{\pm}, T_{lm}] = l(l+1) - m(m \pm 1) T_{l, m \pm 1} \quad (IV.55)$$

$$[I_z, T_{lm}] = m T_{lm} \quad (IV.56)$$

with  $m = -l, -l+1, \dots, l-1, l$ . As results of Eqs.(IV.55) and (IV.56), irreducible tensor operators have the properties that:

$$\exp(-iI_z\phi)T_{lm}\exp(iI_z\phi) = \exp(-im\phi)T_{lm} \quad (\text{IV.57})$$

$$\exp(-iI_y\theta)T_{lm}\exp(iI_y\theta) = \sum d_{m'm}^l(\theta)T_{lm'}, \quad (\text{IV.58})$$

where  $d_{m'm}^l(\theta)$  are elements of a reduced Wigner rotation matrix. An important conclusion to draw from Eqs.(IV.57) and (IV.58) is that the components of a given irreducible tensor operator transform only among themselves under any rotation.

The other components of the second rank tensor are:

$$T_{2\pm1} = \mp \frac{1}{2} I_{\pm} (2I_z \pm 1) \quad (\text{IV.59})$$

$$T_{2\pm2} = \frac{1}{2} I_{\pm}^2 \quad (\text{IV.60})$$

The normalization in Eqs.(IV.54), (IV.59), and (IV.60) follows reference 55.

The above remarks indicate that  $\tilde{V}(t)$  for a dipole or quadrupole coupling is always a sum of terms that are second rank irreducible tensor components.  $V^{(0)}$  is therefore also a sum of second rank irreducible tensor components. Even if  $V$  is the sum of several  $T_{20}$  terms, they all transform in the same way and independently under rotations. There are no cross terms in  $\tilde{V}(t)$  or  $V^{(0)}$ . Therefore it is sufficient to consider only a single  $T_{20}$  term, and take:

$$V = d(3I_z^2 - I^2) \quad (\text{IV.61})$$

The equation  $V^{(0)} = 0$  has five independent operator components, regardless of the number of coupled nuclei and regardless of their total spin quantum numbers.

$v(0)$  for a pulse sequence may be calculated by summing the contributions from individual pulses. The contribution from the  $n^{\text{th}}$  pulse is  $v_n^{(0)}$ :

$$v_n^{(0)} = \exp(iI_{x1}\theta_1)\exp(-iI_{z2}\phi_2)\dots\exp(iI_{xn}\theta_{n-1})\exp[-iI_z(\phi_n - \phi_{n-1})]\tilde{T}_{20}(\theta_n) \\ \times \exp[I_z(\phi_n - \phi_{n-1})]\exp(-iI_{xn}\theta_{n-1})\dots\exp(iI_{z2}\phi_2)\exp(iI_{x1}\theta_1) \quad (\text{IV.62})$$

$$T_{20}(\theta) = \int_0^{\theta/\omega_1^0} dt \exp(iI_{x1}\omega_1^0 t) T_{20} \exp(-iI_{x1}\omega_1^0 t) \quad (\text{IV.63})$$

$$= \frac{0-6}{8}(\theta - \sin\theta\cos\theta)(T_{22} + T_{2-2}) + \frac{6}{4}i\sin^2\theta(T_{21} + T_{2-1}) \\ + \frac{1}{4}(\theta + 3\sin\theta\cos\theta)T_{20} \quad (\text{IV.64})$$

$v_n^{(0)}$  can be evaluated in a loop in a computer program using Eq.(IV.57) and the reduced Wigner matrix  $d^1(\theta)$ , or the matrix representation for  $\exp(iI_{x1}\theta)$  in the operator basis  $\{T_{22}, T_{21}, T_{20}, T_{2-1}, T_{2-2}\}$  derived from Table 3 of reference 55:

$$\begin{pmatrix} \frac{1}{4}(1+\cos\theta)^2 & \frac{i}{2}\sin\theta(1+\cos\theta) & -\frac{\sqrt{6}}{4}\sin^2\theta & -\frac{i}{2}\sin\theta(1-\cos\theta) & \frac{1}{4}(1-\cos\theta)^2 \\ \frac{i}{2}\sin\theta(1+\cos\theta) & \frac{1}{2}(1+\cos\theta)(2\cos\theta-1) & \frac{i\sqrt{6}}{2}\sin\theta\cos\theta & -\frac{1}{2}(1-\cos\theta)(2\cos\theta+1) & -\frac{i}{2}\sin\theta(1-\cos\theta) \\ -\frac{\sqrt{6}}{4}\sin^2\theta & \frac{i\sqrt{6}}{2}\sin\theta\cos\theta & \frac{1}{2}(3\cos^2\theta-1) & \frac{i\sqrt{6}}{2}\sin\theta\cos\theta & -\frac{\sqrt{6}}{4}\sin^2\theta \\ -\frac{i}{2}\sin\theta(1-\cos\theta) & -\frac{1}{2}(1-\cos\theta)(2\cos\theta+1) & \frac{i\sqrt{6}}{2}\sin\theta\cos\theta & \frac{1}{2}(1+\cos\theta)(2\cos\theta-1) & \frac{1}{2}\sin\theta(1+\cos\theta) \\ \frac{1}{4}(1-\cos\theta)^2 & -\frac{1}{2}\sin\theta(1-\cos\theta) & -\frac{\sqrt{6}}{4}\sin^2\theta & \frac{i}{2}\sin\theta(1+\cos\theta) & \frac{1}{4}(1+\cos\theta)^2 \end{pmatrix}$$

(IV.65)

Line (IV.65) is actually the matrix representation of the superoperator, i.e. the linear transformation on operators, corresponding to  $\exp(iI_x\theta)$ . As before, a search through possible flip angle and phase combinations is conducted. Those combinations for which the inversion equation is satisfied and for which the coefficients of the  $T_{2m}$  components in  $V^{(0)}$  are zero to within a specified tolerance are saved.

The number of operator components in the higher-order Magnus expansion terms depends on the size of the spin system. Consider first the case of a single quadrupolar nucleus with total spin  $I$ .  $V^{(n)}$  involves  $n$ -fold commutators of  $T_{2m}$  components.  $V^{(n)}$  may then contain irreducible tensors with ranks from 0 to  $n + 2$  in general. This fact may be seen as follows.

The product  $T_{lm}T_{l'm'}$  of two tensor components may be decomposed into a linear combination of tensor components  $T_{l''m''}$  with  $m'' = m + m'$ :

$$T_{lm}T_{l'm'} = \sum_{l''=|l-l'|}^{l+l'} \langle ll'l''m'' | lm l'm' \rangle T_{l''m''} \quad (\text{IV.66})$$

where  $\langle ll'l''m'' | lm l'm' \rangle$  is a Clebsch-Gordon coefficient. The maximum value of  $l''$  in  $[T_{lm}, T_{l'm'}]$  is  $l + l' - 1$ , however. The only commutator that could have a component of  $T_{l''m''}$  with  $l'' = l + l'$  is  $[T_{11}, T_{1,1}]$ , but this must be zero because:

$$T_{11} \propto (I_+)^1 \quad (\text{IV.67})$$

Therefore:

$$\text{Tr}(T_{(l+l')}(l+l') [T_{lm}, T_{l'm'}]) = 0 \quad (\text{IV.68})$$

for all  $m$  and  $m'$ . For any component  $T_{(l+l')m''}$ , a finite number of rotations  $R_j$  and constants  $c_j$  can be found such that:

$$T_{(l+l')m''} = c_1 R_1 T_{(l+l')(l+l')} R_1^{-1} + c_2 R_2 T_{(l+l')(l+l')} R_2^{-1} + \dots \quad (\text{IV.69})$$

Eqs.(IV.68) and (IV.69) imply:

$$\begin{aligned} \text{Tr}(T_{(l+l')m''} [T_{lm}, T_{l'm'}]) &= c_1^* \text{Tr}(T_{(l+l')(l+l')} [R_1^{-1} T_{lm} R_1, R_1^{-1} T_{l'm'} R_1]) \\ &+ c_2^* \text{Tr}(T_{(l+l')(l+l')} [R_2^{-1} T_{lm} R_2, R_2^{-1} T_{l'm'} R_2]) + \dots \end{aligned} \quad (\text{IV.70})$$

$$= 0 \quad (\text{IV.71})$$

where Eq.(IV.71) follows from Eq.(IV.68). Therefore,  $[T_{lm}, T_{l'm'}]$  has no tensor component of rank  $l + l'$ . The maximum rank tensor in an  $n$ -fold commutator of  $T_{2m}$  components can not be greater than  $n + 2$ .

For the case of a quadrupolar nucleus, an upper limit on the tensor rank in all Magnus expansion terms is set by the total spin quantum number  $I$  to be  $2I$ . Any tensor  $T_{lm}$  with  $l > 2I$  becomes the zero matrix when written in a basis of spin states for a spin- $I$  nucleus.

The other important case to consider is that of a system of  $N$  dipole-coupled spin- $1/2$  nuclei. In this case, only the terms involving  $I_{ij}$  operators are not zero in Eq.(IV.52). A non-zero  $n$ -fold commutator can involve angular momentum operators from at most  $n + 2$  different nuclei, implying a maximum irreducible tensor rank of  $n + 2$ , as before. It is sufficient to consider a system of  $n + 2$  spins when treating  $V^{(n)}$ , since all possible independent terms in  $V^{(n)}$  will then be present.

Unlike the case of a single quadrupolar nucleus, there is generally more than one independent irreducible tensor of a given rank.

One modification of the procedure that proves useful in the case of composite pulses for coupled systems is to replace the  $V^{(n)} = 0$  requirement with the requirement  $[V^{(n)}, I_z] = 0$ . Sequences that satisfy the latter requirement have overall propagators that are still approximately in the form of Eq.(II.59) or (II.70). The propagators are not pure rotations and are not strictly constant over a range of couplings, however. Such sequences are discussed further in Chapter V.

## 5. Limitations of the methods

The practical limitations on the coherent averaging approach to broadband excitation are of two types. First, the expression for  $V^{(n)}$  for a general pulse sequence with many variables can not be written out by hand. Once the contributions to  $V^{(n)}$  have been sorted out and a general form for each contribution has been determined, as in Eqs.(IV.41) and (IV.44) through (IV.46),  $V^{(n)}$  can be evaluated for each combination of flip angles and phases using some arrangement of loops in a computer program. Even this will become tedious and prone to error as  $n$  becomes large, however.

One way around this limitation may be to use symbolic manipulation programs (e.g. MAXIMA or SMP). It may be possible to give such a program the definition of  $V^{(n)}$ , as in Eqs.(IV.10) through (IV.12), and a specific form for  $V$ , as in Eqs.(IV.23) through (IV.26), and have the program produce an expression for  $V^{(n)}$  as a function of the variables in the pulse sequence, using the angular momentum commutation rules and



rotation relationships.

The second limitation on the approach is the amount of computer time required to search for solutions to the required equations in the space of variables  $(\theta_i, \phi_i)$ . For the examples treated in Chapter V, the programs typically tested about  $10^6$  flip angle and phase combinations in several hours of CPU time on VAX 11/780 computers at the Lawrence Berkeley Laboratory computer center. For a four-pulse sequence with four variable flip angles and three variable phases, the required CPU time might limit the initial search to flip angles and phases between  $0^\circ$  and  $360^\circ$  in  $45^\circ$  increments. With existing methods, sequences with more variables can not be tested with sufficiently small flip angle and phase increments in practical amounts of time.

If explicit expressions for  $V^{(n)}$  and  $U_{rf} I_Z U_{rf}^{-1}$  could be derived with symbolic manipulation programs, it is likely that the required equations could be checked in considerably less time, extending the length of the pulse sequences that may be treated practically. Additionally, more intelligent search procedures may help. Rather than testing all combinations of the variables in specified increments, a directed search may be employed. A single quantity  $Q$  that indicates the deviation from a simultaneous solution of the required equations can be defined.  $Q$  is a function with a value at each point in  $(\theta_i, \phi_i)$  space. The gradient of  $Q$  at some initial point can be approximately calculated by evaluating  $Q$  at nearby points. A new point can then be chosen in the direction in  $(\theta_i, \phi_i)$  space along which  $Q$  decreases. Repeating this process may lead to a minimum of  $Q$  that represents an approximate solution to the equations. With such a method, a composite pulse may be found without searching through all flip angle and phase combinations.

## Chapter V: Coherent Averaging Approach to Broadband Excitation: Results

### A. Motivation

In this chapter, composite pulses constructed with the methods of Chapter IV are presented and demonstrated both experimentally and in simulations. The composite pulses may be divided into two categories: those that have large bandwidths with respect to resonance offsets or rf amplitudes and are therefore primarily, but not exclusively, intended for applications in liquid state NMR, and those that have large bandwidths with respect to dipole and quadrupole couplings and are therefore intended for applications in solid state NMR. This division is appropriate partly because dipole and quadrupole couplings are the dominant interaction in solids. Rf inhomogeneity is a factor in solid state NMR experiments, but its most dramatic effects are in NMR experiments that use surface coils [56], as explained later. Surface coils are most commonly used in liquid state, in vivo studies. Resonance offsets and chemical shifts are also present in solids, but they are usually negligible compared to the rf amplitudes typically used in solid state NMR, since large rf amplitudes are required due to the large couplings. In solids, it is common to have  $\omega_1^0/2\pi \approx 100$  kHz. Smaller rf amplitudes are common in liquid state NMR, with  $\omega_1^0/2\pi \approx 10$  kHz. In a 100 kG static magnetic field, not unusual in liquid state NMR, proton chemical shifts in organic compounds span a range of about 5 kHz. In NMR imaging techniques [57-59], the static field may be as

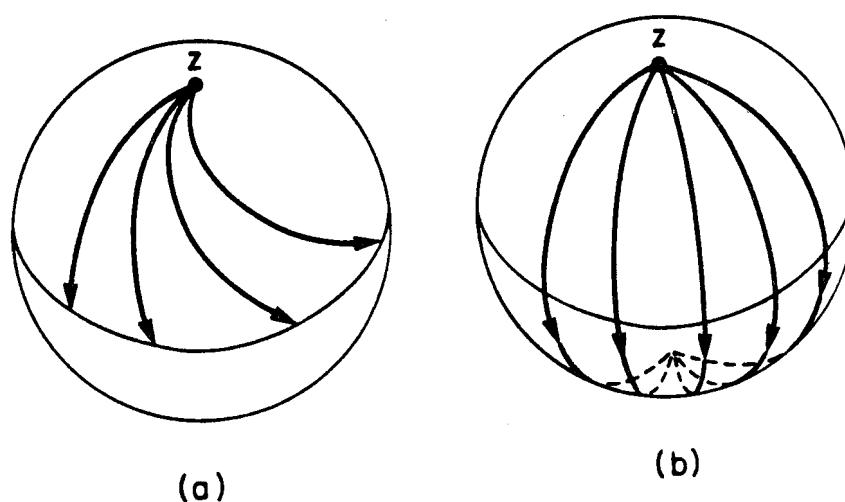
small as 1 kG, but a 10 kHz range of resonance offsets may be produced by static field gradients. In medical NMR imaging, it is particularly difficult to produce a large  $\omega_1^0$ , due to the large sample volume that must be irradiated, so that resonance offsets are particularly significant if rf pulses are applied at the same time that static field gradients are present.

In addition to differences in their applications, one reason for dividing the composite pulses into two categories is that a large body of work that deals with composite pulses that compensate for resonance offsets and rf inhomogeneity exists, some previous to the work described in this dissertation and some concurrent. The distinguishing feature of the composite pulses constructed with the methods of Chapter IV is the fact that they produce constant net rotations, as explained in Chapter IV.C. This feature is emphasized in the demonstrations of composite pulses for resonance offsets and rf inhomogeneity in sections B and C below. The importance of constant rotations is discussed further in section D. Bloch vector pictures illustrating the general case of composite  $\pi/2$  and  $\pi$  pulses are given in Figure V.1.

Considerably less work has been devoted to composite pulses for broadband excitation with respect to dipole and quadrupole couplings. Apart from the composite pulses presented in section E below, there is currently one other publication on the subject, which is also discussed in section E.

## B. Rf inhomogeneity

### 1. Composite $\pi$ pulses



XBL 845-1699

Figure V.1: The general case of phase variations in composite pulses.  
 a) As the resonance offset or the rf amplitude varies, the net rotation angle and the net rotation axis of a composite  $\pi/2$  pulse change. This is indicated by Bloch vector trajectories on a unit sphere, corresponding to the net rotation produced by a hypothetical composite  $\pi/2$  pulse for various values of the resonance offset or rf amplitude.  
 b) For a composite  $\pi$  pulse, it is the net rotation axis that changes, even though magnetization may be inverted over a range of resonance offsets or rf amplitudes.

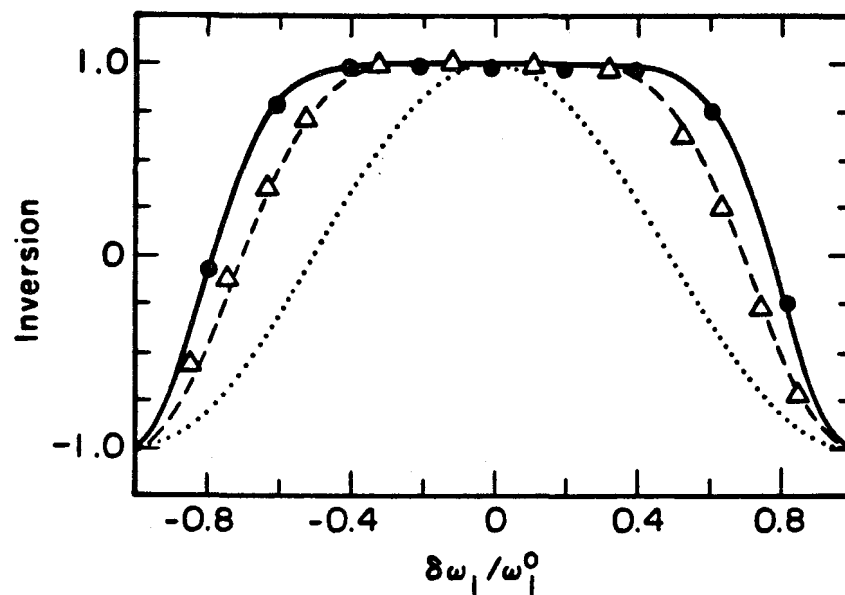
Figure V.2 shows the inversion performance of two composite  $\pi$  pulses designed to cover a large range of rf amplitudes. The sequence  $180_0 180_{120} 180_0$  is a zeroth order composite pulse, with  $V^{(0)} = 0$  exactly.  $180_0 180_{105} 180_{210} 360_{59}$  is a first order composite pulse, with  $V^{(0)} = \delta\omega_1(-0.0016 I_x + 0.0007 I_y)$  and  $V^{(1)} = (\delta\omega_1)^2(0.0004 I_z)/\omega_1^0$ . Note that the required equations  $V^{(0)} = 0$  and  $V^{(1)} = 0$  are nearly, but not exactly, satisfied. The inversion bandwidth increases with order, as predicted theoretically.

The general form of the propagator for a composite  $\pi$  pulse is given in Eq.(II.61). The angle  $\phi$  in that equation characterizes the net rotation axis. For  $180_0 180_{120} 180_0$ ,  $\phi = 240^\circ$  when  $\delta\omega_1 = 0$ . It is generally true of composite  $\pi$  pulses that the rotation axis is a function of  $\omega_1$ , as in Figure V.1b. This can be seen experimentally if the composite  $\pi$  pulse is used as a refocussing pulse in a  $\pi/2-\tau-\pi-\tau$  spin echo sequence [60,61].  $\tau$  represents a delay in which spins evolve under resonance offsets, chemical shifts and scalar couplings. Assuming a perfect  $\pi/2$  pulse and a perfect composite  $\pi$  pulse, the density operator for an isolated spin with resonance offset  $\Delta\omega$  is, after the second delay:

$$\begin{aligned} \rho(2\tau) = & \exp(-iI_z\Delta\omega\tau)\exp(-iI_x\pi)\exp(2iI_z\phi)\exp(-iI_z\Delta\omega\tau)\exp(-iI_x\pi/2)I_z \\ & \times \exp(iI_x\pi/2)\exp(iI_z\Delta\omega\tau)\exp(-2iI_z\phi)\exp(iI_x\pi)\exp(iI_z\Delta\omega\tau) \end{aligned} \quad (V.1)$$

$$= -I_x \sin 2\phi + I_y \cos 2\phi \quad (V.2)$$

The echo sequence results in a spin state at  $2\tau$  that is independent of



XBL 845-1700

Figure V.2: Inversion as a function of the relative miscalibration of the rf amplitude for a single  $\pi$  pulse (simulations in the dotted line), the zeroth order composite  $\pi$  pulse  $180_0 180_{120} 180_0$  (experimental data in triangles, simulations in the dashed line), and the first order composite  $\pi$  pulse  $180_0 180_{105} 180_{210} 360_{59}$  (experimental data in heavy dots, simulations in the solid line). The inversion bandwidth increases with the order to which rf amplitude miscalibration effects are cancelled in the theory.

the evolution during the  $\tau$  periods. In other words, the resonance offset is "refocussed." In a one-dimensional spin echo experiment, the NMR free induction decay (FID) signal, i.e. the signal resulting from the free evolution of a spin system after preparation in a non-equilibrium state by rf pulses, is observed beginning at time  $2\tau$ , which is the peak of the echo. According to Eq.(II.75), the phase of the echo signal is  $2\phi + \pi/2$ . Thus, if  $\phi$  is a function of  $\delta\omega_1$ , then so is the phase of the echo signal.

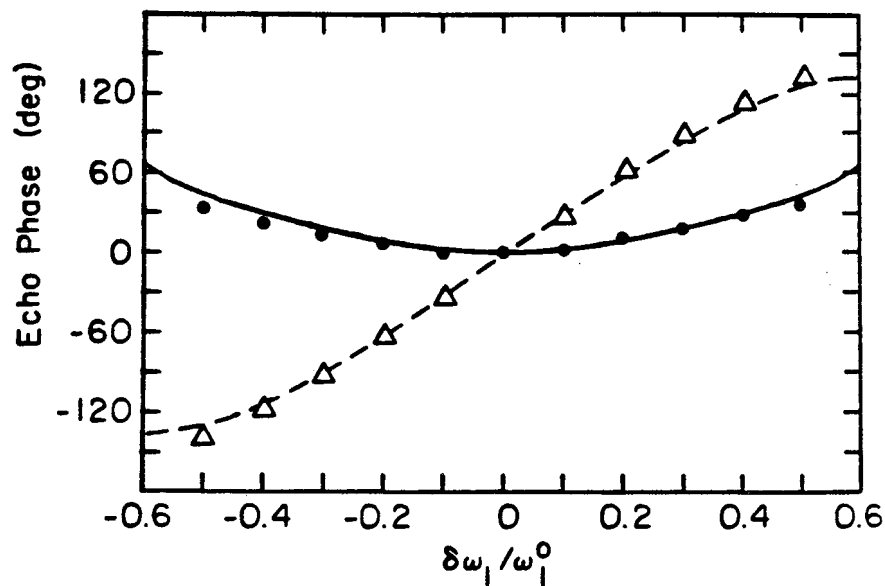
A striking example of the difference between composite pulses derived by the coherent averaging approach and those derived by other means is provided by a comparison of the results of spin echo experiments using  $180_0 180_{120} 180_0$  and  $90_0 360_{120} 90_0$  as refocussing pulses.  $90_0 360_{120} 90_0$  was derived by Levitt [22], as discussed in Chapter III.B. For  $90_0 360_{120} 90_0$ ,  $V^{(0)} = -\delta\omega_1 I_z / \sqrt{3}$ . Surprisingly, the two composite  $\pi$  pulses give the same inversion performance. The inversion  $W$  is:

$$W = -\cos^3 \theta + 3\sin^2 \theta (1 - \cos \theta) / 4 \quad (V.3)$$

$$\theta = (\omega_1^0 + \delta\omega_1) / \omega_1^0 \quad (V.4)$$

The phase of the echo as a function of  $\delta\omega_1$  for the two refocussing pulses is shown in Figure V.3. For variations of  $\delta\omega_1$  between  $-0.4\omega_1^0$  and  $0.4\omega_1^0$ , the echo phase varies over a range of  $224^\circ$  with  $90_0 360_{120} 90_0$ , but only  $31^\circ$  with  $180_0 180_{120} 180_0$ .

For  $180_0 180_{105} 180_{210} 360_{59}$ ,  $\phi = 105^\circ$  when  $\delta\omega_1 = 0$ . When  $180_0 180_{105} 180_{210} 360_{59}$  is used as a composite refocussing pulse, the echo phase varies over a range of  $16^\circ$  for  $-0.4\omega_1^0 < \delta\omega_1 < 0.4\omega_1^0$ .



XBL 845-1696

Figure V.3: The phase of the echo signal in a spin echo experiment using a composite  $\pi$  refocussing pulse, as a function of the relative miscalibration of the rf amplitude. Results are shown for two composite  $\pi$  pulses:  $180_0 180_{120} 180_0$ , with experimental data in dots and simulations in the solid line, and  $90_0 360_{120} 90_0$ , with experimental data in triangles and simulations in the dashed line. Although the two composite pulses invert longitudinal magnetization equally well, their performance in refocussing transverse magnetization is markedly different. The fact that the phase variations with  $180_0 180_{120} 180_0$  are less severe is a consequence of the theoretical method used in the derivation.

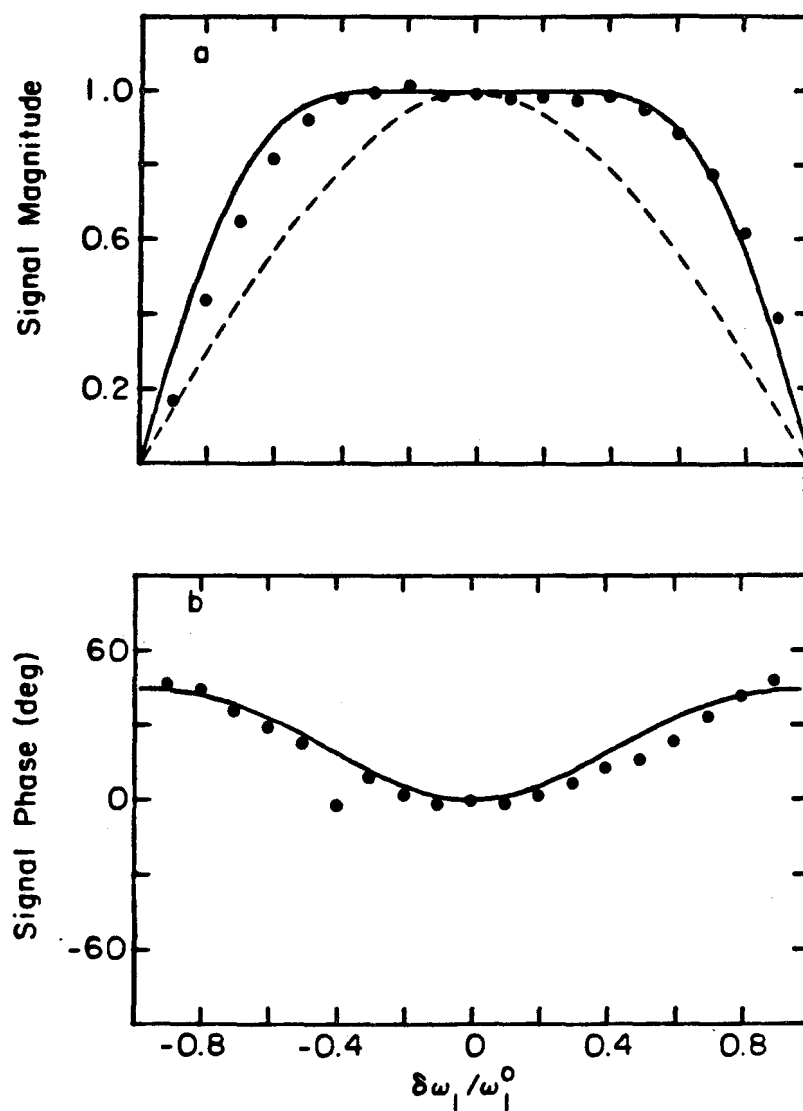


## 2. Composite $\pi/2$ pulses

Figures V.4a and V.5a are plots of the signal magnitude, as defined in Eq.(II.73), following excitation by composite  $\pi/2$  pulses as a function of  $\delta\omega_1$ . Results for two composite  $\pi/2$  pulses are shown. The first,  $90_0^{180}105^{180}315$ , has  $V^{(0)} = -\delta\omega_1(0.0071 I_x)$ . The second,  $270_0^{360}169^{180}33^{180}178$ , has  $V^{(0)} = \delta\omega_1(0.0001 I_x - 0.0002 I_z)$  and  $V^{(1)} = -(\delta\omega_1)^2(0.0003 I_y)/\omega_1^0$ . Again, the excitation bandwidth increases in going from a single  $\pi/2$  pulse to a zeroth order composite  $\pi/2$  pulse to a first order composite  $\pi/2$  pulse.

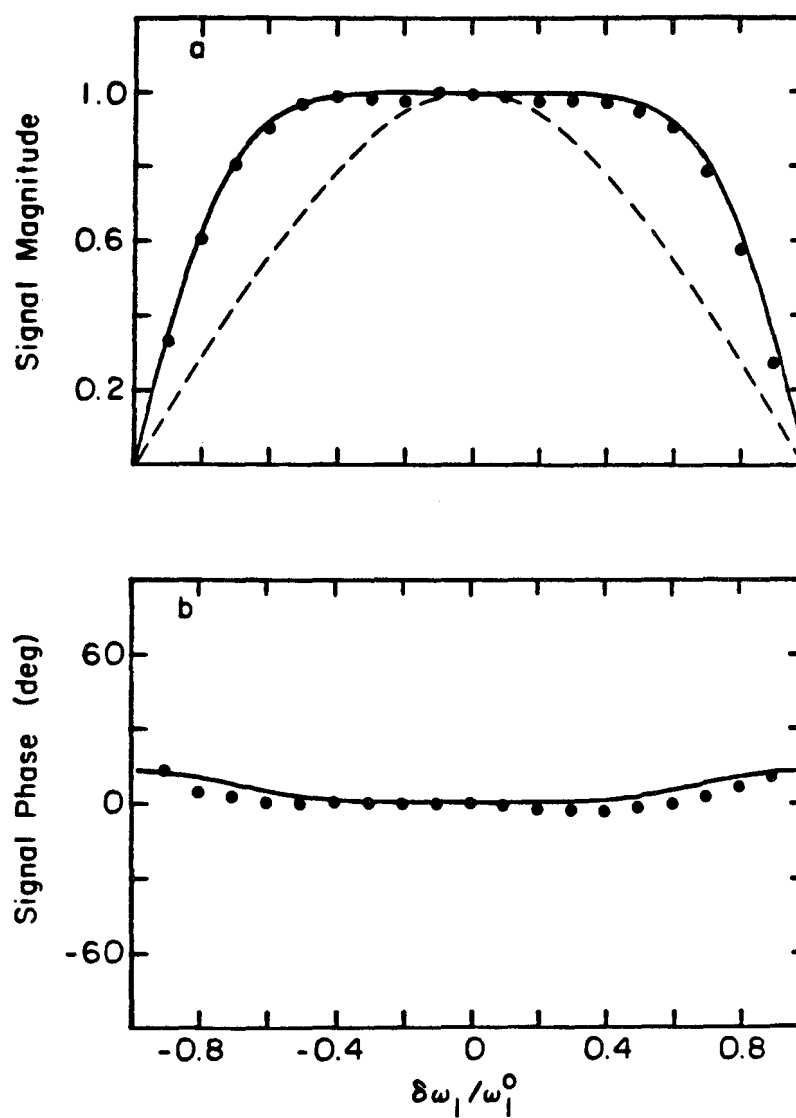
If the propagator for a composite  $\pi/2$  pulse is written in the form of Eq.(II.72), the signal phase after applying the pulse to a system of isolated spins at equilibrium is  $\phi_1 + 3\pi/2$ . This follows from Eqs.(II.74) and (II.75). Plots of the signal phase as a function of  $\delta\omega_1$  for the two sequences are given in Figures V.4b and V.5b. The sequence  $270_0^{360}169^{180}33^{180}178$  is particularly free of phase variations, reflecting the constancy of  $\phi_1$ , with the signal phase remaining within a range of  $15^\circ$  for  $-\omega_1^0 < \delta\omega_1 < \omega_1^0$ .

In the notation of Eq.(II.72),  $\phi_1 = 60^\circ$  and  $\phi_2 = 0$  for  $90_0^{180}105^{180}315$  when  $\delta\omega_1 = 0$ ;  $\phi_1 = 110^\circ$  and  $\phi_2 = 180^\circ$  for  $270_0^{360}169^{180}33^{180}178$ . While  $\phi_2$  does not affect the signal phase after excitation by a single composite  $\pi/2$  pulse, there are other experiments in which  $\phi_2$  does affect the phase. A simple example is a  $\pi/2-\tau_1-\pi/2-\tau_2$  spin echo sequence [60], using two identical composite  $\pi/2$  pulses. The density operator at the end of the sequence for a spin with resonance offset  $\Delta\omega$  is:



XBL B45-1697

Figure V.4: The signal magnitude (a) and phase (b) following excitation by the zeroth order composite  $\pi/2$  pulse  $90_{180}^{180}_{105}180_{315}$ , as a function of the relative rf amplitude miscalibration. Experimental data appears in dots and simulations in the solid lines. For comparison, the signal magnitude following a single  $\pi/2$  pulse is shown in the dashed line.



XBL 845-1696

Figure V.5: Same as Figure V.4, but for the first order composite  $\pi/2$  pulse  $270_0 360_{169} 180_{33} 180_{178}$ . The amount of phase variation decreases significantly as the theoretical order increases.

$$\rho(\tau_1 + \tau_2) = \exp(-iI_z \Delta\omega \tau_2) R(\phi_1, \phi_2) \exp(-iI_z \Delta\omega \tau_1) R(\phi_1, \phi_2) I R(\phi_1, \phi_2)^{-1} \\ \times \exp(iI_z \Delta\omega \tau_1) R(\phi_1, \phi_2)^{-1} \exp(iI_z \Delta\omega \tau_2) \quad (V.5)$$

$$= I_x \sin[\Delta\omega(\tau_1 + \tau_2) + \phi_2 + 2\phi_1] + \sin[\Delta\omega(\tau_1 - \tau_2) + \phi_2] / 2 \\ + I_y \cos[\Delta\omega(\tau_1 - \tau_2) + \phi_2] - \cos[\Delta\omega(\tau_1 + \tau_2) + \phi_2 + 2\phi_1] / 2 \\ - I_z \cos(\Delta\omega \tau_1 + \phi_2 + \phi_1) \quad (V.6)$$

with:

$$R(\phi_1, \phi_2) = \exp(-iI_z \phi_1) \exp(-iI_x \pi/2) \exp(-iI_z \phi_2) \quad (V.7)$$

The echo signal arises from the part of  $\rho(\tau_1 + \tau_2)$  that depends on  $\Delta\omega(\tau_1 - \tau_2)$ , and therefore becomes independent of  $\Delta\omega$  at  $\tau_1 = \tau_2$ . At  $\tau_1 = \tau_2$ , that part is  $\rho'$ :

$$\rho' = (I_x \sin \phi_2) / 2 + (I_y \cos \phi_2) / 2 \quad (V.8)$$

The echo phase is  $\pi/2 - \phi_2$ .

If the signal phase varies with the rf amplitude, and if rf amplitude inhomogeneity exists across the sample, then signals arising from different points in the sample may interfere destructively, thus attenuating or eliminating the advantages of broadband excitation with respect to the rf amplitude. This applies particularly to NMR studies using surface coils [56]. Surface coils are loops of wire placed near the surface of a sample. They are used to excite and detect signals when a small region beneath the surface of a large sample, most commonly tissue or organs within living animals, is of interest. The rf field along the axis perpendicular to the plane of the coil decreases with distance from the coil, i.e. it decreases with increasing depth into the sample. Sometimes it is desirable to use pulse sequences that

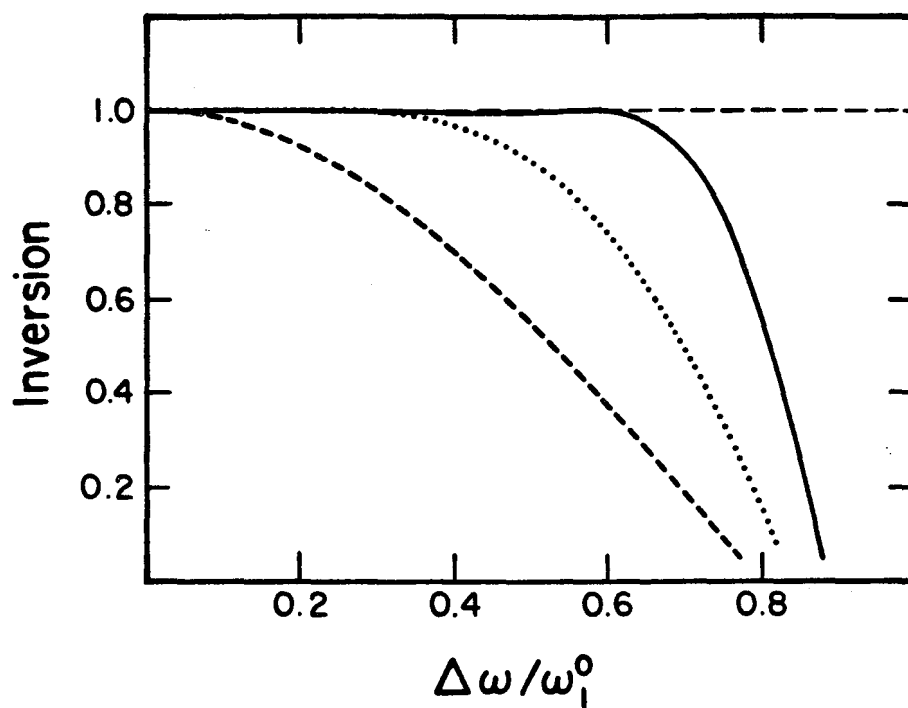
excite spins only over a narrow range of rf amplitudes in order to obtain the spectrum of a localized region in the sample, e.g. a particular organ. Such narrowband excitation sequences are developed in Chapter VIII. In other applications, it may be desirable to excite spins in as large a region as possible to maximize the signal-to-noise ratio, perhaps for examining metabolism in muscles close to the skin or organs that have been surgically exposed. Due to the intrinsic rf inhomogeneity, composite  $\pi/2$  and  $\pi$  pulses for broadband excitation with respect to the rf amplitude may be useful provided that signal phase variations do not lead to destructive interference.

### C. Resonance offsets

#### 1. Composite $\pi$ pulses

Zeroth order composite  $\pi$  pulses for resonance offsets have been treated in Chapter IV.C.2. Figure V.6 shows the inversion performance of the zeroth order sequence  $90_0 270_{90} 90_0$ , with  $V^{(0)} = 0$ , and the first order sequence  $336_0 246_{180} 10_{90} 74_{270} 10_{90} 246_{180} 336_0$ , with  $V^{(0)} = \Delta\omega(0.0005 I_x + 0.0010 I_y)$  and  $V^{(1)} = (\Delta\omega)^2(0.0002 I_x - 0.0001 I_y + 0.0001 I_z)/\omega_1^0$ . In a  $\pi/2$ - $\tau$ - $\pi$ - $\tau$  echo experiment, the first order sequence contributes less than  $1^\circ$  to the variation in the echo signal phase for resonance offsets between  $-0.6\omega_1^0$  and  $0.6\omega_1^0$ . As defined in Eq.(II.61),  $\phi = 135^\circ$  for  $90_0 270_{90} 90_0$  when  $\Delta\omega = 0$ ;  $\phi = -27^\circ$  for  $336_0 246_{180} 10_{90} 74_{270} 10_{90} 246_{180} 336_0$  when  $\Delta\omega = 0$ .

#### 2. Composite $\pi/2$ pulses



XBL 834-9140

Figure V.6: Simulations of inversion as a function of the relative resonance offset for a single  $\pi$  pulse (dashed line), the zeroth order composite  $\pi$  pulse  $90_0 270_{90} 90_0$ , and the first order composite  $\pi$  pulse  $336_0 246_{180} 10_{90} 74_{270} 10_{90} 246_{180} 336_0$ .

Figure II.3 shows that a single  $\pi/2$  pulse already compensates for resonance offset effects to a large extent, at least for the purpose of creating transverse magnetization. The amplitude of the FID signal following a single  $\pi/2$  pulse remains within 0.99 times its maximum for resonance offsets between  $0.9\omega_1^0$  and  $-0.9\omega_1^0$ . The signal phase varies by  $80^\circ$  over that range, but the phase is nearly a linear function of  $\Delta\omega$ . If the spectrum of a sample is obtained by Fourier transformation of the FID signal after a single  $\pi/2$  pulse, the lines arising from nuclei with various chemical shifts can be made to have the same phase by applying a linear phase correction to the spectrum, provided that the individual lines are resolved. If the lines are not resolved, however, it is not possible to correct the phases in the spectrum. Consider an FID signal of the following form:

$$S(t) = \int_{-\infty}^{+\infty} d\omega A(\omega) \exp(-i\omega t) \exp(-t/T_2) \quad (V.9)$$

where  $A(\omega)$  is the complex amplitude of the contribution to the total signal with frequency  $\omega$ .  $T_2$  is the transverse, or spin-spin, relaxation time, assumed to be constant over the spectrum. The spectrum  $F(\omega)$  is:

$$F(\omega) = \int_0^\infty dt \exp(i\omega t) S(t) \quad (V.10)$$

$$= \int_{-\infty}^{+\infty} d\omega' |A(\omega')| \exp[i\phi(\omega')] [f_1(\omega - \omega') + if_2(\omega - \omega')] \quad (V.11)$$

where:

$$f_1(\omega) = [T_2(\omega^2 + 1/T_2^2)]^{-1} \quad (V.12)$$

$$f_2(\omega) = \omega(\omega^2 + 1/T_2^2)^{-1} \quad (V.13)$$

$$A(\omega) = A(\omega) \exp[i\phi(\omega)]$$

$f_1(\omega)$  is a Lorentzian absorption lineshape.  $f_2(\omega)$  is a dispersion lineshape. The spectrum is a superposition of absorption/dispersion pairs centered at each frequency  $\omega'$  with an amplitude  $A(\omega')$  and a phase  $\phi(\omega')$ . In a properly phased spectrum,  $\phi(\omega') = 0$  for all  $\omega'$ . Then all the absorption components are in the real part of  $F(\omega)$  and all the dispersion components are in the imaginary part. If the lines in the spectrum are resolved,  $A(\omega')$  is a sum of delta functions centered at widely separated frequencies. Then:

$$F(\omega) = \sum_n a_n \exp[i\phi(\omega_n)] [f_1(\omega - \omega_n) + if_2(\omega - \omega_n)] \quad (V.14)$$

where the sum is over the resolved lines centered at frequencies  $\omega_n$ .  $a_n$  is the real amplitude of the line at  $\omega_n$ . If  $F(\omega)$  is multiplied by  $\exp[-in(\omega)]$  with  $n(\omega_n) = \phi(\omega_n)$ , the spectrum becomes properly phased at all frequencies  $\omega_n$ , although the phase may still be distorted at intermediate frequencies where the spectral intensity is small. If individual lines are not resolved, however, the spectrum can not be properly phased by multiplying by a phase correction. Significant contributions to the spectral intensity at  $\omega$  arises not only from a line centered at  $\omega$ , but also from the wings of lines centered elsewhere.

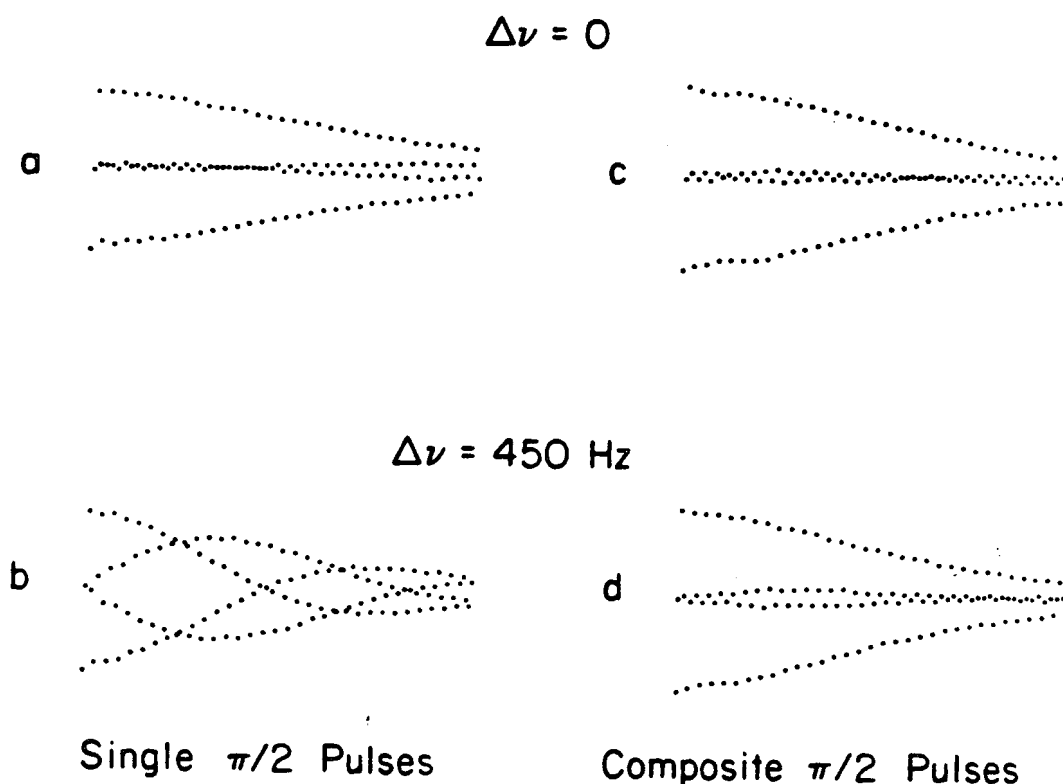
NMR imaging [57-59] is an important case where resolved lines are not to be expected. Static field gradients produce a continuum of transition frequencies. A common trick to eliminate linear phase variations resulting from excitation in a field gradient is to reverse the gradient direction for a short time after the rf pulse [62].



Composite  $\pi/2$  pulses that produce constant net rotations and thus prepare transverse magnetization with a uniform phase may make such gradient switching unnecessary. In addition, gradient switching does not correct for phase variations that are not a linear function of  $\Delta\omega$ .

Other possible applications of composite  $\pi/2$  pulses in which a constant net rotation is essential include multiple pulse line-narrowing [34-45] and time-reversal [45-47] sequences. Such sequences are usually employed in solid state NMR. The discussion in section A indicated that resonance offsets are usually negligible in solid state NMR. However, line-narrowing and time-reversal sequences are used in conjunction with static field gradients in solid state NMR imaging [63,64]. The field gradients may be large enough that the resonance offsets do become considerable, making composite  $\pi/2$  pulses that compensate for resonance offsets applicable. As discussed in Chapter IV.A, line-narrowing and time-reversal sequences work by averaging the internal spin Hamiltonian over a deliberately chosen series of rotations in the toggling frame [34,35,37]. If the net rotation of a composite  $\pi/2$  pulse varies with offset in a general way, it can not be incorporated into multiple pulse techniques.

A simple demonstration of a composite  $\pi/2$  pulse in a multiple pulse experiment is shown in Figure V.7. The composite  $\pi/2$  pulse is  $385_0 320_{180} 25_0$ , for which  $V^{(0)} = \Delta\omega(0.0026 I_z + 0.0026 I_y)$  and  $V^{(1)} = -(\Delta\omega)^2(0.0026 I_x)/\omega_1^0$ . The experiment consists of applying a train of  $\pi/2$  pulses separated by delays, with the signal being sampled once in the center of each delay. This is a commonly used technique for calibrating and adjusting rf amplitudes [65]. When the pulses are applied on resonance, a characteristic signal pattern of three lines



XBL 845-1695

Figure V.7: Signal traces generated by applying a train of closely spaced  $\pi/2$  (a,b) and composite  $\pi/2$  (c,d) pulses to a small bulb of  $\text{H}_2\text{O}(l)$ , with the signal sampled once after each  $\pi/2$  pulse. The composite  $\pi/2$  pulse is  $385_0 320_{180} 25_0$ , designed to be free of resonance offset effects to first order in the theory. In a and c, the pulses are applied on resonance with an rf amplitude of 3 kHz. In b and d, the pulses are off resonance by 450 Hz. The signal trace in b exhibits an obvious offset dependence; the trace in d is largely unaffected by the offset, due to the absence of appreciable phase distortion in the composite  $\pi/2$  pulse.

results. In Figures V.7a and V.7b, it is apparent that the signal pattern deteriorates considerably at resonance offsets of  $0.15\omega_1^0$  when single  $\pi/2$  pulses are used. This is primarily due to variations in the net rotation of the  $\pi/2$  pulses rather than free evolution during the delays, since long  $\pi/2$  pulses (84  $\mu$ s) and short delays (20  $\mu$ s) were used. When composite  $\pi/2$  pulses are substituted for the single  $\pi/2$  pulses, the signal pattern becomes much less sensitive to the resonance offset, as shown in Figures V.7c and V.7d. Again, 20  $\mu$ s delays were used, but the length of each composite  $\pi/2$  pulse was 688  $\mu$ s, so that the signal patterns in Figures V.7c and V.7d represent a longer time than those in V.7a and V.7b.

#### D. The importance of constant net rotations

The arguments in sections B and C demonstrate the need for composite pulses that produce constant net rotations when the simplest one- and two-pulse experiments are performed in the presence of static or rf field gradients. For the sake of completeness, however, it is appropriate to point out that there are situations in which a constant net rotation is not essential.

In some cases, the phase of detected signals is unaffected by the

specific values of  $\phi$  in Eq.(II.61) or  $\phi_1$  and  $\phi_2$  in Eq.(II.72). These cases include the use of composite  $\pi$  pulses for inversion-recovery measurements of spin-lattice relaxation times [19,20] and for heteronuclear decoupling [24,25,29-32]. In other cases, composite pulses are used to overcome a miscalibration of the rf amplitude [28], rather than true rf inhomogeneity. Then the rotation produced by any composite pulse is constant throughout the sample, not because of an intrinsic property of the composite pulse, but simply because the rf amplitude does not vary.

Sometimes the signal phase can be made constant by using multiple composite pulses. This has been demonstrated in multiple spin echo (Carr-Purcell) trains [21], i.e.  $\pi/2-\tau-\pi-2\tau-\pi-2\tau-\dots$ . In such a sequence, only the phase of odd numbered echoes depends on the net rotation axis of the composite  $\pi$  pulse. If only even numbered echoes are observed, there are no signal phase variations induced by the composite  $\pi$  pulses. Similarly, if the single echo sequence  $\pi/2-\tau-\pi-\tau$  is changed to  $\pi/2-\tau-\pi-\tau-\pi$ , the phase of the echo signal becomes independent of  $\phi$ . This is easily seen by examining the density operator  $\rho'(2\tau)$  created by the modified echo sequence.  $\rho'(2\tau)$  is related to  $\rho(2\tau)$  in Eq.(V.1) by:

$$\rho'(2\tau) = \exp(-iI_x\pi)\exp(2iI_z\phi)\rho(2\tau)\exp(-2iI_z\phi)\exp(iI_x\pi) \quad (V.15)$$

$$= -I_y \quad (V.16)$$

Experimentally, it is preferable to use the simpler  $\pi/2-\tau-\pi-\tau$  sequence, however, since the additional composite  $\pi$  pulse in the  $\pi/2-\tau-\pi-\tau-\pi$  sequence may aggravate the effects of pulse imperfections. The

$\pi/2$ - $\tau$ - $\pi$ - $\tau$  sequence also has the advantage of avoiding distortions in the spectrum due to pulse ringdown.

Levitt and Ernst have suggested general principles for incorporating composite pulses into various multiple-quantum, polarization transfer, and two-dimensional NMR techniques in such a way that most effects of variable net rotations cancel between pairs of composite pulses [66]. The composite pulses must be carefully matched. In particular, it is necessary to form composite pulse pairs whose propagators are inverses of one another. If resonance offsets are negligible and the composite pulses compensate for rf inhomogeneity, the inverse of a given pulse sequence is formed by reversing the order of the pulses and phase-shifting them by  $\pi$ . If resonance offsets are significant, an exact inverse can not be constructed by any general method, although an approximate method is demonstrated.

The methods of Levitt and Ernst primarily prevent the effects of variable rotations from accumulating over several composite pulses and allow composite  $\pi/2$  pulses that do not produce rotations by  $\pi/2$  about an axis in the xy plane to be used. Often the signal phase remains sensitive to variations in the net rotation of the final composite pulse, however. Thus, the problems of destructive interference and of improper spectral phasing remain. In addition, the effects of variable rotations can not be cancelled in single pulse,  $\pi/2$ - $\tau$ - $\pi$ - $\tau$  echo, and multiple pulse experiments.

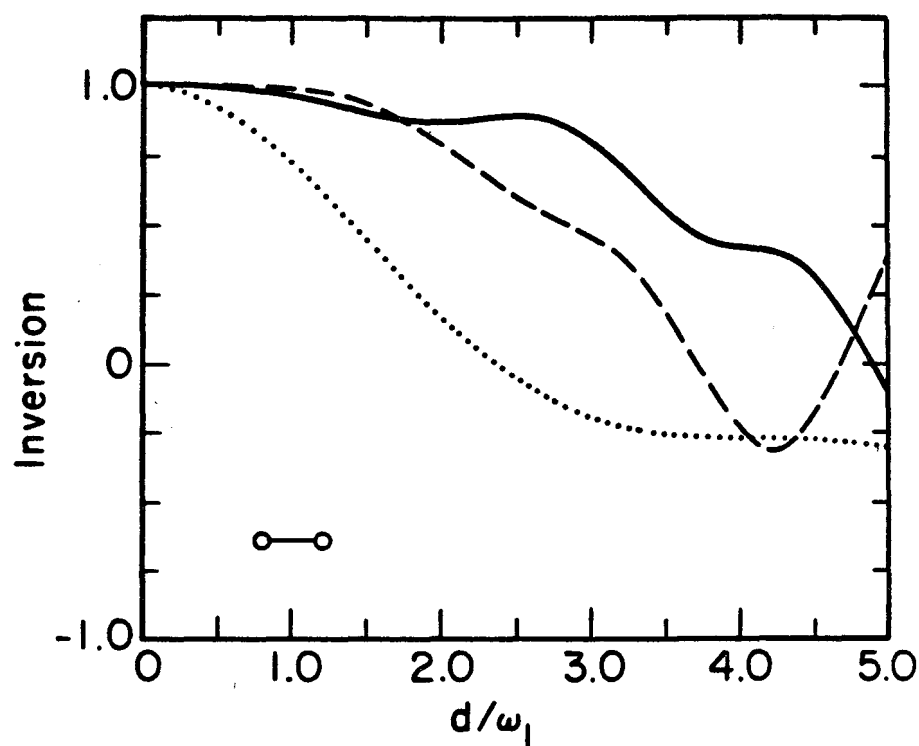
Finally, composite pulses that produce constant rotations prove to be important as models for the design of composite excitation sequences in Chapter VI.

## E. Dipole and quadrupole couplings

### 1. Composite $\pi$ pulses

Figure V.8 shows simulations of the inversion performance as a function of the relative dipole coupling constant in a system of a pair of equivalent spin-1/2 nuclei for two composite  $\pi$  pulses and for a single  $\pi$  pulse. The composite pulses are  $45_0 180_{90} 90_{180} 180_{90} 45_0$ , for which  $V^{(0)} = 0$ , and  $180_0 180_{120} 180_0$ , for which  $V^{(0)} = 0.25 V$ , with  $V$  given by Eq.(IV.25).  $180_0 180_{120} 180_0$  satisfies the requirement  $[V^{(0)}, I_z] = 0$ , rather than  $V^{(0)} = 0$ , as discussed in Chapter IV.C.4. Recall that  $180_0 180_{120} 180_0$  also compensates for rf inhomogeneity to zeroth order, as seen in section B.1. Both  $45_0 180_{90} 90_{180} 180_{90} 45_0$  and  $180_0 180_{120} 180_0$  provide substantial improvements in inversion performance over a single  $\pi$  pulse. Good inversion is accomplished with couplings that are as large as  $2\omega_1$ . The results in Figure V.8 apply identically to the inversion of a quadrupolar spin-1 nucleus, substituting  $2\omega_Q/\omega_1$  for  $d/\omega_1$  on the abscissa. The equivalence of a spin-1 nucleus and a pair of coupled spin-1/2 nuclei is apparent from a comparison of Eq.(IV.26) with Eq.(IV.52) and from the discussion in Chapter IV.C.4.

An interesting feature of Figure V.8 is that  $180_0 180_{120} 180_0$  gives slightly better inversion for small couplings than  $45_0 180_{90} 90_{180} 180_{90} 45_0$ . It is possible that the presence of a non-zero  $V^{(0)}$  term truncates the higher-order terms in the Magnus expansion. For example, if  $V^{(0)}$  is much larger than  $V^{(1)}$ , then only those components of  $V^{(1)}$  that commute with  $V^{(0)}$  will significantly affect the inversion. Such an effect is reminiscent of the "second averaging" technique commonly employed in



XBL 841-301

Figure V.8: Simulations of population inversion for a system of two dipole coupled spin-1/2 nuclei as a function of the ratio of the coupling constant  $d$  to the applied rf amplitude  $\omega_1$ . Results are shown for a single  $\pi$  pulse (dotted line), a  $45_0 180_{90} 90_{180} 180_{90} 45_0$  composite  $\pi$  pulse (solid line), and a  $180_0 180_{120} 180_0$  composite  $\pi$  pulse (dashed line).

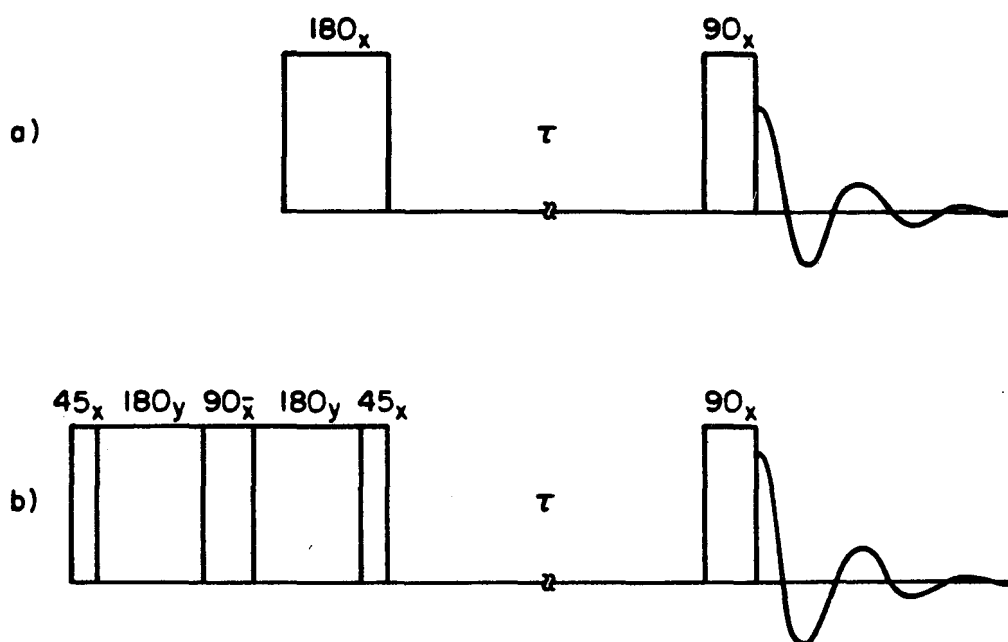
multiple pulse line-narrowing experiments in solid state NMR [35,67]. In second averaging, a deliberately large resonance offset term in  $V^{(0)}$  is introduced to truncate higher-order correction terms.

Figure V.9 illustrates pulse sequences used to experimentally contrast the inversion performance of composite  $\pi$  pulses against that of a single  $\pi$  pulse. Spins initially at equilibrium are inverted by a  $\pi$  (V.9a) or composite  $\pi$  (V.9b) pulse. Coherences dephase during a delay  $\tau$ , leaving the spin system in a state describable by a density operator that commutes with  $I_z$ . The FID signal is then collected following a  $\pi/2$  pulse and Fourier transformed to give the spectrum. Spectral distortions at low rf power reflect imperfect inversion. The sequence of Figure V.9a is commonly used to study spin-lattice relaxation. Figure V.9b represents the analogous experiment employing a composite  $\pi$  pulse.

Figure V.10 shows simulations of powder pattern spectra resulting from the sequence of Figure V.9a applied to an isotropic orientational distribution of pairs of spin-1/2 nuclei. The usual Pake pattern [68] results from the  $3\cos^2\theta - 1$  dependence of the dipolar coupling constant on the angle between the static magnetic field and the internuclear displacement vector. Here the maximum coupling is taken to be  $d/2\pi = 80$  kHz. Clearly, the characteristic spectral features are lost as the rf amplitude is reduced.

Figure V.10 also shows simulated spectra resulting from the sequence of Figure V.9b. The spectral distortion at low rf amplitudes is dramatically reduced by the substitution of a composite  $\pi$  pulse for a single  $\pi$  pulse. The composite  $\pi$  pulse  $180_0 180_{120} 180_0$  gives essentially the same results.





XBL 841-296

Figure V.9: Schematic representation of the pulse sequences used in the simulations of Figure V.10 and the experiments of Figures V.11 and V.13. a) Spins are inverted by a  $\pi$  pulse. Coherences, which are created at low rf amplitudes, dephase during a delay  $\tau$ . The FID signal after the final  $\pi/2$  pulse is digitized and Fourier transformed to give a spectrum that reflects the inversion efficiency of the initial  $\pi$  pulse. b) Same as (a), but with a  $45_0 180_{90} 90_{180} 180_{90} 45_0$  composite  $\pi$  pulse in place of the single  $\pi$  pulse.

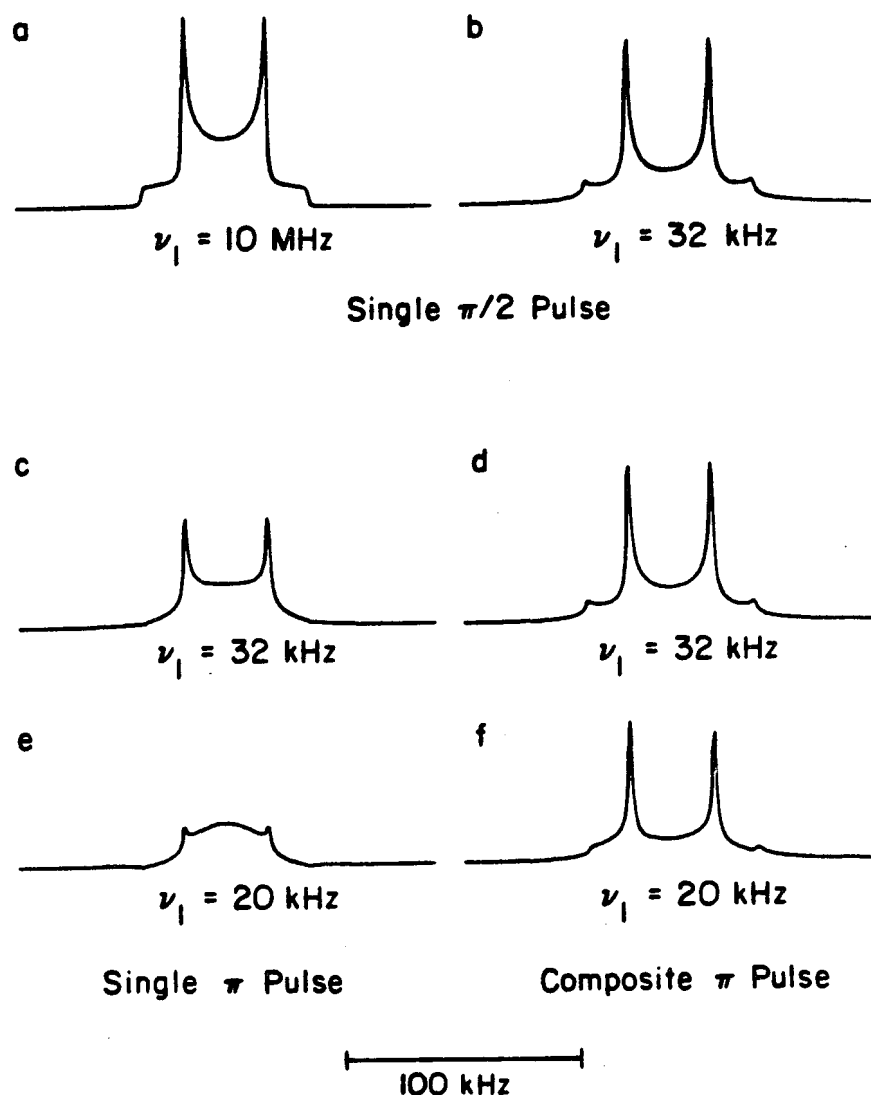


Figure V.10: Simulated NMR spectra of an isotropic orientational distribution of pairs of dipole coupled spin-1/2 nuclei. The maximum coupling is  $d_{\max}/2\pi = 80$  kHz. 1 kHz line-broadening is added. a) Spectrum after a single  $\pi/2$  pulse, with  $\omega_1/2\pi = \nu_1 = 10,000$  kHz. Since  $\omega_1 \gg d_{\max}$ , the spectrum is undistorted. b) Spectrum after a single  $\pi/2$  pulse, with  $\nu_1 = 32$  kHz, illustrating the distortion resulting from a  $\pi/2$  pulse alone at low rf amplitudes. c) Spectrum resulting from sequence a of Figure V.9 with  $\nu_1 = 32$  kHz. d) Spectrum resulting from sequence b with  $\nu_1 = 32$  kHz. e) Spectrum from sequence a with  $\nu_1 = 20$  kHz. f) Spectrum from sequence b with  $\nu_1 = 20$  kHz. The characteristic features of the spectrum, which are lost by a single  $\pi$  pulse at low rf amplitudes, are preserved by a composite  $\pi$  pulse.

The slight asymmetry in the spectrum in Figure V.10f resulting from the composite  $\pi$  pulse requires some explanation. Suppose the coupled spin system is initially described by a density operator  $I_z$ . When a weak pulse sequence is applied to the spin system, the presence of the couplings interferes with the action of the applied rf in such a way that the magnitude of the expectation value of the spin angular momentum changes. In other words, the magnetization shrinks. The density operator evolves into not only a linear combination of  $I_x$ ,  $I_y$ , and  $I_z$ , but also into non-observable coherences and non-equilibrium populations. One part of the non-equilibrium populations is dipolar order [69]. Dipolar order is defined to be a component of the density operator proportional to the dipole coupling term in the Hamiltonian. The spectrum of a dipolar ordered, two-spin state is antisymmetric about the center.

The asymmetry is absent in the spectra resulting from a single  $\pi$  pulse. It can be proved that there can be no dipolar order produced by a single  $\pi$  pulse, regardless of the rf amplitude. The amount of dipolar order is proportional to  $D$ , where:

$$D = \text{Tr}[VU(\tau)I_zU(\tau)^{-1}] \quad (\text{V.17})$$

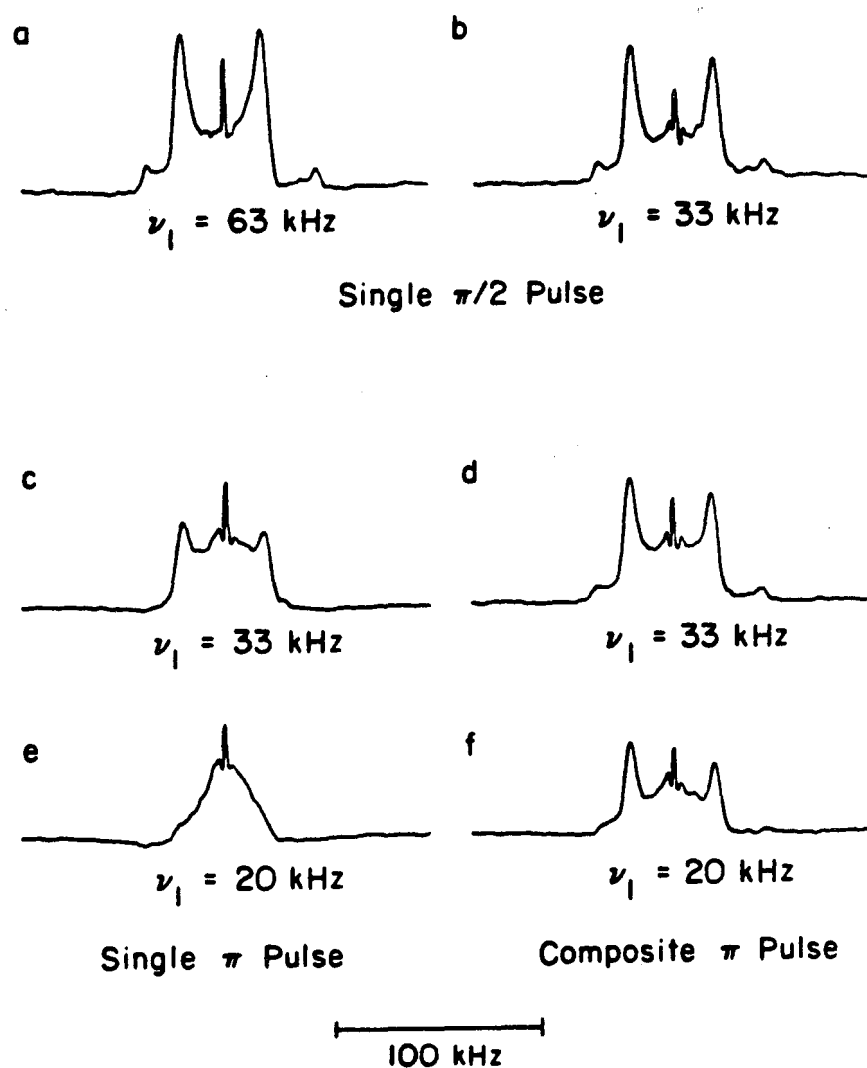
$V$  is given by Eq.(IV.25).  $U(\tau)$  is the propagator for a weak  $180_0$  pulse. Since the trace is invariant to a unitary transformation, all of the operators on the right side of Eq.(V.17) can be rotated by an angle  $\pi$  about the  $x$  axis without changing the validity of the equation. Since that rotation changes  $I_z$  to  $-I_z$  and leaves all the other operators unchanged, the result  $D = -D$  is obtained, implying that  $D = 0$ . The

proof may be extended to show that no dipolar order is created by any pulse sequence in which the rf phase only takes on the values  $\phi$  and  $\phi + \pi$ .

Figure V.11 shows proton NMR spectra of  $\text{Ba}(\text{ClO}_3)_2 \cdot \text{H}_2\text{O}$  powder obtained with the sequences of Figure V.9 applied at two different rf amplitudes. The delay  $\tau$  in Figure V.9 is here taken to be 5 ms. As predicted by the simulations, the spectral distortion with weak rf is quite obviously reduced by the use of a composite  $\pi$  pulse.

The spectrum of  $\text{Ba}(\text{ClO}_3)_2 \cdot \text{H}_2\text{O}$  reflects the fact that individual  $\text{H}_2\text{O}$  molecules are essentially isolated from one another, giving a Pake pattern characteristic of pairs of protons. The experimental pattern is somewhat distorted from the ideal pattern assumed in the simulations by two factors. The first of these is the presence of couplings between  $\text{H}_2\text{O}$  molecules. Such intermolecular couplings have the effect of broadening each individual transition, as reviewed in reference 70. The second factor is the presence of chemical shift anisotropy. The proton chemical shift anisotropy for  $\text{H}_2\text{O}$  in ice has been measured to be about 34 ppm [71]. The sharp peak in the center of the  $\text{Ba}(\text{ClO}_3)_2 \cdot \text{H}_2\text{O}$  spectra arises from residual protons and from  $\text{H}_2\text{O}$  molecules that are free to reorient rapidly and isotropically.

The delay  $\tau$  of 5 ms was chosen to be long compared to the dephasing time ( $T_2$ ) but short compared to the spin-lattice relaxation time ( $T_1$ ).  $T_1$  in  $\text{Ba}(\text{ClO}_3)_2 \cdot \text{H}_2\text{O}$  at room temperature is approximately 10 s. Measurements of  $T_{1d}$ , the relaxation time for dipolar order, using the Jeener-Broekaert technique [69], indicate that  $T_{1d}$  is about equal to  $T_1$ . Hence, a slight asymmetry in the composite  $\pi$  pulse spectra in Figure V.11 is observed, due to the presence of dipolar order. Similar



XBL 841-302

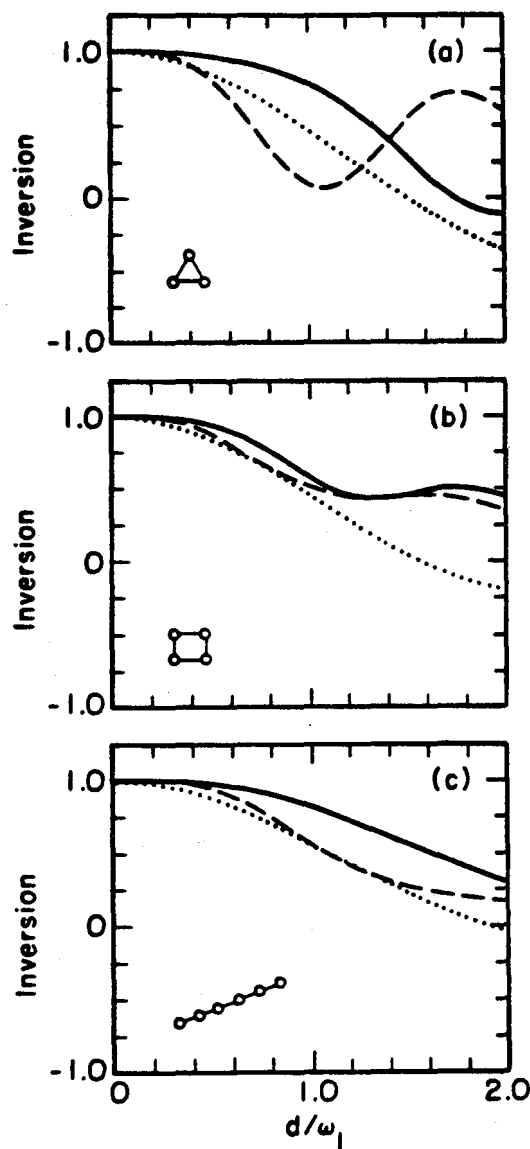
Figure V.11: Experimental proton NMR spectra of  $\text{Ba}(\text{ClO}_3)_2 \cdot \text{H}_2\text{O}$  powder. All spectra are the averages of 60 scans, with a recycle delay of 30 s. a) Spectrum after a single  $\pi/2$  pulse with  $\nu_1 = 63 \text{ kHz}$ . b) Spectrum after a single  $\pi/2$  pulse with  $\nu_1 = 33 \text{ kHz}$ . c) Spectrum from sequence a of Figure V.9 with  $\nu_1 = 33 \text{ kHz}$ . d) Spectrum from sequence b with  $\nu_1 = 33 \text{ kHz}$ . e) Spectrum from sequence a with  $\nu_1 = 20 \text{ kHz}$ . f) Spectrum from sequence b with  $\nu_1 = 20 \text{ kHz}$ . The principal features of the simulations in Figure V.10 are reproduced.

experimental results to those in Figure V.11 were obtained using the  $180_0 180_{120} 180_0$  sequence.

The results in Figures V.8, V.10, and V.11 indicate that zeroth order composite  $\pi$  pulses invert spin populations over a much larger range of couplings than a single  $\pi$  pulse in two-spin systems. This is important because, even in a many-spin system, the strongest couplings may be arranged in pairs, for example as methylene groups in an organic solid. The fact that the two-spin results apply identically to quadrupolar spin-1 nuclei makes the composite  $\pi$  pulses useful in deuterium and  $^{14}\text{N}$  NMR as well.

Coupled spins occur in other configurations, however. For composite  $\pi$  pulses to be of general use in solid state NMR, they should provide an advantage over a single  $\pi$  pulse in an arbitrary coupled system. Therefore, the inversion performance of composite  $\pi$  pulses in systems of more than two coupled spin-1/2 nuclei is investigated.

Figure V.12 presents the results of computer simulations of the inversion performance of the  $45_0 180_{90} 90_{180} 180_{90} 45_0$  and  $180_0 180_{120} 180_0$  composite  $\pi$  pulses, as well as that of a single  $\pi$  pulse, in three different spin systems. The spin system of Figure V.12a consists of three spin-1/2 nuclei arranged in an equilateral triangle perpendicular to the applied static field, so that all dipole coupling constants are equal. Figure V.12b represents a system of four spin-1/2 nuclei in a square, again perpendicular to the applied field. The coupling constants are taken to be proportional to  $r_{ij}^{-3}$ , where  $r_{ij}$  is the distance between nucleus  $i$  and nucleus  $j$ . The spin system of Figure V.12c is a straight row of six, equally spaced spin-1/2 nuclei. Again, the coupling constants are proportional to  $r_{ij}^{-3}$ .



XBL 841-299

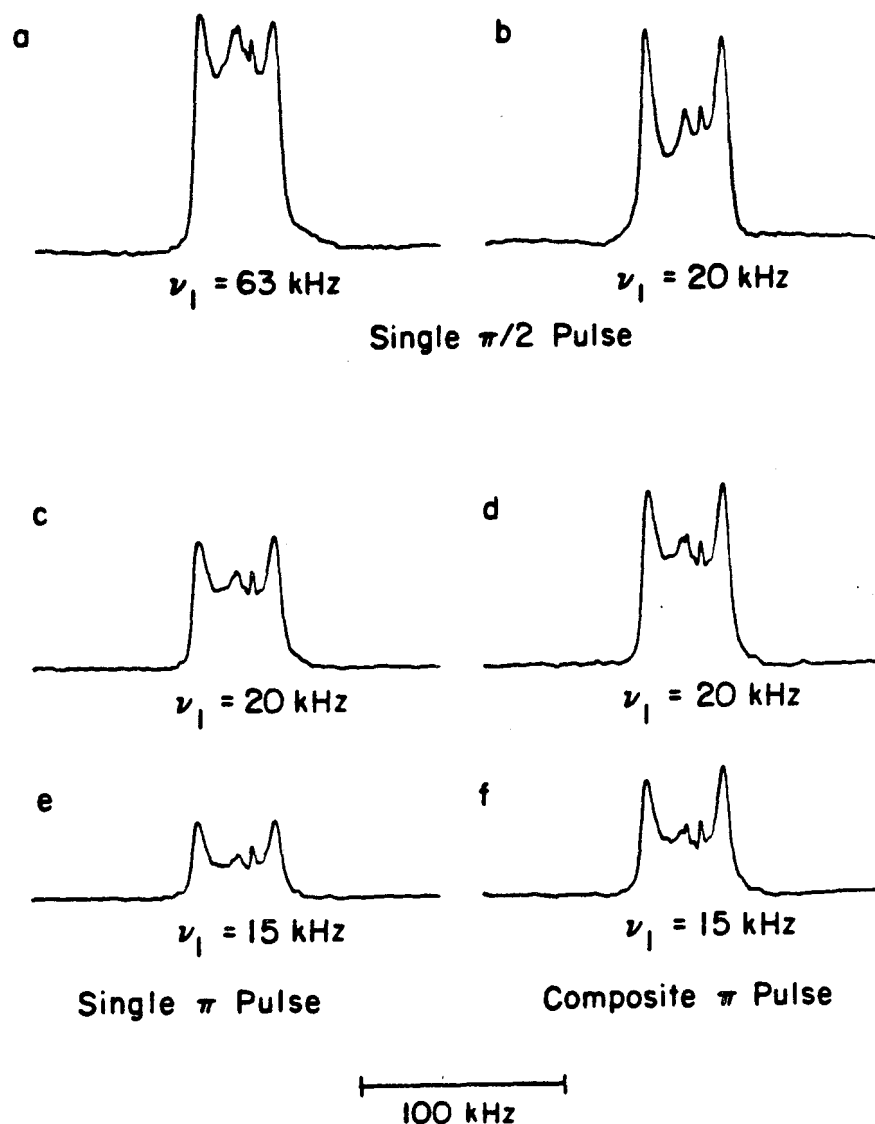
Figure V.12: Simulations of inversion as a function of the ratio of the nearest-neighbor dipole coupling constant  $d$  to the rf amplitude  $\omega_1$  for three possible systems of coupled spin-1/2 nuclei. Results are shown for a single  $\pi$  pulse (dotted lines), a  $45_0 180_{90} 90_{180} 180_{90} 45_0$  composite  $\pi$  pulse (solid lines), and a  $180_0 180_{120} 180_0$  composite  $\pi$  pulse (dashed lines). a) Three spins in an equilateral triangle. b) Four spins in a square. c) Six spins in a row. Coupling constants are taken to be proportional to  $r_{ij}^{-3}$ , where  $r_{ij}$  is the distance between nuclei  $i$  and  $j$ .

In all cases considered, both composite  $\pi$  pulses give better inversion than a single  $\pi$  pulse over some range of couplings. Generally speaking, the  $45_0 180_{90} 90_{180} 180_{90} 45_0$  sequence is the more effective of the two. Note that the range of nearest-neighbor couplings over which good inversion is achieved is substantially smaller than in the two-spin case, for the single  $\pi$  as well as the composite  $\pi$  pulses.

Experimental spectra resulting from the sequences of Figure V.9 applied to a single crystal squaric acid ( $C_4O_4H_2$ ) sample are shown in Figure V.13. In the crystal, squaric acid molecules are arranged in planes in such a way that the hydrogen nuclei, or protons, form chains perpendicular to the molecular planes. The spacing between adjacent protons in a chain is known to be  $2.636 \text{ \AA}$  [72]. Squaric acid has been the subject of NMR [73,74] and other [75,76] studies, in particular due to the observation of a structural phase transition at 370 K which exhibits critical behavior suggestive of a two-dimensional system [75,76]. Squaric acid was chosen for demonstration purposes because it is a true many-spin solid, yet there is resolved structure in its proton NMR spectrum. The spectra in Figure V.13 resulting from the sequence of Figure V.9b have greater overall intensity at low rf amplitudes than those resulting from the sequence of Figure V.9a.

It is worth emphasizing that the spectra in Figure V.13 are from a single crystal, although they superficially resemble a powder pattern. In a powder pattern, as in Figure V.11, the features of the spectrum furthest from the center result from spin pairs with the largest couplings. Therefore, those features are lost first due to poor inversion at low rf amplitudes. The squaric acid spectrum, on the other hand, is the product of an essentially infinite network of coupled





XBL 841-303

Figure V.13: Experimental proton NMR spectra of a squaric acid crystal. All spectra are the averages of 20 scans, with a recycle delay of 30 s. The narrow peak to the right of center of each spectrum results from residual protons. a) Spectrum after a single  $\pi/2$  pulse with  $\nu_1 = 63$  kHz. b) Spectrum after a single  $\pi/2$  pulse with  $\nu_1 = 20$  kHz. Low rf amplitude results in a loss of intensity from the center of the spectrum. c) Spectrum from sequence a of Figure V.9 with  $\nu_1 = 20$  kHz. d) Spectrum from sequence b with  $\nu_1 = 20$  kHz. e) Spectrum from sequence a with  $\nu_1 = 15$  kHz. f) Spectrum from sequence b with  $\nu_1 = 15$  kHz. Use of the composite  $\pi$  pulse results in greater overall intensity, reflecting a more complete inversion.

spins, with the strongest couplings occurring along chains. Each of the individual, unresolved transitions that make up the spectrum is a transition of the spin system as a whole, so that it should not be expected that the outer spectral features would be attenuated at low rf amplitudes.

For the squaric acid experiments, a delay  $\tau$  of 5 ms was used. The crystal was doped with chromium to reduce the proton  $T_1$  to approximately 10 s. The crystal was oriented with the b axis parallel to the static magnetic field. In this orientation, the proton chains are parallel to the field, giving the strongest possible couplings.

## 2. Composite $\pi/2$ pulses

Two composite  $\pi/2$  pulses for broadband excitation in coupled spin systems have been derived with the coherent averaging approach. With  $V = dT_{20}$ , the sequence  $45_0^{135}180^{135}90^{45}270$  has  $V^{(0)} = d[-0.0056 T_{20} - 0.0069 (T_{22} + T_{2-2})]$ . The sequence  $180_{90}^{180}270^{148}0^{86}180^{28}0$  has  $V^{(0)} = d[0.13063 T_{20} + 0.00014i (T_{21} + T_{2-1}) - 0.00049 (T_{22} + T_{2-2})]$ . The irreducible tensor components  $T_{lm}$  are defined in Eqs.(IV.54), (IV.59), and (IV.60). Theoretical signal amplitudes from a system of two coupled spin-1/2 nuclei following excitation by the two composite  $\pi/2$  pulses are plotted as a function of the relative coupling constant in Figure V.14.

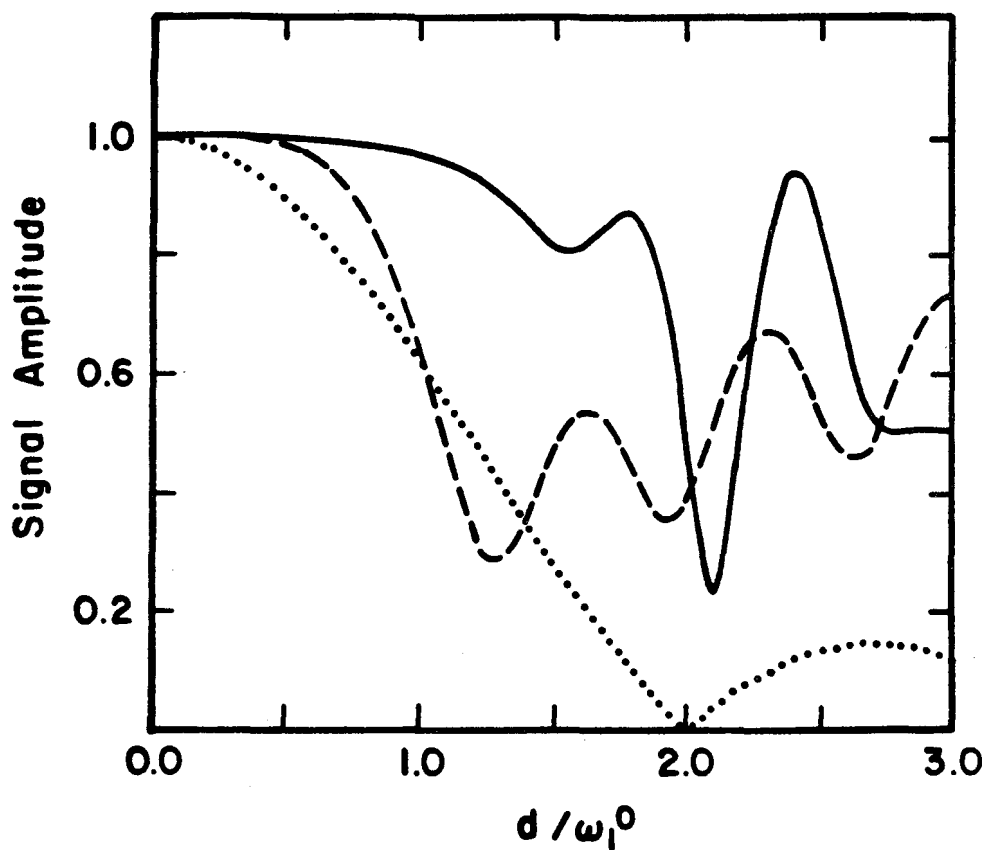


Figure V.14: Simulations of the signal amplitude immediately following excitation by a single  $\pi/2$  pulse (dotted line), a  $45_0 135_{180} 135_{90} 45_{270}$  composite  $\pi/2$  pulse (dashed line), and a  $180_{90} 180_{270} 148_0 86_{180} 28_0$  composite  $\pi/2$  pulse (solid line), as a function of the relative dipole coupling constant in a system of identical pairs of coupled spin-1/2 nuclei.

For comparison, the signal amplitude following excitation by a single  $\pi/2$  pulse is plotted as well.  $45_0^{135}180^{135}90^{45}270$  offers an advantage over a single  $\pi/2$  pulse only over a small range of couplings, while  $180_0^{180}270^{148}0^{86}180^{28}0$  performs considerably better. As suggested in the preceding section, it is possible that the presence of a non-zero  $V^{(0)}$  with  $[V^{(0)}, I_z] \neq 0$  helps the performance by truncating higher-order Magnus expansion terms. The higher-order terms may be particularly unfavorable for  $45_0^{135}180^{135}90^{45}270$ .

Plots such as those in Figure V.14 do not give a complete characterization of the usefulness of composite  $\pi/2$  pulses for obtaining spectra in spin systems with large couplings. The signal amplitude immediately after the composite  $\pi/2$  pulse is proportional to the area of the spectrum if the spectrum is obtained by Fourier transformation of the FID. The signal amplitude arises only from the  $I_x$  and  $I_y$  components of the density operator, i.e. the observable single-quantum coherences. In a coupled system, a composite  $\pi/2$  pulse generally produces a density operator with other, non-observable single-quantum coherences. Initially, these components do not contribute to the signal. However, they may subsequently evolve into observable coherence under the internal Hamiltonian. Thus, they contribute distortions to the spectrum, although they do not contribute to the area of the spectrum.

To classify the types of spectral distortion that appear due to excitation at low rf amplitudes, it is useful to treat the density operator  $\rho(\tau)$  after the single or composite  $\pi/2$  pulse as a linear combination of irreducible tensor operators  $T_{lm}$ . Because  $\rho(\tau)$  is hermitian, and because the tensor components satisfy:

$$T_{1m} = (-1)^m T_{1-m} \quad (V.18)$$

the tensor components must appear in  $\rho(\tau)$  as independent hermitian combinations  $A_{1m}$  and  $B_{1m}$ :

$$A_{1m} = T_{1m} + (-1)^m T_{1-m} \quad (V.19)$$

$$B_{1m} = iT_{1m} - i(-1)^m T_{1-m} \quad (V.20)$$

The tensor operators transform under a rotation about x by  $\pi$  according to:

$$\exp(-iI_x\pi)T_{1m}\exp(iI_x\pi) = (-1)^1 T_{1-m} \quad (V.21)$$

Observable signal arises only from  $A_{11}$  and  $B_{11}$  components. These satisfy:

$$\exp(-iI_x\pi)A_{11}\exp(iI_x\pi) = (-1)^{1+1}A_{11} \quad (V.22)$$

$$\exp(-iI_x\pi)B_{11}\exp(iI_x\pi) = (-1)^1 B_{11} \quad (V.23)$$

The coefficients of  $A_{11}$  and  $B_{11}$  in the density operator after the composite  $\pi/2$  pulse are real numbers  $a_1$  and  $b_1$ :

$$a_1 = \text{Tr}[A_{11}U(\tau)I_zU(\tau)^{-1}]/\text{Tr}(A_{11}^2) \quad (V.24)$$

$$b_1 = \text{Tr}[B_{11}U(\tau)I_zU(\tau)^{-1}]/\text{Tr}(B_{11}^2) \quad (V.25)$$

where  $U(\tau)$  is the pulse sequence propagator. The FID signal and the corresponding spectrum is a superposition of the signals and spectra

arising from each tensor component separately. A signal component  $S_l(t)$  can therefore be defined by:

$$S_l(t) = \text{Tr}[I_+ \exp(-iVt)(a_l A_{ll} + b_l B_{ll}) \exp(iVt)] \quad (\text{V.26})$$

$V$  is the dipole or quadrupole coupling Hamiltonian.  $V$  is invariant to a rotation about  $x$  by  $\pi$ . Then, if the operators in the trace in Eq.(V.26) are all rotated about  $x$  by  $\pi$ , leaving the trace unchanged,  $S_l(t)$  becomes:

$$S_l(t) = \text{Tr}\{I_- \exp(-iVt)[(-1)^{l+1} a_l A_{ll} + (-1)^l b_l B_{ll}] \exp(iVt)\} \quad (\text{V.27})$$

In addition, if the adjoint of the product of the operators in the trace in Eq.(V.26) is taken,  $S_l(t)$  is replaced by its complex conjugate:

$$S_l^*(t) = \text{Tr}[I_- \exp(-iVt)(a_l A_{ll} + b_l B_{ll}) \exp(iVt)] \quad (\text{V.28})$$

Comparison of Eqs.(V.27) and (V.28) reveals the following facts:  $A_{ll}$  components contribute to the real part of the signal when  $l$  is odd and to the imaginary part of the signal when  $l$  is even;  $B_{ll}$  components contribute to the real part of the signal when  $l$  is even and to the imaginary part when  $l$  is odd.

The undistorted spectrum, which would result from the FID following a single or composite  $\pi/2$  pulse with a very large rf amplitude, has absorption lineshapes in the real part and dispersion lineshapes in the imaginary part, as discussed in section C.2 of this chapter. For a

coupled spin system on resonance with no chemical shifts, the real part of the spectrum is symmetric about the center and the imaginary part is antisymmetric, that is:

$$F(\omega) = F(-\omega)^* \quad (\text{V.29})$$

where  $F(\omega)$  is given by Eq.(V.10). Eq.(V.29) holds if the signal is purely real. The imaginary part of the signal results in a contribution to the spectrum with the opposite symmetry. Specifically, imaginary signal makes an antisymmetric contribution to the real part of the spectrum. The resulting asymmetric "absorption" spectrum, even if it has a larger total area than the spectrum obtained with a single  $\pi/2$  pulse, is an undesirable result of composite  $\pi/2$  pulse excitation.

Two possible remedies for asymmetry in the spectrum exist. One is to artificially set the imaginary part of the FID signal to zero before the Fourier transformation. This is justifiable only if the spectrum is known to be symmetric a priori. In addition, it is difficult to determine experimentally that the two recorded signal channels actually correspond to the real and imaginary parts, and not to linear combinations of the real and imaginary parts that require a constant phase correction. It may also not be known with certainty that the spins are being irradiated exactly on resonance.

A second possibility is to collect two FID signals, one from the original composite  $\pi/2$  pulse and one from a new version of that pulse in which all the rf phases are replaced by their negatives. This negation of phases may be called "phase reversal." If  $U(\tau)$  is the propagator for the original composite pulse, then  $U'(\tau)$  is the propagator for the

phase-reversed pulse, with:

$$U'(\tau) = T \exp[-i \int_0^\tau [\omega_1(I_x \cos \phi - I_y \sin \phi) + V] dt] \quad (V.30)$$

$$= \exp(i I_x \pi) U(\tau) \exp(i I_x \pi) \quad (V.31)$$

If the operators in the traces in Eqs. (V.24) and (V.25) are rotated about x by  $\pi$ , the following equations result:

$$a_1 = (-1)^{1+1} \text{Tr}[A_{11} U'(\tau) I_z U'(\tau)^{-1}] / \text{Tr}(A_{11}^2) \quad (V.32)$$

$$= (-1)^{1+1} a_1' \quad (V.33)$$

$$b_1 = (-1)^1 \text{Tr}[B_{11} U'(\tau) I_z U'(\tau)^{-1}] / \text{Tr}(B_{11}^2) \quad (V.34)$$

$$= (-1)^1 b_1' \quad (V.35)$$

Thus, phase reversal changes the sign of the coefficients of the tensor components that contribute to the imaginary part of the signal. If the FID signals from the original and the phase-reversed composite  $\pi/2$  pulses are added either before or after Fourier transformation, and if the undistorted spectrum is truly symmetric, the antisymmetric spectral components are eliminated. This method avoids the a priori assumption of a symmetric spectrum and avoids experimental uncertainties about the adjustment of the signal channels and the rf frequency.

Note that  $U'(\tau)$  equals  $U(\tau)$  if the rf phase in the original composite  $\pi/2$  pulse only takes on the values 0 and  $\pi$ . Such a composite pulse therefore can not introduce asymmetry into the spectrum regardless of the rf amplitude. A single  $\pi/2$  pulse is a special case of such a composite pulse.

Figure V.15 shows simulated powder pattern spectra resulting from



excitation by a single  $\pi/2$  pulse and by the composite  $\pi/2$  pulse  $180_{90}180_{270}148_086_{180}28_0$  at various rf amplitudes. The spin system is an isotropic orientational distribution of either coupled pairs of spin-1/2 nuclei or quadrupolar spin-1 nuclei with an axially symmetric quadrupole interaction. The imaginary signals have been set to zero in the composite pulse case in order to symmetrize the spectra. The same spectra would result from the phase-reversal procedure. At low rf amplitudes, the composite  $\pi/2$  pulse spectra in Figure V.15 clearly have greater areas and less obvious distortion than the single  $\pi/2$  pulse spectra.

The distortions in the spectra of spin-1 nuclei or pairs of spin-1/2 nuclei resulting from single pulse excitation at low rf amplitudes have been well characterized, first by Barnaal and Lowe [77] and later by Bloom et al. [78]. The distortion is a combination of a loss of signal amplitude and a shift in the signal phase. The phase shift is proportional to the coupling constant. As in the discussion in section C.2 above, the phase distortion in a powder pattern can not be corrected after the spectrum is obtained.

An important application of composite  $\pi/2$  pulses is in a solid echo sequence [79], i.e.  $(\pi/2)_0-\tau_1-(\pi/2)_{90}-\tau_2$ . In the case of a spin-1 nucleus or a pair of spin-1/2 nuclei, and in the limit of very large rf amplitude, the signal collected after a solid echo sequence with  $\tau_2 = \tau_1$  is exactly the same as the signal after a single  $\pi/2$  pulse. For a general coupled spin system, the signal from a solid echo sequence is approximately the same as that from a single  $\pi/2$  pulse if  $\tau_1$  and  $\tau_2$  are equal and small. At lower rf amplitudes, the echo signal is attenuated and peaks when  $\tau_2$  is slightly different from  $\tau_1$  [78]. The solid echo is

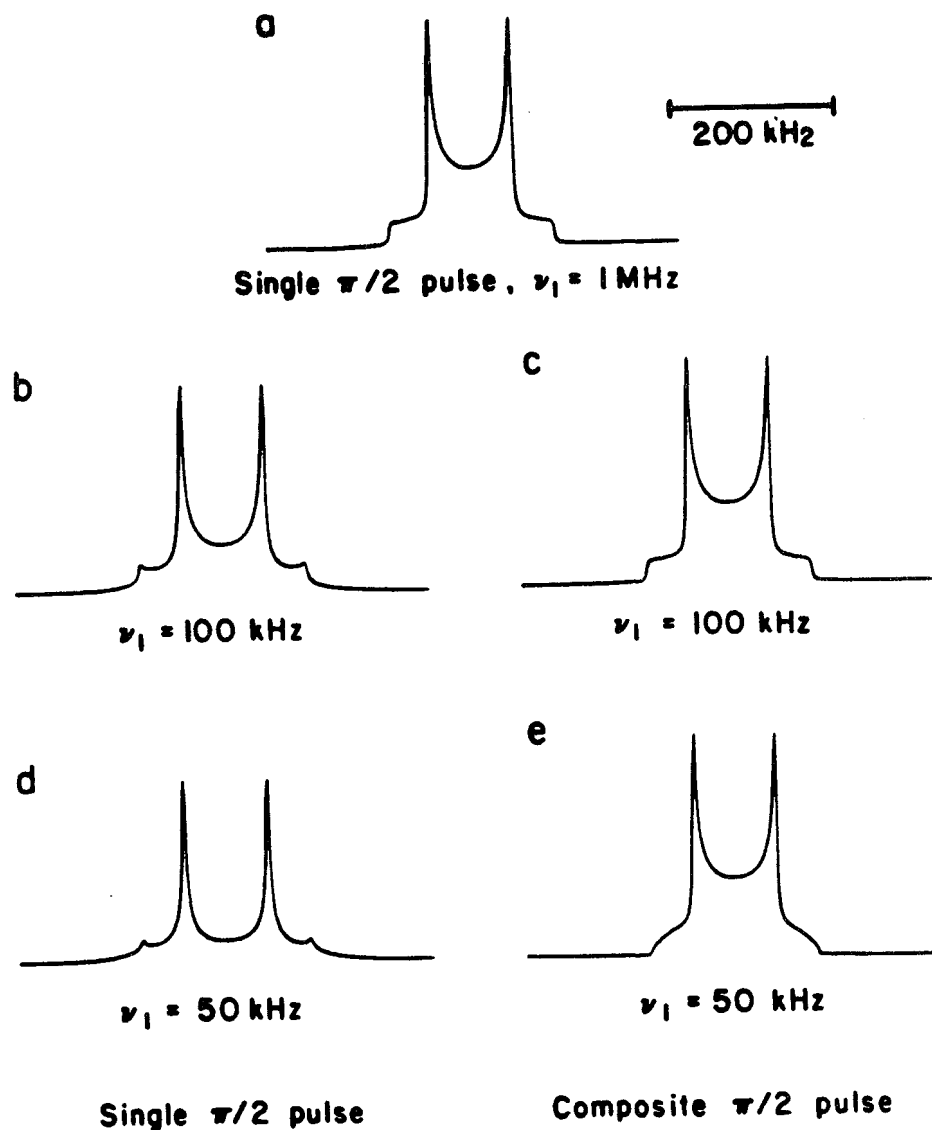


Figure V.15: Simulated powder pattern spectra for an isotropic orientational distribution of pairs of dipole coupled spin-1/2 nuclei, resulting from excitation by a single  $\pi/2$  pulse (a,b,d) and the composite  $\pi/2$  pulse  $180_{90}180_{270}148_{0}86_{180}28_{0}$  (c,e) at various rf amplitudes. The spectrum in a is essentially undistorted. A comparison of b and d with c and e shows that the distortions at low rf amplitudes are less severe when the composite  $\pi/2$  pulse is used.

widely used in place of a single  $\pi/2$  pulse to obtain solid state NMR spectra because the delay  $\tau_2$  allows signal artifacts from the rf pulses to die out before the signal observation begins. If a single  $\pi/2$  pulse is used, such pulse artifacts generally obscure the beginning of the FID, making an accurate spectrum impossible to achieve.

The composite  $\pi/2$  pulse  $180_{90}180_{270}148_{0}86_{180}28_{0}$  can be used in a solid echo sequence with limited success. A difficulty with using the composite solid echo sequence to obtain a powder pattern spectrum is that the optimum difference between  $\tau_2$  and  $\tau_1$  depends on the coupling constant, i.e. different frequency components in the powder pattern echo at different times. This problem does not arise with the solid echo sequence using single  $\pi/2$  pulses, at least not in the spin-1 and pair of spin-1/2 cases [78].

Levitt, Suter, and Ernst [27] have introduced composite  $\pi/2$  pulses specifically for solid echo sequences applied to quadrupolar spin-1 nuclei or pairs of coupled spin-1/2 nuclei. The most effective of these is  $90_{180}180_{0}90_{180}135_{0}45_{180}$ . The spectrum resulting from the FID after one of these composite  $\pi/2$  pulses has severe phase and amplitude distortions, even at an rf amplitude comparable to the spectral width. However, when the composite  $\pi/2$  pulses are used in a solid echo sequence, a virtually undistorted spectrum can be obtained when  $\omega_1/2\pi$  is only one quarter of the spectral width. This is an important example of how distortions can be made to cancel between pairs of composite pulses.

The composite  $\pi/2$  pulses of Levitt, Suter, and Ernst are derived by applying a fictitious spin-1/2 formalism [80-82] to the three-level, spin-1 system. It is shown that certain composite  $\pi$  pulses that

compensate for resonance offsets in systems of isolated spins can be adapted to form composite  $\pi/2$  pulses for anharmonic three-level systems.

The particular composite  $\pi$  pulse used to generate

$90_{180} 180_0 90_{180} 135_0 45_{180}$  was developed by Shaka et al. [25].

Finally, other possible applications of composite  $\pi/2$  pulses compensated for couplings include their incorporation into line-narrowing, spin-locking, time-reversal, and multiple-quantum excitation sequences. In some of those applications, it is common practice to use single  $\pi/2$  pulses arranged so that the average of the coupling Hamiltonian during the pulses vanishes in the interaction representation when calculated over the sequence as a whole. The relative merits of making the average vanish for each composite  $\pi/2$  pulse individually is a matter for further investigation.

## Chapter VI: Broadband Excitation in Other NMR Techniques

### A. Motivation

This chapter deals with broadband excitation problems other than population inversion and the creation of transverse magnetization. There are a number of techniques in NMR in which simple sequences of strong rf pulses separated by delays are used to produce a desired transformation of a spin system. As an example, a sequence that is commonly used in multiple-quantum spectroscopy [83,84] is shown in Figure VI.1. Assuming that the rf pulse amplitudes are very large compared to internal spin couplings, resonance offsets, and chemical shifts, the propagators for the pulse sequences considered in this chapter depend on the products of the coupling constants with the delay lengths. For given delay lengths, the desired transformation is achieved only for specific values of the coupling constants if the standard, simple sequences are used. In many experimental situations, however, a range of coupling constants exists. This range may result from the random orientations of crystallites in a powdered or polycrystalline solid, from differences in bond connectivities between coupled nuclei, from differences in electronic environments of quadrupolar nuclei, or from differences in the motional averaging of couplings.

In certain cases, the pulse sequence propagator can be analyzed as a rotation operator in a fictitious two-level system. The coupling constants determine the rotation rate; the products of coupling

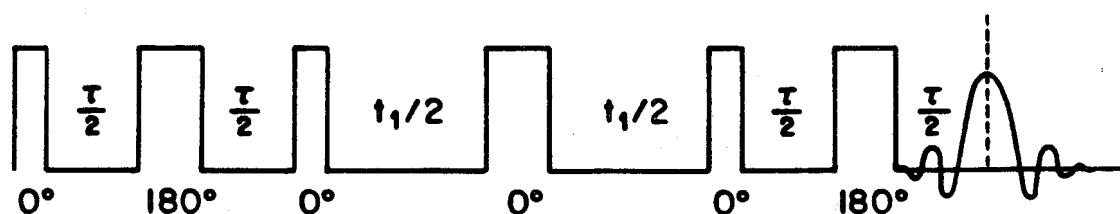


Figure VI.1: A simple sequence for multiple-quantum spectroscopy, composed of  $\pi/2$  and  $\pi$  pulses with the indicated phases. The signal is acquired as a function of  $t_1$ .  $\tau$  is fixed at a value that optimizes the preparation of desired multiple-quantum coherences by the first three pulses. The best value of  $\tau$  depends on the particular arrangement and strengths of couplings in a particular spin system.

constants with delay lengths are rotation angles. The problem of constructing a pulse sequence that is effective over a broad range of coupling constants reduces to the problem of finding a sequence of rotations for which the final net rotation is insensitive to the rotation rate. This is precisely the problem solved by composite pulses that compensate for variations in the rf amplitude, as in Chapter V.B. Thus, it is possible to construct composite excitation sequences by direct analogy to composite pulses.

The first work in which a composite excitation sequence was explicitly based on a composite pulse was the development of homonuclear decoupling sequences for liquid state NMR by Garbow, Weitekamp, and Pines [85]. Their technique, bilinear rotation decoupling (BIRD), depends on the selective population inversion of protons that are bound to  $^{13}\text{C}$  nuclei in an organic molecule. If there is a scalar coupling between a proton and a  $^{13}\text{C}$  nucleus, with coupling constant  $J$ , then the simple sequence  $90_0 - \tau - 90_{180}$  applied to the proton on resonance inverts the proton populations if  $\tau = 2\pi/J$ . In that case,  $90_0 - \tau - 90_{180}$  is a bilinear  $\pi$  pulse, called "bilinear" because of the bilinear form of the scalar coupling. To cover a range of  $J$  values, Garbow, Weitekamp, and Pines suggested replacing the simple bilinear  $\pi$  pulse with the composite bilinear  $\pi$  pulse  $90_0 - \tau/2 - 90_{90} - \tau - 90_{270} - \tau/2 - 90_{180}$ , which is a bilinear analog of the  $90_0 - 180_{90} - 90_0$  composite  $\pi$  pulse of Levitt and Freeman [19].

An earlier technique for cross-polarization in liquids employed a composite excitation sequence as well, but the analogy to composite pulses was not made explicit [86].

Sections B, C, and D of this chapter are devoted to another example

of composite excitation, namely composite double-quantum excitation. Section E describes composite polarization transfer sequences. At this point, it is worthwhile to emphasize the difference between composite excitation sequences and composite pulses. Both may be concerned with uniform excitation over a range of couplings. However, the parameter of interest in a composite excitation sequence is the product of the coupling constant with a delay length, while the parameter of interest in a composite pulse is the ratio of the coupling constant to the rf amplitude. Composite excitation sequences are useful even when the rf amplitude is much greater than all coupling constants. A second difference is that composite excitation sequences are designed to produce a uniform transformation over a range of coupling constants centered around a non-zero value, while composite pulses produce a uniform transformation over a range of coupling constants centered around zero.

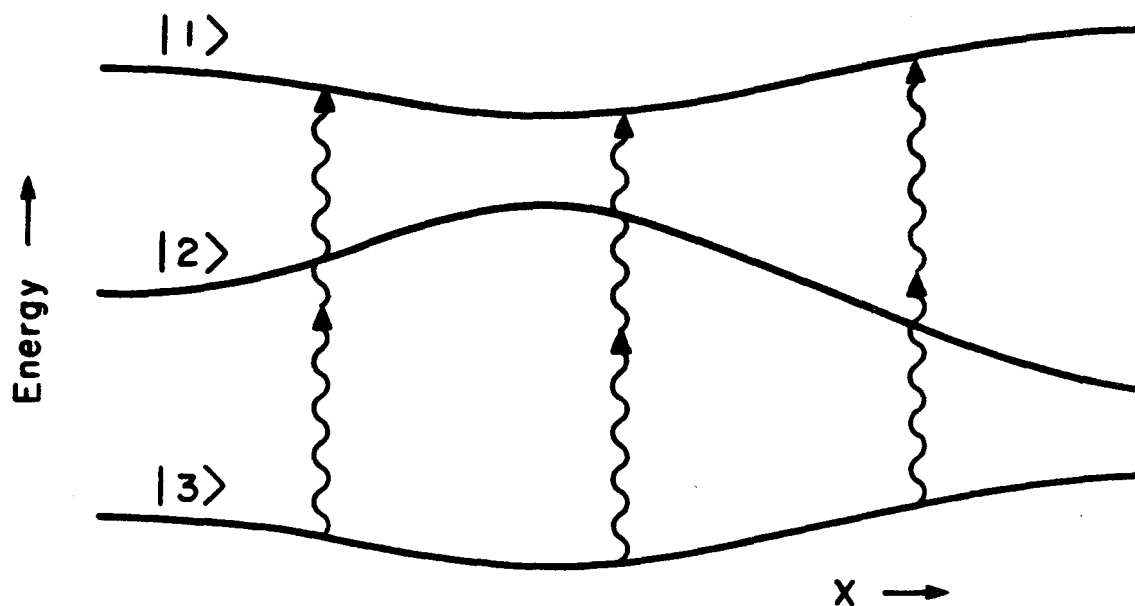
## B. Theory of broadband double-quantum excitation

### 1. Fictitious two-level systems

In this section, a method for constructing pulse sequences for broadband double-quantum (DQ) excitation is developed. The spin systems considered are all effectively three-level systems. The problem of broadband DQ excitation in a three-level system is pictured schematically in Figure VI.2.

Consider first the internal Hamiltonian for a pair of equivalent dipole-coupled spin-1/2 nuclei:





XBL 847-2662

Figure VI.2: The problem of broadband double-quantum excitation. A three-level system with a coupling that depends on a parameter  $x$  is shown. The efficiency of the excitation of coherence between  $|1\rangle$  and  $|3\rangle$  generally depends on the energy mismatch between  $|2\rangle$  and the intermediate, or virtual, state of the double-quantum transition. In solid state NMR,  $x$  may specify the orientation of a molecule or crystallite, as for quadrupolar spin-1 nuclei or pairs of dipole-coupled spin-1/2 nuclei. In liquid state NMR,  $x$  may label different bond connectivities between scalar coupled spin-1/2 nuclei.

$$\mathcal{H} = d(I_{z1}I_{z2} - \frac{1}{3}I_1 \cdot I_2) + \Delta\omega(I_{z1} + I_{z2}) \quad (\text{VI.1})$$

Assuming that the rf amplitude is much larger than  $d$  and  $\Delta\omega$ , the propagator for the pulse sequence  $90_{90}-t/2-180_{270}-t/2-90_{90}$  is:

$$U(t) = \exp(-iI_y\pi/2)\exp(-i t/2)\exp(iI_y\pi)\exp(-i t/2)\exp(-iI_y\pi/2) \quad (\text{VI.2})$$

Using the fact that:

$$\exp(\pm iI_y\pi/2) \exp(\mp iI_y\pi/2) = d(I_{x1}I_{x2} - \frac{1}{3}I_1 \cdot I_2) \mp \Delta\omega(I_{x1} + I_{x2}) \quad (\text{VI.3})$$

Eq.(VI.2) can be rewritten:

$$U(t) = \exp[-id(I_{x1}I_{x2} - \frac{1}{3}I_1 \cdot I_2)t] \quad (\text{VI.4})$$

The fact that the two terms on the right side of Eq.(VI.3) commute with one another is used to derive Eq.(VI.4).

At this point, it is useful to introduce the fictitious spin-1/2 formalism of Vega [82] and Wokaun and Ernst [81]. In an  $n$ -level system, it is possible to define fictitious spin-1/2 operators for each pair of levels  $p$  and  $q$ , as follows:

$$I_x^{p-q} = (|p\rangle\langle q| + |q\rangle\langle p|)/2 \quad (\text{VI.5a})$$

$$I_y^{p-q} = (-i|p\rangle\langle q| + i|q\rangle\langle p|)/2 \quad (\text{VI.5b})$$

$$I_z^{p-q} = (|p\rangle\langle p| - |q\rangle\langle q|)/2 \quad (\text{VI.5c})$$

The fictitious spin-1/2 operators for a given pair of levels satisfy the same commutation relations as standard angular momentum operators:

$$[I_{\alpha}^{p-q}, I_{\beta}^{p-q}] = i I_{\gamma}^{p-q} \quad (\text{VI.6})$$

where  $\{\alpha, \beta, \gamma\}$  is any cyclic permutation of  $\{x, y, z\}$ .

For the Hamiltonian of Eq.(VI.1), the basis of eigenstates is  $\{|1\rangle = |\alpha\alpha\rangle, |2\rangle = (|\alpha\beta\rangle + |\beta\alpha\rangle)/\sqrt{2}, |3\rangle = |\beta\beta\rangle\}$  where  $|\alpha\rangle$  and  $|\beta\rangle$  represent spins in their  $m = 1/2$  and  $m = -1/2$  states, respectively. These eigenstates make up the triplet, i.e. total spin 1, manifold. Additionally, there is a singlet state  $(|\alpha\beta\rangle - |\beta\alpha\rangle)/\sqrt{2}$ , but the singlet state never mixes with triplet manifold under any combination of rf pulses and delays. It is therefore ignored.

Eq.(VI.4) can now be rewritten in terms of fictitious spin-1/2 operators, using:

$$I_{x1}I_{x2} - \frac{1}{3}I_1 \cdot I_2 = \frac{1}{2}I_x^{1-3} - \frac{1}{6}(I_z^{1-2} - I_z^{2-3}) \quad (\text{VI.7})$$

The result is:

$$U(t) = \exp(-idI_x^{1-3}t/2)\exp[id(I_z^{1-2} - I_z^{2-3})t/6] \quad (\text{VI.8})$$

Similarly, the propagator for the sequence  $(90_{90}-t/2-180_{270}-t/2-90_{90})_{\gamma}$ , where  $\gamma$  denotes an overall rf phase shift, is:

$$U(\beta, \gamma) = \exp[-i\beta(I_x^{1-3}\cos 2\gamma + I_y^{1-3}\sin 2\gamma)]\exp[i\beta(I_z^{1-2} - I_z^{2-3})/3] \quad (\text{VI.9})$$

with  $\beta = dt/2$ . The phase shift introduces an angle  $2\gamma$  in Eq.(VI.9)

instead of  $\gamma$  because  $I_z = 2I_z^{1-3}$ . The sequence for which the propagator is  $U(\beta, \gamma)$  will be denoted by  $P(\beta, \gamma)$ .

The initial, equilibrium state of the system is described by a density operator proportional to  $I_z^{1-3}$ . The second exponential operator on the right-hand side of Eq.(VI.9) commutes with all  $I_z^{1-3}$  operators; the first exponential operator produces a rotation in the 1-3 subspace. As long as the total excitation sequence consists only of  $P(\beta, \gamma)$  subcycles, it is possible to disregard the second exponential operator and treat  $U(\beta, \gamma)$  as the operator for a rotation in the xy plane of the 1-3 subspace.  $U(\beta, \gamma)$  is therefore formally analogous to the usual angular momentum rotation operator resulting from a single rf pulse with phase  $2\gamma$  and flip angle  $\beta$ .

## 2. Composite double-quantum excitation sequences

DQ coherence is an off-diagonal density matrix element connecting states  $|1\rangle$  and  $|3\rangle$ , which differ in their Zeeman quantum numbers by 2. DQ coherence is therefore described by a density operator that is a linear combination of  $I_x^{1-3}$  and  $I_y^{1-3}$ . The problem of finding a sequence of  $P(\beta, \gamma)$  subcycles that excites DQ coherence over a range of coupling constants is the same as the problem of finding a sequence of rotations about axes in the xy plane that brings a vector from the z axis into the xy plane over a range of variations in the rotation angles. This problem is solved by composite  $\pi/2$  pulses that compensate for rf inhomogeneity. Thus, as anticipated in section A, it is possible to construct composite preparation sequences directly by analogy to composite  $\pi/2$  pulses. If  $(\theta_1)_{\phi_1}(\theta_2)_{\phi_2}\dots(\theta_N)_{\phi_N}$  is a composite  $\pi/2$

pulse, with  $\theta_i$  and  $\phi_i$  being the flip angle and phase of the  $i$ th pulse, then the corresponding composite DQ excitation sequence is

$P(\theta_1, \phi_1/2)P(\theta_2, \phi_2/2)\dots P(\theta_N, \phi_N/2)$ , with the overall propagator:

$$U_T = U(\theta_N, \phi_N/2)U(\theta_{N-1}, \phi_{N-1}/2)\dots U(\theta_1, \phi_1/2) \quad (\text{VI.10})$$

The particular composite  $\pi/2$  pulse used as the model for the DQ experiments that follow is  $270_0 360_{169} 180_{33} 180_{178}$ , the first order composite pulse presented in Chapter V.B. This choice is explained later.

### 3. Reduced composite sequences

The construction of a composite sequence from  $P(\beta, \gamma)$  subcycles entails juxtaposing the first  $\pi/2$  pulse of one subcycle with the last  $\pi/2$  pulse of the previous subcycle. The juxtaposition of rf pulses of different phases is a common and important feature of composite  $\pi$  and  $\pi/2$  pulses, as in Chapter V. In the case of composite DQ excitation sequences, however, it is merely an artifact of the construction method and is a source of experimental imperfections. Normally, a gap between pulses on the order of microseconds is needed in practice to ensure that their transients do not interfere and to allow for the switching time of an rf phase shifter. Spin evolution due to resonance offsets or chemical shift differences during the gaps can degrade the performance of a composite excitation sequence. The gaps can be eliminated and the total flip angle shortened, without changing the overall propagator in the limit of perfect pulses, by replacing adjoining pairs of  $\pi/2$  pulses

by an equivalent single pulse. The reduction in the number of pulses and the total flip angle should alleviate the effects of rf inhomogeneity, phase transients, and finite pulse amplitudes somewhat. The derivation of the reduced form of a composite excitation sequence depends on the following identity:

$$\begin{aligned} & \exp[-i(I_x \cos \phi_1 + I_y \sin \phi_1)\pi/2] \exp[-i(I_x \cos \phi_2 + I_y \sin \phi_2)\pi/2] \\ &= \exp[-iI_z(\phi_1 - \pi/2)] \exp[-iI_x(\pi + \phi_2 - \phi_1)] \exp[iI_z(\phi_2 + \pi/2)] \end{aligned} \quad (\text{VI.11})$$

The left-hand side of Eq.(VI.11) is the product of the two rotations of a  $90_{\phi_2} 90_{\phi_1}$  pair. The right-hand side is a product of three rotations. The first and third factors are rotations about z that commute with the internal Hamiltonian and merely affect the phases of pulses in a reduced sequence. The second factor is a rotation about x, corresponding to a pulse with a flip angle of  $\pi + \phi_2 - \phi_1$ . If  $\phi_2 - \phi_1 > 0$ , the flip angle may be changed to  $\pi - \phi_2 + \phi_1$  and the sense of the rotation reversed. Using Eq.(VI.11) and this rule, the reduced form of the composite DQ excitation sequence based on  $270_0 360_{169} 180_{33} 180_{178}$  is:

$$90_0 - 3T/2 - 180_{180} - 3T/2 - 95.5_{90} - 2T - 180_0 - 2T - 112_{90} - T - 180_{180} - T - 107.5_{90} - T - 180_0 - T - 90_{180} \quad (\text{VI.14})$$

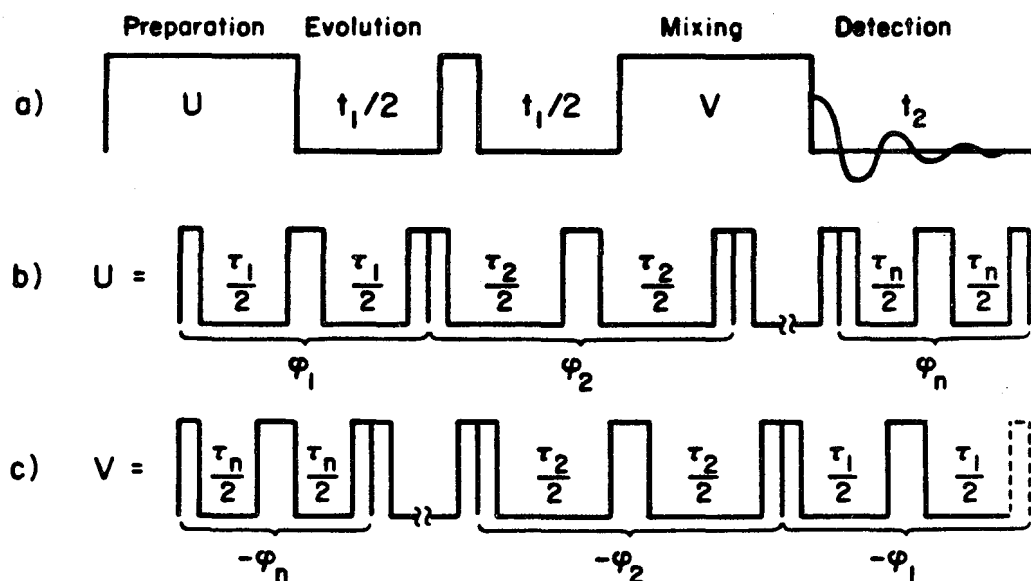
A general composite excitation sequence  $(90_0 - t_1 - 180_{180} - t_1 - 90_0)_0 - (90_0 - t_2 - 180_{180} - t_2 - 90_0)_{\gamma_2} \dots (90_0 - t_n - 180_{180} - t_n - 90_0)_{\gamma_n}$  corresponds to the reduced sequence:

$$\begin{aligned}
 &90_0-t_1-180_{180}-t_1-(180-\gamma_2)90-t_2-180_0-t_2-(180+\gamma_2-\gamma_3)-90-t_3- \\
 &180_{180}-t_3-(180+\gamma_3-\gamma_4) \dots -t_n-90_{180}
 \end{aligned} \tag{VI.15}$$

An interesting bonus of the reduced sequence is that the pulse phases are multiples of  $90^\circ$ . This will be true regardless of which composite  $\pi/2$  pulse is used as the model. It simplifies the experimental requirements since standard phase tune-up procedures are applicable and a small angle phase shifter is not required.

#### 4. The double-quantum experiment

Figure VI.3 depicts the class of pulse sequences which will be demonstrated in the following section. The general form of the multiple quantum (MQ) experiment, the notation, and much of the earlier work are reviewed in references 83 and 84. In general terms, an MQ experiment consists of a preparation sequence that creates MQ coherence from the initial, equilibrium state, an evolution time  $t_1$  in which the system evolves under a Hamiltonian that commutes with  $I_z$ , a mixing sequence that converts part of the MQ coherence to observable single quantum coherence, and a detection period. Signals are recorded as a function of  $t_1$ . Composite DQ excitation can be used in the preparation or the mixing period, or preferably in both. Here the case where the preparation and mixing propagators,  $U$  and  $V$  respectively, are of the form of Eq.(VI.10) is considered. The actual mixing sequence differs



LBL 847-2663

Figure VI.3: a) General form of time domain double-quantum spectroscopy, showing preparation, evolution, mixing, and detection periods. An optional  $\pi$  pulse in the evolution removes chemical shifts and static field inhomogeneity. The detected signal  $S(t_1, t_2)$  may be Fourier transformed with respect to  $t_1$  at  $t_2 = 0$  to give a one-dimensional, double-quantum spectrum; a double Fourier transform with respect to  $t_1$  and  $t_2$  yields a two-dimensional spectrum. b) A composite preparation sequence, based on  $90_{90}-\tau/2-180_{270}-\tau/2-90_{90}$  subcycles. These subcycles, with various values of  $\tau_i$  and overall phase shifts  $\phi_i$ , are combined to form a sequence for preparing double-quantum coherence over a large range of couplings. The  $\tau_i$  and  $\phi_i$  are easily derived from existing composite  $\pi/2$  pulses. c) The matching mixing sequence. The final  $\pi/2$  pulse in  $V$  is omitted to allow the detection of transverse magnetization. If there is no  $\pi$  pulse in the evolution,  $-\phi_i$  is replaced by  $\phi_i$ . Preparation and mixing sequences should be matched to give the maximum signal amplitude and a uniform signal phase.



from V only by the deletion of the final  $\pi/2$  pulse to create transverse magnetization. The signal at the end of the mixing period in the channel orthogonal to this  $\pi/2$  pulse has the form:

$$S_1(t_1) = \text{Tr}[V^{-1}I_z V \exp(-i\mathcal{H}t_1) U I_z U^{-1} \exp(i\mathcal{H}t_1)] \quad (\text{VI.16})$$

Since U and V are DQ selective, it can be shown that the other channel carries no signal at this time, in the absence of pulse errors. The propagator in the evolution period,  $\exp(-i\mathcal{H}t_1)$ , is a rotation about z in the 1-3 subspace by an angle  $2\Delta\omega t_1$ .

Eq.(VI.16) can be analyzed by using the facts that  $I_z = 2I_z^{1-3}$  and that U and V are also rotations in the 1-3 subspace:

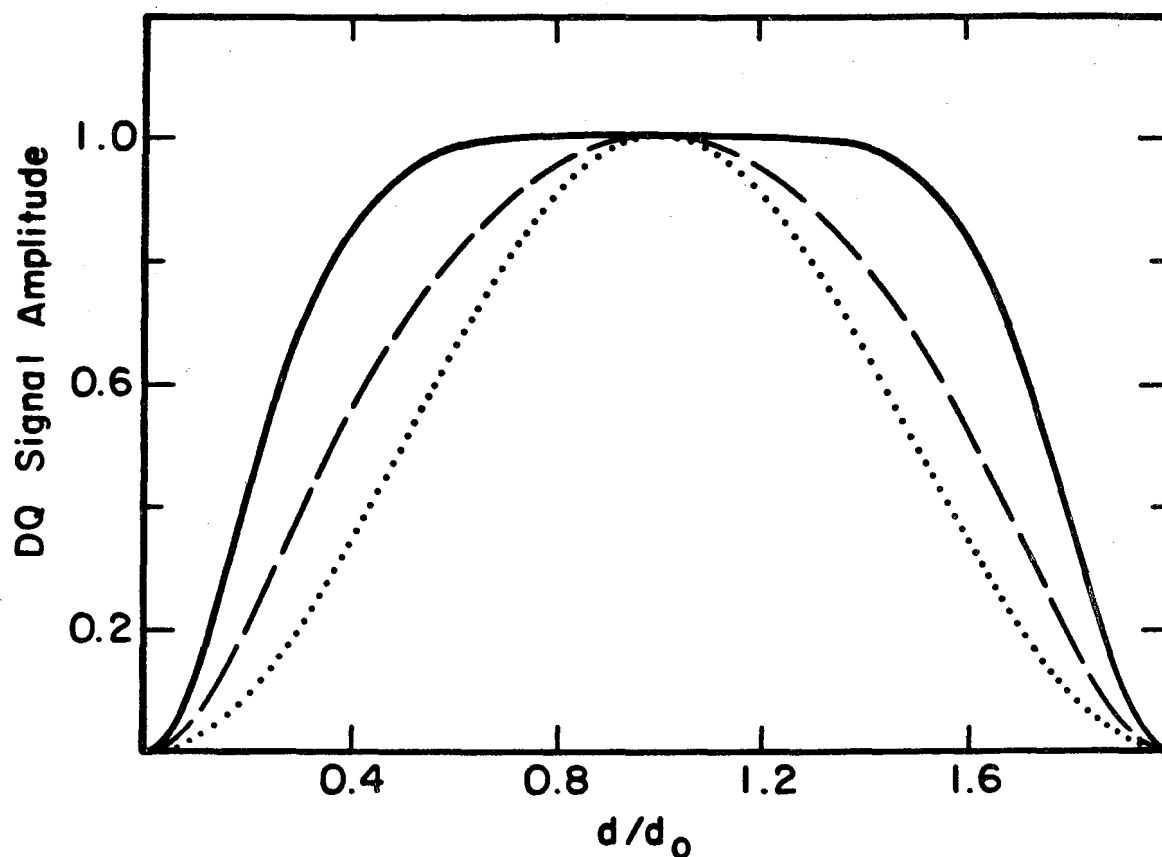
$$U I_z U^{-1} = \alpha_p (I_x^{1-3} \cos \gamma_p + I_y^{1-3} \sin \gamma_p) + \beta_p I_z^{1-3} \quad (\text{VI.17})$$

$$V I_z V^{-1} = \alpha_m (I_x^{1-3} \cos \gamma_m + I_y^{1-3} \sin \gamma_m) + \beta_m I_z^{1-3} \quad (\text{VI.18})$$

The detected DQ signal becomes:

$$S_{\text{DQ}}(t_1) = (1/2) \alpha_m \alpha_p \cos(\gamma_p - \gamma_m + 2\Delta\omega t_1) \quad (\text{VI.19})$$

Two important features of the DQ experiment are apparent in Eq.(VI.19). First, the amplitude of the detected DQ signal depends on both the efficiency with which DQ coherence is prepared ( $\alpha_p$ ) and the efficiency with which it is mixed back to SQ coherence ( $\alpha_m$ ). Calculated plots of the DQ signal amplitude as a function of the coupling constant are shown in Figure VI.4 for the non-composite DQ experiment, the experiment with composite preparation only, and the experiment with both composite



XBL 847-2664

Figure VI.4: Theoretical double-quantum signal amplitudes as a function of the ratio of the actual coupling constant  $d$  to the nominal coupling constant  $d_0$  in a non-composite experiment (dotted line), a composite preparation or composite mixing experiment (dashed line), and a composite preparation and composite mixing experiment (solid line). A composite double-quantum excitation sequence based on the composite pulse  $270_0 360_{169} 180_{33} 180_{178}$  is assumed.

preparation and mixing. Second, the phase of a DQ line is  $\gamma_p - \gamma_m$ . When the signal in Eq.(VI.19) is averaged over a distribution of systems with different couplings, the possibility of overlap in the DQ spectrum must be considered. It is therefore important that the phases be independent of the internal Hamiltonian to avoid destructive interference.

A feature of most composite  $\pi/2$  pulses is that they produce transverse magnetization with a phase that depends on the rf amplitude, as discussed in Chapter V. If such a composite pulse is used as the basis for the composite preparation sequence, the DQ signal phase will generally be a function of the coupling constant. Signal cancellation may result. This could occur if a composite sequence is only used in the preparation period. For such an experiment, the composite sequence should be based on a composite  $\pi/2$  pulse with minimal phase variations. The composite  $\pi/2$  pulse  $270_0 360_{169} 180_{33} 180_{178}$  used here has this property, as shown in Chapter V.B.

Phase variations can be eliminated in more general ways, and the DQ signal amplitude increased, by using composite sequences in both the preparation and the mixing periods. This matching of preparation and mixing periods to maximize signal is a general principle of MQ spectroscopy [84]. If the mixing sequence is the same as the preparation sequence, but with the pulses and delays given in reverse order, then the following equations hold:

$$V = \exp(-iI_z\pi/2)U^{-1}\exp(iI_z\pi/2) \quad (\text{VI.20})$$

$$\alpha_p = -\alpha_m \quad (\text{VI.21})$$

$$\gamma_p = \gamma_m \quad (\text{VI.22})$$

Here the DQ selectivity of U was used.

If, as in the experiments that follow, a  $\pi$  pulse is added to the evolution period (for example at  $t_1/2$  to remove resonance offsets and chemical shifts) the phases  $\phi_i$  in the mixing period must be changed to  $-\phi_i$  to preserve uniform phase. In this form, the experiment is a special case of a general procedure for obtaining spin inversion transitions in phase and does not depend on selectivity [84].

### C. Broadband double-quantum excitation results

#### 1. Experiments and spectra

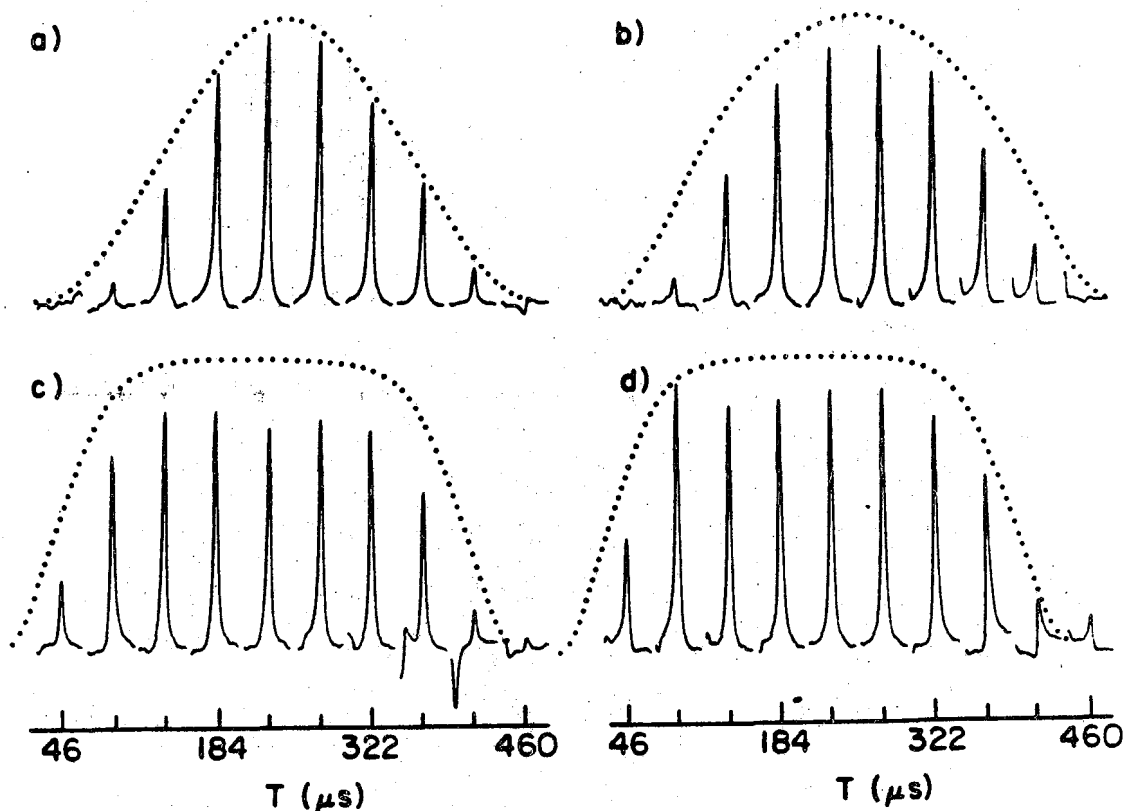
Experiments were performed on a sample of  $\text{CH}_2\text{Cl}_2$  dissolved in Eastman 15320 liquid crystal. Excess  $\text{CH}_2\text{Cl}_2$  was evaporated until the isotropic solution became nematic, at which point it was sealed. For this sample, at 29° C the single quantum spectrum of  $\text{CH}_2\text{Cl}_2$  is a doublet with a splitting of 2.18 kHz, implying  $d/2\pi = 1.09$  kHz. The spectrometer operated at 180 MHz. The rf amplitude was  $\omega_1/2\pi = 50$  kHz. As explained above, the composite excitation sequence  $P(3dT,0)P(4dT,169/2)P(2dT,33/2)P(2dT,178/2)$  was used. The performance of composite sequences over a range of internal couplings was mimicked by varying T around the theoretically optimum value of 230  $\mu\text{s}$ . A  $\pi$  pulse in the middle of the evolution period removed static field inhomogeneity. Zero-, one-, and two-quantum spectral lines were separated using time-proportional phase incrementation (TPPI) [87]. All experiments were performed twice, with an overall phase shift of the

preparation sequence by  $\pi/2$  the second time, and the results added together to cancel artifacts due to imperfections in the TPPI phase cycling. Phase shifts in increments of  $360^\circ/256$  were available from a digitally controlled phase shifter. A delay of  $2.5 \mu\text{s}$  was required for the switching time of the phase shifter.

Figure VI.5 shows DQ lines of  $\text{CH}_2\text{Cl}_2$  obtained by varying  $T$  from  $46 \mu\text{s}$  to  $460 \mu\text{s}$  in  $46 \mu\text{s}$  increments. Figure VI.5a results from experiments with single  $P(dT,0)$  preparation and mixing sequences; Figure VI.5b results from experiments with composite preparation sequences; Figure VI.5c results from experiments with composite preparation and composite mixing sequences. The theoretical signal amplitude as a function of  $T$  is superimposed on the experimental results. As predicted, the range of values of  $dT$  over which the DQ signal amplitude is nearly its maximum is greatly extended by the use of composite excitation sequences. The DQ signal phase remains nearly constant as  $T$  varies. In Figure VI.5b, where the preparation and mixing sequences are not matched, this is a result of the use of a model composite  $\pi/2$  pulse derived with the approach of Chapter IV.

## 2. Effects of pulse imperfections

The theoretical analysis in the preceding section assumed perfect, delta function rf pulses. The existence of pulse imperfections affects the experimental results in several noticeable ways. First, the optimum value of  $T$  is less than the theoretical prediction. This effect is most pronounced in the experiments employing composite preparation and composite mixing, and results from the finite pulse lengths. The



XBL 847-2661

Figure VI.5: Double-quantum  $^1\text{H}$  NMR lines of oriented  $\text{CH}_2\text{Cl}_2$  in a liquid crystal solvent. The lines are shown as a function of the preparation and mixing time for non-composite (a), composite preparation (b), and composite preparation and composite mixing experiments (c). In d, reduced composite preparation and mixing sequences are used, replacing adjoining  $\pi/2$  pulses by a single equivalent pulse and thereby decreasing pulse imperfection effects. Theoretical line amplitudes, normalized to those in a, are shown in dotted lines. The fact that the composite sequences give uniform line amplitudes and phases over a range of  $T$  for a fixed proton-proton coupling implies that they give uniform line amplitudes and phases over a range of couplings for a fixed  $T$ .

simulations in Figure VI.5 have been shifted to coincide with the experimental maxima.

Second, the maximum DQ signal in the composite experiments is about 10% less than that in the experiments with single preparation and mixing. A number of pulse imperfections may be responsible for a loss of signal amplitude. These include pulse length miscalibrations, rf inhomogeneity, rf phase transients, and rf phase misadjustments. Rf inhomogeneity proved to be a particularly significant factor in the experiments, as experiments with a larger sample resulted in larger relative differences in the maximum DQ signals between experiments with different numbers of pulses.

A third, and related, effect is the observation of SQ lines, which appear as artifacts to the left of individual DQ lines in Figure VI.5. Ideally, a sequence of  $P(\beta, \gamma)$  subcycles would prepare no SQ coherence. However, any of the above pulse imperfections may interfere with the DQ selectivity of  $P(\beta, \gamma)$ . The preparation of SQ coherence contributes to the loss of DQ signal amplitude. In addition, the lack of perfect DQ selectivity causes signal to be detected in both receiver channels, rather than the single channel assumed in the theory section.

The presence of signal in both channels as a result of pulse imperfections may produce small signal phase variations as a function of  $dT$  even if the preparation and mixing sequences are matched as in Figure VI.5c. These could be removed by actually giving the final  $\pi/2$  pulse in the mixing sequence of Figure VI.3c, allowing coherences to dephase during a delay, and then sampling longitudinal magnetization with a  $\pi/2$  "read" pulse. This procedure for performing a true single-channel experiment has been followed in reference 47.

Figure VI.5d shows results from the reduced composite preparation and mixing sequence of line (VI.14). In comparison to Figure VI.5c, the overall amplitude in Figure VI.5d is greater and the SQ artifacts are smaller. The improved performance of the reduced composite sequences may be attributed to a reduction in pulse imperfection effects.

The effects of pulse imperfections may be further attenuated by incorporating composite pulses into composite DQ excitation sequences. In particular, composite pulses that compensate for rf inhomogeneity and for dipole and quadrupole couplings may be beneficial.

#### D. Extensions and applications

##### 1. Liquid state NMR

The internal Hamiltonian for a pair of weakly coupled spin-1/2 nuclei in a liquid is:

$$\mathcal{H} = J I_{z1} I_{z2} + \delta_1 I_{z1} + \delta_2 I_{z2} \quad (\text{VI.23})$$

The propagator for the sequence  $90_{90}-t/2-180_{270}-t/2-90_{90}$  is then:

$$U(t) = \exp(-iJ I_{x1} I_{x2} t) \quad (\text{VI.24})$$

$$= \exp(-iJ I_x^{1-3} t/2) \exp[-iJ (I_z^{2-3} - I_z^{1-2}) t/6] \quad (\text{VI.25})$$

A factor of  $\exp(-iJt/12)$  has been dropped from Eq.(VI.25), making it formally the same as Eq.(VI.8). The same derivation of composite sequences follows. Note that the triplet basis of spin states is



assumed in Eq.(VI.25), although those states are not the eigenstates of the Hamiltonian in Eq.(VI.23). This basis is appropriate because the  $\pi$  pulse in the center of a  $P(\beta, \gamma)$  subcycle removes the chemical shifts.

DQ excitation in liquids is used in DQ filtering [88], a technique that allows the spectral lines of pairs of coupled nuclei to be separated from those of isolated nuclei. Two-dimensional DQ spectroscopy in liquids [89,90] is used to establish bond connectivities of carbon atoms in organic molecules. In this technique,  $^{13}\text{C}$  SQ lines are correlated through the DQ spectrum. A range of  $^{13}\text{C}$ - $^{13}\text{C}$  couplings arises due to the variety of C-C bonds.

## 2. $^{13}\text{C}$ spectroscopy in solids

The generalization of Eq.(VI.1) to pairs of inequivalent nuclei is:

$$\mathcal{H} = d(I_{z1}I_{z2} - \frac{1}{3}\mathbf{I}_1 \cdot \mathbf{I}_2) + \delta_1 I_{z1} + \delta_2 I_{z2} \quad (\text{VI.26})$$

In this case, the  $90_{90}-t/2-180_{270}-t/2-90_{90}$  subcycle does not apply when  $|d|$  and  $|\delta_1 - \delta_2|$  are comparable, since the dipole coupling term and the chemical shift terms do not commute. This is likely to be the situation in  $^{13}\text{C}$  NMR in solids. An alternative subcycle for the case in Eq.(VI.26) is simply a strong rf pulse of length  $t$ . If the rf phase is zero, and if  $t$  is a multiple of  $2\pi/\omega_1$ , then the propagator for the effective Hamiltonian in the lowest order of coherent averaging theory is:

$$U(t) = \exp[i d(I_{x1}I_{x2} - \frac{1}{3}\mathbf{I}_1 \cdot \mathbf{I}_2)t/2] \quad (\text{VI.27})$$

Eq.(VI.27) is again formally the same as Eq.(VI.4). Both DQ filtering and the two-dimensional DQ experiment can be applied in solids as well as in liquids [91]. In solids, the need for broadband DQ excitation arises from the distribution of dipole coupling constants due to differences in bond lengths and orientations.

### 3. Quadrupolar spin-1 nuclei

The quadrupole coupling constant  $\omega_Q$  for deuterium and  $^{14}\text{N}$  nuclei in solids is typically much larger than  $\omega_1$ . If  $\omega_1 \ll |\omega_Q|$ , then irradiation at a resonance offset  $\Delta\omega$  leads to an effective Hamiltonian [80]:

$$\mathcal{H}_{xx} = (\omega_1^2/\omega_Q) I_x^{1-3} + (\omega_Q/3)(I_z^{1-2} - I_z^{2-3}) + 2\Delta\omega I_z^{1-3} \quad (\text{VI.28})$$

If  $|\Delta\omega| \ll |\omega_1^2/\omega_Q|$ , Eq.(VI.28) is analogous to Eqs.(VI.4) and (VI.7) so that the same composite excitation sequences can be constructed. If  $\Delta\omega$  can not be ignored, Eq.(VI.28) implies that composite  $\pi/2$  pulses with simultaneous compensation for rf inhomogeneity and resonance offsets should be used as models for composite excitation sequences, since the first and third terms in Eq.(VI.28) look like the rf and offset interactions of an isolated spin. Again, the second term commutes with the others and can be ignored.

DQ spectroscopy is used to obtain chemical shift spectra of deuterium and  $^{14}\text{N}$  nuclei in solids [92-94]. The DQ spectrum displays the chemical shifts, and possibly the dipole couplings, that are otherwise masked by the much larger quadrupole couplings. In powdered,

polycrystalline, or amorphous solids, the randomness of orientations combines with differences in electronic environments to give a range of quadrupole couplings. Magic angle spinning may be used in conjunction with DQ spectroscopy to acquire chemical shift spectra [94]. Otherwise, chemical shift powder patterns are obtained.

Regardless of the sequence used for DQ excitation, no DQ coherence can be excited at molecular orientations where the quadrupole couplings are zero. Thus, if for example a deuterium chemical shift powder pattern is recorded, there will necessarily be an intensity deficit at chemical shift values corresponding to those orientations. However, if the maximum coupling in an axially symmetric quadrupole powder pattern is  $\omega_Q^{\max}$ , the bandwidth of uniform excitation for the composite sequences described above is sufficient that the signal amplitude arising from all orientations with couplings between the singularities at  $\omega_Q^{\max}$  and  $\omega_Q^{\max}/2$  will be within 0.99 of the maximum, provided that the composite sequence is optimized for a coupling of  $3\omega_Q^{\max}/4$ . The shape, but not the area, of the observed chemical shift powder pattern will depend on the relative orientation of the principle axes of the quadrupole coupling tensor and the chemical shift anisotropy tensor.

## E. Broadband polarization transfer

### 1. Background

In a given static magnetic field, the equilibrium polarization of a

particular nuclear isotope is proportional to its gyromagnetic ratio. This is apparent in Eq.(II.40). The initial polarization limits the maximum signal amplitude in any experiment. Therefore, to increase the sensitivity of experiments performed on nuclei with small gyromagnetic ratios, techniques have been developed for transferring polarization from nuclei with higher gyromagnetic ratios to those with lower gyromagnetic ratios. Polarization transfer (PT) relies on couplings between the different isotopes, i.e. heteronuclear couplings. In the most common case, the transfer is from protons to  $^{13}\text{C}$  nuclei in organic compounds. In this case, there are the additional advantages that the proton spin-lattice relaxation times are typically shorter than those of  $^{13}\text{C}$  nuclei and that several protons may contribute polarization to a single  $^{13}\text{C}$  nucleus.

A commonly used PT method in  $^{13}\text{C}$  NMR in solids is cross-polarization, developed by Pines, Gibby, and Waugh [95] based on earlier work of Hartmann and Hahn [96]. Cross-polarization is usually accomplished by giving a  $\pi/2$  pulse to protons, followed by long (several milliseconds) rf pulses applied simultaneously to protons and  $^{13}\text{C}$  nuclei satisfying the Hartmann-Hahn condition  $\omega_{1I} = \omega_{1S}$ , where I and S label protons and carbons respectively. Cross-polarization in solids is analyzed as an incoherent process, using kinetic and thermodynamic formalisms, due to the large number of protons coupled to one another.

Cross-polarization in liquids has been demonstrated as well [86]. In liquids, the proton-proton couplings are insignificant, allowing cross-polarization to be analyzed coherently, i.e. using exact quantum mechanical calculations of the spin evolution. Composite cross-polarization sequences have been developed for liquids in order to

extend the range of heteronuclear couplings for which PT is effective [86].

Other PT techniques for liquids have appeared, in particular INEPT [97] and DEPT [98]. In place of long pulses satisfying the Hartmann-Hahn condition, these make use of simple sequences of  $\pi/2$  and  $\pi$  pulses and delays similar to those used in MQ spectroscopy as discussed above. The INEPT sequence is shown in Figure VI.6. The delays are adjusted for optimal transfer for a single value of the heteronuclear coupling. In what follows, composite versions of INEPT are suggested to increase the range of couplings over which the transfer is nearly optimal. The composite sequences are again based on a formal analogy to composite pulses. The analogy in this case is the one introduced by Garbow, Weitekamp, and Pines for composite BIRD sequences [85].

## 2. Polarization transfer in an I-S spin system

To describe experiments in which rf pulses are applied near the Larmor frequencies of two different isotopes I and S, it is useful to use a doubly rotating frame of reference, related to the laboratory frame by the transformation  $\exp[-i(\omega_{0I}I_z + \omega_{0S}S_z)t]$ . With I and S labelling a single proton and a carbon, respectively, the doubly rotating frame internal Hamiltonian for a C-H fragment in a liquid is given by:

$$\mathcal{H} = \delta_I I_z + \delta_S S_z + J I_z S_z \quad (\text{VI.29})$$

A version of the INEPT sequence may be written:

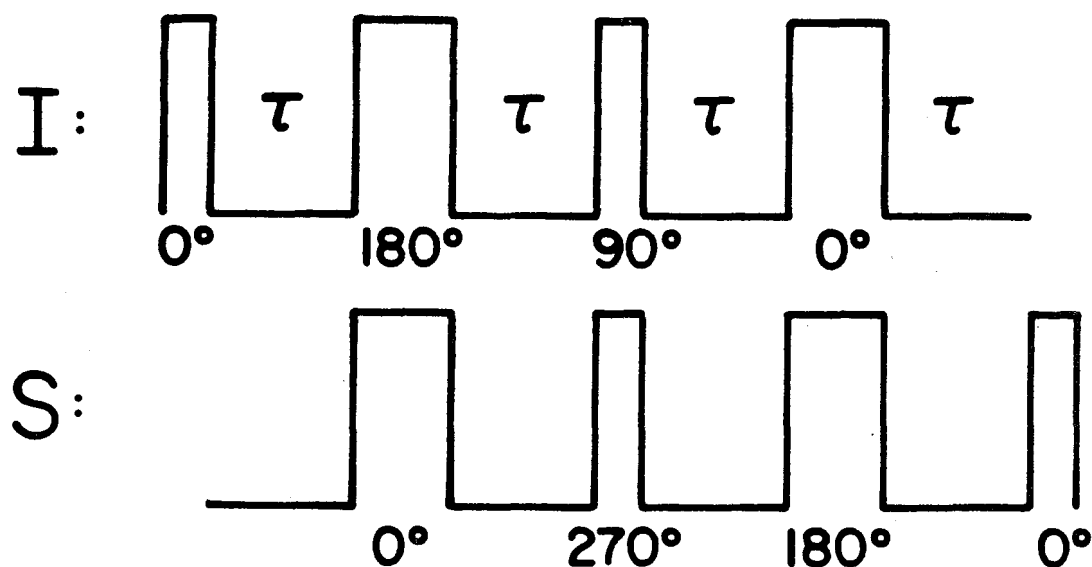


Figure VI.6: A simple sequence of the INEPT type for transferring polarization from a nucleus I to a nucleus S (e.g. a proton to a  $^{13}\text{C}$  nucleus), composed of  $\pi/2$  and  $\pi$  pulses with indicated phases. For optimal transfer, the delay  $\tau$  is set to  $\pi/(2J)$ , where  $J$  is the scalar coupling constant between I and S.

$$I: 90_0 - \tau - 180_{180} - \tau - 90_0 \quad -90_{90} - \quad \tau - 180_0 - \tau \quad (VI.30a)$$

$$\begin{array}{ccc} & : & : \\ 1 & : & 2 & : & 3 \\ & : & : \end{array}$$

$$S: -\tau - 180_0 - \tau - \quad -90_{270} - \quad 90_0 - \tau - 180_{180} - \tau - 90_0 \quad (VI.30b)$$

Line (VI.30a) is the sequence applied to the proton; line (VI.30b) is the sequence applied to the carbon. The sequence in Figure VI.6 is a reduced form of (VI.30). The form in (VI.30) is chosen to emphasize the symmetry of the proton and carbon sequences and to facilitate the following discussion by dividing PT into three steps.

Assume an initial density operator  $I_z$ . The aim of PT is to create a final density operator with a large component of  $S_z$ . The propagator for part 1 of line (VI.30) is:

$$U_1 = \exp(-iI_x\pi/2)\exp(-i\mathcal{H}\tau)\exp(iI_x\pi)\exp(-iS_x\pi)\exp(-i\mathcal{H}\tau)\exp(-iI_x\pi/2) \quad (VI.31)$$

$$= \exp(i2JI_yS_z\tau)\exp(-iS_x\pi) \quad (VI.32)$$

Since S refers to a spin-1/2 nucleus,  $S_z^2 = 1/4$ . Then the density operator after part 1 is:

$$\rho_1 = \exp(i2JI_yS_z\tau)I_z\exp(-i2JI_yS_z\tau) \quad (VI.33)$$

$$= I_z\cos(2JS_z\tau) - I_x\sin(2JS_z\tau) \quad (VI.34)$$

$$= I_z\cos(J\tau) - 2S_zI_x\sin(J\tau) \quad (VI.35)$$

The step from Eq.(VI.34) to (VI.35) can be seen by expanding the cosine and sine in their Taylor series [99]. Assuming  $J\tau = \pi/2$ , the density operator after part 2 is:

$$\rho_2 = -2\exp(-iI_y\pi/2)\exp(iI_y\pi/2)S_zI_x\exp(iS_y\pi/2)\exp(iI_y\pi/2) \quad (\text{VI.36})$$

$$= -2I_zS_x \quad (\text{VI.37})$$

The propagator for part 3 is:

$$U_3 = \exp(iI_x\pi)\exp(-iJI_zS_y\tau) \quad (\text{VI.38})$$

$U_3$  is related to  $U_1^{-1}$  by an exchange of the labels I and S. Therefore, since  $U_1$  converts  $I_z$  to  $-2S_zI_x$  when  $J\tau = \pi/2$ ,  $U_3$  converts  $-2I_zS_x$  to  $S_z$  when  $J\tau = \pi/2$ . The polarization transfer is complete. For other values of J, the final coefficient of  $S_z$  in the density operator is  $\sin^2(J\tau)$ .

The key element in the PT process is the conversion of  $I_z$  to an operator of the form  $2S_z(I_x\cos\gamma + I_y\sin\gamma)$ . This conversion can be treated as a rotation in the operator space spanned by the set  $\{2S_zI_x, 2S_zI_y, I_z\}$ , which satisfies the same commutation rules as  $\{I_x, I_y, I_z\}$ . The desired rotation is analogous to the creation of transverse magnetization. As in the theory of broadband DQ excitation, composite sequences can be constructed from basic units of the form of part 1 of line (VI.30), with various values of  $\tau_i$  and with overall phase shifts  $\phi_i$  of the proton rf. The basic unit is denoted by  $Q(\beta, \phi)$ , where  $\beta = J\tau$  and  $\phi$  is the phase shift. The propagator for the sequence  $Q(\beta_1, \phi_1)Q(\beta_2, \phi_2)\dots Q(\beta_n, \phi_n)$  is:



$$U = \exp(2iS_z I_{\phi_n} \beta_n) \exp(-2iS_z I_{\phi_{n-1}} \beta_{n-1}) \dots \exp(2iS_z I_{\phi_2} \beta_2) \exp(-2iS_z I_{\phi_1} \beta_1) \quad (\text{VI.39})$$

The alternation of the signs in the exponents is due to the factor  $\exp(-iS_x \pi)$  in Eq.(VI.32).  $n$  is assumed to be even in Eq.(VI.39). Eq.(VI.39) shows that composite sequences can be modelled after composite  $\pi/2$  pulses that compensate for rf inhomogeneity. The composite pulse  $(\theta_1)_{\phi_1} (\theta_2)_{\phi_2} \dots (\theta_n)_{\phi_n}$  becomes the composite sequence  $Q(\theta_1, \phi_1) Q(\theta_2, \phi_2 + \pi) \dots Q(\theta_n, \phi_n + \pi)$ .

A composite sequence may convert  $I_z$  to  $2S_z(I_x \cos \gamma + I_y \sin \gamma)$  over a large range of values of  $J$ . If  $\gamma$  is constant, the second step of PT, namely the conversion to  $2I_z(S_x \cos \gamma + S_y \sin \gamma)$ , can be accomplished with a pair of single  $\pi/2$  pulses, one on the proton and one on the carbon. If  $\gamma$  varies with  $J$ , the second step can not be accomplished efficiently. Therefore, it is important to use a composite  $\pi/2$  pulse that produces a constant net rotation as the model. Again, a good choice is

$$270_0 360_{169} 180_{33} 180_{178}.$$

The final step, the conversion of  $2I_z(S_x \cos \gamma + S_y \sin \gamma)$  to  $S_z$ , is achieved by a pulse sequence whose propagator is the inverse of that in Eq.(VI.39), but with the I and S labels reversed. Such a pulse sequence is easily constructed by reversing the order of pulses in the composite sequence in the first step and applying the I pulses to the S spins and the S pulses to the I spins. A general composite PT sequence is shown in Figure VI.7.

The plots of DQ signal amplitude as a function of the coupling constant for composite DQ excitation sequences in Figure VI.4 apply to

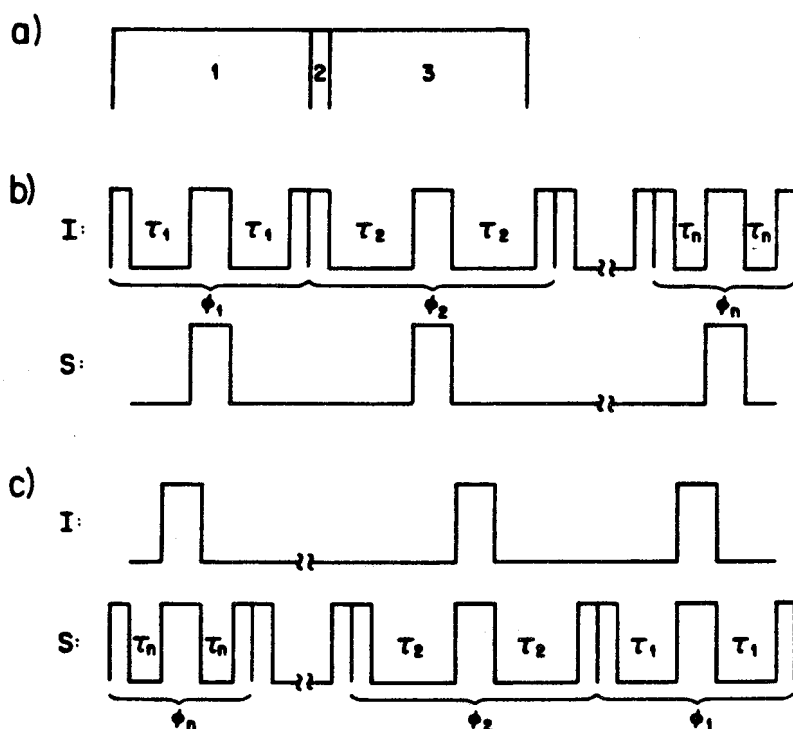


Figure VI.7: General form for a composite polarization transfer sequence, a generalization of Figure VI.6. The overall sequence is composed of three parts (a). The sequence of part 1 (b) converts an initial density operator  $I_z$  to  $I_\phi S_z$ . The second part is a pair of  $\pi/2$  pulses that convert the density operator to  $I_z S_\phi$ . The sequence of part 3 (c) converts  $I_z S_\phi$  to  $S_z$ , completing the transfer.

composite PT sequences as well if the ordinate is considered to be the final coefficient of  $S_z$ .

The composite PT sequences may be converted to reduced forms by combining adjoining  $\pi/2$  pulses as discussed in section B.3 above. The effects of rf inhomogeneity and of resonance offsets acting during the rf pulses can be further weakened by incorporating composite pulses into the composite PT sequences.

### 3. Polarization transfer in $I_n$ -S systems.

In organic molecules, coupled protons and  $^{13}\text{C}$  nuclei exist as  $\text{CH}_2$  and  $\text{CH}_3$  groups in addition to CH groups. Spin evolution in PT sequences differs for the different groups. This fact is used to selectively polarize  $^{13}\text{C}$  nuclei of one type, e.g.  $\text{CH}_2$  groups, and obtain the  $^{13}\text{C}$  spectrum of that type alone [98,100]. The impact of multiple I spins on the construction of composite PT sequences is that the evolution during the third step of the process is no longer a rotation. For example, consider a  $\text{CH}_2$  group. Eq.(VI.29) still applies, but with  $I_z = I_{z1} + I_{z2}$ . Eq.(VI.38) applies as well, but the final density operator becomes:

$$\rho_3 = \exp(iI_x\pi)\exp(-2iJI_{z1}S_y\tau)\exp(-2iJI_{z2}S_y\tau)(-2I_zS_x)\exp(2iJI_{z2}S_y\tau) \\ \times \exp(2iJI_{z1}S_y\tau)\exp(-iI_x\pi) \quad (\text{VI.40})$$

$$= 2I_zS_x\cos(2J\tau) + 4I_{z1}I_{z2}S_z\sin(2J\tau) + S_z\sin(2J\tau) \quad (\text{VI.41})$$

It is not guaranteed that composite sequences based on composite pulses in the third PT step will increase the effective bandwidth.

However, the evolution in the first step is formally the same for all  $I_n$ -S systems, so that composite sequences always apply. In addition, the S signal is sometimes acquired immediately after step 2, omitting step 3 entirely. This leads to a spectrum with zero area.

## Chapter VII: Iterative Schemes: Fixed Point Theory and Application to Broadband Population Inversion

### A. Background

#### 1. Definition of iterative schemes

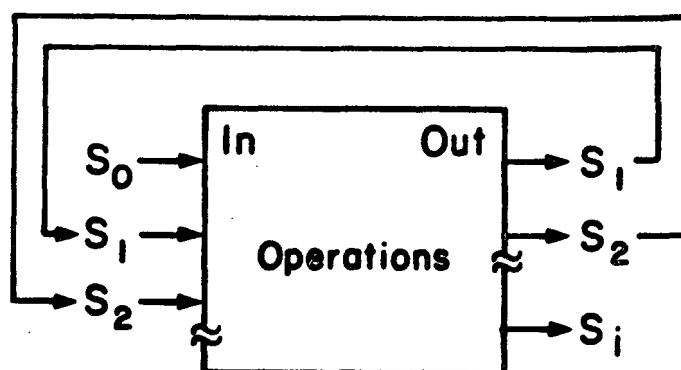
The approach to broadband excitation in Chapters IV and V is based on the well established methods of coherent averaging theory. The work described in Chapter III is also in the spirit of a great deal of previous work in NMR, relying as it does on Bloch vector trajectories. In very general terms, all of these approaches are similar in that they proceed by evaluating specific proposed pulse sequences in detail.

Recently, a qualitatively different approach to pulse sequence design has appeared in several areas of NMR. Rather than examining specific pulse sequences, the approach is to propose a set of operations that may be applied iteratively to any initial pulse sequence  $S_0$ , or any of a class of pulse sequences, to generate a series of iterate sequences  $S_1, S_2, S_3$ , etc., usually with increasing lengths. If a pulse sequence with a propagator of the form  $U_D$  is desired, the goal is to find operations such that the propagators  $U_0, U_1, U_2, U_3$ , etc. corresponding to the iterate sequences converge to  $U_D$  regardless of the choice of  $S_0$ . Thus, the theoretical emphasis is on evaluating the proposed operations, rather than the specific sequences. A set of operations that may be performed repetitively on a large class of initial sequences is called an iterative scheme. A schematic illustration of the action of an

iterative scheme is given in Figure VII.1. Iterative schemes are ideally suited for generating very long pulse sequences, which can not be derived by traditional methods due to the complexity of the calculations or due to practical computer time limitations, in cases where shorter sequences do not have the desired propagator. Iterative schemes have been used previously to construct pulse sequences for order-selective multiple-quantum excitation [46] and for heteronuclear decoupling [32,54], and to construct composite  $\pi/2$  pulses [101]. The purpose of this chapter is to present a unified theoretical framework for iterative schemes and to show how that framework can be used to analyze iterative schemes for broadband population inversion in systems of isolated spins. Chapter VIII extends those iterative schemes to the problem of narrowband population inversion. Chapter IX contains analyses of iterative schemes proposed by other authors, in order to demonstrate the wide applicability of the theory presented here.

## 2. Iterative schemes as functions on the propagator space

In any  $n$ -dimensional space of spin states, for example corresponding to a system of  $\log n / \log 2$  coupled spin-1/2 nuclei, there are  $n^2 - 1$  independent operators, excluding the identity operator. The operator space spanned by the operators is called Liouville space [35,102]. The density operator that describes the spin system exists in a subspace of Liouville space corresponding to Hermitian operators. Similarly, the propagator  $U$  that describes the transformation resulting from a pulse sequence exists in a subspace corresponding to some subset of all possible unitary operators. The space in which  $U$  lies may be



$S_0 =$ 

--	--	--

$S_1 =$ 

--	--	--	--	--	--

$S_2 =$ 

--	--	--	--	--	--	--	--	--	--	--	--	--

Figure VII.1: Schematic illustration of an iterative scheme for generating pulse sequences. Starting with an initial sequence  $S_0$ , a set of operations are performed iteratively to generate sequences  $S_1$ ,  $S_2$ , etc. that typically become increasingly complex, but produce the desired transformation of a spin system with increasing accuracy.

called the propagator space. It is sometimes convenient to write:

$$U = \exp(-iA) \quad (\text{VII.1})$$

where  $A$  is a Hermitian operator. Thus, for a spin system with given internal interactions, the effect of a pulse sequence is described either by a point in the propagator space or by a point in a topologically equivalent subspace of the space of Hermitian operators.

When an iterative scheme acts on a pulse sequence, it generates a new pulse sequence. To the new sequence, there corresponds a new propagator  $U'$ . This suggests that an iterative scheme may be viewed as a function  $F$  on the propagator space, with  $U' = F(U)$ . Equivalently,  $F$  may be considered to act on the space of Hermitian operators, with  $A' = F(A)$ . For certain iterative schemes, this is actually the case; for others,  $F$  is not single-valued. Nevertheless, an interpretation of iterative schemes in terms of functions on an operator space proves to be useful and forms the basis of the theoretical approach. Chapter IX gives examples of iterative schemes that are not described by a single function. The necessary modifications to the theory are discussed there.

### 3. An example of a function

#### a. Iterates, fixed points, and attractors

As a means of introducing the principles and terminology of the theory that follows, consider a simple class of functions  $f$  of a single



variable:

$$f(x) = \lambda x - x^3 \quad (\text{VII.2})$$

$\lambda$  is a parameter that characterizes members of this class of functions. A plot of  $f$  with  $\lambda = 3/2$  is given in Figure VII.2.

Beginning with any initial point  $x_0$ ,  $f$  can be used to generate a series of iterates  $x_1, x_2, x_3$ , etc. with  $x_1 = f(x_0)$ ,  $x_2 = f(x_1)$ ,  $x_3 = f(x_2)$ , etc. The iterates satisfy  $x_n = f^n(x_0)$ . Certain initial points have the property  $x_0 = f(x_0)$ ; this implies  $x_n = x_0$ , for all  $n$ . Such points are called fixed points of  $f$ . In the example of Eq. (VII.2), the fixed points are 0 and  $\pm(\lambda-1)^{1/2}$ , provided that  $\lambda > 1$ . For  $\lambda < 1$ , 0 is the only fixed point.

The properties of the iterates of a function may be called the dynamics of that function [103]. Fixed points have an important influence on the dynamics of a function, particularly if they are stable. A fixed point  $\bar{x}$  is stable if the iterates  $x_n$  of all initial points in the neighborhood of  $\bar{x}$  converge to  $\bar{x}$  as  $n$  increases. The stability of  $\bar{x}$  is determined by evaluating the derivative of  $f$  at  $\bar{x}$ , i.e.  $f'(\bar{x})$ . If  $f'(\bar{x}) < 1$ ,  $\bar{x}$  is stable; if  $f'(\bar{x}) > 1$ ,  $\bar{x}$  is unstable. Stable fixed points are sometimes called attractors. Initial points in the neighborhood of an attractor converge geometrically if  $0 < f'(\bar{x}) < 1$ ; that is  $x_n - \bar{x} \approx f'(\bar{x})(x_{n-1} - \bar{x})$ . The most rapid convergence occurs when  $f'(\bar{x}) = 0$ . In that case,  $\bar{x}$  is called superstable. In the example of Eq. (VII.2), 0 is an attractor when  $\lambda < 1$ . It is superstable when  $\lambda = 0$ . The points  $\pm(\lambda-1)^{1/2}$  are attractors when  $1 < \lambda < 2$ , and superstable when  $\lambda = 3/2$ .

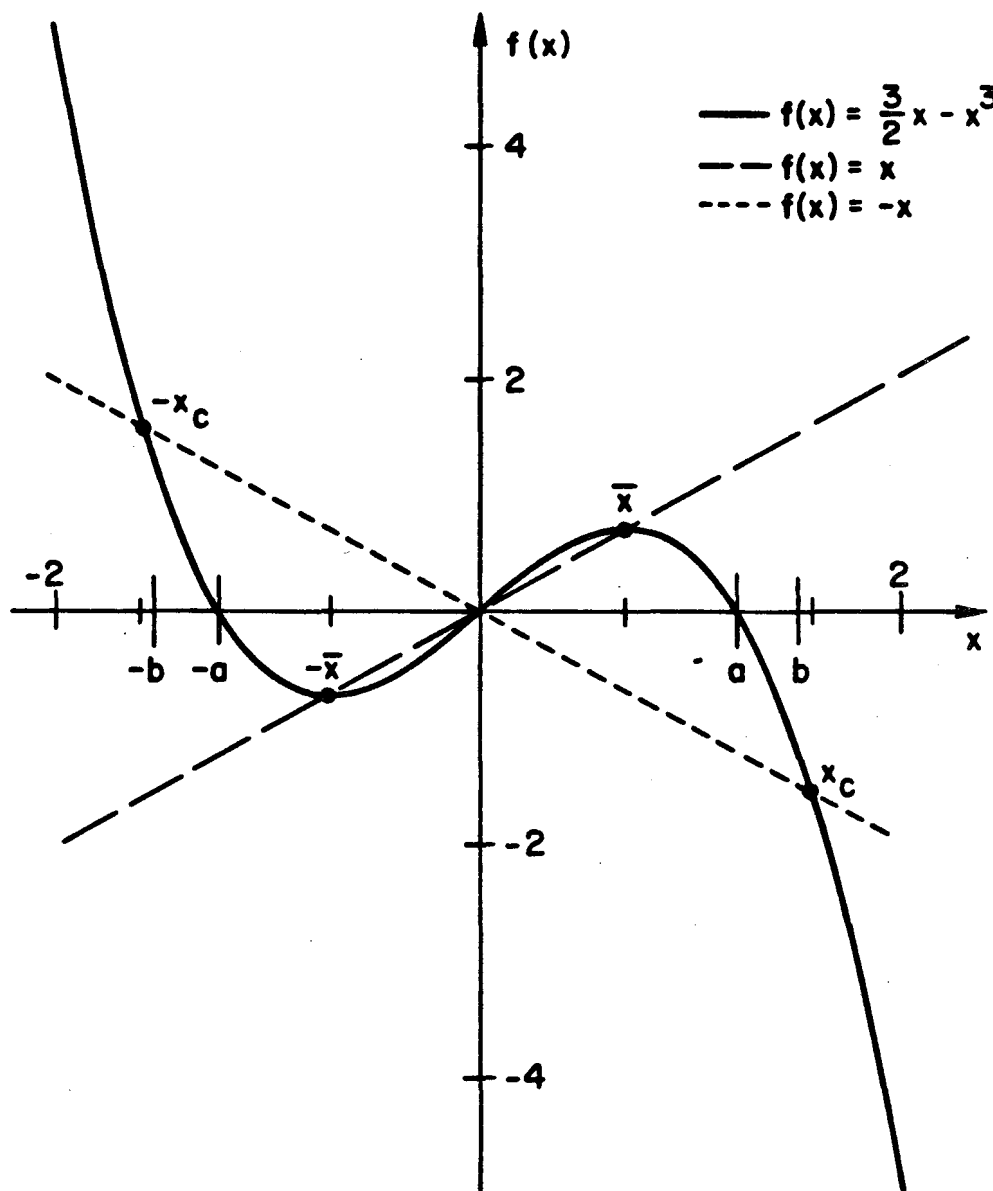


Figure VII.2: An example of a function of a single variable  $x$  that illustrates the concepts and behavior that underlies the analysis of iterative schemes. The points  $\pm\bar{x} = \pm\sqrt{1/2}$  are superstable fixed points; the point  $x = 0$  is an unstable fixed point. All initial points between  $-x_c$  and  $+x_c$ , with  $x_c = \sqrt{5/2}$ , converge to  $\bar{x}$ ,  $-\bar{x}$ , or 0 upon iteration. The open intervals  $(0,a)$ ,  $(-b,-a)$ ,  $(b,c)$ , etc. converge to  $\bar{x}$ , and therefore constitute the basin of  $\bar{x}$ . The points  $a, b, c$ , etc. converge to 0.

## b. Basins of attractors

The assessment of the stability of a fixed point is based on a linearization of the function in the neighborhood of the fixed point. Only the first derivative is considered. However, when a fixed point is stable, it can affect the dynamics of the function far beyond its immediate neighborhood, i.e. in the non-linear regime. Large regions of initial points, not just the nearby initial points, may converge to an attractor. The set of points that converge to an attractor is called the basin of that attractor.

For the function of Eq.(VII.2), with  $\lambda = 3/2$ , the iterates of all initial points in the open interval  $(-\sqrt{5/2}, \sqrt{5/2})$  converge to one of the three fixed points.  $(-\sqrt{5/2}, \sqrt{5/2})$  may be divided into subintervals that converge to one or the other of the superstable fixed points as depicted in Figure VII.2. First, note that it is sufficient to examine  $(0, \sqrt{5/2})$ , since  $f^n(-x) = -f^n(x)$  for all  $n$ . All initial points in the open interval  $(0, \sqrt{3/2})$  converge to the superstable fixed point at  $x = \sqrt{1/2}$ . This interval is denoted by  $I_a$ . The point  $a = \sqrt{3/2}$  satisfies  $f(a) = 0$ . Beyond  $a$ , there is an open interval  $I_b$  that maps onto  $(-a, 0)$  on the first iteration, and therefore converges to  $-\sqrt{1/2}$ . The upper bound of  $I_b$  is a point  $b$  that satisfies  $f(b) = -a$ , or  $f^2(b) = 0$ . Beyond  $b$ , there is an open interval  $I_c$  that maps onto  $(-b, -a)$ , which converges to  $\sqrt{1/2}$ .  $I_c$  is bounded by a point  $c$  that satisfies  $f(c) = -b$ , or  $f^3(c) = 0$ . Continuing in this way, the interval  $(0, \sqrt{5/2})$  is decomposed into open intervals that converge alternately to  $\sqrt{1/2}$  and  $-\sqrt{1/2}$ . The intervals are separated by isolated points  $a, b, c$ , etc. that map onto 0 with

increasing numbers of iterations. The sequence  $a, b, c, \dots$  converges to the point  $x_c = \sqrt{5}/2$ . This point satisfies  $f^n(x_c) = (-1)^n x_c$ . Its iterates alternate between  $-x_c$  and  $x_c$ .  $x_c$  may be called a fixed point with a period of 2. For  $x > x_c$ ,  $|f(x)| > |x|$ . Therefore, the iterates of points in  $(-\infty, -x_c)$  and  $(x_c, \infty)$  diverge.

#### 4. Remarks

The example of Eq.(VII.2) and Figure VII.2 illustrates a number of general features. A function may have more than one fixed point. The attractors influence the dynamics of the function over large ranges of initial points. The basins may consist of many disconnected regions.

The fact that  $f$  in Eq.(VII.2) is a simple function of a single variable makes the dynamics easy to analyze in detail by algebraic and graphical means. The analysis of more complicated cases follows the same steps, although a complete description of the dynamics may not be possible. First, the fixed points are found. In the NMR examples in the following sections, certain fixed points are known a priori. Others can be found numerically. Next, a linear analysis is performed in the neighborhood of the fixed points. In general, a function of many variables is equivalent to a linear transformation in the neighborhood of a fixed point. The stability of a fixed point is determined by examining the features of that linear transformation, in particular its eigenvalues. If the magnitudes of all the eigenvalues are less than or equal to 1, the fixed point is stable. Finally, the basins are examined. If the function is complicated, as in the examples below, the basins must be determined numerically.

In the following sections, the above principles are applied to iterative schemes that generate composite  $\pi$  pulses. Algebraic and numerical methods for analyzing the dynamics of the corresponding functions are developed.

## B. Iterative schemes for broadband population inversion

### 1. Propagator space for an isolated spin or two-level system

The propagator for a pulse of length  $\tau$  is:

$$R = \exp(-i\tilde{\alpha} \cdot \tilde{I}) \quad (\text{VII.3})$$

where:

$$\tilde{\alpha} = (\omega_1 \tau \cos \phi, \omega_1 \tau \sin \phi, \Delta \omega \tau) \quad (\text{VII.4})$$

$R$  is a rotation operator in the spin angular momentum vector space. The density operator describing the initial, equilibrium spin state is proportional to  $I_z$ ; rf pulses merely rotate the density operator to a linear combination of  $I_x$ ,  $I_y$ , and  $I_z$ . Therefore, the relevant space of Hermitian operators is the three-dimensional space spanned by  $I_x$ ,  $I_y$  and  $I_z$ . For describing the propagator, only a subspace of this space is required. Any sequence of rf pulses produces a transformation that is a product of rotations, equivalent to a single net rotation. The net

rotation is completely characterized by a vector  $\underline{\alpha}$ , as in Eq.(VII.3), where the magnitude of  $\underline{\alpha}$  is the net rotation angle and the direction of  $\underline{\alpha}$  is the net rotation axis.  $\underline{\alpha}$  is determined by the pulse lengths and phases of the sequence, and by the values of  $\Delta\omega$  and  $\omega_1$ . Since any product of rotations is equivalent to a net rotation of  $\pi$  or less,  $\underline{\alpha}$  lies in a sphere with a radius of  $\pi$ . Since rotations of  $\pi$  about antiparallel axes are equivalent, antipodal points on the surface of the sphere are identified. This spherical subspace represents the group of rotations, called  $SO(3)$  or  $O^+(3)$  [104]. It is pictured in Figure VII.3.

## 2. An iterative scheme and the corresponding function

A class of iterative schemes that may be applied to any initial pulse sequence  $S_0$  is defined by the following operations:

1. Construct  $N$  phase-shifted versions of  $S_0$ , with overall phase shifts  $\phi_i$ . The phase-shifted versions may be denoted by  $S_0^{(i)}$ .  $N$  is taken to be an odd integer.
2. Concatenate the phase-shifted versions, producing a new sequence  $S_1 = S_0^{(1)} S_0^{(2)} \dots S_0^{(N)}$ .

The operations may be applied to  $S_1$  to generate  $S_2$ , and so forth. An iterative scheme of this class is specified by the notation  $[\phi_1, \phi_2, \dots, \phi_N]$ , with the phase shifts given in degrees. Under such a scheme,  $S_n$  is  $N^n$  times longer than  $S_0$ .

A  $[\phi_1, \phi_2, \dots, \phi_N]$  scheme dictates a function on  $SO(3)$  space. If  $S_0$  produces a rotation corresponding to the point  $\underline{\alpha}_0 = (\alpha_x, \alpha_y, \alpha_z)$ , then  $S_1$  produces a rotation corresponding to the unique point  $\underline{\alpha}_1$  satisfying:

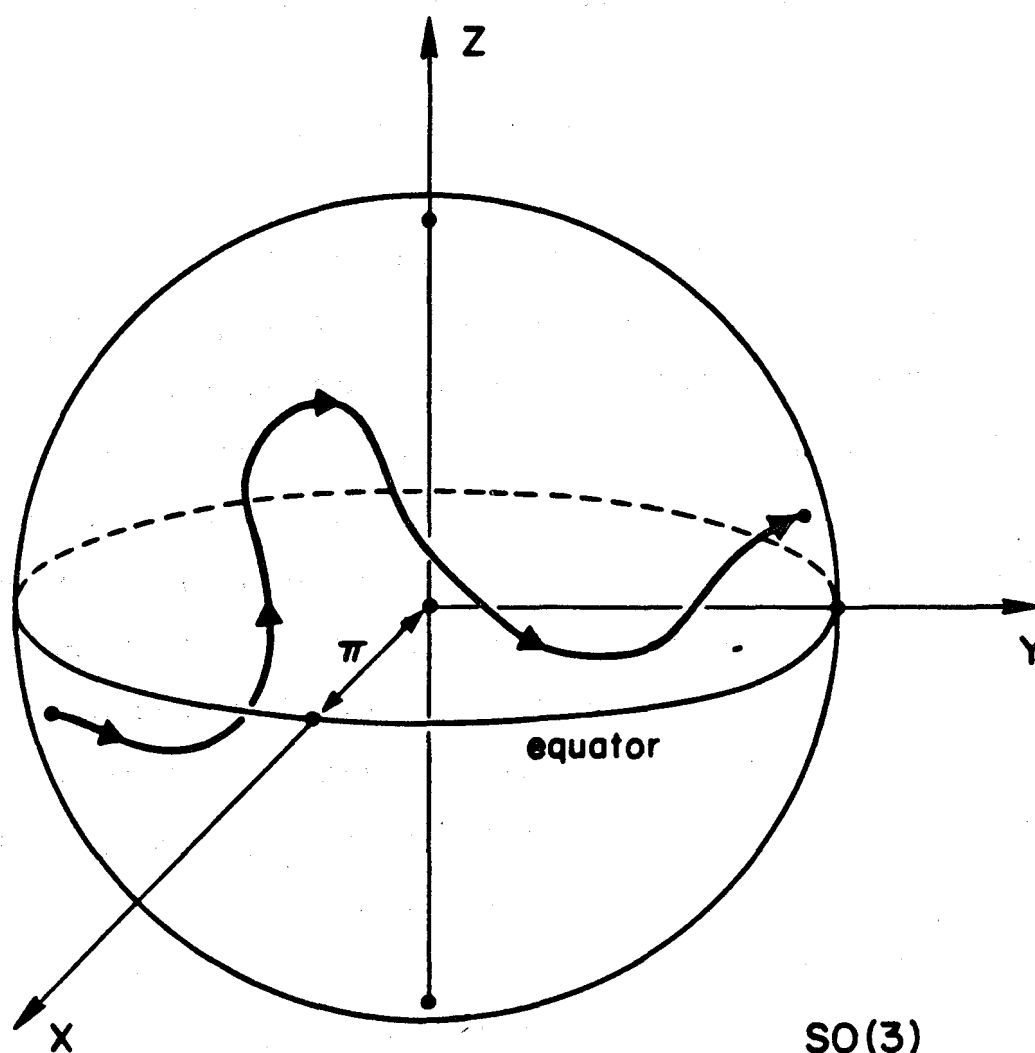


Figure VII.3: The spherical space that represents the group of rotations  $SO(3)$ . Each distinct rotation corresponds to a point in the space whose distance and direction from the origin are respectively the angle and axis of rotation. The space has a radius of  $\pi$ , and antipodal points are identified (correspond to the same rotation). A closed path in the space is shown. Iterative schemes that generate pulse sequences that act on isolated spins are treated as functions on the space. The equator corresponds to rotations, or pulse sequences, that invert spin populations.

$$\exp(-i\alpha_1 \cdot \underline{I}) = \exp(-i\alpha_0^N \cdot \underline{I}) \exp(-i\alpha_0^{N-1} \cdot \underline{I}) \dots \exp(i\alpha_0^1 \cdot \underline{I}) \quad (\text{VII.5})$$

with:

$$\alpha_0^i = (\alpha_x \cos \phi_i - \alpha_y \sin \phi_i, \alpha_y \cos \phi_i + \alpha_x \sin \phi_i, \alpha_z) \quad (\text{VII.6})$$

Eq.(VII.6) is a statement of the fact that an overall rf phase shift by  $\phi_i$  rotates a pulse sequence propagator about  $z$  by  $\phi_i$ . The only possible ambiguity in the definition of  $\alpha$  arises if the right-hand side of Eq.(VII.5) is equivalent to a net rotation of  $\pi$ , but this ambiguity is resolved by the identification of antipodal points in  $SO(3)$ . The mapping of  $\alpha_0$  to  $\alpha_1$ , and then to higher iterates, makes no reference to the details of the pulse sequence  $S_0$ . If two different sequences produce the same net rotation, possibly with different values of  $\Delta\omega$  and  $\omega_1$ , then their iterates will produce the same net rotations, corresponding to the same series of points  $\alpha_0, \alpha_1, \alpha_2$ , etc. The function that generates these points is  $F$ , with  $\alpha_n = F^n(\alpha_0)$ .

Certain fixed points of  $F$  are immediately obvious and are common to all  $[\phi_1, \phi_2, \dots, \phi_N]$  schemes with odd  $N$ . First, if  $\alpha_0 = 0$ , then the right-hand side of Eq.(VII.5) is the unit operator, making  $\alpha_1 = 0$ . Thus, the origin of  $SO(3)$  is always a fixed point.

A second type of fixed point appears from the following considerations. Suppose  $\alpha_0 = (\pi \cos \gamma, \pi \sin \gamma, 0)$ . Then  $S_0$  produces a rotation of  $\pi$  about an axis in the  $xy$  plane, taking  $I_z$  to  $-I_z$ . Any phase-shifted version of  $S_0$  also produces a rotation of  $\pi$  about an axis in the  $xy$  plane. An odd number of these rotations will again take  $I_z$  to  $-I_z$ , and is therefore equivalent to a net rotation of  $\pi$  about an axis in the  $xy$  plane. In fact:



$$\underline{g}_1 = (\pi \cos(\gamma + \phi_T), \pi \sin(\gamma + \phi_T), 0) \quad (\text{VII.7})$$

with:

$$\phi_T = \sum_{i=1}^N (-1)^{i+1} \phi_i \quad (\text{VII.8})$$

$\underline{g}_0$  and  $\underline{g}_1$ , as well as higher iterates generated by  $F$ , lie on the equator of  $S(3)$ , although they are generally different points. To describe this situation, in which  $F$  generates iterates that are all contained in a specific set of points, the definition of a fixed point must be generalized somewhat. The equator of  $S(3)$  is called a fixed, or invariant, set of points. Note that there are schemes in which all points on the equator are individually fixed, in particular when  $\phi_T = 0$  or  $\phi_T = \pi$ . The equator is an especially significant set of points, since a rotation that takes a density operator of  $I_z$  to  $-I_z$  corresponds to perfect population inversion.

The third fixed set of points common to all  $[\phi_1, \phi_2, \dots, \phi_N]$  schemes is the  $z$  axis of  $S(3)$ . If  $\underline{g}_0$  lies on the  $z$  axis, then the right-hand side of Eq.(VII.5) is a product of rotations about the  $z$  axis, equivalent to a net rotation about the  $z$  axis. Thus,  $\underline{g}_1$  lies on the  $z$  axis as well. Specifically,  $\underline{g}_1 = (0, 0, N\alpha_z)$ . Points along the  $z$  axis for which  $\alpha_z = 2n\pi/(N-1)$  for some integer  $n$  are individually fixed points.

### 3. Stability of the fixed points

#### a. The origin

As discussed in Section A, the stability of a fixed point is assessed by a linearization of the function in the neighborhood of the fixed point. A linearization of  $F$  about the origin of  $SO(3)$  is effected by evaluating the right-hand side of Eq.(VII.5) to first order in  $|\alpha_0|$ . The result is:

$$\alpha_1 = \alpha_0^N + \alpha_0^{N-1} + \dots + \alpha_0^1 \quad (\text{VII.9})$$

Eq.(VII.9) expresses a linear transformation, which can be written as  $\alpha_1 = T_0 \alpha_0$ . The linear operator  $T_0$  is a sum of rotations about the  $z$  axis by angles  $\phi_i$ :

$$T_0 = R_z(\phi_N) + R_z(\phi_{N-1}) + \dots + R_z(\phi_1) \quad (\text{VII.10})$$

In the  $\{x,y,z\}$  basis,  $T_0$  is:

$$T_0 = \begin{pmatrix} N & \sum_{n=1}^N \cos \phi_n & \sum_{n=1}^N \sin \phi_n & 0 \\ -\sum_{n=1}^N \sin \phi_n & N & \sum_{n=1}^N \cos \phi_n & 0 \\ 0 & 0 & 0 & N \end{pmatrix} \quad (\text{VII.11})$$

One eigenvector of  $T_0$  is  $(0,0,1)$ , a vector along the  $z$  axis of  $SO(3)$ . Its eigenvalue is  $N$ . Since  $N > 1$ , the  $z$  axis is an unstable direction. The other eigenvectors are  $(1,i,0)$  and  $(1,-i,0)$ , with eigenvalues  $\lambda_0^+$  and  $\lambda_0^-$  respectively:

$$\lambda_0^\pm = \sum_{n=1}^N \exp(\pm i\phi_n) \quad (\text{VII.12})$$

The existence of complex eigenvectors and eigenvalues is indicative of a rotation.  $T_0$  stretches or shrinks vectors in the  $xy$  plane by a factor of  $|\lambda_0^+|$  and rotates them about  $z$  by an angle  $\phi_+$ , where  $\phi_+$  is the phase of  $\lambda_0^+$ . The stability of the origin of  $SO(3)$  along directions in the  $xy$  plane is thus determined by  $|\lambda_0^+|$ . Eq.(VII.12) implies:

$$|\lambda_0^+| = \left[ \left( \sum_{n=1}^N \cos\phi_n \right)^2 + \left( \sum_{n=1}^N \sin\phi_n \right)^2 \right]^{1/2} \quad (\text{VII.13})$$

If  $|\lambda_0^+| < 1$ , the origin is stable with respect to displacements in the  $xy$  plane.

b. The equator

The assessment of the stability of the equator of  $SO(3)$  is complicated by the fact that points on the equator are not individually fixed under  $F$ , but constitute an invariant set. The linear analysis can take two forms. One is to write  $\alpha_0$  as  $\alpha_0 = \beta_0 + \delta$ , where  $\beta_0$  lies on the equator and  $\delta$  is small. The right-hand side of Eq.(VII.5) can then be evaluated to first order in  $|\delta|$  using relations such as:

$$\exp[-i(\beta_0 + \delta) \cdot \underline{I}] = \exp(-i\beta_0 \cdot \underline{I}) \exp(-i\delta \cdot \underline{I}) \quad (\text{VII.14})$$

where:

$$\begin{aligned} \underline{\varepsilon} = & (-2\delta_z \sin\gamma/\pi + \delta_x \cos^2\gamma + \delta_y \sin\gamma \cos\gamma, 2\delta_z \cos\gamma/\pi \\ & + \delta_x \sin\gamma \cos\gamma + \delta_y \sin^2\gamma, 2\delta_x \sin\gamma/\pi - 2\delta_y \cos\gamma/\pi) \end{aligned} \quad (\text{VII.15})$$

Eq.(VII.15) assumes that  $\underline{g}_0 = (\pi \cos \gamma, \pi \sin \gamma, 0)$ , and is valid to first order in  $|\underline{\delta}|$ . In fact, the analysis can be somewhat simplified by requiring that  $\delta_x \sin \gamma - \delta_y \cos \gamma = 0$ . This may be done because  $\delta_x \sin \gamma - \delta_y \cos \gamma$  is the projection of  $\underline{\delta}$  onto a direction in the xy plane perpendicular to  $\underline{g}_0$ , namely  $(\sin \gamma, -\cos \gamma, 0)$ . To first order, the component of  $\underline{\delta}$  perpendicular to  $\underline{g}_0$  merely converts  $\underline{g}_0$  to another point on the equator, still in the invariant set of points. Thus, there are really only two significant directions for displacements from the equator, which may be obvious in retrospect.

A more concise way of treating the linearization about the equator, and one that simplifies the algebra, is to write the propagator for  $S_0$  in the form of the right-hand side of Eq.(VII.14) immediately, with the restriction  $\epsilon_z = 0$ . Such an expression is actually completely general, regardless of  $|\underline{\epsilon}|$ . In other words, any net rotation at all can be expressed as the product of two rotations in the xy plane, the first by  $|\underline{\epsilon}|$  and the second by  $180^\circ$ . Again, this fact may not be surprising in retrospect, since there are still three variables in such an expression, i.e. the direction of  $\underline{g}_0$  and the magnitude and direction of  $\underline{\epsilon}$ . For a given net rotation, those three variables are uniquely determined in all cases except when the net rotation is about the z axis.

A linear analysis using an expression for the net rotation in the form of the right-hand side of Eq.(VII.14) proceeds as follows. If:

$$\exp(-i \underline{g}_0 \cdot \underline{I}) = \exp[-i(I_x \cos \gamma + I_y \sin \gamma) \pi] \exp(-i \underline{\epsilon} \cdot \underline{I}) \quad (\text{VII.16})$$

then, to first order in  $|\underline{\varepsilon}|$  :

$$\exp(-i\underline{\alpha}_1 \cdot \underline{I}) = \exp[-i(I_x \cos(\gamma + \phi_T) + I_y \sin(\gamma + \phi_T))\pi] \exp(-i\underline{\varepsilon}_T \cdot \underline{I}) \quad (\text{VII.17})$$

where:

$$\underline{\varepsilon}_T = \sum_{n=1}^N (\varepsilon_x \cos \Gamma_n - \varepsilon_y \sin \Gamma_n, (-1)^{n+1} \varepsilon_y \cos \Gamma_n + (-1)^{n+1} \varepsilon_x \sin \Gamma_n, 0) \quad (\text{VII.18})$$

$$\Gamma_n = \phi_n + \sum_{m=1}^{n-1} (-1)^{m+1} 2\phi_m, \quad n \text{ odd} \quad (\text{VII.19})$$

$$= \phi_n - 2\gamma + \sum_{m=1}^{n-1} (-1)^m 2\phi_m, \quad n \text{ even} \quad (\text{VII.20})$$

Eq.(VII.16) presents the initial rotation as the product of an error rotation characterized by  $\underline{\varepsilon}$  with a perfect  $\pi$  rotation with a phase  $\gamma$ . Eq.(VII.17) indicates that the effect of  $F$  is to transform that rotation to a new rotation of the same form, but with the error  $\underline{\varepsilon}_T$  and the phase  $\gamma + \phi_T$ .  $\underline{\varepsilon}_T$  is related to  $\underline{\varepsilon}$  by a linear transformation  $T_e$ .  $T_e$  can be expressed in terms of rotations as:

$$T_e = [R_z(\Gamma_N) + R_z(\Gamma_{N-2}) + \dots + R_z(\Gamma_1)] \\ + R_x(\pi)[R_z(\Gamma_{N-1}) + R_z(\Gamma_{N-3}) + \dots + R_z(\Gamma_2)] \quad (\text{VII.21})$$

$(0,0,1)$  is always an eigenvector of  $T_e$  with eigenvalue 1, but this is not a significant direction since  $\underline{\varepsilon}$  always has a  $z$  component of 0. In the  $\{x,y\}$  basis,  $T_e$  is:

$$T_e = \begin{pmatrix} \sum_{n=1}^N \cos \Gamma_n & -\sum_{n=1}^N \sin \Gamma_n \\ \sum_{n=1}^N (-1)^{n+1} \sin \Gamma_n & \sum_{n=1}^N (-1)^{n+1} \cos \Gamma_n \end{pmatrix} \quad (\text{VII.22})$$

In investigating the dynamics of  $F$  near the equator, the phase shift  $\phi_T$  is ignored due to the fact that the equator is generally an invariant set of points within which individual points are not fixed. Therefore, in studying the transformation of  $\underline{\varepsilon}$ , it is the direction of  $\underline{\varepsilon}$  relative to the phase  $\gamma$  and the direction of  $\underline{\varepsilon}_T$  relative to the phase  $\gamma + \phi_T$  that are important. For this reason, it is convenient to rewrite Eq.(VII.17) as:

$$\begin{aligned} \exp(-i\alpha_1 \cdot \underline{I}) &= \exp(-iI_Z \phi_T) \exp[-i(I_X \cos \gamma + I_Y \sin \gamma) \pi] \\ &\quad \times \exp[(-i\underline{\varepsilon}_T' \cdot \underline{I}) \exp(iI_Z \phi_T)] \end{aligned} \quad (\text{VII.23})$$

where:

$$\underline{\varepsilon}_T' = R_Z(-\phi_T) \underline{\varepsilon}_T \quad (\text{VII.24})$$

The significant linear transformation is no longer  $T_e$ , but is the product  $R_Z(-\phi_T) T_e$ , denoted by  $T_e'$ . Eq.(VII.21) implies that  $T_e'$  has the same matrix form as  $T_e$  in Eq.(VII.22), but with a redefinition of  $\Gamma_n$ :

$$T_e' = \begin{pmatrix} \sum_{n=1}^N \cos \Gamma_n' & -\sum_{n=1}^N \sin \Gamma_n' \\ \sum_{n=1}^N (-1)^{n+1} \sin \Gamma_n' & \sum_{n=1}^N (-1)^{n+1} \cos \Gamma_n' \end{pmatrix} \quad (\text{VII.25})$$

$$\Gamma_n' = \Gamma_n + (-1)^n \phi_T \quad (\text{VII.26})$$

The eigenvectors and eigenvalues depend on the choice of the iterative scheme. Three possible scenarios exist: First, the eigenvalues can be

real and distinct, implying the existence of two real eigenvectors. Second, the two eigenvalues can be complex and conjugate to one another, implying two complex conjugate eigenvectors. Third, the two eigenvalues can be real and degenerate. In this last case, there may be either one or two independent real eigenvectors. It should be realized that  $T'_e$  and  $T_e$  are generally not hermitian, and so need not have a complete basis of eigenvectors. This statement is generally true of iterative schemes.

The eigenvalues of  $T'_e$  are  $\lambda_e^\pm$ , given by:

$$\lambda_e^\pm = (\cos\Gamma_1' + \cos\Gamma_3' + \dots + \cos\Gamma_N') \pm [(\cos\Gamma_2' + \cos\Gamma_4' + \dots + \cos\Gamma_{N-1}')^2 + (\sin\Gamma_2' + \sin\Gamma_4' + \dots + \sin\Gamma_{N-1}')^2 - (\sin\Gamma_1' + \sin\Gamma_3' + \dots + \sin\Gamma_N')^2]^{1/2} \quad (\text{VII.27})$$

The criteria for stability at the equator are  $|\lambda_e^+| < 1$  and  $|\lambda_e^-| < 1$ .

The eigenvalues are independent of  $\gamma$  but the eigenvectors are not. The eigenvectors for  $\gamma \neq 0$  are related to those for  $\gamma = 0$  by a rotation about  $z$  by  $\gamma$ .

#### 4. Schemes for which the equator of $SO(3)$ is superstable

Iterative schemes can be found with various stability properties at the equator and the origin. One way to find iterative schemes is to make use of vector diagrams. This is particularly useful for finding schemes for which the fixed points are superstable. For example, Eqs.(VII.18) through (VII.21) suggest the following picture:  $\underline{x}_T$  is the sum of  $N$  vectors of equal magnitudes in the  $xy$  plane, rotated about  $z$  by  $\Gamma_n$ . These vectors may be divided into two groups, those with odd  $n$  and

those with even  $n$ . Those with even  $n$ , in addition to being rotated about  $z$ , are rotated about  $x$  by  $\pi$ . Now, if  $\Gamma_n$  can be found such that the two groups of vectors separately add up to zero,  $\underline{\varepsilon}_T$  will be zero regardless of  $\underline{\varepsilon}$  and regardless of  $\gamma$ . Then the equator is superstable. Examples of vector diagrams that imply iterative schemes for which the equator is superstable are given in Figure VII.4. A minimum  $N$  of 5 is required. Once the  $\Gamma_n$  are determined, the phase shifts  $\phi_n$  can be derived with Eqs.(VII.19) and (VII.20). For  $N = 5$ , possible superstability conditions are:

$$\Gamma_3 = \Gamma_1 + 2\pi/3 \quad (\text{VII.28a})$$

$$\Gamma_4 = \Gamma_2 + \pi \quad (\text{VII.28b})$$

$$\Gamma_5 = \Gamma_1 + 4\pi/3 \quad (\text{VII.28c})$$

Two schemes that satisfy Eq.(VII.28) are  $[0,0,120,60,120]$  and  $[0,330,60,330,0]$ . If the initial sequence is chosen to be  $180_0$ , i.e. a single  $\pi$  pulse, these schemes generate sequences of  $5^n$   $\pi$  pulses. Table VII.1 lists the phases of the  $\pi$  pulses in the first three iterate sequences generated by  $[0,0,120,60,120]$ .

The arguments above make no reference to the source of the error  $\underline{\varepsilon}$ . Thus, errors due to rf inhomogeneity and miscalibration or resonance offsets are both cancelled by iteration. Figures VII.5 through VII.8 show inversion plots for the iterate sequences of  $180_0$  under  $[0,0,120,60,120]$  and  $[0,330,60,330,0]$  as functions of  $\Delta\omega/\omega_1^0$  and  $\omega_1/\omega_1^0$ . Note that large bandwidths of essentially perfect inversion are achieved with respect to both parameters. A contour plot of the inversion as a function of  $\Delta\omega/\omega_1^0$  and  $\omega_1/\omega_1^0$  simultaneously for the 25-pulse sequence



Table VII.1: Rf phases in degrees of individual  $\pi$  pulses in the broadband inversion sequences  $S_1$ ,  $S_2$ , and  $S_3$  generated from an initial pulse  $180_0$  by the iterative scheme  $[0,0,120,60,120]$

---

$S_1$ : 0,0,120,60,120

$S_2$ : 0,0,120,60,120,0,0,120,60,120,120,120,240,180,240,60,60,180,  
120,180,120,120,240,180,240

$S_3$ : 0,0,120,60,120,0,0,120,60,120,120,120,240,180,240,60,60,180,  
120,180,120,120,240,180,240,0,0,120,60,120,0,0,120,60,120,  
120,120,240,180,240,60,60,180,120,180,120,120,240,180,240,  
120,120,240,180,240,120,120,240,180,240,240,240,0,300,0,180,  
180,300,240,300,240,240,0,300,0,60,60,180,120,180,60,60,  
180,120,180,180,180,300,240,300,120,120,240,180,240,180,  
180,300,240,300,120,120,240,180,240,120,120,240,180,240,240,  
240,0,300,0,180,180,300,240,300,240,240,0,300,0



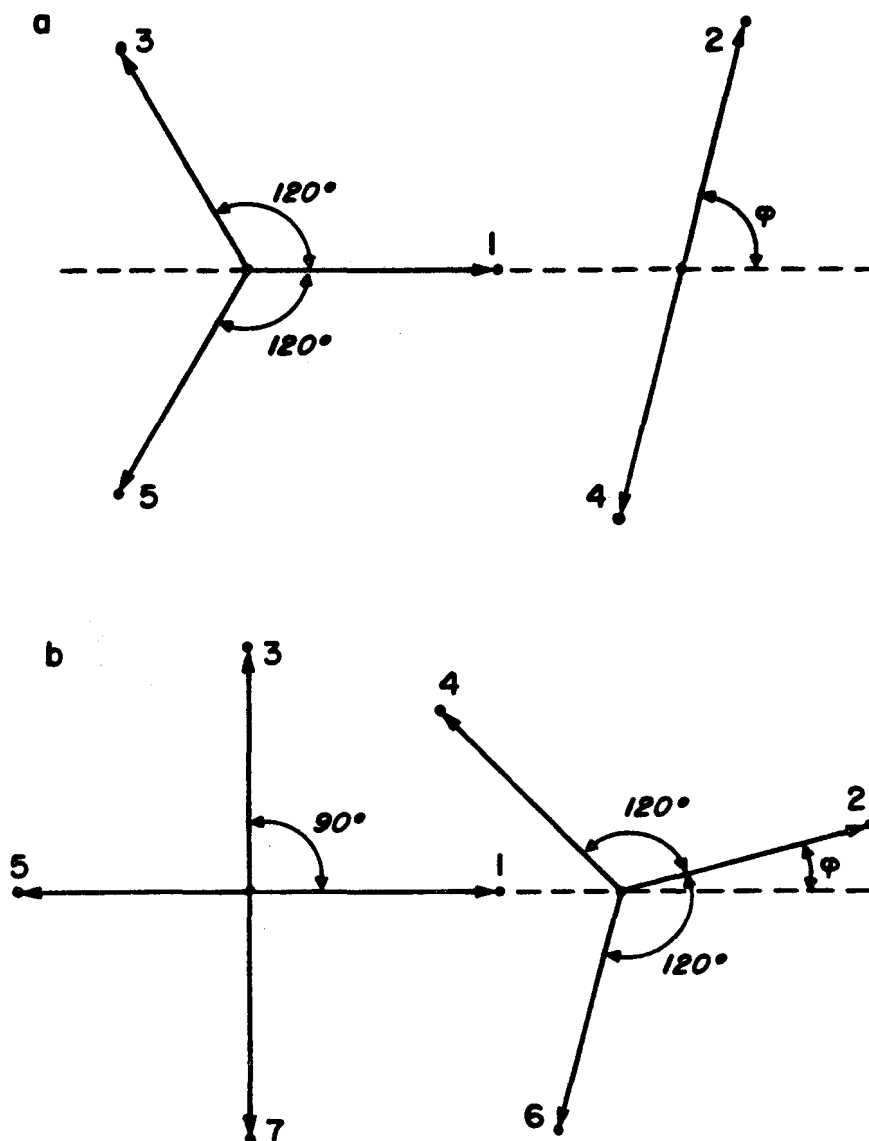
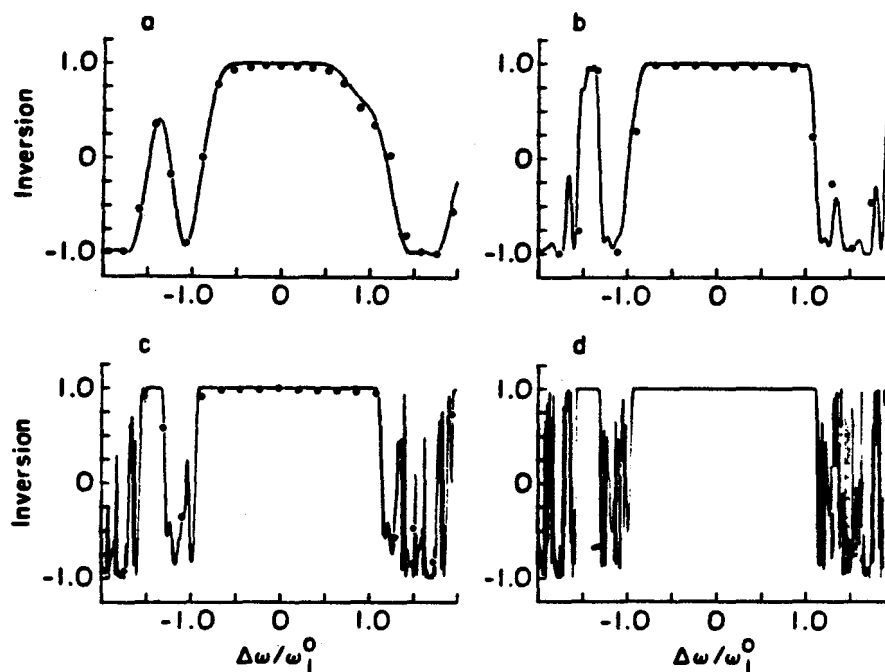
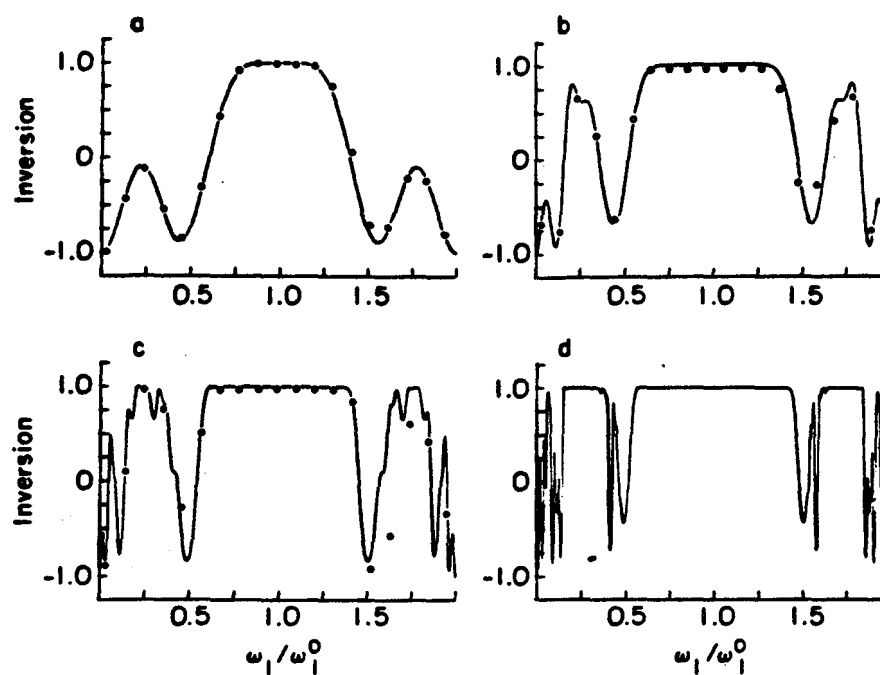


Figure VII.4: Vector diagrams that describe iterative schemes for which the equator of  $SO(3)$  is superstable. Such schemes generate broadband population inversion sequences. a) A diagram that describes schemes of the form  $[0, \phi, 120+2\phi, 60+3\phi, 120+4\phi]$ . b) A diagram that describes schemes of the form  $[0, \phi, 90+2\phi, 300+3\phi, 240+4\phi, 300+5\phi, 90+6\phi]$ . See Eqs. (VII.19) and (VII.20) and section B.4 of Chapter VII.



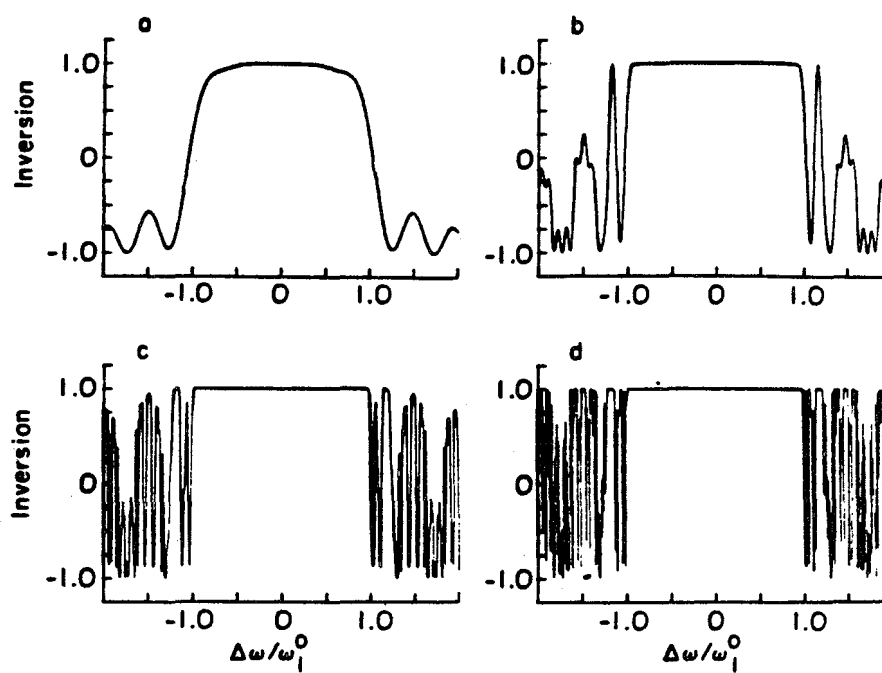
XBL 846-2381

Figure VII.5: Inversion as a function of the relative resonance offset for pulses sequences generated iteratively according to the scheme  $[0,0,120,60,120]$ . From a to d, the pulse sequences are composed of 5, 25, 125, and 625 phase-shifted  $\pi$  pulses, with the phase shifts given in Table VII.1. Simulations appear in the solid lines. Experimental measurements appear in dots. The results apply to isolated spins or to two-level systems in general.



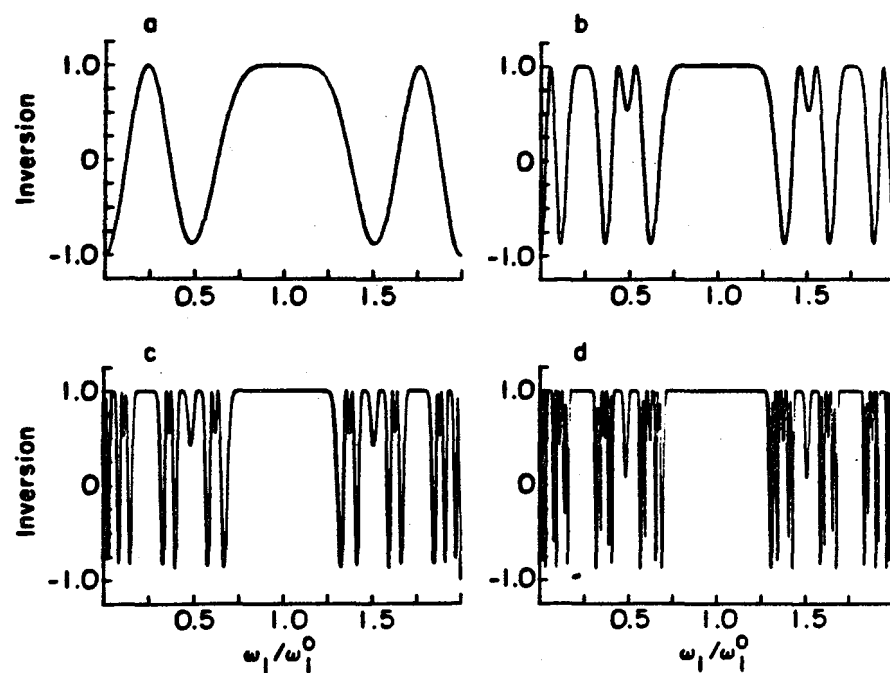
XBL B46-2376

Figure VII.6: Same as Figure VII.5, but with the inversion plotted as a function of the relative rf amplitude.



XBL 846-2379

Figure VII.7: Same as Figure VII.5, but for the scheme  $[0,330,60,330,0]$ .



XBL 846-238C

Figure VII.8: Same as Figure VII.7, but with the inversion plotted as a function of the relative rf amplitude.

generated by  $[0,0,120,60,120]$  is shown in Figure VII.9.

Iteration also cancels errors that arise from experimental pulse imperfections. These include pulse shape errors and phase transients. Other errors, such as amplitude imbalances among the rf pulse channels or rf phase misadjustments, may also cancel, depending on how the experiment is performed. The requirement for cancellation is that the error transform under a phase shift as a rotation about  $z$ . The cancellation of experimental imperfections probably contributes to the good agreement between the simulations and experimental measurements in Figures VII.5 and VII.6.

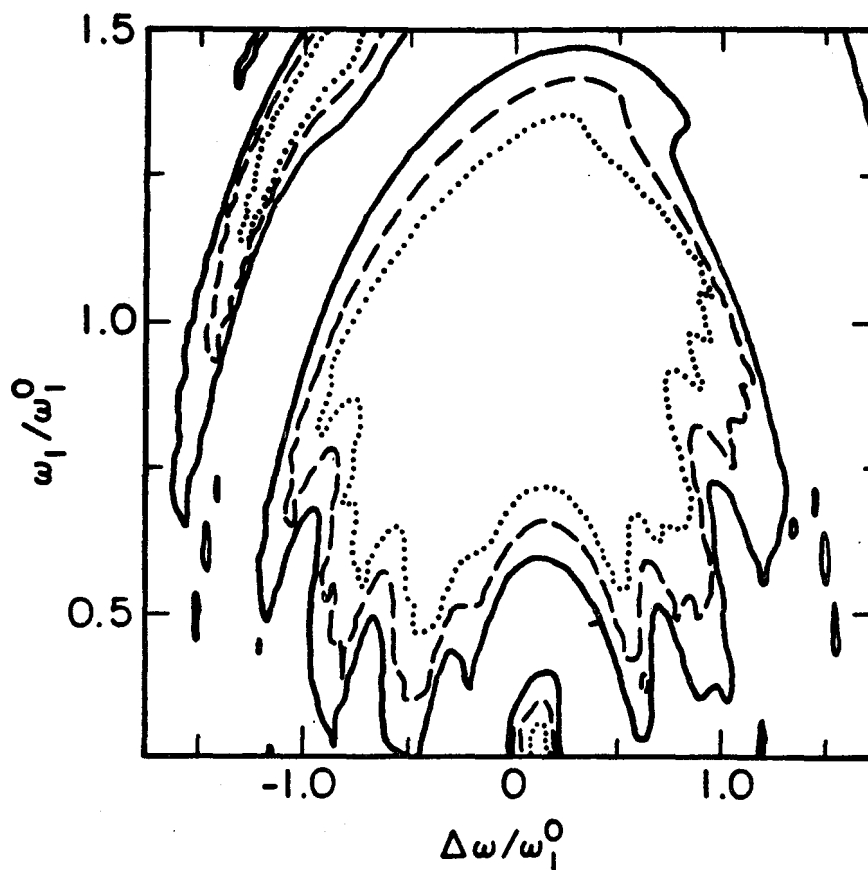
Similar vector diagrams apply to the linear analysis about the origin of  $SO(3)$ . Eqs.(VII.9) and (VII.10) indicate that the origin will be superstable with respect to displacements in the  $xy$  plane if the sum of  $N$  unit vectors in the  $xy$  plane making angles  $\phi_n$  with  $x$  is zero. In fact,  $|\lambda_0^+|$  is the magnitude of the resultant vector, as is clear in Eq.(VII.13). For  $[0,0,120,60,120]$ , then,  $|\lambda_0^+| = 3$ . For  $[0,330,60,330,0]$ ,  $|\lambda_0^+| = (11 + 4\sqrt{3})^{1/2}$ . The origin is unstable in all directions for both schemes.

### C. Numerical analysis of iterative schemes in $SO(3)$

#### 1. Motivation

In section B, iterative schemes were constructed so that the fixed points at the origin and the equator of  $SO(3)$  were unstable and





XBL 846-2383

Figure VII.9: A calculated contour plot of the population inversion performance of the 25-pulse sequence of Figures VII.5b and VII.6b, illustrating broadband inversion with respect to the resonance offset and the rf amplitude simultaneously. In the region enclosed by the dotted line, the inversion is greater than 0.99. Contours corresponding to an inversion of 0.90 (dashed line) and 0.50 (solid line) are shown as well.

superstable, respectively. The stability determines how the function  $F$  corresponding to some scheme transforms points in  $S(3)$  that are close to the fixed points. However, it would seem that most points in  $S(3)$  are not close to the fixed points. In the example of section A.3, the fixed points were shown to affect the dynamics of a function far from the fixed points. Methods for examining the dynamics of  $F$  over its entire domain are needed.

For the problem of broadband population inversion, the stability of the equator is most important, since points on the equator correspond to rotations that produce complete inversion. Typically,  $S_0$  is chosen to be a pulse sequence that produces complete inversion when  $\Delta\omega = 0$  and  $\omega_1 = \omega_1^0$ . There will necessarily be small ranges of  $\Delta\omega$  and  $\omega_1$  for which the rotation vector  $\alpha_0$  lies close to the equator. If the equator is an attractor, then the iterates of  $S_0$  will produce increasingly good inversion over those ranges. However, it is possible that the ranges of  $\Delta\omega$  and  $\omega_1$  for which the iterates of  $\alpha_0$  converge to the equator can be quite large. This is apparent in the results in section B. A method of determining which initial rotations will converge to the attractor, i.e. the basin of the attractor, and the number of iterations required for convergence is needed. In particular, it is desirable to know the region of  $S(3)$  that converges quickly. Knowledge of the rapidly convergent region allows  $S_0$  to be chosen so that the iterative scheme acts most efficiently.

If a fixed point is unstable or only stable in certain directions, as is always the case for the origin for the schemes considered here and is sometimes the case for the equator, then other points may not converge to the fixed point. However, with successive iterations, they

may approach the fixed point along a stable direction before diverging along an unstable direction. Thus, an initial sequence  $S_0$  may approach a desired form in a transient way. In the neighborhood of a fixed point, the linear analysis implies that the dynamics of  $F$  may be pictured in terms of smooth flows. Away from the fixed points, the dynamics may be apparently irregular or random. A method of illustrating the flows and defining the regions in which they apply is needed.

Finally there may be fixed points, either stable or unstable, that are not anticipated a priori. Locating them and determining their basins or flows may assist in the selection of  $S_0$ .

## 2. Maps of basins

Since a simple expression for  $F$  is not available, basins must be mapped with a computer program. The rotation corresponding to a vector  $\underline{\alpha}$  in  $S(3)$  can be represented by a  $3 \times 3$  real matrix  $R(\underline{\alpha})$ :

$$\begin{pmatrix} \sin^2\theta\cos^2\phi+\sin^2\phi\cos\alpha & -\cos\theta\sin\alpha & \sin\theta\sin\phi\sin\alpha \\ +\cos^2\theta\cos^2\phi\cos\alpha & +\sin^2\theta\cos\phi\sin\phi(1-\cos\alpha) & +\cos\theta\sin\theta\cos\phi(1-\cos\alpha) \\ \cos\theta\sin\alpha & \sin^2\theta\sin^2\phi+\cos^2\phi\cos\alpha & -\sin\theta\cos\phi\sin\alpha \\ +\sin^2\theta\cos\phi\sin\phi(1-\cos\alpha) & +\cos^2\theta\sin^2\phi\cos\alpha & +\cos\theta\sin\theta\sin\phi(1-\cos\alpha) \\ -\sin\theta\sin\phi\sin\alpha & \sin\theta\cos\phi\sin\alpha & \cos^2\theta+\sin^2\theta\cos\alpha \\ +\cos\theta\sin\theta\cos\phi(1-\cos\alpha) & +\cos\theta\sin\theta\sin\phi(1-\cos\alpha) & \end{pmatrix} \quad (\text{VII.29})$$

where  $\alpha$  is  $|\underline{\alpha}|$  and  $\theta$  and  $\phi$  are the polar and azimuthal angles defining  $\underline{\alpha}$  in polar coordinates. Given any initial vector  $\underline{\alpha}_0$  in  $SO(3)$ , the corresponding rotation matrix  $R(\underline{\alpha}_0)$  can be constructed. Phase-shifted versions  $R^{(n)}(\underline{\alpha}_0)$  are formed according to  $R^{(n)}(\underline{\alpha}_0) = R_z(\phi_n)R(\underline{\alpha}_0)R_z(\phi_n)^{-1}$ . Finally, these are multiplied together:

$$R(\underline{\alpha}_1) = R^{(N)}(\underline{\alpha}_0)R^{(N-1)}(\underline{\alpha}_0)\dots R^{(1)}(\underline{\alpha}_0)$$

By examining the matrix elements of  $R(\underline{\alpha}_1)$ ,  $\underline{\alpha}_1$  may be extracted. Repeating this process, the series of iterates of  $\underline{\alpha}_0$  can be generated numerically for any  $\underline{\alpha}_0$  and iterative scheme of the form  $[\phi_1, \phi_2, \dots, \phi_N]$ .

The task of mapping the dynamics of  $F$  is greatly simplified by symmetry with respect to rotations about  $z$ . If  $\underline{\alpha}_0$  and  $\underline{\alpha}'_0$  are related by a rotation about  $z$ , then their iterates  $\underline{\alpha}_n$  and  $\underline{\alpha}'_n$  are related by the same rotation, as follows from Eq.(VII.5). A corollary is that the fixed points must have symmetry about  $z$ , i.e. if  $\underline{\alpha}_0$  is a fixed point, or a member of a fixed set of points, then so is any other vector related to  $\underline{\alpha}_0$  by a rotation about  $z$ . Thus, in what follows it is sufficient to consider any single half slice through  $SO(3)$  containing the  $z$  axis. For the following maps, the slice defined by  $y = 0$  and  $x > 0$  is chosen.

The series of iterates of a representative grid of points in the slice are generated. A criterion for convergence to a fixed point must be established. In the following maps, the criterion for convergence on  $k$  iterations is:

$$|\underline{\alpha}_k - \underline{\alpha}_{k-1}| < 0.01 \text{ rad.} \quad (\text{VII.30})$$

This criterion is necessarily somewhat arbitrary, with consequences that are discussed below. In checking Eq.(VII.30), the vectors are always rotated about  $z$  so that they both lie in the  $xz$  plane with  $x > 0$ . In other words, the phase shift  $\phi_T$  is removed. A maximum value  $k_{\max}$  is defined so that, if a particular initial point does not converge after  $k_{\max}$  iterations, the iteration process stops and  $k_{\max}$  is assigned to that point. Thus, an integer  $k$  is assigned to every initial point on the grid. This constitutes a map of the basins. The map only specifies the number of iterations required to reach a fixed point, and not the fixed point itself. If there were multiple attractors, it would be necessary to examine the vectors  $g_k$  to determine which attractor corresponded to a basin.

Figure VII.10 is a basin map of the scheme  $[0,0,120,60,120]$ . Initial points were examined in  $\pm 5^\circ$  increments in both the  $x$  and  $z$  directions, starting with the point  $(2.5^\circ, 0, 2.5^\circ)$ . The map was displayed on a graphics terminal by shading  $5^\circ \times 5^\circ$  blocks, centered at the initial points, according to  $k$ .

Figure VII.10 reveals a large region near the equator that converges to the equator after only several iterations. Except for a small number of isolated points, the rest of  $SO(3)$  also converges to the equator. Those isolated points apparently converge elsewhere, but that convergence is probably an artifact of the mapping procedure, as explained later. These results suggest that very high iterations of  $[0,0,120,60,120]$ , applied to an arbitrary initial sequence, will generate sequences that invert spin populations for most values of  $\Delta\omega$  and  $\omega_1$ . Of course, experimental hardware and software limitations, as

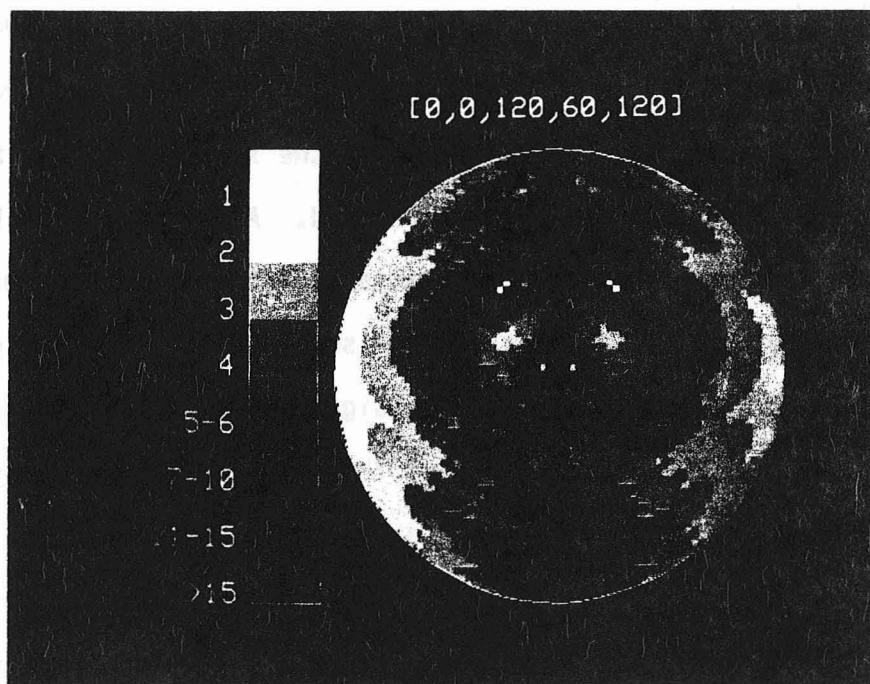


Figure VII.10: Basin map of the scheme  $[0,0,120,60,120]$ . Shown is the  $xz$  plane in  $SO(3)$ . Regions are shaded according to the number of iterations required for an initial point in a given region to converge to a fixed point. The shade scale is shown to the left.

well as intrinsic factors such as relaxation processes restrict the length of a useful sequence and thus the feasible number of iterations. Thus, it is the size and structure of the rapidly convergent region that is of practical importance.

Figure VII.11 is a basin map for the scheme  $[0,330,60,330,0]$ . The region of  $S0(3)$  that converges rapidly is somewhat different than in Figure VII.10. However, the most striking qualitative difference is the symmetry with respect to a reflection in the  $xy$  plane in Figure VII.11. This symmetry is a consequence of the symmetry of the phase shifts in  $[0,330,60,330,0]$ . In general, if  $\phi_n = \phi_{N-n+1}$  and if two initial vectors  $\alpha_0$  and  $\alpha'_0$  are related by reflection in the  $xy$  plane, then  $\alpha_i$  and  $\alpha'_i$  are related by the same reflection. Again, an obvious corollary is that, if  $\alpha_0$  is a fixed point, there must be a fixed point related to  $\alpha_0$  by reflection in the  $xy$  plane. A second corollary, which will be important in Chapter VIII, is that the iterates of an initial point in the  $xy$  plane must all remain in the  $xy$  plane.

### 3. Maps of fixed points and the flow of iterates

As mentioned above, certain isolated initial points in the basin maps apparently converge to points not on the equator. This suggests the existence of unanticipated fixed points. It is unlikely that unanticipated attractors exist in the schemes considered, since an attractor would probably have a basin large enough to be apparent in Figure VII.10 or VII.11. However, even if a fixed point is unstable, initial points move slowly in its neighborhood. Consequently, due to the criterion in Eq.(VII.30), there may be an apparent convergence to an

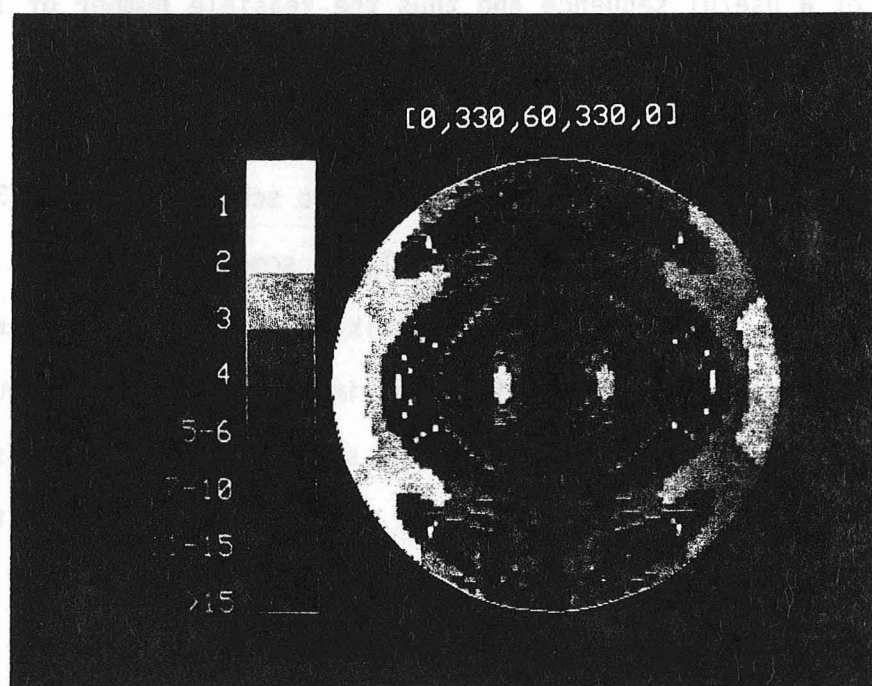


Figure VII.11: Basin map of the scheme [0,330,60,330,0].



unstable fixed point.

Unstable fixed points are difficult to identify in the basin mapping procedure for two reasons. First, initial points can only be examined in increments of some finite spacing. It is likely that fixed points will be missed. Second, the calculation of the iterates of an initial point involves many matrix multiplications. Inevitably, round-off errors become significant, so that a point that should remain fixed will apparently move. It is therefore not possible to distinguish conclusively between a fixed point and a region in which the movement of iterates is merely slow. For the purpose of designing pulse sequences, however, such a distinction is not necessary. One method for finding unanticipated fixed points is as follows. The first iterates of initial points in a slice through  $S^2$  with a spacing of  $2^\circ$  in the  $x$  and  $z$  directions are calculated. If an initial point  $g_0$  and its first iterate  $g_1$  satisfy:

$$|g_1 - g_0| < 20^\circ \quad (\text{VII.31})$$

then  $g_0$  may be close to a fixed point. Again the choice of  $20^\circ$  is somewhat arbitrary. All initial points satisfying Eq.(VII.31) are plotted. The plot that results from the procedure applied to the scheme  $[0,0,120,60,120]$  is shown in Figure VII.12a. The anticipated fixed points at the equator and along the  $z$  axis are clearly visible. The structure of the plotted points near  $(0,0,\pi/2)$  suggests the existence of another unstable fixed point. A more detailed examination indicates that there is probably a fixed point at approximately  $(\pi/4,0,0.39\pi)$ , since initial points near  $(\pi/4,0,0.39\pi)$  appear to rotate around that

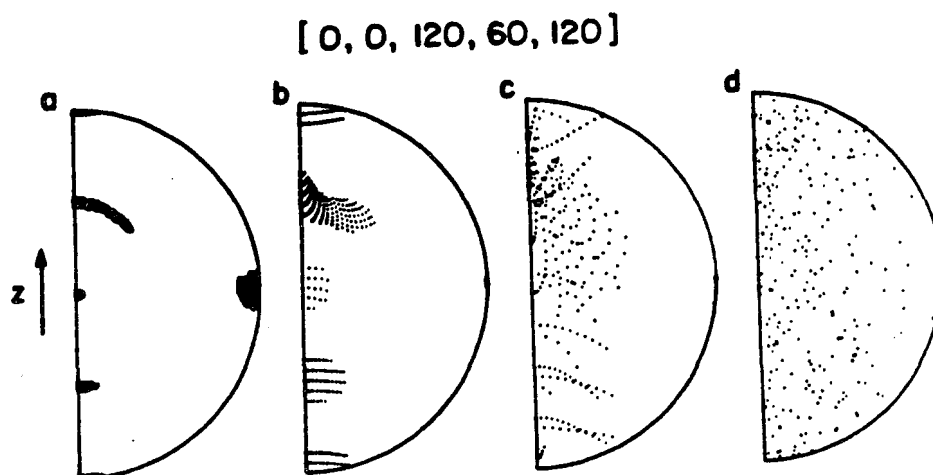


Figure VII.12: Fixed point map of the scheme  $[0, 0, 120, 60, 120]$ . Half of the  $xz$  plane of  $SO(3)$  is shown. Initial points that move less than  $20^\circ$  on the first iteration are plotted in a, revealing regions around possible fixed points. The first, second, and third iterates of the points in a are plotted in b, c, and d, revealing the stability properties of the fixed points.

point and diverge from it. Again, it is impossible to distinguish definitively between a true unstable fixed point and a region in which the flow of iterates is merely very slow. It should also be realized that the fixed points may actually be fixed sets of points, related by a rotation about  $z$ .

Figure VII.12 traces the flow of iterates initially near the fixed points. The superstability of the equator is apparent, as is the instability of the other fixed points.

Figure VII.13 is a fixed point map for the scheme  $[0,330,60,330,0]$ . There are two unanticipated fixed points along the  $x$  axis, at approximately  $(0.3989\pi, 0, 0)$  and  $(0.7035\pi, 0, 0)$ . The fixed point at  $(0.3989\pi, 0, 0)$  is unstable. The eigenvalue in the direction of the origin is approximately  $-3.6$ ; the eigenvalue along  $z$  is approximately  $-1.7$ . The fixed point at  $(0.7035\pi, 0, 0)$  is stable along  $z$ , with an eigenvalue of  $0.19$ , and unstable towards the origin, with an eigenvalue of  $2.4$ . The eigenvalues and the positions of the fixed points are determined by a detailed examination of the flow of initial points in the dotted regions of Figure VII.13a. The fixed points could be localized precisely in this case because the symmetry of  $[0,330,60,330,0]$  results in a one-dimensional movement of points along the  $x$  axis. The instability of the origin and the other fixed points on the  $z$  axis, the superstability of the equator, and the one stable direction near  $(0.7035\pi, 0, 0)$  are apparent.

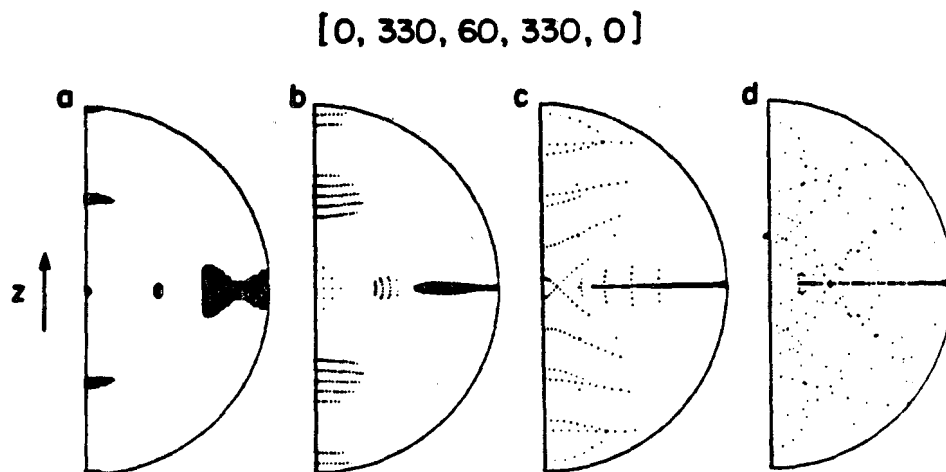


Figure VII.13: Fixed point map of the scheme  $[0, 330, 60, 330, 0]$ . In this case, in addition to the superstable fixed point at the equator and the unstable fixed point at the origin, two other fixed points in the  $xy$  plane appear. One of these is stable with respect to displacements in the  $z$  direction.

#### D. Generation of pulse sequences for broadband population inversion

The schemes  $[0,0,120,60,120]$  and  $[0,330,60,330,0]$  can be used to generate sequences for broadband population inversion, as in Figures VII.5 through VII.9. Here it is shown how the maps of section C can be used to guide the selection of an initial pulse sequence  $S_0$  whose iterates have larger inversion bandwidths than the iterates of a single  $\pi$  pulse.

The selection of  $S_0$  is based on the idea that, for any  $S_0$ , there is a locus of initial points  $\alpha_0$  in  $S_0(3)$  that corresponds to the experimentally relevant ranges of  $\Delta\omega$  and  $\omega_1$ . As an example, Figure VII.14 shows the loci for a single  $\pi$  pulse that arise from variations of  $\Delta\omega$  and  $\omega_1$  separately. A comparison of Figure VII.14 with Figures VII.10 and VII.11 reveals the ranges of  $\Delta\omega$  and  $\omega_1$  for which the inversion will be nearly complete for sequences resulting from a small number of iterations of  $[0,0,120,60,120]$  and  $[0,330,60,330,0]$  acting on an initial single  $\pi$  pulse. Those ranges are given by the portions of the loci in Figure VII.14 that lie inside the rapidly convergent regions in Figures VII.10 and VII.11.

The iterates of initial sequences for which the analogous loci lie inside the rapidly convergent regions for larger ranges of  $\Delta\omega$  and  $\omega_1$  will produce nearly complete inversion over larger ranges of  $\Delta\omega$  and  $\omega_1$ . Such sequences can be found by means of a computer search. For example, the rapidly convergent region of the scheme  $[0,0,120,60,120]$  is roughly defined by the requirements:

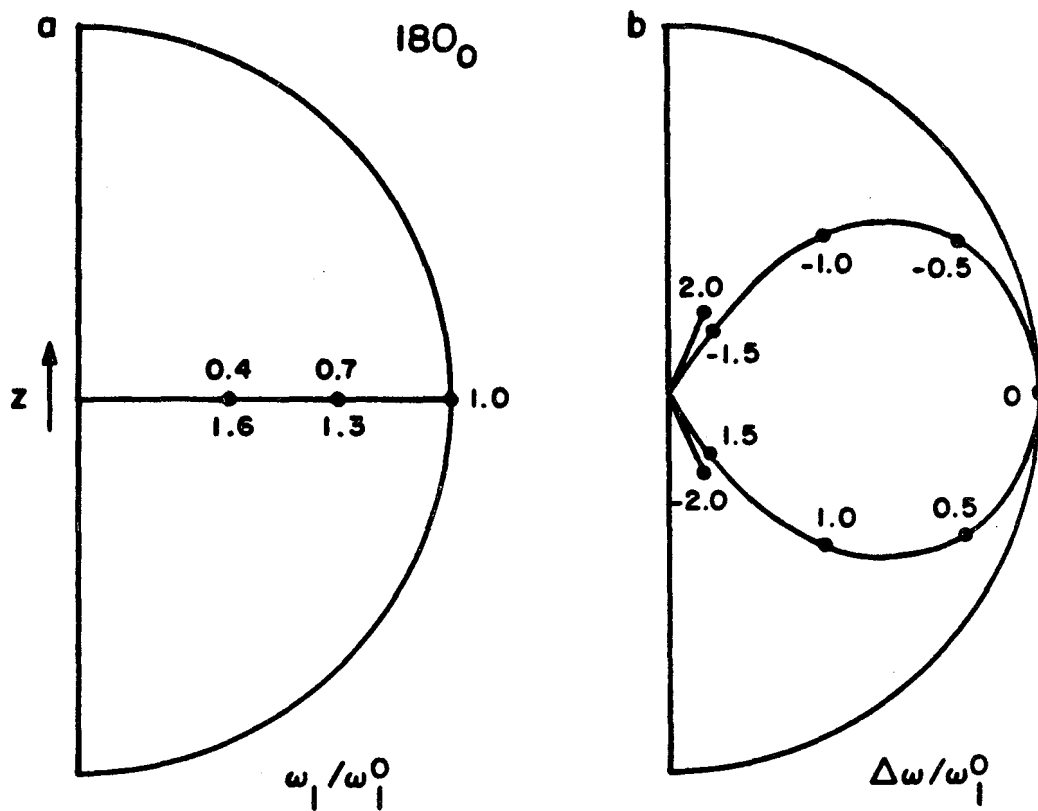


Figure VII.14: Loci of points in  $SO(3)$  corresponding to a single  $\pi$  pulse, resulting from variations in the relative rf amplitude (a) and the relative resonance offset (b).

$$40^\circ < \phi < 140^\circ \quad (\text{VII.32a})$$

$$125^\circ < r < 180^\circ \quad (\text{VII.32b})$$

where  $\phi$  and  $r$  are polar coordinates in  $S(3)$ . A search is conducted over possible initial sequences consisting of two pulses with phases of  $0^\circ$  and  $180^\circ$  and flip angles in increments of  $10^\circ$ . For each possible sequence, the point  $\alpha_0$  is calculated for all values of  $\Delta\omega$  between  $-1.4\omega_1^0$  and  $1.4\omega_1^0$ , in increments of  $0.1\omega_1^0$ . This is done by treating the pulse sequences as a product of  $3 \times 3$  rotation matrices and extracting  $\alpha_0$  as in section C.2. One sequence for which  $\alpha_0$  lies inside the region defined by Eq.(VII.32) for  $-1.4\omega_1^0 < \Delta\omega < 1.4\omega_1^0$  is the sequence  $300_0 120_{180}$ . The corresponding locus of initial points is shown in Figure VII.15.

Simulations of the population inversion as a function of  $\Delta\omega$  for the first four iterates of  $300_0 120_{180}$  under the scheme  $[0,0,120,60,120]$  are given in Figure VII.16. Figure VII.16 shows nearly complete inversion for  $-1.8\omega_1^0 < \Delta\omega < 1.8\omega_1^0$ . For comparison, the results in Figure VII.5 using  $180_0$  as the initial sequence showed nearly complete inversion for  $-0.9\omega_1^0 < \Delta\omega < 1.1\omega_1^0$ . Thus, the inversion bandwidth is nearly doubled by the choice of an appropriate initial sequence.

In any experimental situation, there is a range of  $\omega_1$  values as well as  $\Delta\omega$  values. Figure VII.17a shows the locus of points in  $S(3)$  corresponding to a single  $\pi$  pulse with simultaneous variations of  $\Delta\omega$  between  $-\omega_1^0$  and  $\omega_1^0$  and  $\omega_1$  between  $0.4\omega_1^0$  and  $1.6\omega_1^0$ . For the scheme  $[0,330,60,330,0]$ , this locus extends outside of the rapidly convergent region. In particular, the rapidly convergent region is limited in its extent along the  $x$  axis, due to the existence of the fixed point at  $(0.7035\pi, 0, 0)$  seen in Figure VII.13. This fixed point primarily limits

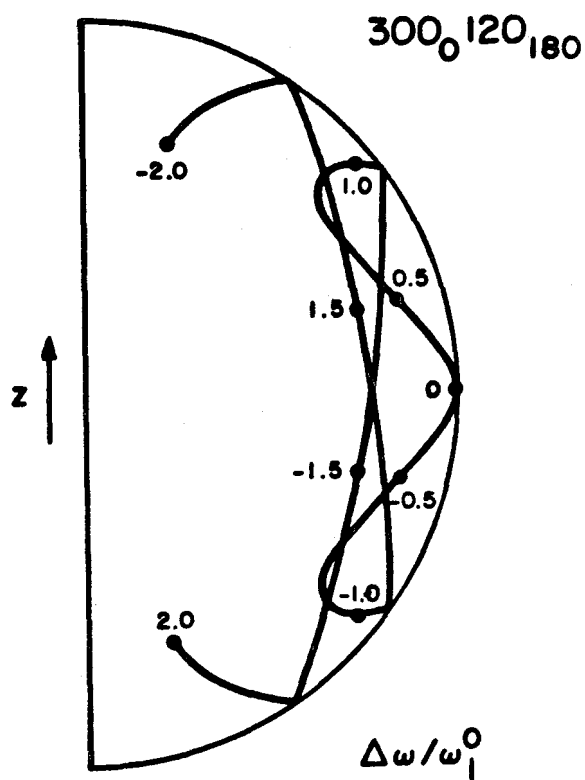


Figure VII.15: Locus of points in  $SO(3)$  corresponding to the sequence  $300_0 120_{180}$  with variations in the resonance offset. Comparison with Figures VII.14b and VII.10 reveals that the locus for  $300_0 120_{180}$  conforms to the basin of the equator under the scheme  $[0, 0, 120, 60, 120]$  over a larger range of offsets than the locus for  $180_0$ .



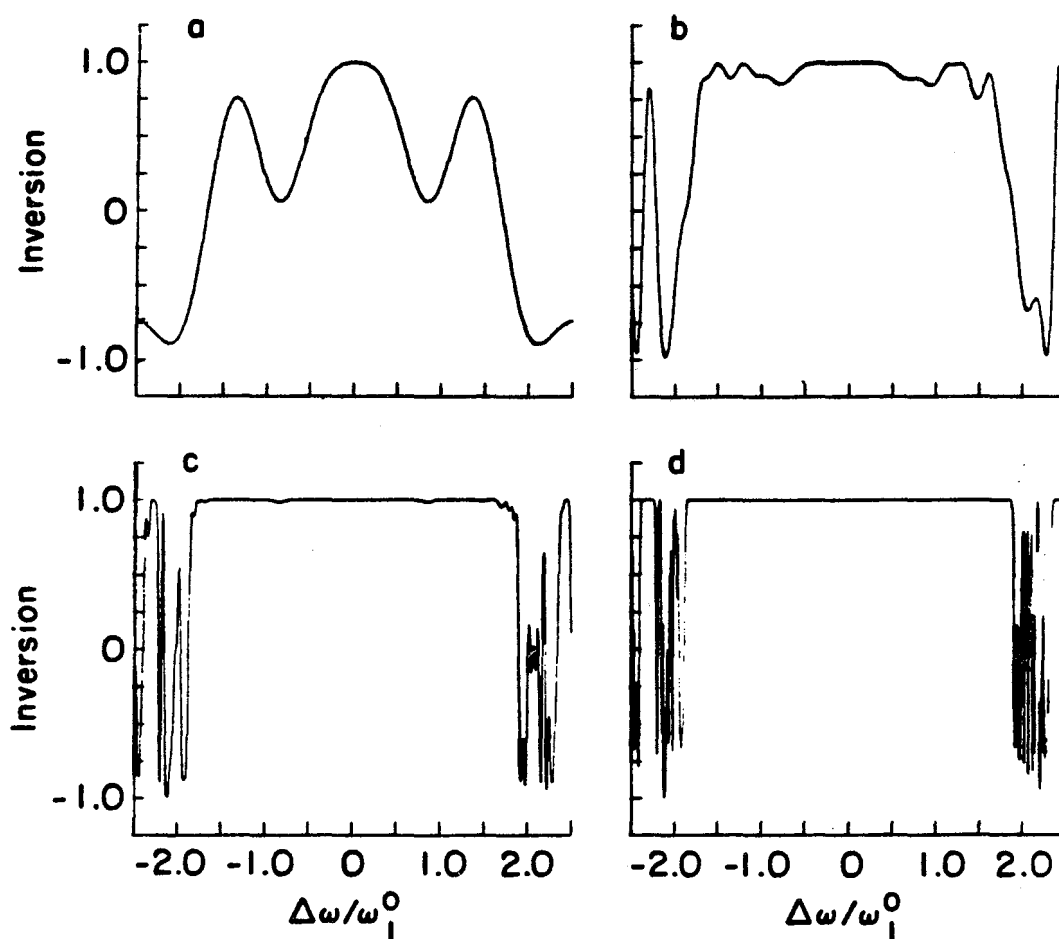


Figure VII.16: Simulations of inversion as a function of the relative resonance offset for sequences generated iteratively from  $300_0120_{180}$  by the scheme  $[0,0,120,60,120]$ . The performance of  $300_0120_{180}$  alone (a), and of its first, second, and third iterates (b through d) is shown. Comparison with Figure VII.5 demonstrates that the inversion bandwidths of the iterate sequences are substantially improved by choosing an initial sequence for which the locus of points in  $S(3)$  conforms to the basin of the equator.

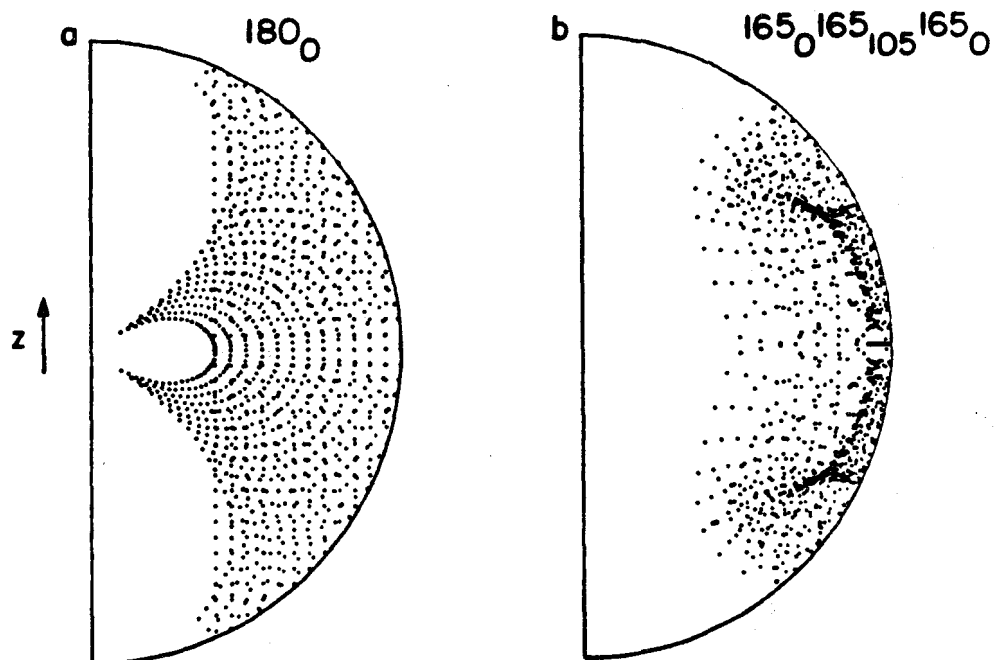


Figure VII.17: Loci of points in  $SO(3)$  for the pulse sequences  $180_0$  (a) and  $165_0 165_{105} 165_0$  (b) resulting from simultaneous variations of the resonance offset and the rf amplitude. Points for offsets in the range  $-1 \leq \omega/\omega_1^0 \leq 1$  in increments of 0.05 and rf amplitudes in the range  $0.4 \leq \omega_1/\omega_1^0 \leq 1.6$  in increments of 0.05 are plotted.  $165_0 165_{105} 165_0$  is chosen because its locus of points conforms to the basin of the equator under the scheme  $[0, 330, 60, 330, 0]$ .

the range of  $\omega_1$  for which inversion is achieved if a single  $\pi$  pulse is used for  $S_0$ . Figure VII.17b shows the locus of initial points for the sequence  $165_0 165_{105} 165_0$ , for the same variations of  $\Delta\omega$  and  $\omega_1$ . This sequence was found by a computer search, fitting the initial points into a region defined by:

$$40^\circ < \phi < 140^\circ \quad (\text{VII.33a})$$

$$130^\circ < r < 180^\circ \quad (\text{VII.33b})$$

for  $-0.8\omega_1^0 < \Delta\omega < 0.8\omega_1^0$  and  $0.7\omega_1^0 < \omega_1 < 1.3\omega_1^0$ . The locus of initial points is clearly more concentrated in the rapidly convergent region for  $165_0 165_{105} 165_0$  than for a single  $\pi$  pulse.

Figure VII.18 shows inversion contour plots for sequences generated by two iterations of  $[0, 330, 60, 330, 0]$ , where  $S_0$  is either a single  $\pi$  pulse or the sequence  $165_0 165_{105} 165_0$ . As anticipated, the inversion is nearly complete for larger simultaneous variations of  $\Delta\omega$  and  $\omega_1$  when  $S_0$  is  $165_0 165_{105} 165_0$ . The bandwidth is especially enlarged in the  $\omega_1$  dimension.

#### E. Summary of principles of the fixed point theory

The viewpoint of the fixed point theory is that an iterative scheme for generating pulse sequences corresponds to an underlying function on the propagator space. The fixed points of the function and their

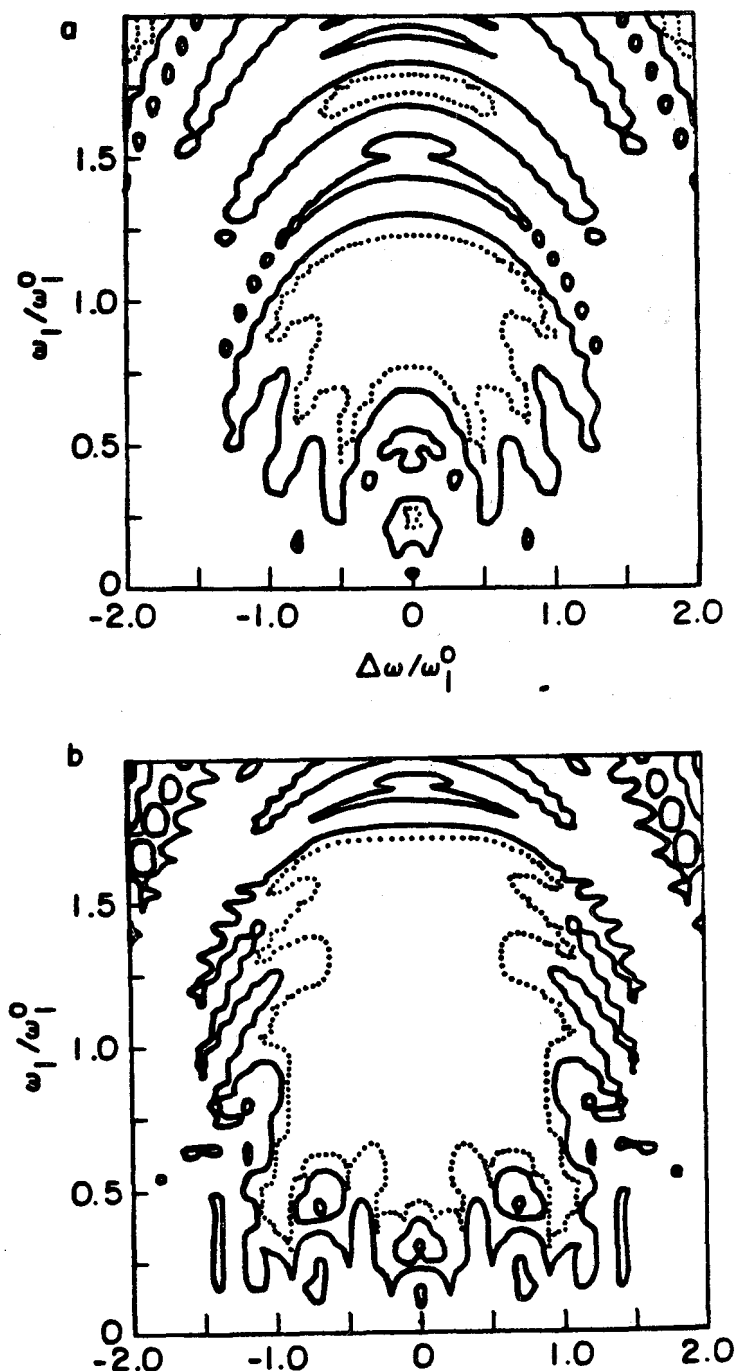


Figure VII.18: Inversion contour plots for pulse sequences that are the second iterates of  $180_0$  (a) and  $165_0 165_{105} 165_0$  (b) under the scheme  $[0, 330, 60, 330, 0]$ . Shown are the 0.99 (dotted line) and the 0.50 (solid line) inversion contours. The results demonstrate that the area of uniform population inversion is enlarged by choosing an initial pulse sequence for which the locus of points in  $S(3)$  conforms to the basin of the equator for simultaneous variations of the offset and the rf amplitude.

stability determine the behavior of the scheme.

The process of designing an iterative scheme begins with the identification of a general form for the desired propagator. The relevant propagator space and the locus of points in that space that corresponds to the desired propagator are determined. Next, a class of operations on pulse sequences for which that locus is a fixed point or an invariant set of points must be discovered. The stability properties of that fixed point or set of points, as well as other fixed points that are known a priori, may be calculated for a general member of the class of operations. A particular member with the desired properties is then selected.

The choice of the particular scheme may be made with the help of the mapping techniques of section C. As in section D, those techniques also may be used to select an initial sequence on which the iterative scheme acts most effectively.

The mapping techniques are quite feasible in problems where the relevant propagator space is three-dimensional, e.g. all isolated spin problems. In higher dimensions, or in problems where the number of dimensions is arbitrary, representative maps are more difficult to compute. For those cases, a qualitative understanding of the variety of types of behavior is provided by the three-dimensional examples.

## Chapter VIII: Iterative Schemes for Narrowband Population Inversion

### A. Motivation

Certain members of the class of iterative schemes introduced in Chapter VII can generate pulse sequences for narrowband, rather than broadband, population inversion of isolated spins. Of particular interest are pulse sequences that invert populations only over a narrow range of  $\omega_1$  centered at  $\omega_1^0$  and leave populations undisturbed at other values of  $\omega_1$ . Such sequences can be incorporated into a method for spatially localizing NMR signals in an rf field gradient. This method is discussed in section C.

The fixed point theory of Chapter VII can be used to analyze the narrowband inversion schemes. The basic idea is as follows. While the equator of  $S(3)$ , pictured in Figure VII.3, is stable for broadband inversion schemes, it is unstable for narrowband inversion schemes. The origin of  $S(3)$  is stable with respect to displacements in the xy plane for narrowband schemes. Points close to the origin move towards the origin upon iteration. If the initial sequence is chosen to be  $180_0$ , points close to the origin correspond to rf amplitudes that are close to even multiples of  $\omega_1^0$ , as shown in Figure VII.14. Points at the equator, which remain at the equator upon iteration, correspond to rf amplitudes that are odd multiples of  $\omega_1^0$ . Points close to the equator are repelled from the equator. Thus, the iterate sequences are expected to develop the desired narrow inversion profile.

## B. Generation of pulse sequences.

The simplest example of an iterative scheme based on phase shifts for which the origin is superstable with respect to displacements in the  $xy$  plane is  $[0,120,240]$ . The superstability follows from the discussion in Chapter VII.B. The equator is unstable, with  $\lambda_e^\pm = -1 \pm \sqrt{2} i$  as defined in Eq.(VII.27). A fixed point map for  $[0,120,240]$ , produced according to the procedure in Chapter VII.C.3, is shown in Figure VIII.1. The instability of the equator and the stability of the origin in the  $xy$  plane are apparent.

Inversion plots as a function of  $\omega_1$  for the first four iterates of  $180_0$  under  $[0,120,240]$  are shown in Figure VIII.2. The narrowband property is obvious. However, it appears that significant inversion develops at intermediate values of  $\omega_1$  in the higher iterations. This is because the origin of  $S(3)$  is unstable along the  $z$  axis and because the  $z$  axis itself is not stable. Thus, points may move towards the origin on the first few iterations, then escape along  $z$  to become rotations that affect spin populations. This behavior is depicted in Figure VIII.3. The development of the desired inversion profile is only a transient property of  $[0,120,240]$ . It is nonetheless useful, however, and serves as an illustration of the significance of fixed points that are not unconditionally stable.

One way to prevent the escape of points along  $z$  is to use an iterative scheme with symmetric phase shifts, as discussed in Chapter VII. Initial points in the  $xy$  plane are constrained to remain in the  $xy$  plane by the symmetry.  $[180-\cos^{-1}0.25, 180+\cos^{-1}0.25, 0, 180+\cos^{-1}0.25, 180-\cos^{-1}0.25]$ , or roughly  $[104.5, 255.5, 0, 255.5, 104.5]$ , is an example of

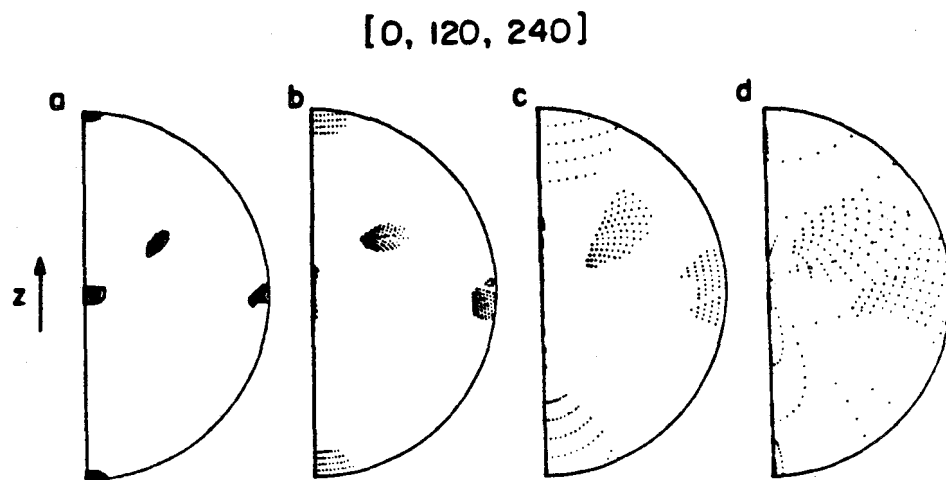
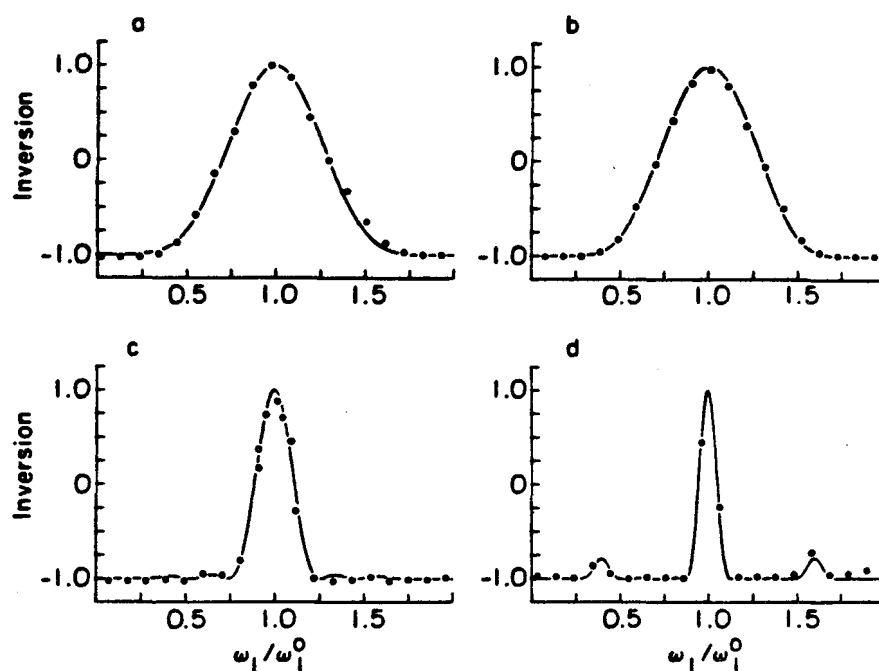


Figure VIII.1: Fixed point map for  $[0, 120, 240]$ , showing that the origin of  $SO(3)$  is superstable with respect to displacements in the  $xy$  plane and the equator is unstable.





XBL 846-2376

Figure VIII.2: The extent of population inversion as a function of the relative rf amplitude for pulse sequences generated from an initial single  $\pi$  pulse by the scheme [0,120,240]. From a to d, the pulse sequences are composed of 3, 9, 27, and 81 phase-shifted  $\pi$  pulses. Pulse sequences generated by [0,120,240] exhibit narrowband inversion.

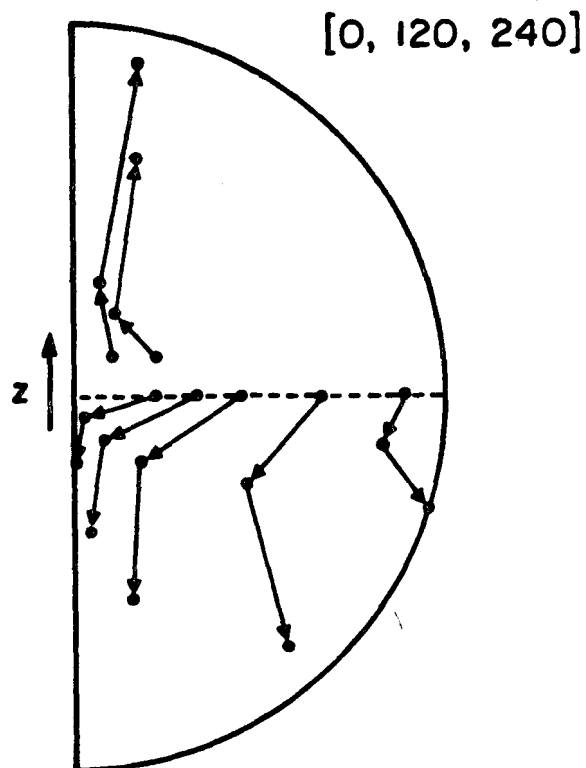


Figure VIII.3: The movement of iterates in  $SO(3)$  under  $[0, 120, 240]$ . Initial points in the  $xy$  plane first move towards the origin, but diverge on higher iterations. This results in the reappearance of significant inversion at rf amplitudes far from  $\omega_1 = \omega_1^0$  in Figure VIII.2d.

a symmetric scheme for which the origin is superstable in the xy plane and the equator is unstable. A fixed point map for this scheme is shown in Figure VIII.4. Since there are no other fixed points in the xy plane, the iterates of initial points in the xy plane flow from the equator to the origin. Inversion plots as a function of  $\omega_1$  for sequences generated from an initial  $180_0$  sequence are shown in Figure VIII.5. The narrowband inversion profile is clearly not transient.

### C. Application to the spatial localization of NMR signals

If rf inhomogeneity is deliberately introduced, pulse sequences that are sensitive to the value of  $\omega_1$  can be used to spatially localize NMR signals [105-107], i.e. selectively observe those signals that arise from a region in space where  $\omega_1$  has a particular value. This is particularly useful for in vivo studies using surface coils [56,108]. Typically, it is desirable to observe signals from a single organ without interference from surrounding tissue. If signals are excited with a single pulse, the degree of spatial localization is often insufficient, requiring that the organ be surgically exposed [109,111]. A higher degree of spatial localization can be achieved if surface coils are used in conjunction with following method, called NOBELS (Narrowband Excitation for Localization in Space).

Let P be a narrowband inversion sequence and R be a "read" pulse or pulse sequence. As illustrated in Figure VIII.6, NOBELS consists of the following steps:

- 1) Digitize and store the FID following R alone, as in Figure VIII.6a.

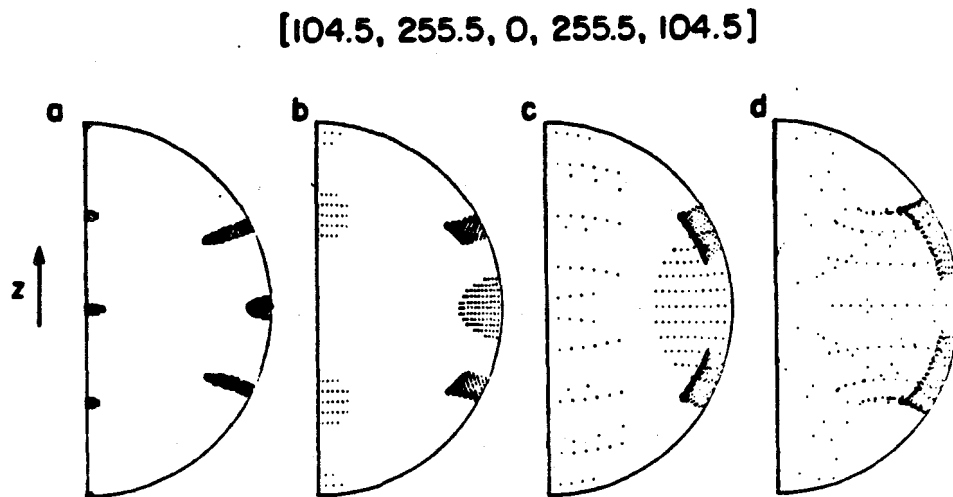


Figure VIII.4: Fixed point map for  $[104.5, 255.5, 0, 255.5, 104.5]$ , showing the instability of the equator of  $SO(3)$ , the superstability of the origin with respect to displacements in the  $xy$  plane, and the absence of other fixed points in the  $xy$  plane. The symmetry of the scheme constrains points in the  $xy$  plane to remain in the  $xy$  plane, flowing towards the origin on successive iterations.

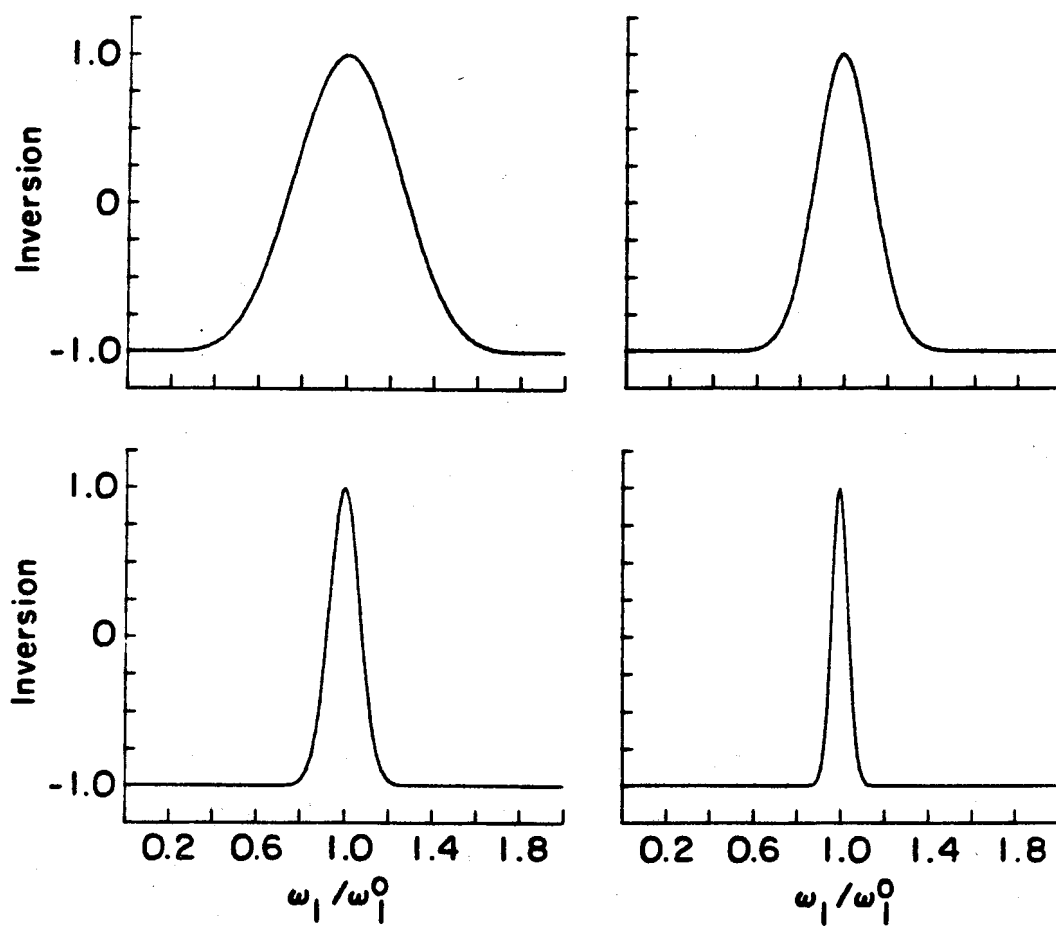
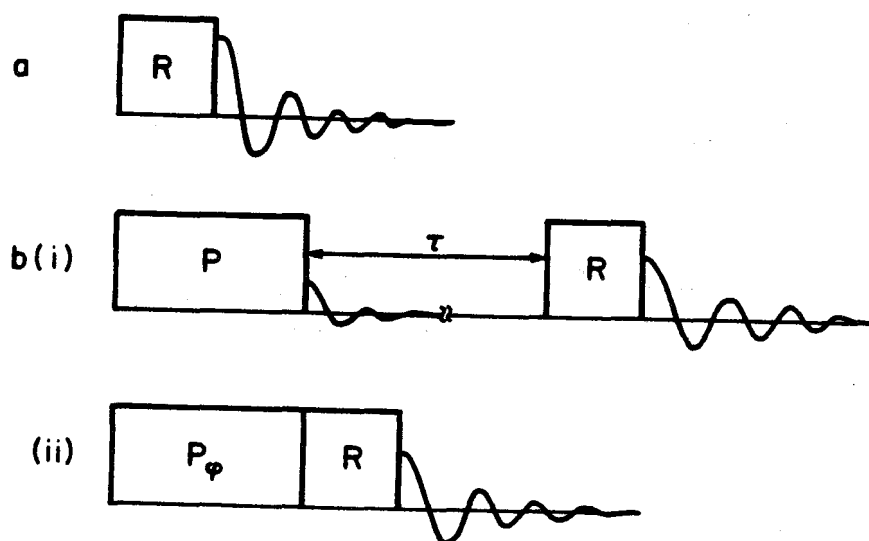


Figure VIII.5: Simulations of inversion as a function of the relative rf amplitude for the first four iterates of  $180_0$  under  $[104.5, 255.5, 0, 255.5, 104.5]$ . a, b, c, and d result from sequences of 5, 25, 125, and 625  $\pi$  pulses, respectively.



XBL 844-1579

Figure VIII.6: Schematic representation of NOBELS. P is a narrowband inversion sequence, inverting spins over a small range of rf amplitudes as in Figures VIII.2 and VIII.5. R is a "read" pulse or pulse sequence. The FID signal in b(i) or b(ii) is subtracted from the FID in a. Contributions from transverse magnetization created by P are eliminated by dephasing during  $\tau$  in b(i) or by phase cycling in b(ii), with  $\phi = 0$  and  $\phi = \pi$ . When the pulses are applied with a surface coil, the remaining signal arises only from the localized spatial region in which P inverts spins and R excites signal.

- 2) Digitize and store the FID following the sequence of Figure VIII.6b(i).  $\tau$  is a delay during which residual transverse magnetization dephases. A static field gradient may be required during the delay. In the FID, signals arising from the spatial region in which P inverts spins are themselves inverted.
- 3) Subtract the FID of step 2 from that of step 1. Only spins inverted by P contribute to the remaining signal.

The need for a pulsed field gradient may be eliminated by a variant of NOBELS:

- 1') Digitize and store two FIDs following R alone.
- 2') Digitize and store two FIDs from the sequence in Figure VIII.6b(ii). The notation  $P_\phi$  indicates that the overall rf phase of P is cycled between 0 and  $\pi$ .
- 3') Subtract the sum of the FIDs of step 2' from the sum of the FIDs of step 1'. The phase cycling in step 2' cancels the effects of residual transverse magnetization following P.

In principle, the two forms of NOBELS produce the same spatial localization. The choice is a matter of experimental convenience. One effective narrowband inversion sequence is the sequence of 27 phase-shifted pulses, each with a nominal flip angle of  $\pi$ , illustrated in Figure VIII.2c.

The inversion produced by the 27-pulse sequence is periodic in  $\omega_1/\omega_1^0$ , with a period of 2. Any sequence of  $\pi$  pulses will be periodic in this way. Thus, spins are inverted in regions of space where the rf

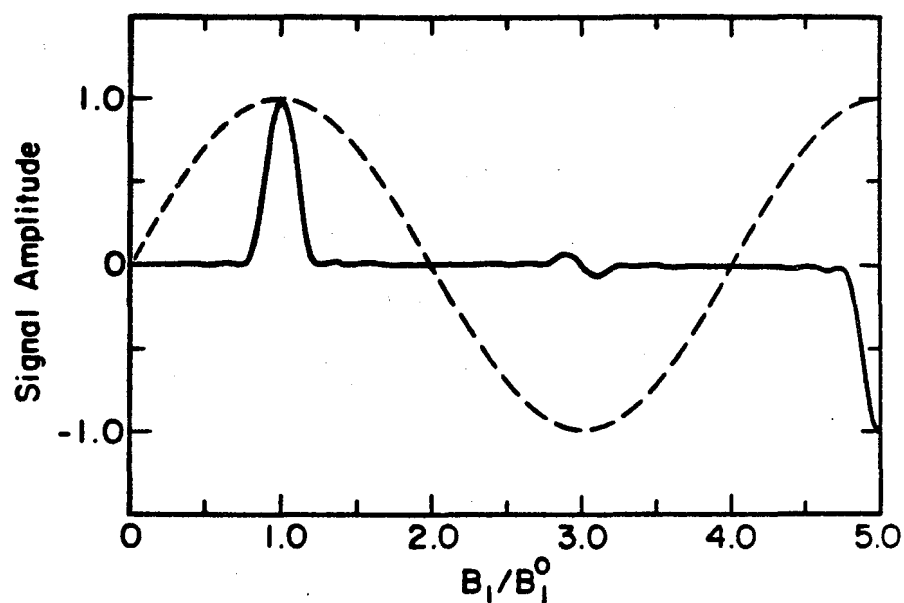
amplitude is any odd multiple of  $\omega_1^0$ . This presents a problem for spatial localization. If  $\omega_1^0$  is taken to be the rf amplitude at a region of interest at some distance from a surface coil, there will be regions closer to the coil where the rf amplitude is  $3\omega_1^0$ ,  $5\omega_1^0$ , etc. These regions may contribute to the signal collected with NOBELS. If a gap between the surface coil and the sample is permitted, the problem is alleviated somewhat. However, it is still desirable to minimize at least the contributions from the  $3\omega_1^0$  region.

One way to eliminate signal from the  $3\omega_1^0$  region is to use a nominal  $\pi/3$  pulse as the read pulse R. Then, at  $3\omega_1^0$ , R is in fact a  $\pi$  pulse and does not excite signal. In Figure VIII.7, a calculated plot of the signal amplitude as a function of  $\omega_1/\omega_1^0$  resulting from either version of NOBELS is shown, using the 27-pulse sequence of Figure VIII.2c for P and a nominal  $\pi/3$  pulse for R. The signal amplitude is normalized to its value at  $\omega_1 = \omega_1^0$ . Note that the maximum signal in the  $3\omega_1^0$  region is smaller than that at  $\omega_1^0$  by a factor of 0.07.

Figure VIII.7 applies to any surface coil geometry. It may be desirable to design a coil such that the size and shape of the  $\omega_1^0$  region conforms to that of the interesting sample region. If the same coil is used for both the excitation and the detection of signals, then the observed signal amplitude is further weighted by a factor of  $\omega_1/\omega_1^0$ . This is because the intrinsic sensitivity at a given point in space is proportional to the transverse field amplitude that would be produced at that point by a unit current flowing in the detection coil [112].

Figure VIII.7 is intended as an indication of the high degree of spatial localization that is possible with NOBELS. The qualitative features are independent of the specific pulse sequences used. Other





XBL 844-1576

Figure VIII.7: Simulation of the signal resulting from NOBELS as a function of the relative rf amplitude (solid line). The narrowband inversion sequence of Figure VIII.c is used for P. A nominal  $\pi/3$  pulse is used for R. For comparison, the signal amplitude resulting from a single nominal  $\pi/2$  pulse is shown (dashed line). Signal amplitudes are normalized to their value at  $B_1^0$ .

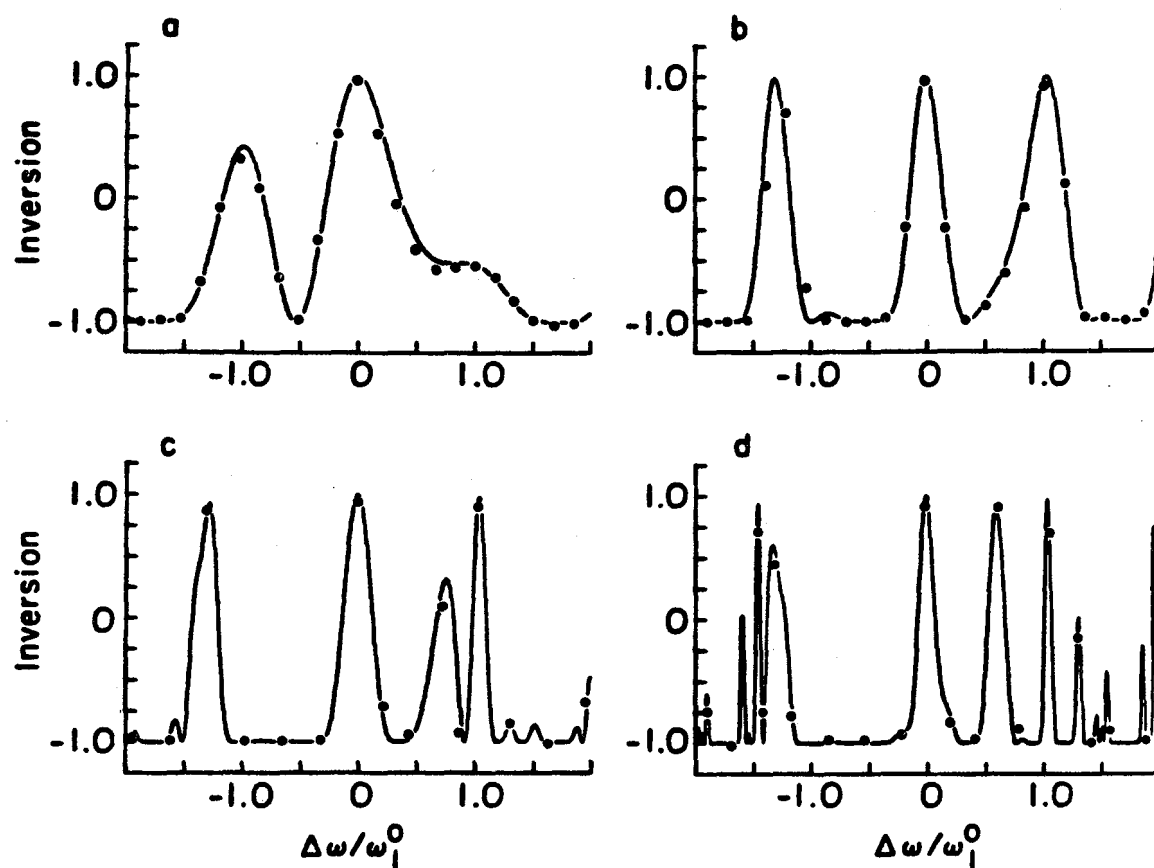
choices for P, perhaps with a different periodicity, are possible. R may be a sequence of pulses, rather than a single pulse, with its own narrowband properties. It may also be profitable to combine NOBELS with shaping of the static magnetic field to further localize signals.

With both the surface coil and the sample held fixed, it is possible to move the region from which signals are detected in two equivalent ways. Either the rf power is varied while maintaining constant pulse lengths, or all pulse lengths in P and R are varied proportionally while maintaining a constant rf power. A series of NMR spectra from various spatial regions may thus be collected.

#### D. Resonance offset behavior

The pulse sequences generated by [0,120,240] and [104.5,255.5, 0,255.5,104.5] also invert spin populations over narrow resonance offset ranges, with  $\omega_1 = \omega_1^0$ . Inversion as a function of offset for sequences generated from an initial single  $\pi$  pulse by [0,120,240] is shown in Figure VIII.8. If the chemical shift range of a sample is significant, the narrowband behavior with respect to the resonance offset makes spatial localization in an rf field gradient with these sequences impossible. The acquired signal will arise from nuclei with different chemical shifts located in different parts of the sample. In order to observe signal from all chemically shifted nuclei in a single spatial region, sequences that invert populations over a broad range of offsets and a narrow range of rf amplitudes are needed.

As a step towards the derivation of broadband/narrowband combination sequences, consider the iterative scheme [0,200,230,30,95].



XBL 846-2377

Figure VIII.8: Population inversion as a function of the relative resonance offset for the iterates of  $180_0$  under  $[0,120,240]$ . Simulations (solid lines) and experimental data (dots) are shown for the first four iterates in a through d.

As is apparent in the fixed point map in Figure VIII.9, for this scheme the origin of  $S(3)$  is stable with respect to displacements in the  $xy$  plane. The equator is unstable towards the origin but stable along the  $z$  direction. Specifically,  $\lambda_0^\pm = 0.196 \pm 0.388i$  and  $\lambda_e^\pm = 0.826 \pm 0.845i$ . Displacements along  $z$  arise from resonance offsets if the initial pulse sequence is a single  $\pi$  pulse. Thus, resonance offset effects should be removed by iteration, at least near the equator, due to the stability with respect to displacements along  $z$ .

Plots of inversion as a function of  $\omega_1/\omega_1^0$  for the 25-pulse sequence that is the second iterate of  $180_0$  under  $[0,200,230,30,95]$  are shown in Figure VIII.10 for several values of  $\omega/\omega_1^0$ . Near  $\omega_1/\omega_1^0 = 1$ , the inversion is insensitive to the offset as expected. Elsewhere, however, the inversion is still dependent on the offset. These other values of  $\omega_1/\omega_1^0$  correspond to initial points in  $S(3)$  that are not near the equator, so that their offset dependence is not removed by iteration.

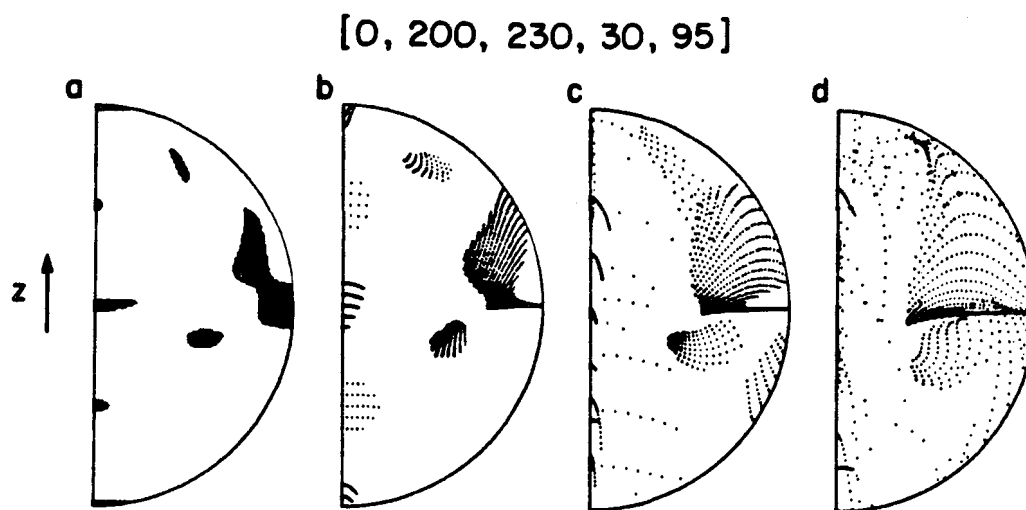


Figure VIII.9: Fixed point map in  $S0(3)$  for the scheme  $[0, 200, 230, 30, 95]$ . The origin is stable with respect to displacements in the  $xy$  plane. The equator has one stable and one unstable direction.

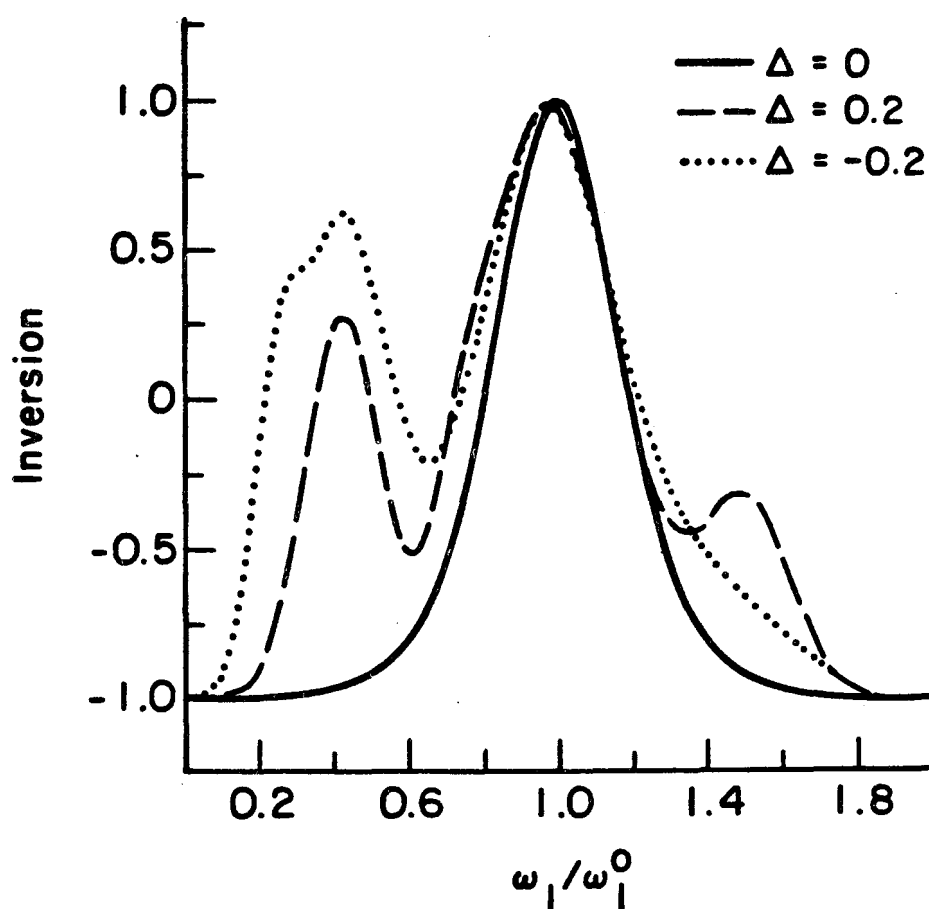


Figure VIII.10: Simulations of the inversion as a function of the relative rf amplitude for the second iterate of  $180_0$  under  $[0, 200, 230, 30, 95]$ . Plots for irradiation on resonance (solid line) and off resonance (dotted and dashed lines,  $\Delta = \Delta\omega/\omega_1^0$ ) are shown. Near  $\omega_1 = \omega_1^0$ , narrowband inversion with respect to  $\omega_1$  and broadband inversion with respect to  $\Delta\omega$  are achieved simultaneously.

## Chapter IX: Fixed Point Theory Analyses of Other Iterative Schemes

### A. Motivation

In this chapter, iterative schemes developed by other authors for various purposes in NMR are examined. The treatments of those schemes are not intended to be complete descriptions; complete descriptions are given in the original papers. The intention is only to demonstrate the applicability of the fixed point theory. Modifications that are required when an iterative scheme is not strictly equivalent to a function on the propagator space are discussed. In addition, an example in which the relevant space is not the three-dimensional space  $SO(3)$  is treated.

### B. Heteronuclear decoupling in liquids

Recently, several authors have demonstrated pulse sequences, and iterative schemes for generating such sequences, designed to remove heteronuclear couplings in liquids, e.g. to decouple protons from carbon-13 nuclei by applying a pulse sequence to the protons, allowing the observation of the carbon-13 spectrum without line splittings caused by the coupled protons. The decoupling sequences are designed to compensate for the existence of a large range of proton chemical shifts.

#### 1. Waugh's theory of decoupling

Waugh has given a criterion for evaluating decoupling sequences: A good decoupling sequence is one for which the net rotation experienced by isolated spins is independent of the resonance offset over a large range of offsets [53]. In addition, Waugh has demonstrated a particular iterative scheme that produces pulse sequences that are equivalent to net rotations of nearly zero over a large range of offsets [54]. They are therefore good decoupling sequences. It is shown here that, for a specific range of offsets, the scheme leads to a stable fixed point at the origin of the space  $SO(3)$ .

The iterative scheme may be applied to any initial sequence of  $\pi/2$  pulses. The operations are to permute a  $\pi/2$  pulse from the end of the sequence to the beginning, to form a version of the permuted sequence phase-shifted by  $180^\circ$ , and finally to concatenate the permuted sequence with the phase-shifted, permuted sequence. These operations generate a new pulse sequence that is twice as long as the original one. The new sequence is also made up of  $\pi/2$  pulses, so that the operation may be applied iteratively.

Since the criterion for decoupling involves a single, isolated spin, the pulse sequence propagators are described by points in the spherical space in Figure VII.3. For particular values of  $\Delta\omega$  and  $\omega_1$ , the initial sequence corresponds to an initial vector  $\underline{\epsilon}$  in  $SO(3)$ . Assuming for simplicity that the phase of the last  $\pi/2$  pulse in the initial sequence is 0, the propagator for the new sequence is a rotation  $R$  given by:

$$R = \exp[i(\delta I_x - \Delta I_z)\pi/2] \exp(-i\underline{\epsilon} \cdot \underline{I}) \exp[-i(\delta I_x - \Delta I_z)\pi/2] \exp[-i(\delta I_x + \Delta I_z)\pi/2] \\ \times \exp(-i\underline{\epsilon} \cdot \underline{I}) \exp[i(\delta I_x + \Delta I_z)\pi/2] \quad (IX.1)$$



with:

$$\bar{\epsilon} = (-\epsilon_x, -\epsilon_y, \epsilon_z) \quad (\text{IX.2})$$

$\delta$  and  $\Delta$  are the relative rf amplitude and the relative resonance offset, respectively, defined as the ratios of  $\omega_1$  and  $\Delta\omega$  to the nominal rf amplitude  $\omega_1^0$ . The net rotation vector associated with R is  $\beta$ . If  $\epsilon = (0,0,0)$ , then  $R = 1$  and  $\beta = (0,0,0)$ . Therefore the origin of  $S(3)$  is a fixed point of the relation implied by Eq.(IX.1). To determine its stability, Eq.(IX.1) is linearized. To first order in  $|\epsilon|$ , it can be shown that:

$$\beta = (0, 0, 2\epsilon_x \cos\theta \sin\theta (1 - \cos\xi) + 2\epsilon_y \sin\xi \cos\theta + 2\epsilon_z (\cos^2\theta \cos\xi + \sin^2\theta)) \quad (\text{IX.3})$$

where:

$$\xi = (\delta^2 + \Delta^2)^{1/2} \pi/2 \quad (\text{IX.4})$$

$$\tan\theta = \Delta/\delta \quad (\text{IX.5})$$

The linear transformation relating  $\epsilon$  and  $\beta$  in Eq.(IX.3) has a doubly degenerate eigenvalue of 0 and another eigenvalue  $\lambda_W$ , with:

$$\lambda_W = 2(\cos^2\theta \cos\xi + \sin^2\theta) \quad (\text{IX.6})$$

The eigenvector with eigenvalue  $\lambda_W$  is  $(0,0,1)$ . This eigenvalue and eigenvector are independent of the phase of the permuted  $\pi/2$  pulse. There are two other eigenvectors with eigenvalue 0 except in the case where  $\lambda_W = 0$  and either  $\cos\theta \sin\theta (1 - \cos\xi) \neq 0$  or  $\sin\xi \cos\theta \neq 0$ . In that case, there are altogether two eigenvectors.

The dynamics given by Eq.(IX.3) has a simple interpretation. Near the origin, points are either taken directly to the origin on a single iteration, or they are taken to the  $z$  axis. Once on the  $z$  axis, they move either towards the origin or away from the origin, dictated by the magnitude of  $\lambda_W$ . Thus, if  $|\lambda_W| < 1$ , the origin is stable.

If  $\delta = 1.0$ , Eq.(IX.6) shows that the origin is stable if  $|\Delta| < 1.732$ . If  $\delta = 0.8$ , the origin is stable if  $|\Delta| < 1.216$ . If  $\Delta = 0$ , the origin is stable if  $\delta < 2/3$ . When the origin is unstable, successive iterations of Waugh's scheme may not be expected to generate pulse sequences that produce net rotations successively closer to zero. Thus, the fixed point analysis leads to a prediction of intrinsic limits on the offset and rf amplitude ranges for which the scheme may be effective.

Finally, it has been suggested that the scheme be applied to initial sequences composed of composite, rather than single,  $\pi/2$  pulses [25]. This may increase the accessible offset or rf amplitude ranges. In addition, it has been shown that an appropriate initial sequence can improve the decoupling performance of the iterate sequences [24,25].

## 2. MLEV decoupling sequences

Levitt, Freeman et al. have demonstrated heteronuclear decoupling sequences, called MLEV-4, MLEV-16, etc., that are also derived with an iterative scheme. These sequences provided the impetus for much of the subsequent work on decoupling sequences and composite pulses. The original development of the MLEV scheme [32] was in terms of coherent averaging theory. Successive iterations eliminate successive terms in a Magnus expansion of the effective heteronuclear coupling. However,

Waugh's criterion for decoupling may also be applied to the MLEV sequences. Here it is shown that the origin of  $SO(3)$  is a stable fixed point under the MLEV scheme for specific ranges of  $\omega_1$  and  $\Delta\omega$ .

The MLEV scheme operates on an initial sequence composed of an even number of composite  $\pi$  pulses. The composite  $\pi$  pulses are all of the same type, with overall phases of either 0 or  $180^\circ$ . Four versions of the initial sequence are formed: the initial sequence itself; the initial sequence with an overall phase shift of  $180^\circ$ ; the initial sequence with one composite  $\pi$  pulse permuted from the end to the beginning; the permuted sequence with an overall phase shift of  $180^\circ$ . In the simplest example of the MLEV scheme, the four versions are concatenated to generate a new sequence, still composed of composite  $\pi$  pulses, that is four times longer than the original one. Although the full MLEV theory allows considerably more flexibility in the construction of iterates, only this simplest case is considered for the sake of clarity. If the initial sequence produces a rotation corresponding to the point  $\underline{\varepsilon}$  in  $SO(3)$ , and if the permuted composite  $\pi$  pulse produces a rotation  $P$ , then the new sequence produces a net rotation  $R$ , given by:

$$R = \bar{P} \exp(-i\bar{\varepsilon} \cdot \underline{I}) \bar{P}^{-1} P \exp(-i\underline{\varepsilon} \cdot \underline{I}) P^{-1} \exp(-i\bar{\varepsilon} \cdot \underline{I}) \exp(-i\underline{\varepsilon} \cdot \underline{I}) \quad (IX.7)$$

where:

$$\bar{P} = \exp(-iI_z\pi) P \exp(iI_z\pi) \quad (IX.8)$$

and  $\bar{\varepsilon}$  is as in Eq.(IX.2). Again, the question is what point  $\underline{g}$  is associated with  $R$ . If  $\underline{\varepsilon} = (0,0,0)$ , then  $\underline{g} = (0,0,0)$ , so that the origin of  $SO(3)$  is a fixed point. To assess its stability,  $P$  may be expressed

in the following form:

$$P = \exp(-iI_z\gamma_1)\exp(-iI_x\gamma_2)\exp(-iI_z\gamma_3) \quad (\text{IX.9})$$

Evaluating the right-hand side of Eq.(IX.7) to first order in  $|\xi|$ :

$$\underline{\beta} = (0, 0, 2\sin\gamma_2\sin\gamma_3\varepsilon_x + 2\sin\gamma_2\cos\gamma_3\varepsilon_y + 2(\cos\gamma_2+1)\varepsilon_z) \quad (\text{IX.10})$$

The MLEV scheme is thus equivalent to a linear transformation on  $SO(3)$  in the neighborhood of the origin. Eq.(IX.10) is obviously analogous to Eq.(IX.3), so that the dynamics of the MLEV and Waugh schemes are similar. Eq.(IX.10) defines a linear transformation with a doubly degenerate eigenvalue of 0 and a third eigenvalue  $\lambda_M$ :

$$\lambda_M = 2(\cos\gamma_2+1) \quad (\text{IX.11})$$

In view of Eq.(IX.11), the stability condition  $\lambda_m < 1$  is the same as the requirement that the population inversion produced by  $P$  be greater than or equal to  $1/2$ , since the inversion is  $-\cos\gamma_2$ . For a given composite  $\pi$  pulse, this inversion requirement dictates particular ranges of  $\omega_1$  and  $\Delta\omega$ .

### 3. Remarks

The MLEV and Waugh iterative schemes for heteronuclear decoupling differ in several ways from the schemes for population inversion presented in Chapters VII and VIII.

To begin with, the equator of  $S(3)$  is not a fixed point in the decoupling schemes as it is in the inversion schemes. The origin of  $S(3)$  is stable in all directions under certain conditions in the decoupling schemes, while it is always unstable along  $z$  in the inversion schemes. These differences are in accordance with the different purposes of the schemes. The purpose of a decoupling scheme is to produce net rotations of nearly zero, while the purpose of an inversion scheme is to produce rotations of  $\pi$ .

There are other, more qualitative differences that affect the applicability of an analysis, such as that in Chapter VII.C, designed to map out the dynamics of a function. First, the decoupling schemes act only on pulse sequences of a particular form, i.e. composed of  $\pi/2$  or  $\pi$  pulses. In itself, this fact is not very significant. However, it is related to a second, important difference. The decoupling schemes are based on the creation of new versions of an initial sequence by the permutation of pulses. If an initial sequence, with propagator  $U_0$ , is composed of  $M$  pulses with propagators  $V_i$ , then:

$$U_0 = V_M V_{M-1} \cdots V_1 \quad (\text{IX.12})$$

Permuting a pulse gives a new version with propagator  $U_0^{(1)}$ , given by:

$$U_0^{(1)} = V_{M-1} \cdots V_1 V_M \quad (\text{IX.13})$$

$$= V_M^{-1} U_0 V_M \quad (\text{IX.14})$$

Since the transformation  $V_M$  depends on parameters in the Hamiltonian, for example  $\omega_1$  and  $\Delta\omega$ , as well as the form of the permuted

pulse, or composite pulse, the relationship between  $U_0^{(1)}$  and  $U_0$  depends on those parameters. Consequently, if the initial sequence corresponds to a point  $\alpha_0$  in  $SO(3)$ , the first iterate  $\alpha_1$  depends on parameters in the Hamiltonian and the form of the permuted pulses. An iterative scheme is therefore generally not equivalent to a single function when it relies on the permutation of pulses. The fixed points, their stability, and their basins are not determined by the iterative scheme alone. This is apparent in the above discussion of decoupling schemes, where the stability of the origin depends on  $\Delta$  and  $\delta$ , as in Eq.(IX.6), as well as the form of the permuted pulses, as in Eq.(IX.11).

Despite the fact that a function on  $SO(3)$  is not uniquely defined, useful results are obtained from a fixed point analysis of decoupling schemes, specifically the limits on the stability of the origin of  $SO(3)$ . In addition, a function does exist for each pair of values of  $\Delta$  and  $\delta$  and for a particular form of the permuted pulses. For example, if an MLEV sequence is composed entirely of composite  $\pi$  pulses of the form  $90_0 180_{180} 90_0$ , and if  $\Delta = 0.5$  and  $\delta = 1.0$ , then the MLEV scheme, in the simplest case discussed above, defines a function  $F_0$  on  $SO(3)$  when the overall phase of the permuted composite  $\pi$  pulse is 0. If the overall phase of the permuted composite  $\pi$  pulse is  $\phi$ , then the function is  $F_\phi$ .  $F_\phi$  and  $F_0$  are related by:

$$F_\phi(\alpha) = R_z(\phi) F_0(R_z(-\phi)\alpha) \quad (IX.15)$$

Eq.(IX.15) implies that it is sufficient to study the single function  $F_0$ .

With the above complications in mind, the development of decoupling

sequences based on a fixed point analysis might proceed as follows:

1. Decide on the experimentally relevant ranges of  $\Delta$  and  $\delta$ .
2. Study the properties of  $F_0$  for representative values of  $\Delta$  and  $\delta$ , using various composite  $\pi$  pulses (for the MLEV scheme) or composite  $\pi/2$  pulses (for the Waugh scheme). In particular, find a composite pulse for which the basin of the origin is large and converges rapidly for the chosen values of  $\Delta$  and  $\delta$ .
3. Select an initial sequence, made up of the chosen composite pulses, for which the locus of relevant initial points lies within the basin of the origin.

A generalization of this procedure would apply to other iterative schemes for other purposes in which the function on Liouville space depends on parameters in the Hamiltonian and on the structure of the pulse sequences.

### C. Composite Pulses

#### 1. Recursive Expansion Procedure

Levitt and Ernst have proposed the recursive expansion procedure for generating broadband composite  $\pi/2$  pulses [101]. Operating on any initial pulse sequence, the recursive expansion procedure depends on the existence of an inverse sequence, i.e. a sequence that produces the inverse rotation. When  $\Delta = 0$ , inverse sequences are easily constructed by phase shifting the initial sequence by  $180^\circ$  and reversing the order

of the pulses. When  $\Delta \neq 0$ , there is no general method for constructing an exact inverse sequence, although an approximate method has been proposed [66]. Thus, the recursive expansion procedure, and other iterative schemes that rely on inverse sequences, are primarily useful for problems in which the resonance offsets are small.

The propagator  $R_0$  for an arbitrary initial sequence can be written:

$$R_0 = \exp(-iI_z\gamma_1)\exp[-iI_x(\pi/2+\epsilon)]\exp(-iI_z\gamma_2) \quad (\text{IX.16})$$

where  $\epsilon$  reflects the deviation from a perfect composite  $\pi/2$  pulse.

Recursive expansion consists of concatenating the initial sequence with its inverse, phase-shifted by  $90^\circ$ . If the initial sequence is  $S_0$ , the new sequence may be symbolized by  $S_1 = S_0 (S_0^{-1})_{90}$ .  $S_1$  has a propagator  $R_1$  given by:

$$R_1 = \exp(-iI_z\pi/2)\exp(iI_z\gamma_2)\exp[iI_x(\pi/2+\epsilon)]\exp(iI_z\pi/2) \\ \times \exp[-iI_x(\pi/2 + \epsilon)]\exp(-iI_z\gamma_2) \quad (\text{IX.17})$$

To first order in  $\epsilon$ :

$$R_1 = \exp[-iI_z(-\gamma_2+\epsilon)]\exp(-iI_x\pi/2)\exp[-iI_z(\pi/2+\gamma_2+\epsilon)] \quad (\text{IX.18})$$

$R_1$  in Eq.(IX.18) is a rotation that brings a vector from the  $z$  axis into the  $xy$  plane, exactly. Eqs.(IX.10) through (IX.18) show that such rotations form a superstable invariant set under the recursive expansion procedure. The explicit form of the vectors  $\underline{g}$  in  $SO(3)$  that belong to that set is:



$$\underline{\alpha} = |\underline{\alpha}| (\sin\theta\cos\phi, \sin\theta\sin\phi, \cos\theta) \quad (\text{IX.19})$$

with:

$$\cos |\underline{\alpha}| = -\cot^2(\theta) \quad (\text{IX.20})$$

These vectors define a closed surface in  $SO(3)$ , pictured in Figure IX.1. There is only one significant direction of deviations from that surface, i.e. the direction normal to the surface, as indicated by the fact that only one error parameter,  $\epsilon$ , appears in Eq.(IX.16).

## 2. Composite $\pi$ pulses

Shaka and Freeman have introduced iterative schemes that generate pulse sequences for population inversion that are either broadband or narrowband with respect to the rf amplitude [113]. These schemes rely on inverse sequences, so that they are most useful in cases where  $\Delta\omega \approx 0$ . One scheme that produces narrowband inversion sequences may be represented by  $S_1 = S_0(S_0^{-1})_{60}(S_0)_{120}$ , i.e. a concatenation of the initial sequence, the inverse sequence with a phase shift of  $60^\circ$ , and the initial sequence with a phase shift of  $120^\circ$ . Using the methods of Chapter VII, it can be shown that the equator of  $SO(3)$  is an unstable fixed set of points under this scheme. However, every point on the  $z$  axis is superstable with respect to displacements in the  $x$  and  $y$  directions. To see this, write the propagator  $R_0$  for  $S_0$  in the general form:

$$R_0 = \exp(-iI_{zY})\exp(-i\underline{\epsilon}\cdot\underline{I}) \quad (\text{IX.21})$$

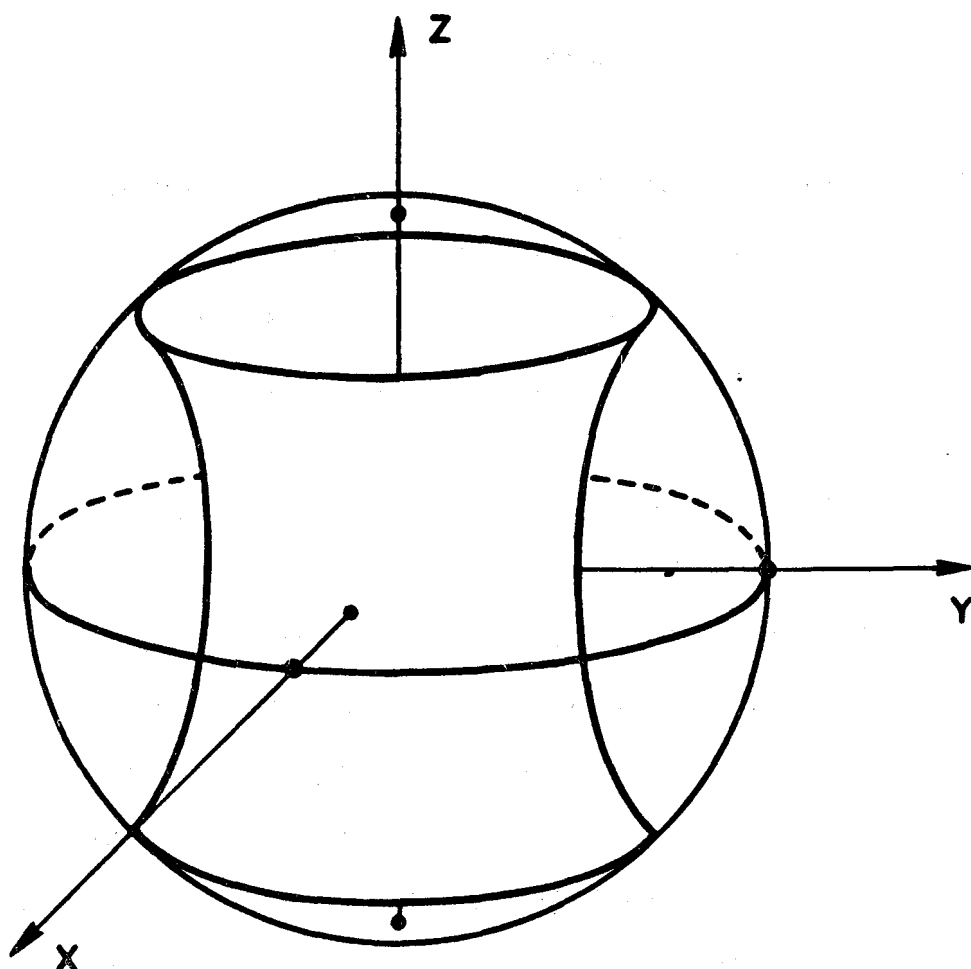


Figure IX.1: The surface contained in  $SO(3)$  that is the locus of points that correspond to rotations, or pulse sequences, that create transverse magnetization when acting on isolated spins at equilibrium.

where the  $z$  component of  $\underline{\xi}$  is zero. The propagator  $R_1$  for  $S_1$  is then:

$$R_1 = \exp[-iI_z(\gamma+2\pi/3)]\exp(-i\underline{\xi}\cdot\underline{I})\exp(iI_z\pi/3)\exp(i\underline{\xi}\cdot\underline{I}) \\ \times \exp(iI_z\pi/3)\exp(-i\underline{\xi}\cdot\underline{I}) \quad (\text{IX.22})$$

To first order in  $|\underline{\xi}|$ , Eq.(IX.22) reduces to:

$$R = \exp(-iI_z\gamma) \quad (\text{IX.23})$$

Since the  $z$  axis is an attractor, points in  $SO(3)$  that are not on the equator converge to the  $z$  axis, corresponding to rotations that do not invert populations at all. Points on the equator, corresponding to perfect inversion, remain there. This leads to narrowband inversion, as in the schemes  $[0,120,240]$  and  $[180-\cos^{-1}0.25, 180+\cos^{-1}0.25, 0, 180+\cos^{-1}0.25, 180-\cos^{-1}0.25]$  discussed in Chapter VIII, although in those schemes it is only the origin that is superstable to displacements in the  $xy$  plane, rather than the entire  $z$  axis.

Shaka and Freeman also suggest a scheme in which  $S_1 = S_0(S_0^{-1})_{300}S_0$ . For this scheme, the equator of  $SO(3)$  is a superstable fixed set of points, leading to broadband population inversion. In addition, they demonstrate a scheme represented by  $S_1 = S_0(S_0^{-1})_{270}S_0$ . This scheme leads to broadband inversion, but the equator of  $SO(3)$  is not an attractor. It can be shown that, in a linear analysis, the eigenvalues at the equator are  $\lambda_e^{\pm} = 1$ , using the notation of Chapter VII.B.3. Broadband inversion is instead the result of the fact that this scheme converts rotations of the form of Eq.(IX.18) or Eqs.(IX.19) and (IX.20) to rotations that produce complete inversion. In other

words this scheme maps the surface in Figure IX.1 onto the equator.

Finally, Shaka and Freeman demonstrate a scheme for which

$S_1 = S_0(S_0^{-1})_{90}(S_0)_{180}$ . This scheme maps the surface of Figure IX.1 onto the z axis, and leads to narrowband inversion.

Inversion plots for the last two examples do not exhibit the smooth regions of uniform inversion seen in Chapters VII and VIII. Rather, the inversion as a function of  $\omega_1$  displays ripples [113]. This is due to the fact that the points in  $SO(3)$  that correspond to the desired transformations are not attractors.

### 3. Remarks

The mapping techniques developed in Chapter VII.C can be applied to the above iterative schemes to investigate basins, fixed points, and flows. As in Section III, these techniques can aid in the selection of an initial sequence and in the development of new schemes.

Several operations on pulse sequences that may be used in iterative schemes have been encountered, namely phase shifting, pulse permutation, and the reversal of the order of pulses. These operations are intended to produce some transformation of the pulse sequence propagator. In general, the effect that an operation has on the propagator is dependent on the Hamiltonian, as has been seen particularly in the cases of pulse permutation and order reversal.

#### D. Selective excitation of multiple quantum coherence

The first true iterative scheme for generating pulse sequences for NMR applications was developed by Warren, Weitekamp, and Pines for selectively exciting multiple quantum coherences in coupled spin systems [46]. The objective was to excite coherences only between spin states that differ in their Zeeman quantum number by a multiple of a particular integer  $n$ , i.e.  $nk$ -quantum coherences. The propagator for a pulse sequence in a coupled spin system is a general transformation  $U_0$  which may be written in terms of irreducible tensor operators  $T_{lm}(q)$ , where the index  $q$  is necessary because there may be several, independent operators with the same  $l$  and  $m$ :

$$U_0 = \exp(-iQ) \quad (IX.24)$$

$$Q = \sum_q \sum_l \sum_{m=-l}^l C_{lm}(q) T_{lm}(q) \quad (IX.26)$$

$A$  must be Hermitian, which implies:

$$C_{l-m}(q) = (-1)^m C_{lm}^*(q) \quad (IX.26)$$

Alternatively, instead of using the irreducible tensors themselves as a basis, a basis of Hermitian combinations  $A_{lm}(q)$  and  $B_{lm}(q)$ , as defined in Eqs.(V.18) and (V.19) may be used:

$$Q = \sum_q \sum_l [C_{l0}(q) T_{l0}(q) + \sum_{m=1}^l (a_{lm}(q) A_{lm}(q) + b_{lm}(q) B_{lm}(q)) \quad (IX.27)$$

The coefficients  $a_{lm}(q)$ ,  $b_{lm}(q)$  and  $C_{10}(q)$  are real. The set of these real coefficients is a generalization of the vector  $\underline{g}$  in  $SO(3)$  that describes the transformation of a system of uncoupled, isolated spins. For a system of  $N$  coupled spin-1/2 nuclei, there are  $4^N - 1$  independent, real numbers that specify  $Q$ . Thus, the relevant propagator space is  $(4^N - 1)$ -dimensional. The pulse sequence propagator is characterized by a point in that space.

The selective excitation scheme employs the phase shifting and concatenation operations discussed in Chapters VII and VIII. For selective  $nk$ -quantum excitation, the scheme  $[0, 1 \times 360/n, 2 \times 360/n, \dots, (n-1) \times 360/n]$  may be used. Phase shifting has the effect of rotating  $Q$  about  $z$ , so that, if the initial sequence has the propagator  $U_0$  of Eq.(IX.24), the first iterate sequence has the propagator  $U_1$ :

$$U_1 = \exp(-iQ_{n-1})\exp(-iQ_{n-2})\dots\exp(-iQ_0) \quad (\text{IX.28})$$

with:

$$Q_p = \sum_q \sum_l \sum_{m=-l}^l \exp[-im(2\pi p/n)] C_{lm}(q) T_{lm}(q) \quad (\text{IX.29})$$

Eq.(IX.29) depends on the property of irreducible tensor operators that:

$$\exp(-iI_{z\phi}) T_{lm}(q) \exp(iI_{z\phi}) = \exp(-im\phi) T_{lm}(q) \quad (\text{IX.30})$$

To first order in the coefficients  $C_{lm}(q)$ , the exponents in Eq.(IX.28) can be added. Using the identity:

$$\sum_{p=0}^{n-1} \exp[-im(2\pi p/n)] = \begin{cases} n, & m \text{ a multiple of } n \\ 0, & \text{otherwise} \end{cases} \quad (\text{IX.31})$$

$U_1$  becomes:

$$U_1 = \exp(-iQ_T) \quad (\text{IX.32})$$

$$Q_T = \sum_q \sum_l \sum'_m n C_{lm}(q) T_{lm}(q) \quad (\text{IX.33})$$

where the sum over  $m$  in Eq.(IX.33) is restricted to multiples of  $n$ .

Since the propagator in Eq.(IX.32) contains only  $T_{lm}(q)$  operators with  $m$  a multiple of  $n$ , it generates coherences only between spin states that differ in their Zeeman quantum number by a multiple of  $n$ , i.e.

$nk$ -quantum coherences, when it acts on a spin system initially at equilibrium.

In terms of a fixed point analysis, the origin of the propagator space is a fixed point. Eqs.(IX.24) through (IX.33) show that the origin is superstable along directions corresponding to  $T_{lm}(q)$  with  $m$  not a multiple of  $n$ , and unstable, with an eigenvalue of  $n$ , along directions corresponding to  $T_{lm}(q)$  with  $m$  a multiple of  $n$ . The situation is formally analogous to the scheme [0,120,240] in  $SO(3)$  where the origin is superstable along  $x$  and  $y$  and unstable along  $z$ . If the scheme for selective excitation is to be successful, the initial sequence must be such that  $Q$  in Eq.(IX.24) is small, i.e. close to the origin. Then the first several iterations may produce sequences for which the desirable tensor components are much larger than the undesirable ones. However, with higher iterations, the point that describes the sequence propagator will move away from the origin, and may develop large components of undesirable tensors. In other words,

the scheme may only be effective in a transient way. This is because the axes in the propagator space that correspond to the desired transformations are a fixed set of points, but are not stable. Behavior analogous to that in Figure VII.3 is expected.

The development of the iterative schemes for selective excitation of multiple quantum coherences was originally based on coherent averaging theory. It was shown that successive iterations cause the undesirable tensor components to vanish from successively higher terms in a Magnus expansion of the propagator. The need for an initial sequence for which  $A$  is small was recognized as a requirement for the convergence of the Magnus expansion [46].



## Chapter X: Conclusion

The previous chapters describe in detail two methods for deriving pulse sequences for broadband excitation. The work described in those chapters does not exhaust the potential of either method, however. Some extensions and areas for improvement of the methods are listed here.

Two obvious extensions of the coherent averaging approach are the derivation of higher-order composite pulses and the derivation of composite pulses with broadband properties with respect to two different experimental parameters at once. Both extensions require improvements in the numerical methods to allow more complicated equations to be generated and solved. Promising avenues to pursue are the use of symbolic manipulation programs and directed searches, as described in Chapter IV.C.5. It may also prove fruitful to lift the restriction to constant pulse amplitudes and piecewise-constant phase functions. Piecewise-constant or continuously varying pulse amplitudes and continuously varying rf phases may result in improved excitation sequences.

Coherent averaging theory calculations by the direct numerical evaluation of the Magnus expansion have not been employed in NMR problems outside of the construction of composite pulses. Such an approach may be useful in other problems when suitable sequences can not be found by the usual means. Even when sequences can be found by other means, those that are derived numerically may turn out to be more effective.

The generation of pulse sequences by iterative schemes is an area

of NMR whose potential is as yet unknown, beyond what has been presented in Chapters VII through IX. Some problems that deserve attention are the generation of pulse sequences that produce constant net rotations, pulse sequences that are broadband with respect to one parameter and narrowband with respect to a different parameter, pulse sequences for broadband excitation in coupled spin systems, and improved sequences for selective multiple quantum excitation. All of these problems are likely to require an investigation of new classes of operations that may be applied iteratively to an initial pulse sequence.

Finally, the incorporation of broadband excitation sequences into NMR experiments in general, and the comparison with the more traditional forms of those experiments, is an important area for future research.

## Appendix A: Experimental Methods

### 1. Spectrometers

Experiments were performed on two home-built NMR spectrometers that have been described in detail in other dissertations [99,114]. One spectrometer, operating at a proton Larmor frequency of 360 MHz, was used to obtain the data and spectra in Chapters II and V. The other, operating at a proton Larmor frequency of 180 MHz, was used to obtain the data and spectra in Chapters VI and VII.

Both spectrometers are based on Bruker superconducting magnets (42 and 84 kG). The timing sequence of rf pulses, delays, and signal acquisition is stored in and controlled by a pulse programmer with an independent microprocessor. Overall triggering of the pulse programmer, data storage and averaging, Fourier transformation, and other data manipulations and analysis are accomplished by Data General Nova computers, running the SPEC operating system [115]. The principal components of the spectrometer are diagrammed in Figure A.1.

An unusual feature of many of the pulse sequences investigated in this dissertation, from the experimental standpoint, is their uncommon rf phase shifts. The spectrometers normally operate with four proton rf pulse channels and four X nucleus channels, each producing pulses with relative phases of 0°, 90°, 180°, and 270°. Phase generation and pulse gating takes place at an intermediate frequency (IF) of 30 MHz. In addition, there is a digital phase shifter capable of producing overall phase shifts in increments of  $360^\circ/256$  [87,114]. The overall phase

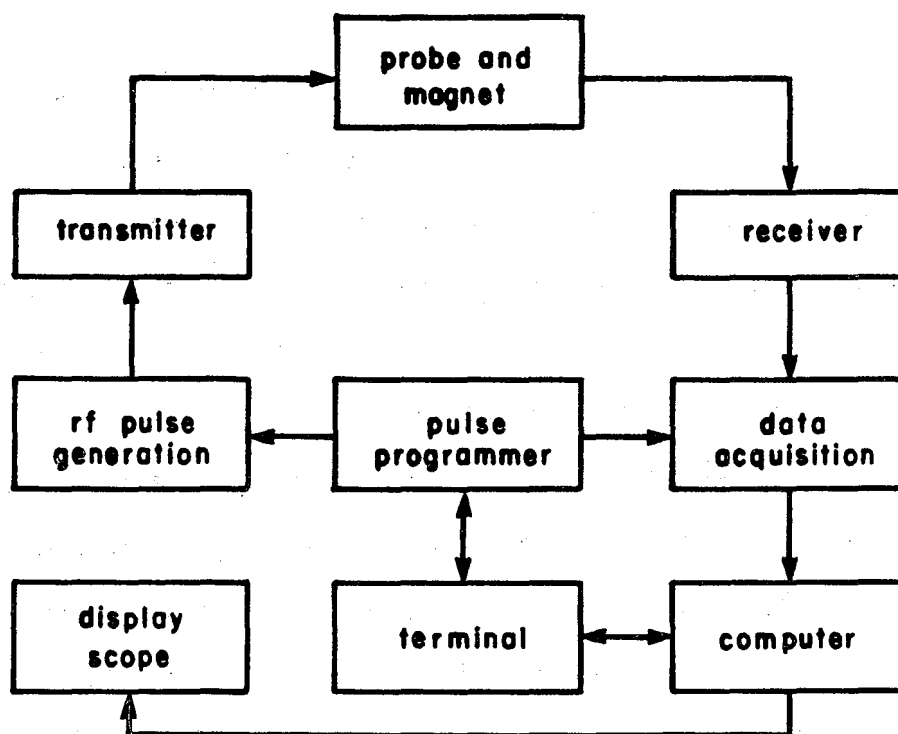


Figure A.1: Block diagram of the principal components of the pulsed NMR spectrometers used in the studies described in this dissertation.

shift produced by the phase shifter can be determined by an eight bit binary number stored in a RAM. Thus, the overall phases can be set to any value within a nominal precision of  $360^\circ/512$  by loading the appropriate numbers into successive RAM locations. Approximately  $2.5 \mu\text{s}$  is required for the phase shifter to change state, however, so that  $2.5 \mu\text{s}$  gaps are required between pulses if the phase shifter RAM is used to set the pulse phases. Pulse phases were set in this way for experiments whose results are given in Figures V.2, V.4, V.5, and VI.5.

In cases where gaps between pulses would degrade the performance of a sequence due to the presence of large resonance offsets or dipole couplings, or in cases where the required phase shifts were comparatively simple, the phase shifter was not used. This applies to data in Figures V.2, V.3, V.7, V.11, V.13, VI.5, VII.5, and VII.6. Where necessary, the relative phases of the rf channels were readjusted with a combination of delay cables and phase tweakers. Relative phases were measured with a vector voltmeter. For the experiments that produced the data in Figures VII.5 and VII.6, six rf channels with phases in increments of  $60^\circ$  were required. Therefore, the outputs of two of the X nucleus channels were combined with the outputs of the four proton channels and the relative phases were adjusted appropriately.

A schematic diagram of the phase generation circuitry is given in Figure A.2.

## 2. NMR probes

The two probe circuits used in the experiments are given in Figure A.3. The 360 MHz probe in Figure A.3a was designed and built by Erika

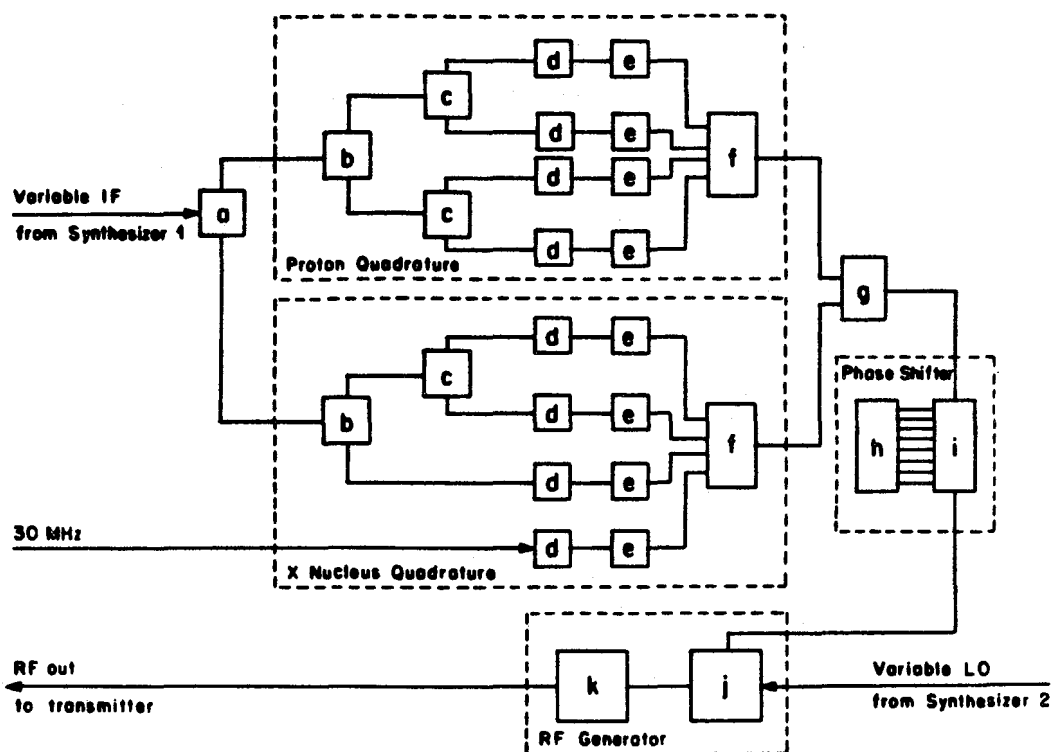


Figure A.2: Block diagram of circuitry for generating phase-shifted rf pulses. The components are: divider (a), 0°/180° hybrid (b), 0°/90° hybrid (c), phase and amplitude tweakers (d), rf switch (e and k), four-way combiner (f), two-way combiner (g), RAM circuit (h), Daico phase shifter (i), mixer (j). This set up allows pulses with seven chosen phases to be given at one frequency and pulses of a single phase to be given at another frequency. In addition, overall phase shifts in increments of  $360^\circ/256$  can be performed by the phase shifter.

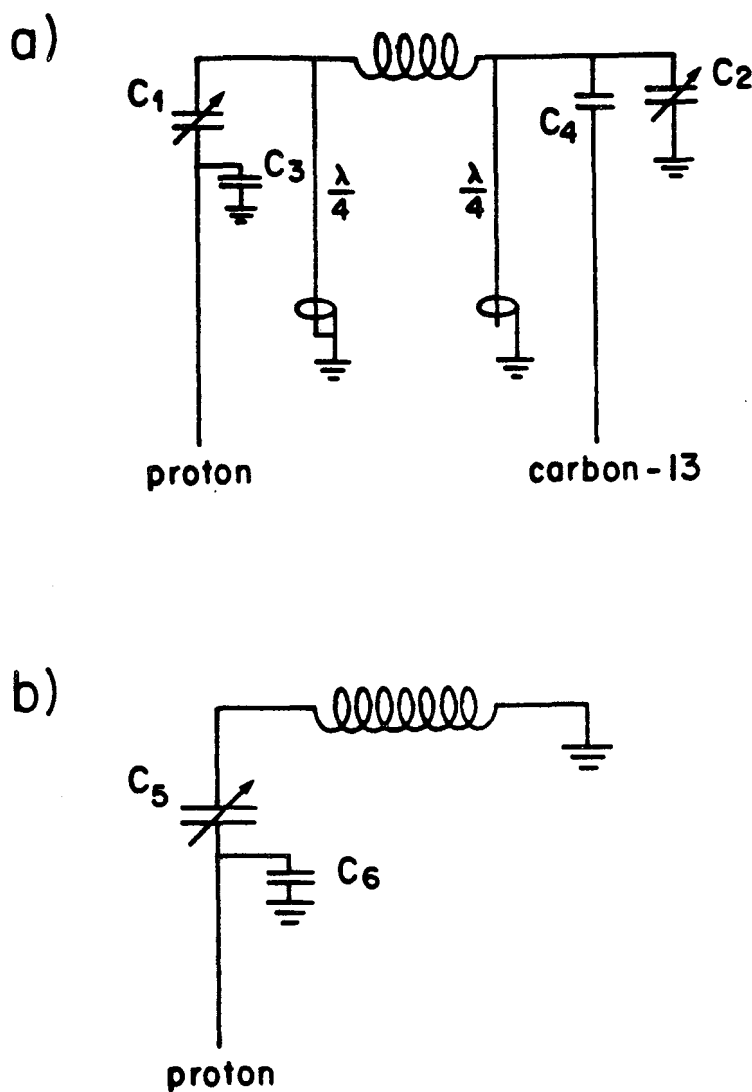


Figure A.3: NMR probe circuits. a) Double-tuned circuit for proton (360 MHz) and  $^{13}\text{C}$  studies.  $C_1$  and  $C_2$  are tuning capacitors.  $C_3$  and  $C_4$  are for impedance matching. Isolation between the proton and  $^{13}\text{C}$  sides is provided by the open and closed  $\lambda/4$  cables on either side of the coil. b) Circuit for proton (180 MHz) studies.

Schneider and Kurt Zilm. It is a double-tuned probe, suitable for irradiating and detecting signals from protons and  $^{13}\text{C}$  nuclei simultaneously, although only the proton side was used in the experiments in this dissertation. The coil consists of four turns of 2 mm wide, flattened copper wire. The coil is 10 mm long, with an inside diameter of 7 mm.

The 180 MHz probe in Figure A.3b was built by Warren Warren. The probe is designed for liquid crystal experiments, requiring the capability of controlling the sample temperature. An auxiliary temperature controller is used to read the voltage from a thermocouple positioned near the sample and switch current through a heater. Temperature regulation was employed in the experiments of Figure VI.5.

The coil in the 180 MHz probe is wound from 7 turns of 2 mm wide, flattened copper wire, with a length of 22 mm and an inside diameter of 8 mm.

### 3. Samples

Experiments to demonstrate the performance of composite pulses as a function of the resonance offset or the rf amplitude were performed on an  $\text{H}_2\text{O}_{(l)}$  sample in a glass bulb with an inside diameter of 3 mm. The spectra in Figure V.11 were obtained from a sample of  $\text{Ba}(\text{ClO}_3)_2 \cdot \text{H}_2\text{O}$  powder packed into a glass tube with an inside diameter of 3 mm. The sample was 5 mm long. The dimensions of the squaric acid crystal used in the experiments of Figure V.13 were approximately 5 mm by 6 mm by 8 mm.

The sample of  $\text{CH}_2\text{Cl}_2$  dissolved in Eastman 15320 liquid crystal for



Figure VI.5 was prepared as described in Chapter VI.C.1. The sample was sealed in a glass bulb with an inside diameter of 4 mm.

#### 4. Additional remarks on techniques

Population inversion measurements were made with sequences analogous to that in Figure V.9b. Variations in  $\omega_1$  were mimicked by equivalent variations in pulse lengths in the inverting sequence, since it is experimentally easier to calibrate  $\omega_1$  once and then vary the pulse lengths rather than varying  $\omega_1$  and recalibrating it for every data point. The length of the  $\pi/2$  "read" pulse was kept constant. The inversion was measured by the peak height in a magnitude spectrum, normalized to the peak height after the read pulse alone.

When the inversion is incomplete, transverse magnetization is created by the composite  $\pi$  pulse. The transverse magnetization dephases due to static field inhomogeneity during  $\tau$  in Figure V.9, but is partially refocussed at a time  $\tau$  after the read pulse, giving an echo signal. In the  $H_2O$  inversion experiments,  $\tau$  was taken to be 20 ms. The static field homogeneity was spoiled by missetting the magnet shims so that the FID after the read pulse did not overlap with the echo. Typically, the inhomogeneous linewidth was several hundred Hz.

In order to measure inversion as a function of  $\Delta\omega$ , it was necessary to give the composite  $\pi$  pulse off resonance while keeping the read pulse on resonance. An independent rf gate, fed by a fixed 30 MHz IF source, was used to give the read pulse. The remaining gates were fed by a variable IF from a frequency synthesizer. The outputs of all gates were combined. Thus, the frequency of the composite  $\pi$  pulse could be

varied at will without affecting the read pulse.

Pulse lengths corresponding to flip angles in multiples of  $\pi/4$  were calibrated by giving a sequence of four identical pulses and observing the ensuing FID. The pulse lengths were adjusted to produce a null in the FID signal. When necessary, pulse lengths for other flip angles were interpolated.

Measurements of signal phases were made directly from the FID, using Eq.(II.75).

## Appendix B: Computer Programs

### 1. Simulations

Simulations of signal amplitude, signal phase, or inversion as a function of  $\Delta\omega/\omega_1^0$  or  $\omega_1/\omega_1^0$  were accomplished with FORTRAN programs similar to DELTA.FOR, reproduced along with the necessary subroutines in Figure B.1. Specifically, DELTA.FOR calculates the final x, y, and z components of a Bloch vector as a function of  $\Delta\omega/\omega_1^0$  for any given pulse sequence. The pulses are treated as a sequence of rotations applied to an initial vector aligned with the z axis.

Simulations of signal amplitude or inversion as a function of dipole coupling constants in a system of coupled spin-1/2 nuclei were carried out with NROT.FOR and its associated subroutines, reproduced in Figure B.2. The number of spins and the nominal values of  $d_{ij}/\omega_1^0$  are entered, along with the pulse sequence. The final density matrix in a direct product basis is calculated as a function of an overall factor C that multiplies all coupling constants.

Simulations of powder pattern spectra for an isotropic orientational distribution of pairs of coupled spin-1/2 nuclei were produced by WQDP.FOR and FFT.FOR in Figure B.3. WQDP.FOR generates the FID after a given sequence of pulses and delays. FFT.FOR Fourier transforms the FID, using the IMSL subroutine FFT2C.

### 2. Derivation of pulse sequences in the coherent averaging theory approach

Figure B.1: DELTA.FOR

```

      DIMENSION P(2000),F(2000),FF(2000)
C
C   PROGRAM CALCULATES INVERSION FOR ANY SEQUENCE
C   FOR SPECIFIED RANGE OF RESONANCE OFFSET
C
      TYPE 100
      FORMAT(1X,'ENTER NUMBER OF PULSES')
      ACCEPT 8,NP
      TYPE 101
      FORMAT(1X,'ENTER FLIP ANGLES')
      ACCEPT 8,(F(I),I=1,NP)
      TYPE 102
      FORMAT(1X,'ENTER PHASES')
      ACCEPT 8,(P(I),I=1,NP)
      TYPE 103
      FORMAT(1X,'ENTER LOW OFFSET, HIGH OFFSET, INCREMENT')
      ACCEPT 8,DL,DH,DINC
      PRINT 8,'PHASES: ',(P(I),I=1,NP)
      PRINT 8,'FLIPS : ',(F(I),I=1,NP)
      CONV=4.0*ATAN(1.0)/180.0
      DO 30 I=1,NP
      P(I)=P(I)*CONV
      F(I)=F(I)*CONV
      30  CONTINUE
      D=DL
      35  X=0.0
      Y=0.0
      Z=1.0
      DO 50 I=1,NP
      CALL ROT(D,F(I),P(I),X,Y,Z,U,V,W)
      X=U
      Y=V
      Z=W
      50  CONTINUE
      PRINT 8,D,X,Y,Z
      D=D+DINC
      IF(D.LE.DH) GO TO 35
      STOP
      END

      SUBROUTINE ROT(D,F,P,X,Y,Z,U,V,W)
C
C   GIVES RIGHT HAND ROTATION
C   D=OFFSET; F=FLIP ANGLE; P=PHASE
C   (X,Y,Z)=INITIAL VECTOR; (U,V,W)=FINAL VECTOR
C
      CALL ROTZ(-P,X,Y,Z,U,V,W)
      CALL ROTX(D,F,U,V,W,X,Y,Z)
      CALL ROTZ(P,X,Y,Z,U,V,W)
      RETURN
      END

      SUBROUTINE ROTX(D,F,X,Y,Z,U,V,W)
      A=ATAN(D)
      B=F*SQRT(1+D*D)
      CA=COS(A)
      SA=SIN(A)
      CB=COS(B)
      SB=SIN(B)
      U=X*(CA*CA+SA*SA*CB)-Y*SB*SA-Z*(CA*SA*CB-CA*SA)
      V=X*SA*SB+Y*CB-Z*CA*SB
      W=X*(CA*SB-SA*CB)+Y*SB*CA+Z*(CA*CB*CB+SA*SA)
      RETURN
      END

      SUBROUTINE ROTZ(P,X,Y,Z,U,V,W)
      M=Z
      CP=COS(P)
      SP=SIN(P)
      U=X*CP-Y*SP
      V=X*SP+Y*CP
      RETURN
      END

```

Figure B.2: NROT.FOR

```

C      PROGRAM PERFORMS ARBITRARY PULSE SEQUENCE
C      ON SYSTEM OF UP TO 4 SPINS
C
C      DIMENSION F(20),P(20),D(8,8),Z(64,64)
C      DIMENSION X(64,64),WD(64,64),HT(2080),ST(4096)
C      COMPLEX Y(64,64),RHD(64,64),HAM(64,64),ROT(64,64)
C      COMPLEX RM1
C      COMPLEX Y(64,64),V(64)
C
C      SET PARAMETERS
C
C      TYPE *, 'ENTER # OF SPINS, # OF PULSES'
C      ACCEPT *, NS, NP
C      N=2*NS
C
C      TYPE *, 'ENTER FLIP ANGLES'
C      ACCEPT *, (F(I), I=1, NP)
C      TYPE *, 'ENTER PHASES'
C      ACCEPT *, (P(I), I=1, NP)
C      DO 20 I=1, NS-1
C      DO 10 J=I+1, NS
C      TYPE 3, I, J
C      FORMAT(1X, 'ENTER COUPLING OF', I3, ' TO', I3)
C      ACCEPT *, D(I, J)
C      CONTINUE
C      CONTINUE
C      TYPE *, 'ENTER LOW, HIGH COUPLING MULTIPLIER, INCREMENT'
C      ACCEPT *, CL, CH, CINC
C      DO 30 I=1, N
C      DO 25 J=1, N
C      Z(I, J)=0.0
C      X(I, J)=0.0
C      HD(I, J)=0.0
C      Y(I, J)=(0.0, 0.0)
C      CONTINUE
C      CONTINUE
C      SET UP IZ
C
C      DO 45 J=1, NS
C      N=2*NS(J-1)
C      DO 40 I=1, N
C      K=(I-1)/N
C      Z(I, I)=Z(I, I)+0.5*((-1)**K)
C      CONTINUE
C      CONTINUE
C      SET UP IX AND IY
C
C      DO 55 I=1, NS
C      N=2*NS(I-1)
C      DO 50 J=1, N
C      IF(((J-1).AND.N).NE.0) GO TO 50
C      K=J+N
C      X(J, K)=0.5
C      X(K, J)=0.5
C      Y(J, K)=(0.0, -0.5)
C      Y(K, J)=(0.0, 0.5)
C      CONTINUE
C      CONTINUE
50      CONTINUE
55      CONTINUE

```

```

C
C      SET UP COUPLING MATRIX
C
DO 70 I=1,NS-1
DO 65 J=I+1,NS
MI=2*H(I-1)
MJ=2*H(J-1)
M=MI+MJ
DD=-D(I,J)/6.0
DO 60 K=I+N
KH=(K-1).AND.M
HD(K,K)=HD(K,K)+DD
IF((KH.EQ.M).OR.(KH.EQ.0)) HD(K,K)=HD(K,K)-2.0*DD
IF(KH.NE.MI) GO TO 60
L=K-MI+MJ
HD(K,L)=DD
HD(L,K)=DD
60  CONTINUE
65  CONTINUE
70  CONTINUE
CONV=ATAN(1.0)/45.0
DO 71 I=1,NP
P(I)=P(I)*CONV
F(I)=F(I)*CONV
71  CONTINUE
TYPE 8, 'DONE WITH SET-UP PART'
INC=1
C=CL
RM1=(0.0,1.0)
C
C      MAIN LOOP: STEP THROUGH COUPLINGS
C
73  DO 80 I=1,N
DO 75 J=I+N
RHO(I,J)=Z(I,J)
75  CONTINUE
80  CONTINUE
K=0
DO 90 I=1,N
DO 85 J=I+1
K=K+1
H(K)=X(J,I)+C*RHO(J,I)
85  CONTINUE
90  CONTINUE
CALL REIGEN(H,S,N)
C
C      STEP THROUGH PULSES
C
DO 150 II=1,NP
DO 100 I=1,N
DO 95 J=1,N
HAM(I,J)=(0.0,0.0)
ROT(I,J)=(0.0,0.0)
T(J,I)=S(J+(I-1)*N)
95  CONTINUE
100 CONTINUE
DO 105 I=1,N
ROT(I,I)=CEXP(-RM1*P(I))*Z(I,I)
HAM(I,I)=CEXP(-RM1*H(I))*F(II)
105 CONTINUE
CALL UMUA2(T,HAM,N,64,U)
CALL UMUA2(ROT,HAM,N,64,V)
CALL UMUA2(HAM,RHO,N,64,V)
150 CONTINUE
W=0.0
DO 160 I=1,N
DO 155 J=1,N
W=W+Z(I,J)*RHO(J,I)
155 CONTINUE
160 CONTINUE
W=4.0*W/(N*NS)
PRINT 8,C,W
TYPE 8, 'DONE WITH POINT 0',INC
INC=INC+1
C=C+CINC
IF(C.LE.CN) GO TO 73
STOP
END

```

```

      subroutine unua2(u,b,a,n,v)
c
c  performs unitary transformation
c  b=usb2uadjoint
c
c  complex u(n,n),b(n,n),v(n)
c  call matral(u,b,a,n,v)
c  call matam1(b,u,a,n,v)
c  return
c  end
c
c
c  subroutine matam1(a,b,a,n,rv)
c  complex a(n,n),b(n,n),rv(n),s
c  do 14 i=1,n
c  do 12 j=1,n
c  s=0.0
c  do 11 k=1,n
11  s=s+a(i,k)*conjs(b(j,k))
12  rv(j)=s
c  do 13 j=1,n
13  a(i,j)=rv(j)
14  continue
c  return
c  end
c
c
c  subroutine matral(a,b,a,n,cv)
c  complex a(n,n),b(n,n),cv(n),s
c  do 14 j=1,n
c  do 12 i=1,n
c  s=0.0
c  do 11 k=1,n
11  s=s+a(i,k)*b(k,j)
12  cv(i)=s
c  do 13 i=1,n
13  b(i,j)=cv(i)
14  continue
c  return
c  end
c
c
c  diagonalizes a real hamiltonian.
c  h is a one-dimensional vector whose elements
c  are successive columns in the upper half of the
c  hamiltonian. on return, the eigenvalues are
c  in the first n locations in h. s is a vector
c  whose elements are successive eigenvectors.
c  n is the dimensionality.
c
c  subroutine reisen(h,s,n)
c  dimension h(1),s(1)
c  mat(i,j)=js(j-1)/2+i
c  an=n
c  range=1.0e-7
c  ij=0
c  do 20 j=1,n
c  do 20 i=1,n
c  ij=ij+1
c  s(ij)=0.0
20  if(1.0e-7) s(ij)=1.0
c  anora=0.0
c  do 30 j=2,n
c  jal=j-1
c  do 30 i=1,jal
c  ij=mat(i,j)
30  anora=anorath(ij)*h(ij)
c  anora=sqrt(2.0*anora)
c  if(anora.lt.range) go to 125
c  anorax=anora*range/an
c  ind=0
c  thr=anora
40  thr=thr/an

```

```

30      do 100 m=2,n
      mm=m-1
      do 100 l=1,mm1
      la=mat(l,m)
      if(abs(h(la)).lt.thr) go to 100
      ind=1
      ll=mat(l,1)
      mm=mat(mm,m)
      diff=h(mm)-h(ll)
      if(diff.eq.0.0) diff=1.0e-15
      aa=0.5*atan(2.0*h(la)/diff)
      sina=sin(aa)
      cosa=cos(aa)
      sina2=sina*sina
      cosa2=cosa*cosa
      do 70 k=1,n
      if(k-1) 61,70,62
61      kl=mat(k,1)
      km=mat(k,m)
      go to 65
62      if(k-m) 63,70,64
63      kl=mat(l,k)
      km=mat(k,m)
      go to 65
64      kl=mat(l,k)
      km=mat(m,k)
65      hh=cosa*h(kl)-sina*h(km)
      h(km)=sina*h(kl)+cosa*h(km)
      h(kl)=hh
70      continue
      ss=2.0*sina*cosa*h(la)
      hh=cosa2*h(ll)+sina2*h(mm)-ss
      h(mm)=sina2*h(ll)+cosa2*h(mm)+ss
      h(ll)=hh
      h(la)=0.0
      do 80 i=1,n
      il=(l-1)*n+i
      im=(m-1)*n+i
      ss=cosa*s(il)-sina*s(im)
      s(im)=sina*s(il)+cosa*s(im)
      s(il)=ss
80      continue
100     continue
      if(ind.eq.0) go to 120
      ind=0
      go to 30
120     if(thr.gt.enorax) go to 40
125     do 130 i=2,n
      ii=mat(i,i)
      h(ii)=h(ii)
130     continue
      return
      end

```



Figure B.3: WQDP.FOR and FFT.FOR

## WQDP.FOR

```

dimension sr(1024),si(1024),npsv(20),t(20),ph(20)
dimension e(3),x(3,3),h(6),s(9)
complex rho(3,3),ham(3,3),r(3),w(3,3)
complex rpp(3,3),z,u(3,3)
twopi=8.020.0018atan(1.0)
rput=1.0
ncoso=0
do 5 i=1,1024
  sr(i)=0.0
  si(i)=0.0
  if(i.st.20) go to 5
  npsv(i)=0.0
  t(i)=0.0
  ph(i)=0.0
5  continue
  do 15 i=1,3
  do 15 j=1,3
  x(i,j)=0.0
  w(i,j)=cmplx(0.0,0.0)
15  continue
  x(1,2)=1/(sqrt(2.0))
  x(2,1)=x(1,2)
  x(2,3)=x(1,2)
  x(3,2)=x(1,2)
  w(1,2)=cmplx(0.0,-x(1,2))
  w(2,3)=w(1,2)
  w(2,1)=cmplx(0.0,x(1,2))
  w(3,2)=w(2,1)
  type 8,'how many quadrupole frequencies?'
  accept 8,nhw
  type 8,'powder pattern?'
  accept 8,npp
  if(npp.eq.1) type 8,'very wa from -wa/2 to wa'
  type 8,'enter low and high wa values'
  accept 8,wel,wef
  type 8,'how many steps in pulse sequence?'
  accept 8,np
  type 8,'enter pulse strength (khz)'
  accept 8,w1
  type 8,'enter sequence vector'
  accept 8,(npsv(i),i=1,np)
  type 8,'enter phases'
  accept 8,(ph(i),i=1,np)
  do 10 i=1,np
  ph(i)=ph(i)*1000.0twopi/360.0
10  continue
  type 8,'enter pulse lengths (usec)'
  accept 8,(t(i),i=1,np)
  type 8,'remove coherences after some step?'
  accept 8,mcoh
  if(mcoh.eq.0) go to 20
  type 8,'after which step?'
  accept 8,ncoso
20  type 8,'enter # of points, sampling rate for fid (usec)'
  accept 8,nfid,tfid
  print 8,nfid,tfid
  weinc=0.0
  if(nwe.eq.1) go to 190
  weinc=(wef-wel)/(nwe-1)
190  do 100 iwe=1,nwe
  if(iwe.eq.1) we=wei-weinc
  we=we+weinc
  do 30 i=1,3
  do 30 j=1,3
  rho(i,j)=cmplx(0.0,0.0)
  ham(i,j)=cmplx(0.0,0.0)
30  continue
  rho(1,1)=cmplx(1.0,0.0)
  rho(3,3)=cmplx(-1.0,0.0)
  h(1)=we/3.0
  h(2)=w1/sqrt(2.0)
  h(3)=-2.0sh(1)
  h(4)=0.0
  h(5)=h(2)
  h(6)=h(1)

```

```

      call reisen(h,s,3)
      do 40 i=1,3
      s(i)=h(i)
40      continue
      u(1,1)=s(1)
      u(1,2)=s(4)
      u(1,3)=s(7)
      u(2,1)=s(2)
      u(2,2)=s(5)
      u(2,3)=s(8)
      u(3,1)=s(3)
      u(3,2)=s(6)
      u(3,3)=s(9)
      do 110 ip=1,np
      if(nrev(ip).eq.0) go to 50
      do 70 i=1,3
      do 70 j=1,3
      if(i.eq.j) go to 50
      haa(i,j)=cplx(0.0,0.0)
      go to 70
50      z=cplx(0.0,-s(i)/st(ip)*twopi)
      haa(i,i)=cexp(z)
70      continue
      call umus(u,haa,3,r)
      do 80 i=1,3
      do 80 j=1,3
      rpp(i,j)=cplx(0.0,0.0)
80      continue
      z=cplx(0.0,ph(ip))
      rpp(1,1)=cexp(-z)
      rpp(2,2)=cplx(1.0,0.0)
      rpp(3,3)=cexp(z)
      call umus(rpp,haa,3,r)
      go to 90
60      do 120 i=1,3
      do 120 j=1,3
      haa(i,j)=cplx(0.0,0.0)
120      continue
      z=cplx(0.0,wst(ip)*twopi/3.0)
      haa(1,1)=cexp(-z)
      haa(2,2)=cexp(2.0*z)
      haa(3,3)=haa(1,1)
90      call umus(haa,rho,3,r)
      if(acoh.eq.0) go to 110
      if(ip.ne.ncosu) go to 110
      do 220 i=1,3
      do 220 j=1,3
      if(i.eq.j) go to 220
      rho(i,j)=cplx(0.0,0.0)
220      continue
110      continue
      do 160 i=1,3
      do 160 j=1,3
      haa(i,j)=cplx(0.0,0.0)
160      continue
      z=cplx(0.0,wst(fid)*twopi/3.0)
      haa(1,1)=cexp(-z)
      haa(2,2)=cexp(2.0*z)
      haa(3,3)=haa(1,1)
      if(nre.eq.1) call ppsen(iwa,nwa,rput)
      do 130 ifid=1,nfid
      if(ifid.eq.1) go to 150
      call umus(haa,rho,3,r)
150      avex=0.0
      avev=0.0
      do 140 i=1,3
      do 140 j=1,3
      avex=avex+x(i,j)*rho(j,i)
      avev=avev+v(i,j)*rho(j,i)
140      continue
      sr(ifid)=sr(ifid)+avex*rput/2.0
      si(ifid)=si(ifid)+avev*rput/2.0
130      continue
      type s,'spin 0 ',iwa
100      continue
      do 170 i=1,nfid
      sr(i)=sr(i)/nwa
      si(i)=si(i)/nwa
      print s,i,sr(i),si(i)
170      continue
      stop
      end

```

```

      subroutine unus(u,b,n,v)
c
c   performs unitary transformation
c   b=usbsuadjoint
c
c   complex u(n,n),b(n,n),v(n)
c   call matrai(u,b,n,v)
c   call matrai(b,u,n,v)
c   return
c   end
c
c
c   subroutine matrai(a,b,n,r)
c   complex a(n,n),b(n,n),rv(n),s
c   do 14 i=1,n
c   do 12 j=1,n
c   s=0.0
c   do 11 k=1,n
c   s=s+a(i,k)*conjg(b(j,k))
11  s=rv(j)+s
12  rv(j)=s
c   do 13 j=1,n
c   a(i,j)=rv(j)
13  continue
14  return
c   end
c
c
c   subroutine matrai(a,b,n,cv)
c   complex a(n,n),b(n,n),cv(n),s
c   do 14 j=1,n
c   do 12 i=1,n
c   s=0.0
c   do 11 k=1,n
c   s=s+a(i,k)*b(k,j)
11  s=s+b(k,j)*cv(k)
12  cv(j)=s
c   do 13 i=1,n
c   b(i,j)=cv(i)
13  continue
14  return
c   end
c
c
c   subroutine ppsen(iw,nw,pput)
c   pput=sqrt(2.0*(nw-1))
c   if(iw.ne.1) pput=sqrt(1.0*(nw-1)/(iw-1))
c   return
c   end

```

## FFT.FOR

```

character*15 fname
dimension ar(1024),ai(1024)
dimension iuk(12)
complex a(1024)
type *, 'enter power of 2 for fid length'
accept *,a
type *, 'output real(1) or imag(2) spectrum?'
accept *,is
type *, 'enter name of fid file'
accept 20,n,fname(1:n)
format(a,a)
open(unit=2,name=fname(1:n),status='old',readonly)
nfid=256
type *, 'clear one buffer of fid ?'
accept *,icb
icb=0
if(icb.ne.0) type *, 'which one (1 or 2) ?'
if(icb.ne.0) accept *,ibc
read(2,*) nn,nfid
do 30 i=1,nfid
read(2,*) nn,ar(i),ai(i)
if(ibc.eq.1) ar(i)=0.0
if(ibc.eq.2) ai(i)=0.0
a(i)=cmplx(ar(i),ai(i))
30 continue
type *, 'enter damping (taus per 128 pts)'
accept *,damp
damp=damp/128
do 25 i=1,nfid
a(i)=a(i)*exp(-damp*i)
25 continue
call fft2c(a,a,iuk)
if(is.ne.1) go to 50
do 40 i=1,nfid/2
k=i+nfid/2
print *,i,real(a(k))
40 continue
do 42 i=1,nfid/2
k=i+nfid/2
print *,k,real(a(i))
42 continue
go to 70
50 do 60 i=1,nfid/2
k=i+nfid/2
print *,i,imag(a(k))
60 continue
do 62 i=1,nfid/2
k=i+nfid/2
print *,k,imag(a(i))
62 continue
70 width=1000.0/nfid
type *, 'spectral width(khz) = ',width
close(unit=2)
stop
end

```

The programs HOPE.FOR and RF2180.FOR were used to find first order composite  $\pi$  pulses that are broadband with respect to resonance offsets and rf amplitudes, respectively. Q180.FOR was used to find zeroth order composite  $\pi$  pulses that are broadband with respect to dipole and quadrupole couplings. HOPE.FOR, RF2180.FOR, and Q180.FOR are reproduced in Figures B.4 through B.6. They follow the procedures outlined in Chapter IV.C.3 and IV.C.4.

### 3. Generation of maps for iterative schemes

The program CARTMAP.FOR, along with subroutines ITER.FOR, EXTRACT.FOR, and REFINE.FOR was used to generate data for the maps of attractor basins in Chapter VII.C.2. The programs are given in Figure B.7. CARTMAP.FOR accepts information that specifies a scheme. That information is passed to ITER.FOR, along with the coordinates of an initial point in  $SO(3)$ . ITER.FOR sets up the corresponding  $3 \times 3$  rotation matrix and applies the scheme to generate a new  $3 \times 3$  matrix corresponding to the next iterate. The new point in  $SO(3)$  is calculated by EXTRACT.FOR and REFINE.FOR. ITER.FOR then checks for convergence to a fixed point, according to the discussion in Chapter VII.C.2.

Related calculations, leading to data of the type presented in Figures VII.12 and VII.15, were carried out with programs that were modified versions of those in Figure B.7.

Figure B.4: HOPE.FOR

```

      DIMENSION C(6,7)
      DIMENSION CT(1000),ST(1000),CF(7),SF(7),CP(7),SP(7),N(7)
      G(A1,A2,A3,A4)=A1*(1.-A3)+A2*A4
      ISA=0
      IKT=0
C
C      CREATE COSINE AND SINE TABLES
C      FOR ANGLES BETWEEN -360 AND +360 DEGREES
C      ANGLE I IS -361+I
C
      PI=4.*ATAN(1.)
      DO 10 I=1,721
      CT(I)=COS((-361+I)*PI/180)
      ST(I)=SIN((-361+I)*PI/180)
10    CONTINUE
C
C      GET RANGES OF PARAMETERS, CRITERIA
C
      TYPE 600
600    FORMAT (1X,'ENTER LOW VALUES FOR 3 PHASES')
      ACCEPT 8,M2L,M3L,M4L
      TYPE 601
601    FORMAT (1X,'ENTER HIGH VALUES FOR 3 PHASES')
      ACCEPT 8,M2H,M3H,M4H
      TYPE 602
602    FORMAT (1X,'ENTER LOW VALUES FOR 4 FLIPS')
      ACCEPT 8,N1L,N2L,N3L,N4L
      TYPE 603
603    FORMAT (1X,'ENTER HIGH VALUES FOR 4 FLIPS')
      ACCEPT 8,N1H,N2H,N3H,N4H
      TYPE 604
604    FORMAT (1X,'ENTER PHASE INCREMENT')
      ACCEPT 8,MINC
      TYPE 605
605    FORMAT (1X,'ENTER FLIP INCREMENT')
      ACCEPT 8,NINC
      TYPE 606
606    FORMAT (1X,'ENTER INVERSION, H(0), H(1) CRITERIA')
      ACCEPT 8,MIN,WHO,WHI
C
C      INITIALIZE PARAMETERS
C
      M2=M2L
      M3=M3L
      M4=M4L
      N(1)=N1L
      N(2)=N2L
      N(3)=N3L
      N(4)=N4L
      N(5)=N(3)
      N(6)=N(2)
      N(7)=N(1)

```

C  
C  
C     GET SINES AND COSINES FROM TABLES

20     CP(2)=CT(M2+361)  
       CP(3)=CT(M3-M2+361)  
       CP(4)=CT(M4-M3+361)  
       CP(5)=CP(4)  
       CP(6)=CP(3)  
       CP(7)=CP(2)  
       SP(2)=ST(M2+361)  
       SP(3)=ST(M3-M2+361)  
       SP(4)=ST(M4-M3+361)  
       SP(5)=-SP(4)  
       SP(6)=-SP(3)  
       SP(7)=-SP(2)  
       CF(1)=CT(N(1)+361)  
       CF(2)=CT(N(2)+361)  
       CF(3)=CT(N(3)+361)  
       CF(4)=CT(N(4)+361)  
       CF(5)=CF(3)  
       CF(6)=CF(2)  
       CF(7)=CF(1)  
       SF(1)=ST(N(1)+361)  
       SF(2)=ST(N(2)+361)  
       SF(3)=ST(N(3)+361)  
       SF(4)=ST(N(4)+361)  
       SF(5)=SF(3)  
       SF(6)=SF(2)  
       SF(7)=SF(1)

C  
C  
C     CHECK INVERSION EQUATION

1     X1=CF(1)\*CF(2)\*CF(3)-SF(1)\*CP(2)\*SF(2)\*CF(3)  
       -SF(1)\*CP(2)\*CF(2)\*CP(3)\*SF(3)-CF(1)\*SF(2)\*CP(3)\*SF(3)  
       +SF(1)\*SP(2)\*SP(3)\*SF(3)  
       X2=-SF(1)\*CP(2)\*CF(2)\*CF(3)-CF(1)\*SF(2)\*CP(3)\*CF(3)  
       +SF(1)\*SP(2)\*SP(3)\*CF(3)-CF(1)\*CF(2)\*SF(3)  
       +SF(1)\*CP(2)\*SF(2)\*SF(3)  
       X3=-SF(1)\*SP(2)\*CP(3)-SF(1)\*CP(2)\*CF(2)\*SP(3)  
       -CF(1)\*SF(2)\*SP(3)  
       X4=X1\*(CF(4)\*CF(3)-SF(4)\*CP(4)\*SF(3))+X2\*(CP(4)\*SF(4))  
       +CF(3)\*CP(4)\*CF(4)\*CP(4)\*SF(3)+SP(4)\*SP(4)\*SF(3)  
       +X3\*(-SP(4)\*SF(4)\*CF(3)-SP(4)\*CF(4)\*CP(4)\*SF(3)  
       +CP(4)\*SP(4)\*SF(3))  
       X5=X1\*(-SF(4)\*CP(4)\*CF(3)-CF(4)\*SF(3))+X2\*(CP(4)  
       \*CF(4)\*CP(4)\*CF(3)+SP(4)\*SP(4)\*CF(3)-CP(4)\*SF(4)\*SF(3))  
       +X3\*(-SP(4)\*CF(4)\*CP(4)\*CF(3)+CP(4)\*SP(4)\*CF(3)  
       +SP(4)\*SP(4)\*SF(3))  
       X6=X1\*SF(4)\*SP(4)+X2\*(SP(4)\*CP(4)-CP(4)\*CF(4)\*SP(4))  
       +X3\*(CP(4)\*CP(4)+SP(4)\*CF(4)\*SP(4))  
       X=X4\*(CF(2)\*CF(1)-SF(2)\*CP(2)\*SF(1))+X5\*(CP(3)\*SF(2)  
       \*CF(1)+CP(3)\*CF(2)\*CP(2)\*SF(1)-SP(3)\*SP(2)\*SF(1))  
       +X6\*(SP(3)\*SF(2)\*CF(1)+SP(3)\*CF(2)\*CP(2)\*SF(1)  
       +CP(3)\*SP(2)\*SF(1))  
       IF (X.GT.WIN) GO TO 500

C  
C  
C     GET C(I,J) MATRIX

      C(1,1)=0.  
       C(2,1)=1.  
       C(3,1)=1.  
       C(4,1)=0.  
       C(5,1)=0.  
       C(6,1)=0.  
       DO 100 K=2,7  
       C(1,K)=0.  
       C(2,K)=1.  
       C(3,K)=1.  
       C(4,K)=0.  
       C(5,K)=0.  
       C(6,K)=0.

```

DO 30 LL=2,K
L=K+2-LL
J=L-1
D1=C(1,K)*CF(J)-C(3,K)*CP(L)*SF(J)-C(5,K)*SP(L)*SF(J)
D2=C(2,K)*CF(J)-C(4,K)*CP(L)*SF(J)-C(6,K)*SP(L)*SF(J)
D3=C(3,K)*CP(L)*CF(J)+C(5,K)*SP(L)*CF(J)+C(1,K)*SF(J)
D4=C(4,K)*CP(L)*CF(J)+C(6,K)*SP(L)*CF(J)+C(2,K)*SF(J)
D5=C(5,K)*CP(L)-C(3,K)*SP(L)
D6=C(6,K)*CP(L)-C(4,K)*SP(L)
C(1,K)=D1
C(2,K)=D2
C(3,K)=D3
C(4,K)=D4
C(5,K)=D5
C(6,K)=D6
30 CONTINUE
100 CONTINUE
C
CHECK H(0)
C
WX=G(C(5,1),C(6,1),CF(1),SF(1))+G(C(5,2),C(6,2),
1 CF(2),SF(2))+G(C(5,3),C(6,3),CF(3),SF(3))
1 +G(C(5,4),C(6,4),CF(4),SF(4))+G(C(5,5),C(6,5),CF(5),
1 SF(5))+G(C(5,6),C(6,6),CF(6),SF(6))+G(C(5,7),C(6,7),
1 CF(7),SF(7))
WX=WX*WX
IF (WX.GT.WH0) GO TO 500
WY=G(C(3,1),C(4,1),CF(1),SF(1))+G(C(3,2),C(4,2),
1 CF(2),SF(2))+G(C(3,3),C(4,3),CF(3),SF(3))
1 +G(C(3,4),C(4,4),CF(4),SF(4))+G(C(3,5),C(4,5),CF(5),
1 SF(5))+G(C(3,6),C(4,6),CF(6),SF(6))+G(C(3,7),C(4,7),
1 CF(7),SF(7))
WY=WY*WY
IF (WY.GT.WH0) GO TO 500

C
C CHECK H(1)
C
PFI=PI/180
VZ=0.
DO 110 I=1,7
VZ=VZ+(SF(I)-N(I)*PFI)*C(3,I)*C(6,I)-C(4,I)*C(5,I)
110 CONTINUE
DO 130 I=2,7
DO 120 J=1,I
VZ=VZ+G(C(5,I),C(6,I),CF(I),SF(I))*G(C(3,J),C(4,J),
1 CF(J),SF(J))-G(C(3,I),C(4,I),CF(I),SF(I))*G(C(5,J),
1 C(6,J),CF(J),SF(J))
120 CONTINUE
130 CONTINUE
VZ=VZ*VZ
IF (VZ.GT.WH1) GO TO 500
VX=0.
DO 140 I=1,7
VX=VX+(SF(I)-N(I)*PFI)*C(1,I)*C(4,I)-C(3,I)*C(2,I)
140 CONTINUE
DO 160 I=2,7
DO 150 J=1,I
VX=VX+G(C(3,I),C(4,I),CF(I),SF(I))*G(C(1,J),C(2,J),
1 CF(J),SF(J))-G(C(3,I),C(4,I),CF(I),SF(I))*G(C(1,J),
1 C(2,J),CF(J),SF(J))
150 CONTINUE
160 CONTINUE
VX=VX*VX
IF (VX.GT.WH1) GO TO 500
VY=0.
DO 170 I=1,7
VY=VY+(SF(I)-N(I)*PFI)*C(2,I)*C(5,I)-C(1,I)*C(6,I)
170 CONTINUE
DO 190 I=2,7
DO 180 J=1,I
VY=VY+G(C(1,I),C(2,I),CF(I),SF(I))*G(C(5,J),C(6,J),
1 CF(J),SF(J))-G(C(5,I),C(6,I),CF(I),SF(I))*G(C(1,J),
1 C(2,J),CF(J),SF(J))
180 CONTINUE
190 CONTINUE

```



```

      VY=VY8UY
      IF (VY.GT.WH1) GO TO 500
      ISA=ISA+1
      PRINT 620,M2,M3,M4,N(1),N(2),N(3),N(4),ISA
620   FORMAT (1X,8I5)
      PRINT 621,X,WX,WY,UX,VY,VZ
621   FORMAT (1X,6F10.5)
500   M2=M2+MINC
      IF (M2.LE.M2H) GO TO 20
      M2=M2L
      M3=M3+MINC
      IF (M3.LE.M3H) GO TO 20
      M3=M3L
      M4=M4+MINC
      IF (M4.LE.M4H) GO TO 20
      M4=M4L
      N(1)=N(1)+MINC
      N(7)=N(1)
      IF (N(1).LE.N1H) GO TO 20
      N(1)=N1L
      N(7)=N(1)
      N(2)=N(2)+MINC
      N(6)=N(2)
      IF (N(2).LE.N2H) GO TO 20
      N(2)=N2L
      N(6)=N(2)
      N(3)=N(3)+MINC
      N(5)=N(3)
      IF (N(3).LE.N3H) GO TO 20
      N(3)=N3L
      N(5)=N(3)
      IKT=IKT+1
      TYPE 777,IKT
777   FORMAT(1X,'INCREMENTATION 0',I4)
      N(4)=N(4)+MINC
      IF (N(4).LE.N4H) GO TO 20
      STOP
      END

```

Figure B.5: RF2180.FOR

```

C ----- PROGRAM SEARCHES FOR 4 PULSE INVERTING SEQUENCE
C
C WITH H(0)=0 AND H(1)=0 FOR RF INHOMOGENEITY
C
C DIMENSION CT(2000),ST(2000),CF(4),SF(4),CP(4)
C DIMENSION SP(4),N(4),U(3,4)
C
C ISA=0
C IKT=0
C
C CREATE COSINE AND SINE TABLES
C FOR ANGLES BETWEEN -360 AND +720 DEGREES
C ANGLE I IS -361+I
C
C PI=4.*ATAN(1.)
C DO 10 I=1,1081
C CT(I)=COS((-361+I)*PI/180)
C ST(I)=SIN((-361+I)*PI/180)
10 CONTINUE
C
C GET RANGES OF PARAMETERS, CRITERIA
C
C TYPE 600
600 FORMAT (1X,'ENTER LOW VALUES FOR 3 PHASES')
C ACCEPT *,M2L,M3L,M4L
C TYPE 601
601 FORMAT (1X,'ENTER HIGH VALUES FOR 3 PHASES')
C ACCEPT *,M2H,M3H,M4H
C TYPE 602
602 FORMAT (1X,'ENTER LOW VALUES FOR 4 FLIPS')
C ACCEPT *,N1L,N2L,N3L,N4L
C TYPE 603
603 FORMAT (1X,'ENTER HIGH VALUES FOR 4 FLIPS')
C ACCEPT *,N1H,N2H,N3H,N4H
C TYPE 604
604 FORMAT (1X,'ENTER PHASE INCREMENT')
C ACCEPT *,MINC
C TYPE 605
605 FORMAT (1X,'ENTER FLIP INCREMENT')
C ACCEPT *,NINC
C TYPE 606
606 FORMAT (1X,'ENTER INVERSION, H(0), H(1) CRITERIA')
C ACCEPT *,WIN,UH0,UH1
C
C INITIALIZE PARAMETERS
C
C M2=M2L
C M3=M3L
C M4=M4L
C N(1)=N1L
C N(2)=N2L
C N(3)=N3L
C N(4)=N4L
C
C GET SINES AND COSINES FROM TABLES
C
20 CP(2)=CT(M2+361)
C CP(3)=CT(M3-M2+361)
C CP(4)=CT(M4-M3+361)
C SP(2)=ST(M2+361)
C SP(3)=ST(M3-M2+361)
C SP(4)=ST(M4-M3+361)
C CF(1)=CT(N(1)+361)
C CF(2)=CT(N(2)+361)
C CF(3)=CT(N(3)+361)
C CF(4)=CT(N(4)+361)
C SF(1)=ST(N(1)+361)
C SF(2)=ST(N(2)+361)
C SF(3)=ST(N(3)+361)
C SF(4)=ST(N(4)+361)

```

```

C
C      CHECK INVERSION EQUATION
C
      X1=CP(1)*CP(2)*CF(3)-SF(1)*CP(2)*SF(2)*CF(3)
1  -SF(1)*CP(2)*CF(2)*CP(3)*SF(3)-CF(1)*SF(2)*CP(3)*SF(3)
1  +SF(1)*SP(2)*SP(3)*SF(3)
      X2=-SF(1)*CP(2)*CF(2)*CP(3)*CF(3)-CF(1)*SF(2)*CP(3)*CF(3)
1  +SF(1)*SP(2)*SP(3)*CF(3)-CF(1)*CF(2)*SF(3)
1  +SF(1)*CP(2)*SF(2)*SF(3)
      X3=-SF(1)*SP(2)*CP(3)-SF(1)*CP(2)*CF(2)*SP(3)
1  -CF(1)*SF(2)*SP(3)
      X=X1*CF(4)+X2*CP(4)*SF(4)-X3*SP(4)*SF(4)
      IF (X.GT.MIN) GO TO 500

C
      CP(1)=1.0
      SP(1)=0.0
      CONV=PI/180.0
      CONV2=CONV*CONV

C
C      CREATE TOGGING FRAME RF VECTOR
C
      V(1,1)=1.0
      V(2,1)=0.0
      V(3,1)=0.0
      DO 50 I=2,4
      V(1,I)=1.0
      V(2,I)=0.0
      V(3,I)=0.0
      DO 40 J=2,I
      K=I-J+1
      L=K+1
      VX=V(1,I)*CP(L)-V(2,I)*SP(L)
      VY=V(1,I)*SP(L)*CF(K)+V(2,I)*CP(L)*CF(K)+V(3,I)*SF(K)
      VZ=-V(1,I)*SP(L)*SF(K)-V(2,I)*CP(L)*SF(K)+V(3,I)*CF(K)
      V(1,I)=VX
      V(2,I)=VY
      V(3,I)=VZ
40  CONTINUE
50  CONTINUE

C
C      CHECK H(0)
C
      AX=0.0
      AY=0.0
      AZ=0.0
      DO 60 I=1,4
      AX=AX+V(1,I)*N(I)
      AY=AY+V(2,I)*N(I)
      AZ=AZ+V(3,I)*N(I)
60  CONTINUE
      AX=AX*CONV
      AY=AY*CONV
      AZ=AZ*CONV
      A=AX*AX+AY*AY+AZ*AZ
      IF (A.GT.WHO) GO TO 500

```

```

C
C
C      CHECK N(1)
-----
      BX=0.0
      BY=0.0
      BZ=0.0
      DO 80 I=2,4
      DO 70 J=1,I
      BX=BX+(V(2,I)*V(3,J)-V(3,I)*V(2,J))*N(1)*N(J)
      BY=BY+(V(3,I)*V(1,J)-V(1,I)*V(3,J))*N(1)*N(J)
      BZ=BZ+(V(1,I)*V(2,J)-V(2,I)*V(1,J))*N(1)*N(J)
70      CONTINUE
80      CONTINUE
      BX=BX*CONV2
      BY=BY*CONV2
      BZ=BZ*CONV2
      R=BX*BX+BY*BY+BZ*BZ
      IF (B.GT.WH1) GO TO 500
      ISA=ISA+1
      PRINT 620,M2,M3,M4,N(1),N(2),N(3),N(4),ISA
820     FORMAT(1X,8I5)
      PRINT 621,X,AX,AY,AZ,BX,BY,BZ
621     FORMAT(1X,6F10.5)
500     M2=M2+MINC
      IF (M2.LE.M2H) GO TO 20
      M2=M2L
      M3=M3+MINC
      IF (M3.LE.M3H) GO TO 20
      M3=M3L
      M4=M4+MINC
      IF (M4.LE.M4H) GO TO 20
      M4=M4L
      N(1)=N(1)+NINC
      IF (N(1).LE.N1H) GO TO 20
      N(1)=N1L
      N(2)=N(2)+NINC
      IF (N(2).LE.N2H) GO TO 20
      N(2)=N2L
      N(3)=N(3)+NINC
      IF (N(3).LE.N3H) GO TO 20
      N(3)=N3L
      IKT=IKT+1
      TYPE 777,IKT
777     FORMAT(1X,'INCREMENTATION 0',I4)
      N(4)=N(4)+NINC
      IF (N(4).LE.N4H) GO TO 20
      STOP
      END

```

Figure B.6: Q180.FOR

```

      DIMENSION CT(1000),ST(1000),CF(7),SF(7),CP(7),SP(7),N(7)
      DIMENSION T(S,7,2),R(S,5,6),S(S,2)
      R6DB=SQRT(6.0)/8.0
      CONV=4.0*ATAN(1.0)/180.0
      DO 10 I=1,721
-----
        A=(-361+I)*CONV
        CT(I)=COS(A)
        ST(I)=SIN(A)
10      CONTINUE
        ISA=0
        IKT=0
-----
        TYPE 600
        600      FORMAT(1X,'ENTER LOW VALUES FOR 3 PHASES')
               ACCEPT 8,M2L,M3L,M4L
        TYPE 601
        601      FORMAT(1X,'ENTER HIGH VALUES FOR 3 PHASES')
               ACCEPT 8,M2H,M3H,M4H
-----
        TYPE 602
        602      FORMAT(1X,'ENTER LOW VALUES FOR 4 FLIPS')
               ACCEPT 8,N1L,N2L,N3L,N4L
        TYPE 603
        603      FORMAT(1X,'ENTER HIGH VALUES FOR 4 FLIPS')
               ACCEPT 8,N1H,N2H,N3H,N4H
-----
        TYPE 604
        604      FORMAT(1X,'ENTER PHASE INCREMENT')
               ACCEPT 8,MINC
        TYPE 605
        605      FORMAT(1X,'ENTER FLIP INCREMENT')
               ACCEPT 8,NINC
-----
        TYPE 606
        606      FORMAT(1X,'ENTER INVERSION, H(0) CRITERIA')
               ACCEPT 8,WIN,UH0
               M2=M2L
               M3=M3L
               M4=M4L
               N(1)=N1L
               N(2)=N2L
               N(3)=N3L
               N(4)=N4L
               N(5)=N(3)
               N(6)=N(2)
               N(7)=N(1)
20      M2P=M2+361
               M3P=M3-M2+361
               M4P=M4-M3+361
               N1P=N(1)+361
               M2P=N(2)+361
-----
               M3P=N(3)+361
               M4P=N(4)+361
               CP(2)=CT(M2P)
               CP(3)=CT(M3P)
               CP(4)=CT(M4P)
               CP(5)=CP(4)
-----
               CP(6)=CP(3)
               CP(7)=CP(2)
               SP(2)=ST(M2P)
               SP(3)=ST(M3P)
               SP(4)=ST(M4P)
               SP(5)=-SP(4)
-----
               SP(6)=-SP(3)
               SP(7)=-SP(2)

```

```

CF(1)=CT(N1P)
CF(2)=CT(N2P)
CF(3)=CT(N3P)
CF(4)=CT(N4P)
CF(5)=CF(3)
CF(6)=CF(2)
CF(7)=CF(1)
SF(1)=ST(N1P)
SF(2)=ST(N2P)
SF(3)=ST(N3P)
SF(4)=ST(N4P)
SF(5)=SF(3)
SF(6)=SF(2)
SF(7)=SF(1)

X1=CF(1)*CF(2)*CF(3)-SF(1)*CF(2)*SF(2)*CF(3)
1 -SF(1)*CF(2)*CF(2)*CF(3)*SF(3)-CF(1)*SF(2)*CF(3)*SF(3)
1 +SF(1)*SF(2)*SF(3)*SF(3)
X2=-SF(1)*CF(2)*CF(2)*CF(3)*CF(3)-CF(1)*SF(2)*CF(3)*CF(3)
1 +SF(1)*SF(2)*SF(3)*CF(3)-CF(1)*CF(2)*SF(3)
1 +SF(1)*CF(2)*SF(2)*SF(3)
X3=-SF(1)*SF(2)*CF(3)-SF(1)*CF(2)*CF(2)*SF(3)
1 -CF(1)*SF(2)*SF(3)
X4=X1*(CF(4)*CF(3)-SF(4)*CF(4)*SF(3))+X2*(CF(4)*SF(4)
1 *CF(3)+CF(4)*CF(4)*CF(3)+SF(4)*SF(4)*SF(3))
1 +X3*(-SF(4)*SF(4)*CF(3)-SF(4)*CF(4)*CF(4)*SF(3)
1 +CF(4)*SF(4)*SF(3))
X5=X1*(-SF(4)*CF(4)*CF(3)-CF(4)*SF(3))+X2*(CF(4)
1 *CF(4)*CF(4)*CF(3)+SF(4)*SF(4)*CF(3)-CF(4)*SF(4)*SF(3))
1 +X3*(-SF(4)*CF(4)*CF(4)*CF(3)+CF(4)*SF(4)*SF(4)*CF(3)
1 +SF(4)*SF(4)*SF(3))
X6=X1*(SF(4)*SF(4)+X2*(SF(4)*CF(4)-CF(4)*CF(4)*SF(4))
1 +X3*(CF(4)*CF(4)+SF(4)*CF(4)*SF(4))
X=X4*(CF(2)*CF(1)-SF(2)*CF(2)*SF(1))+X5*(CF(3)*SF(2)
1 *CF(1)+CF(3)*CF(2)*CF(2)*SF(1)-SF(3)*SF(2)*SF(1))
1 +X6*(SF(3)*SF(2)*CF(1)+SF(3)*CF(2)*CF(2)*SF(1)
1 +CF(3)*SF(2)*SF(1))
IF (X.GT.WIN) GO TO 500
DO 40 I=1,7
T(1,I,1)=-R6DB*(N(I)*CONV-SF(I)*CF(I))
T(1,I,2)=0.0
T(2,I,1)=0.0
T(2,I,2)=2.0*R6DB*SF(I)*SF(I)
T(3,I,1)=(N(I)*CONV+3.0*SF(I)*CF(I))*0.25
T(3,I,2)=0.0
T(4,I,1)=0.0
T(4,I,2)=T(2,I,2)
T(5,I,1)=T(1,I,1)
T(5,I,2)=0.0
40 CONTINUE
DO 50 I=1,6
CPL1=CF(I)+1.0
CH1=CF(I)-1.0
R(1,1,I)=CPL1*CPL1*0.25
R(1,2,I)=SF(I)*CPL1*0.5
R(1,3,I)=-R6DB*2.0*SF(I)*SF(I)
R(1,4,I)=SF(I)*CH1*0.5
R(1,5,I)=CH1*CH1*0.25
R(2,2,I)=CPL1*(2.0*CF(I)-1.0)*0.5
R(2,3,I)=R6DB*4.0*SF(I)*CF(I)
R(2,4,I)=CH1*(2.0*CF(I)+1.0)*0.5
R(2,5,I)=R(1,4,I)
R(3,3,I)=(3.0*CF(I)*CF(I)-1.0)*0.5
R(3,4,I)=R(2,3,I)
R(3,5,I)=R(1,3,I)
R(4,4,I)=R(2,2,I)
R(4,5,I)=R(1,2,I)
R(5,5,I)=R(1,1,I)
R(2,1,I)=R(1,2,I)
R(3,2,I)=R(2,3,I)
R(3,1,I)=R(1,3,I)
R(4,3,I)=R(3,4,I)
R(4,2,I)=R(2,4,I)
R(4,1,I)=R(1,4,I)
R(5,4,I)=R(4,5,I)
R(5,3,I)=R(3,5,I)
R(5,2,I)=R(2,5,I)
R(5,1,I)=R(1,5,I)
50 CONTINUE

```

```

DO 70 I=2,7
DO 60 J=2,I
K=I-J+2
L=K-1
BE=CP(K)*CP(K)-SP(K)*SP(K)
BF=2.0*CP(K)*SP(K)
HR=T(1,I,1)*BE+T(1,I,2)*BF
HI=T(1,I,2)*BE-T(1,I,1)*BF
T(1,I,1)=HR
T(1,I,2)=HI
HR=T(2,I,1)*CP(K)+T(2,I,2)*SP(K)
HI=T(2,I,2)*CP(K)-T(2,I,1)*SP(K)
T(2,I,1)=HR
T(2,I,2)=HI
HR=T(4,I,1)*CP(K)-T(4,I,2)*SP(K)
HI=T(4,I,2)*CP(K)+T(4,I,1)*SP(K)
T(4,I,1)=HR
T(4,I,2)=HI
HR=T(5,I,1)*BE-T(5,I,2)*BF
HI=T(5,I,2)*BE+T(5,I,1)*BF
T(5,I,1)=HR
T(5,I,2)=HI

DO 55 II=1,5,2
S(II,1)=R(II,1,L)*ST(1,I,1)-R(II,2,L)*ST(2,I,2)
1 +R(II,3,L)*ST(3,I,1)-R(II,4,L)*ST(4,I,2)
1 +R(II,5,L)*ST(5,I,1)
S(II,2)=R(II,1,L)*ST(1,I,2)+R(II,2,L)*ST(2,I,1)
1 +R(II,3,L)*ST(3,I,2)+R(II,4,L)*ST(4,I,1)
1 +R(II,5,L)*ST(5,I,2)
55 CONTINUE
DO 56 II=2,4,2
S(II,1)=-R(II,1,L)*ST(1,I,2)+R(II,2,L)*ST(2,I,1)
1 -R(II,3,L)*ST(3,I,2)+R(II,4,L)*ST(4,I,1)
1 -R(II,5,L)*ST(5,I,2)
S(II,2)=R(II,1,L)*ST(1,I,1)+R(II,2,L)*ST(2,I,2)
1 +R(II,3,L)*ST(3,I,1)+R(II,4,L)*ST(4,I,2)
1 +R(II,5,L)*ST(5,I,1)
56 CONTINUE
T(1,I,1)=S(1,1)
T(1,I,2)=S(1,2)
T(2,I,1)=S(2,1)
T(2,I,2)=S(2,2)
T(3,I,1)=S(3,1)
T(3,I,2)=S(3,2)
T(4,I,1)=S(4,1)
T(4,I,2)=S(4,2)
T(5,I,1)=S(5,1)
T(5,I,2)=S(5,2)
60 CONTINUE
70 CONTINUE
DO 80 I=2,7
T(1,I,1)=T(1,I,1)+T(1,I,1)
T(1,I,2)=T(1,I,2)+T(1,I,2)
T(2,I,1)=T(2,I,1)+T(2,I,1)
T(2,I,2)=T(2,I,2)+T(2,I,2)
T(3,I,1)=T(3,I,1)+T(3,I,1)
T(3,I,2)=T(3,I,2)+T(3,I,2)
T(4,I,1)=T(4,I,1)+T(4,I,1)
T(4,I,2)=T(4,I,2)+T(4,I,2)
T(5,I,1)=T(5,I,1)+T(5,I,1)
T(5,I,2)=T(5,I,2)+T(5,I,2)
80 CONTINUE
XX=T(1,1,1)*T(1,1,1)+T(1,1,2)*T(1,1,2)
1 +T(2,1,1)*T(2,1,1)+T(2,1,2)*T(2,1,2)
1 +T(3,1,1)*T(3,1,1)+T(3,1,2)*T(3,1,2)
1 +T(4,1,1)*T(4,1,1)+T(4,1,2)*T(4,1,2)
1 +T(5,1,1)*T(5,1,1)+T(5,1,2)*T(5,1,2)
IF(XX.GT.WHO) GO TO 500
ISA=ISA+1
PRINT 620,M2,M3,M4,N(1),N(2),N(3),N(4)
620 FORMAT(1X,7I3)
PRINT 621,X,XX,ISA
621 FORMAT(1X,2F10.5,I10)

```

```

500  M2=M2+MINC
      IF (M2.LE.M2H) GO TO 20
      M2=M2L
-----
      M3=M3+MINC
      IF (M3.LE.M3H) GO TO 20
      M3=M3L
      M4=M4+MINC
      IF (M4.LE.M4H) GO TO 20
      M4=M4L
-----
      N(1)=N(1)+MINC
      N(7)=N(1)
      IF (N(1).LE.N1H) GO TO 20
      N(1)=N1L
      N(7)=N(1)
      N(2)=N(2)+MINC
-----
      N(8)=N(2)
      IF (N(2).LE.N2H) GO TO 20
      N(2)=N2L
      N(6)=N(2)
      N(3)=N(3)+MINC
      N(5)=N(3)
      CALL TIME(THME)
      TYPE 776,THME
776  FORMAT(1X,A15)
      IF (N(3).LE.N3H) GO TO 20
      N(3)=N3L
      N(5)=N(3)
-----
      IKT=IKT+1
      TYPE 777,IKT
777  FORMAT(1X,'INCREMENTATION #',I4)
      N(4)=N(4)+MINC
      IF (N(4).LE.N4H) GO TO 20
      STOP
-----
      END

```



Figure B.7: CARTMAP.FOR

```

C      PROGRAM MAPS OUT FIXED POINT OF
C      PHASE-SHIFT ITERATION IN CARTESIAN
C      COORDS
C
      DOUBLE PRECISION AM,AT,AP,P(20),X,Z,CINC
      DOUBLE PRECISION CONV,C,XX,RAD
      DATA CONV,C/3.1415926535897932384626434,180.0/
      DATA X,Z/0.07,180.0/

      TYPE *, 'ENTER ITERATION LENGTH, MAX # OF ITERATIONS'
      ACCEPT *, NS, NI
      TYPE *, 'ENTER PHASE SHIFTS (FIRST SHOULD BE ZERO)'
      ACCEPT *, (P(I), I=1, NS)
      TYPE *, 'ENTER RESOLUTION OF GRID'
      ACCEPT *, CINC
      DO 10 I=1, NS
        P(I)=P(I)*CONV/C
      CONTINUE
10      IF (X*X.LT.0.0001) GO TO 100
20      RAD=XXX+Z*Z
      IF (RAD.GT.32400.0) GO TO 100
      AM=DSQRT(RAD)
      XX=DABS(X)
      AT=CONV/2.0-DATAN(Z/XX)
      AT=AT*C/CONV
      AP=0.0
      CALL ITER(AM,AT,AP,P,NS,NI,N)
      IF (N.EQ.-1) N=NI+1
100     PRINT *, X, Z, N
      X=X+CINC
      IF (X.LE.180.0) GO TO 20
      X=0.0
      Z=Z+CINC
      IF (Z.LE.180.0) GO TO 20
      STOP
      END

      SUBROUTINE ITER(AM,AT,AP,P,NS,NI,N)
C      PROGRAM APPLIES SPECIFIED PHASE-SHIFT
C      ITERATION TO GIVEN INITIAL ROTATION,
C      GIVES RESULTING ROTATION_
C
      DOUBLE PRECISION R(3,3),A(3),T(3,3,20),UT(3,3),P(20)
      DOUBLE PRECISION CONV,AM,AT,AP,CAH,SAH,CAT,SAT,U
      DOUBLE PRECISION CAP,SAP,C,S,C2,S2,SC,AMH,ATT,APP
      CONV=3.1415926535897932384626434/180.0

C      CONSTRUCT INITIAL ROTATION MATRIX
C
      NNI=0
      AM=AM*CONV
      AT=AT*CONV
      AP=AP*CONV
20      AMH=AM
      ATT=AT
      APP=AP
      CAH=DCOS(AM)
      SAH=DSIN(AM)
      CAT=DCOS(AT)
      SAT=DSIN(AT)
      CAP=DCOS(AP)
      SAP=DSIN(AP)

```

```

R(1,1)=SAT$SAT$CAP$CAP+SAP$SAP$CAN+CAT$CAT$CAP$CAP$CAN
R(2,2)=SAT$SAT$SAP$SAP+CAP$CAP$CAN+CAT$CAT$SAP$SAP$CAN
R(3,3)=CAT$CAT$SAT$SAT$CAN
R(1,2)=-CAT$SAP$SAP+SAT$SAT$CAP$CAP*(1.0-CAN)
R(2,1)=R(1,2)+2.0$CAT$SAP
R(1,3)=SAT$SAP$SAP+CAT$SAT$CAP*(1.0-CAN)
R(3,1)=R(1,3)-2.0$SAT$SAP$SAP
R(2,3)=-SAT$CAP$SAP+CAT$SAT$SAP*(1.0-CAN)
R(3,2)=R(2,3)+2.0$SAT$CAP$SAP
30 DO 100 J=2,NS
C=DCOS(P(J))
S=DSIN(P(J))
C2=C*C
S2=S*S
SC=S*C
T(1,1,J)=R(1,1)*C2-R(1,2)*SC-R(2,1)*SC+R(2,2)*S2
T(2,1,J)=R(1,1)*SC-R(1,2)*S2+R(2,1)*C2-R(2,2)*SC
T(3,1,J)=R(3,1)*C-R(3,2)*S
T(1,2,J)=R(1,1)*SC+R(1,2)*C2-R(2,1)*S2-R(2,2)*SC
T(2,2,J)=R(1,1)*S2+R(1,2)*SC+R(2,1)*SC+R(2,2)*C2
T(3,2,J)=R(3,1)*S+R(3,2)*C
T(1,3,J)=R(1,3)*C-R(2,3)*S
T(2,3,J)=R(1,3)*S+R(2,3)*C
T(3,3,J)=R(3,3)
100 CONTINUE
DO 150 J=2,NS
DO 130 K=1,3
DO 120 L=1,3
U(K,L)=T(K,1,J)*R(1,L)+T(K,2,J)*R(2,L)+T(K,3,J)*R(3,L)
120 CONTINUE
130 CONTINUE
DO 140 K=1,3
DO 135 L=1,3
R(K,L)=U(K,L)
135 CONTINUE
140 CONTINUE
150 CONTINUE
W=R(1,1)*R(1,1)+R(1,2)*R(1,2)+R(1,3)*R(1,3)
1 +R(2,1)*R(2,1)+R(2,2)*R(2,2)+R(2,3)*R(2,3)
1 +R(3,1)*R(3,1)+R(3,2)*R(3,2)+R(3,3)*R(3,3)
W=DSQRT(3.0/W)
R(1,1)=W*R(1,1)
R(1,2)=W*R(1,2)
R(1,3)=W*R(1,3)
R(2,1)=W*R(2,1)
R(2,2)=W*R(2,2)
R(2,3)=W*R(2,3)
R(3,1)=W*R(3,1)
R(3,2)=W*R(3,2)
R(3,3)=W*R(3,3)
CALL EXTRACT(R,A)
NNI=NNI+1
AM=A(1)
AT=A(2)
AP=A(3)
IF(AM.LT.0.001) GO TO 50
DIFF=AM$AH+AMH$AHM-2.0$AH$AHM$DCOS(AT-ATT)
AMH=AM
ATT=AT
APP=AP
IF((DIFF.GT.0.01).AND.(NNI.LT.NI)) GO TO 30
IF(NNI.EQ.NI) NNI=-1
50 WH=WH/CONV
AT=AT/CONV
AP=AP/CONV
RETURN
END

```

```

C SUBROUTINE FINDS ROTATION VECTOR A(3)
C FROM ROTATION MATRIX R(3,3)
C
SUBROUTINE EXTRACT(R,A)
DOUBLE PRECISION R(3,3),A(3)
PI=3.1415926535897932384626434
T=(R(1,1)-R(2,2))/R(3,3)-1.0/2.0
IF(T.GT.1.0) T=1.0
IF(T.LT.-1.0) T=-1.0
AL=ACOS(T)
IF(AL.GT.0.01) GO TO 10
T=0.0
P=0.0
GO TO 500
10 IF((PI-AL).LT.0.01) GO TO 100
SA=SIN(AL)
T=(R(2,1)-R(1,2))/(2.0*SA)
IF(T.GT.1.0) T=1.0
IF(T.LT.-1.0) T=-1.0
T=ACOS(T)
P=0.0
IF(T.LT.0.01) GO TO 500
IF((PI-T).LT.0.01) GO TO 500
ST=SIN(T)
CP=(R(3,2)-R(2,3))/(2.0*ST*SA)
SP=(R(1,3)-R(3,1))/(2.0*ST*SA)
CALL INVCOS(CP,SP,P)
GO TO 500
C
C ALPHA=PI SECTION
C
100 T=R(3,3)
IF(T.GT.1.0) T=1.0
IF(T.LT.-1.0) T=-1.0
TT=ACOS(T)
P=0.0
T=TT/2.0
IF(TT.LT.0.01) GO TO 500
IF((PI-TT).LT.0.01) GO TO 200
STT=SIN(TT)
CP=R(1,3)/STT
SP=R(2,3)/STT
CALL INVCOS(CP,SP,P)
ST=SIN(T)
X=2*ST*ST*CP*SP
X=(X-R(1,2))/(X-R(1,2))
IF(X.LT.0.001) GO TO 500
T=PI-T
P=PI+P
GO TO 500
C
C ALPHA=PI AND THETA=PI/2 SECTION
C
200 CTP=R(1,1)
STP=R(1,2)
CALL INVCOS(CTP,STP,TP)
P=TP/2.0
C
C FINAL SECTION
C
500 A(1)=AL
A(2)=T
A(3)=P
IF(A(1).GT.0.01) CALL REFINE(R,A)
RETURN
END
C
C SUBROUTINE FINDS ANGLE BETWEEN 0 AND 2*PI
C FROM SINE AND COSINE
C SUBROUTINE INVCOS(C,S,A)
IF(C.GT.1.0) C=1.0
IF(C.LT.-1.0) C=-1.0
A=ACOS(C)
TPI=8.0*ATAN(1.0)
IF(S.LT.0.0) A=TPI-A
RETURN
END

```

```

C      SUBROUTINE TO REFINE ROTATION AXIS
C      EXTRACTED BY SUBROUTINE EXTRACT
C
SUBROUTINE REFINE(R,N)
DOUBLE PRECISION R(3,3),A(3),AX,AY,AZ,BX,BY,BZ
DOUBLE PRECISION AA(3),DOT,DOTO
N=0
ND=0
AA(2)=A(2)
AA(3)=A(3)
W=0.1
10  AZ=A(1)*DCOS(AA(2))
    AX=A(1)*DSIN(AA(2))*DCOS(AA(3))
    AY=A(1)*DSIN(AA(2))*DSIN(AA(3))
    BX=R(1,1)*AX+R(1,2)*AY+R(1,3)*AZ
    BY=R(2,1)*AX+R(2,2)*AY+R(2,3)*AZ
    BZ=R(3,1)*AX+R(3,2)*AY+R(3,3)*AZ
    DOT=(AX*BX+AY*BY+AZ*BZ)/(A(1)*A(1))
    DOTO=(DOT-1.0)*(DOT-1.0)
    IF(N.EQ.0) DOTO=DOT
    IF(DOT.GE.DOTO) GO TO 15
    IF(N.NE.0) N=N-1
    ND=0
    A(2)=AA(2)
    A(3)=AA(3)
    DOTO=DOT
    GO TO 20
15  IF(N.EQ.0) GO TO 20
    IF(K.EQ.0) AA(2)=AA(2)-W
    IF(K.EQ.1) AA(2)=AA(2)+W
    IF(K.EQ.2) AA(3)=AA(3)-W
    IF(K.EQ.3) AA(3)=AA(3)+W
    N=N+1
    ND=ND+1
    IF(ND.GE.5) GO TO 200
    K=N-4*(N/4)
    IF(K.EQ.0) AA(2)=AA(2)+W
    IF(K.EQ.1) AA(2)=AA(2)-W
    IF(K.EQ.2) AA(3)=AA(3)+W
    IF(K.EQ.3) AA(3)=AA(3)-W
    GO TO 10
200 W=W/10.0
    N=0
    ND=0
    IF(W.GE.0.0005) GO TO 20
    RETURN
END

```

## References

---

1. R. Tycko, Phys. Rev. Lett. 51, 775 (1983).
2. R. Tycko, E. Schneider, and A. Pines, J. Chem. Phys. 81, 680 (1984).
3. R. Tycko and A. Pines, J. Magn. Reson, in press.
4. R. Tycko and A. Pines, Chem. Phys. Lett., in press.
5. R. Tycko, H.M. Cho, E. Schneider, and A. Pines, J. Magn. Reson., in press.
6. R. Tycko, J. Guckenheimer, and A. Pines, in preparation.
7. J. Baum, R. Tycko, and A. Pines, J. Chem. Phys., 79, 4643 (1983).
8. J. Baum, R. Tycko, and A. Pines, in preparation.
9. T.M. Barbara, R. Tycko, and D.P. Weitekamp, J. Magn. Reson., in press.
10. A. Abragam, "The Principles of Nuclear Magnetism", (Oxford University Press, London, 1961).
11. C.P. Slichter, "Principles of Magnetic Resonance", second ed., (Springer-Verlag, New York, 1980).
12. I.I. Rabi, N.F. Ramsey, and J. Schwinger, Rev. Mod. Phys. 26, 169 (1954).
13. A. Messiah, "Quantum Mechanics", (John Wiley and Sons, New York, 1976).
14. B.L. Silver, "Irreducible Tensor Methods", (Academic Press, New York, 1976).
15. F.J. Dyson, Phys. Rev. 75, 486 (1949).

16. M. Goldman, "Spin Temperature and Nuclear Magnetic Resonance in Solids", (Oxford University Press, London, 1970).
17. F. Bloch, Phys. Rev. 70, 460 (1946).
18. R.P. Feynman, F.L. Vernon, and R.W. Hellwarth, J. Appl. Phys. 28, 49 (1957).
19. M.H. Levitt and R. Freeman, J. Magn. Reson. 33, 473 (1979).
20. R. Freeman, S.P. Kempell, and M.H. Levitt, J. Magn. Reson., 38, 453 (1980).
21. M.H. Levitt and R. Freeman, J. Magn. Reson. 43, 65 (1981).
22. M.H. Levitt, J. Magn. Reson. 48, 234 (1982).
23. M.H. Levitt, J. Magn. Reson. 50, 95 (1982).
24. A.J. Shaka, J. Keeler, T. Frenkiel, and R. Freeman, J. Magn. Reson. 52, 335 (1983).
25. A.J. Shaka, J. Keeler, and R. Freeman, J. Magn. Reson. 53, 313 (1983).
26. A.J. Shaka and R. Freeman, J. Magn. Reson. 55, 487 (1983).
27. M.H. Levitt, D. Suter, and R.R. Ernst, J. Chem. Phys. 80, 3064 (1984).
28. R. Freeman and J. Keeler, J. Magn. Reson. 43, 484 (1981).
29. M.H. Levitt and R. Freeman, J. Magn. Reson. 43, 502 (1981).
30. M.H. Levitt, R. Freeman, and T. Frenkiel, J. Magn. Reson. 47, 328 (1982).
31. M.H. Levitt, R. Freeman, and T. Frenkiel, J. Magn. Reson. 50, 157 (1982).
32. M.H. Levitt, R. Freeman, and T. Frenkiel, in "Advances in Magnetic Resonance", vol. 11, (Academic Press, New York, 1983).

33. L. Allen and J.H. Eberly, "Optical Resonance and Two-Level Atoms", (John Wiley and Sons, New York, 1975).
34. U. Haeberlen, "High Resolution NMR in Solids: Selective Averaging", (Academic Press, New York, 1976).
35. M. Mehring, "Principles of High Resolution NMR in Solids", second ed., (Springer-Verlag, New York, 1983).
36. J.S. Waugh, L.M. Huber, and U. Haeberlen, Phys. Rev. Lett. 20, 180 (1968).
37. U. Haeberlen and J.S. Waugh, Phys. Rev. 175, 453 (1968).
38. P. Mansfield, J. Phys. C 4, 1444 (1971).
39. W.-K. Rhim, D.D. Elleman, and R.W. Vaughan, J. Chem. Phys. 59, 3740 (1973).
40. W.-K. Rhim, D.D. Elleman, L.B. Schreiber, and R.W. Vaughan, J. Chem. Phys. 60, 4595 (1974).
41. D.P. Burum and W.-K. Rhim, J. Chem. Phys. 71, 944 (1979).
42. M. Mehring, Z. Naturforsch. 27a, 1634 (1972).
43. M. Mehring, Rev. Sci. Instrum. 44, 64 (1973).
44. D.P. Burum, M. Linder, and R.R. Ernst, J. Magn. Reson. 44, 173 (1981).
45. W.-K. Rhim, A. Pines, and J.S. Waugh, Phys. Rev. B 3, 684 (1971).
46. W.S. Warren, D.P. Weitekamp, and A. Pines, J. Chem. Phys. 73, 2084 (1980).
47. Y.-S. Yen and A. Pines, J. Chem. Phys. 78, 3579 (1983).
48. W. Magnus, Commun. Pure Appl. Math. 7, 649 (1954).
49. P. Pechukas and J.C. Light, J. Chem. Phys. 44, 3897 (1966).
50. R.M. Wilcox, J. Math. Phys. 8, 962 (1967).
51. I. Bialynicki-Birula, B. Mielnik, and J. Plebanski, Ann. Phys.

- 51, 187 (1969).
52. C.H. Wang and J.D. Ramshaw, Phys. Rev. B 6, 3253 (1972).
53. J.S. Waugh, J. Magn. Reson. 49, 517 (1982).
54. J.S. Waugh, J. Magn. Reson. 50, 30 (1982).
55. H.A. Buckmaster, R. Chatterjee, and Y.H. Shing, Phys. Status Solidi 13, 9 (1972).
56. J.J.H. Ackerman, T.H. Grove, G.C. Wong, D.B. Gadian, and G.K. Radda, Nature 283, 169 (1980).
57. P.C. Lauterbur, Nature 242, 190 (1973).
58. P.A. Bottomley, Rev. Sci. Instrum. 53, 1319 (1982).
59. P. Mansfield and P.G. Morris, "NMR Imaging in Biomedicine", (Academic Press, New York, 1982).
60. E.L. Hahn, Phys. Rev. 80, 580 (1950).
61. H.Y. Carr and E.M. Purcell, Phys. Rev. 94, 630 (1954).
62. J.M.S. Hutchison, R.J. Sutherland, and J.R. Mallard, J. Phys. E 11, 217 (1978).
63. P. Mansfield and P.K. Grannell, Phys. Rev. B 12, 3618 (1975).
64. A.N. Garroway, J. Baum, M.G. Munowitz, and A. Pines, J. Magn. Reson., in press.
65. R.W. Vaughan, D.D. Elleman, L.M. Stacey, W.-K. Rhim, and J.W. Lee, Rev. Sci. Instrum. 43, 1356 (1972).
66. M.H. Levitt and R.R. Ernst, Molec. Phys. 50, 1109 (1983).
67. A. Pines and J.S. Waugh, J. Magn. Reson. 8, 354 (1972).
68. G.E. Pake, J. Chem. Phys. 16, 327 (1948).
69. J. Jeener and P. Broekaert, Phys. Rev. 157, 232 (1967).
70. L.W. Reeves, in "Progress in Nuclear Magnetic Resonance Spectroscopy", vol. 4, (Pergamon Press, New York, 1969).



71. A. Pines, D.J. Ruben, S. Vega, and M. Mehring, Phys. Rev. Lett. 36, 110 (1976).
72. D. Semmingsen, Tetrahedron Lett. 11, 807 (1973).
73. D. Suwelack, J. Becker, and M. Mehring, Solid State Commun. 22, 597 (1977).
74. J.D. Becker, D. Suwelack, and M. Mehring, Solid State Commun. 25, 1145 (1978).
75. D. Semmingsen and J. Feder, Solid State Commun. 15, 1369 (1974).
76. E.J. Samuelsen and D. Semmingsen, Solid State Commun. 15, 217 (1975).
77. D. Barnaal and I.J. Lowe, Phys. Rev. Lett. 11, 258 (1963).
78. M. Bloom, J.H. Davis, and M.I. Valic, Can. J. Phys. 58, 1510 (1980).
79. J.G. Powles and J.H. Strange, Proc. Phys. Soc. 82, 6 (1963).
80. S. Vega and A. Pines, J. Chem. Phys. 66, 5624 (1977).
81. A. Wokaun and R.R. Ernst, J. Chem. Phys. 67, 1752 (1977).
82. S. Vega, J. Chem. Phys. 68, 5518 (1978).
83. G. Bodenhausen, in "Progress in Nuclear Magnetic Resonance Spectroscopy", vol. 14, (Pergamon Press, New York, 1980).
84. D.P. Weitekamp, in "Advances in Magnetic Resonance", vol. 11, (Academic Press, New York, 1983).
85. J.R. Garbow, D.P. Weitekamp, and A. Pines, Chem. Phys. Lett. 93, 504 (1982).
86. G.C. Chingas, A.N. Garroway, R.D. Bertrand, and W.B. Moniz, J. Chem. Phys. 74, 127 (1981).
87. G. Drobny, A. Pines, S. Sinton, D.P. Weitekamp, and D. Wemmer, Symp. Faraday Soc. 13, 49 (1979).

88. A. Bax, R. Freeman, and S.P. Kempell, J. Am. Chem. Soc. 102, 4849 (1980).
89. A. Bax, R. Freeman, and S.P. Kempell, J. Magn. Reson. 41, 349 (1980).
90. D.L. Turner, Molec. Phys. 44, 1051 (1981).
91. E.M. Menger, S. Vega, and R.G. Griffin, J. Magn. Reson. 56, 338 (1984).
92. S. Vega, T.W. Shattuck, and A. Pines, Phys. Rev. Lett. 37, 43 (1976).
93. D.E. Wemmer, Ph.D. Dissertation, University of California, Berkeley (1978).
94. R. Eckman, L. Muller, and A. Pines, Chem. Phys. Lett. 74, 376 (1980).
95. A. Pines, M.G. Gibby, and J.S. Waugh, J. Chem. Phys. 59, 569 (1973).
96. S.R. Hartmann and E.L. Hahn, Phys. Rev. 128, 2042 (1962).
97. G.A. Morris and R. Freeman, J. Am. Chem. Soc. 101, 760 (1979).
98. D.T. Pegg, D.M. Doddrell, and M.R. Bendall, J. Chem. Phys. 77, 2745 (1982).
99. J.R. Garbow, Ph.D. Dissertation, University of California, Berkeley (1983).
100. D.T. Pegg, D.M. Doddrell, W.M. Brooks, and M.R. Bendall, J. Magn. Reson. 44, 32 (1981).
101. M.H. Levitt and R.R. Ernst, J. Magn. Reson. 55, 247 (1983).
102. A. Abragam and M. Goldman, "Nuclear Magnetism: Order and Disorder", (Oxford University Press, New York, 1982).
103. R.H. Abraham and C.D. Shaw, "Dynamics--The Geometry of Behavior",

(Aerial Press, Santa Cruz).

104. M.I. Petrashen and E.D. Trifonov, "Applications of Group Theory in Quantum Mechanics", (Iliffe Books Ltd., 1969).
105. M.R. Bendall and R.E. Gordon, J. Magn. Reson. 53, 365 (1983).
106. M.R. Bendall and W.P. Aue, J. Magn. Reson. 54, 149 (1983).
107. M.R. Bendall, Chem. Phys. Lett. 99, 310 (1983).
108. B. Chance, S. Eleff, and J.S. Leigh, Jr., Proc. Natl. Acad. Sci. U.S.A. 77, 7430 (1980).
109. R.L. Nunnally and P.A. Bottomley, Science 211, 177 (1981).
110. K.J. Neurohr, E.J. Barrett, and R.G. Shulman, Proc. Natl. Acad. Sci. U.S.A. 80, 1603 (1983).
111. A.P. Koretsky, S. Wang, J. Murphy-Boesch, M.P. Klein, T.L. James, and M.W. Weiner, Proc. Natl. Acad. Sci. U.S.A. 80, 7491 (1983).
112. D.I. Hoult and R.E. Richards, J. Magn. Reson. 24, 71 (1976).
113. A.J. Shaka and R. Freeman, J. Magn. Reson. 59, 169 (1984).
114. G. Drobny, Ph.D. Dissertation, University of California, Berkeley (1982).
115. S. Sinton, J.R. Garbow, J.L. Ackerman, G. Drobny, D.J. Ruben, and A. Pines, Lawrence Berkeley Laboratory Report PUB-3033 (1983).



This report was done with support from the Department of Energy. Any conclusions or opinions expressed in this report represent solely those of the author(s) and not necessarily those of The Regents of the University of California, the Lawrence Berkeley Laboratory or the Department of Energy.

Reference to a company or product name does not imply approval or recommendation of the product by the University of California or the U.S. Department of Energy to the exclusion of others that may be suitable.

TECHNICAL INFORMATION DEPARTMENT  
LAWRENCE BERKELEY LABORATORY  
UNIVERSITY OF CALIFORNIA  
BERKELEY, CALIFORNIA 94720